Missouri S&T Library and Learning Resources

Scholars' Mine

Doctoral Dissertations | Student Theses and Dissertations

Spring 2010

Theoretical study of electron impact-ionization of molecules

Ola Al-Hagan

Follow this and additional works at: https://scholarsmine.mst.edu/doctoral_dissertations

 Part of the Physics Commons

Department: Physics

Recommended Citation

Al-Hagan, Ola, "Theoretical study of electron impact-ionization of molecules" (2010). *Doctoral Dissertations*. 1898.
https://scholarsmine.mst.edu/doctoral_dissertations/1898

This thesis is brought to you by Scholars' Mine, a service of the Missouri S&T Library and Learning Resources. This work is protected by U. S. Copyright Law. Unauthorized use including reproduction for redistribution requires the permission of the copyright holder. For more information, please contact scholarsmine@mst.edu.

THEORETICAL STUDY OF ELECTRON IMPACT-IONIZATION OF MOLECULES

by

OLA AL-HAGAN

A DISSERTATION

Presented to the Faculty of the Graduate School of the

MISSOURI UNIVERSITY OF SCIENCE AND TECHNOLOGY

In Partial Fulfillment of the Requirements for the Degree

DOCTOR OF PHILOSOPHY

in

PHYSICS

2010

Approved by

Don H. Madison, Co-Advisor
Jerry L. Peacher, Co-Advisor
Michael Schulz
Barbara N. Hale
Shari Dunn-Norman

© 2010
Ola Al-Hagan
All Rights Reserved

PUBLICATION DISSERTATION OPTION

This dissertation has been prepared in publication format. The first section has been added to supply background information and general theory. The second section is a collection of published papers and the third section is a summary and conclusions of the all of the work presented.

SECTION:

1. INTRODUCTION
2. THEORY OF ELECTRON IMPACT IONIZATION

PAPERS:

Paper I. *Nature physics* **5** 59 (January 2009) Pages 28-41

Paper II. *Phys. Rev.* A **79** 052704 (May 2009) Pages 42-58

Paper III. *J. Phys.* B **42** 171001 (August 2009) Pages 59-73

Paper IV. *Phys. Rev.* A. **81** 030701(R) (March 2010) Pages 74-85

Paper V. *J. Phys.* B **41** 025204 (January 2008) Pages 86-101

Paper VI. *Phys. Rev.* A **80** 062704 (December 2009) Pages102-118

Paper VII. *J. Phys.* B **43** 035201(January 2010) Pages119-135

Paper VIII. *J. Phys.* B **42** 235207 (December 2009) Pages 136-151

Paper IX. *J. Phys.: Conf. Ser.* **212** 012004 (2010) Pages 152-163

Paper X. *J. Phys.* B. **43** No 8 (April 2010) 081002 Pages 164-174

Paper XI. *Journal of Chemical Physics* (submitted April 2010) Pages 175-193

SECTION:

3. CONCLUSIONS

ABSTRACT

There has been impressive progress in the area of theoretical treatments of electron impact ionization (e,2e) of atoms and molecules in the last decade. Most recently, low to intermediate incident electron energies have been reported for molecular systems. In this dissertation, different theoretical models will be used to calculate the fully differential cross section (FDCS) for (e,2e) processes for low to intermediate incident electron energies for a variety of final state electron angles and energies for the diatomic molecules H_2 and N_2, the triatomic molecule H_2O, and the boimolecule $HCOOH$.

In addition, there has been a large amount of interest in diatomic molecules inspired by the possibility of observing an interference effect due to the two molecular centers playing the role of a double slit. In this dissertation, the interference effect for the diatomic molecules H_2 and N_2 will be examined.

Finally, there is presently considerable experimental effort directed towards measuring the FDCS for a specific molecular orientation. Most recently, the FDCS for single ionization of aligned hydrogen molecules was measured by Alexander Dorn's experimental group in Heidelberg, Germany. These measurements were successful for the first time to observe features of the FDCS for different alignment of H_2. Theoretical calculations for aligned H_2 will be presented. These calculations were able to obtain good agreement with the experimental data especially in the binary peak region.

ACKNOWLEDGMENTS

I could never have succeeded in the manner that I have if it were not for the support and love furnished by my family especially my father. He always believed in me, stood behind me; gave me the encouragement and the support to come to the U.S.A to pursue my PhD. So, here's to my family for supporting and believing in me.

My deepest gratitude and appreciation goes to my advisors Dr. Madison and Dr. Peacher for their guidance and support throughout this study. I am especially grateful to my advisor, Dr. Madison, for his unending patience as I completed my PhD. Also, I extend my gratitude to my advisory committee, Dr. Michael Schulz, Dr. Barbara N. Hale and Dr. Shari Dunn-Norman, for adding breadth to my doctorate.

To all the people and friends I have worked with, worked beside, and learned from, to Tina and Allison whose friendship I enjoyed, to my brothers (AbdulRahman and Wael) who stayed with me in the USA and supported me, thank you.

Finally, thank you to everyone in the physics department for making Missouri S&T a great environment for students with full support and inspiration and surrounded by knowledgeable faculty with great motivation. Thanks to the Ministry of Higher Education in Saudi Arabia and the King Abdullah Bin Abdul-Aziz Scholarship for financial support.

TABLE OF CONTENTS

Page

PUBLICATION DISSERTATION OPTION iii
ABSTRACT iv
ACKNOWLEDGMENTS v
TABLE OF CONTENTS vi
LIST OF ILLUSTRATIONS xi
LIST OF TABLES xxi
SECTION
1. INTRODUCTION 1
2. THEORY OF ELECTRON IMPACT IONIZATION 10
2.1. INTRODUCTION 10
2.2. IONIZATION PROCESSES 10
2.2.1. Electron Impact Ionization. 10
2.3. DIFFERENTIAL CROSS SECTIONS 11
2.4. GENERAL SCATTERING THEORY 12
2.4.1. The Lippmann-Schwinger Equation 13
2.4.2. Born Approximations 15
2.4.3. First Born Approximation. 16
2.5. DISTORTED WAVE BORN APPROXIMATION 17
2.6. THREE-BODY DISTORTED WAVE APPROXIMATION 20
PAPER
I. Atomic and Molecular Signatures for Charged Particle Ionization 28
Abstract 28
Introduction 29
1. Experimental arrangement and results 30
2. Possible types of collision 32
3. Quantum mechanical calculation 34
4. Using quantum mechanics to identify collision types 35
5. Nuclear distribution causes the difference 36

6. Generalizing the model to larger molecules 38

Acknowledgements 40

Author contributions 40

References 40

II. Triple Differential Cross Sections for the Electron-Impact Ionization of H_2 Molecules for Equal and Unequal Outgoing Electron Energies 42

Abstract 42

1. Introduction 43

2. Theoretical approach 44

2.1. 3DW theory 44

2.2. Time-dependent close-coupling method 45

3. Experimental setup 48

4. Results and discussion 50

4.1. Equal-energy sharing 50

4.2. Unequal-energy sharing 54

5. Conclusions 54

Acknowledgements 56

References 57

III. Deep Interference Minima in Non-coplanar Triple Differential Cross Sections for the Electron-Impact Ionization of Small Atoms and Molecules 59

Abstract 59

1. Introduction 60

2. Theoretical approach 62

3. Results and discussions 64

Acknowledgments 72

References 72

IV. Electron Impact Ionization Cross Sections of H_2 for Low Energy Outgoing Electrons from 1 eV to 10 eV 74

Abstract 74

References 85

V. (e,2e) Ionization of Helium and the Hydrogen Molecule: Signature of Two-Centre Interference Effects 86

Abstract 86
1. Introduction 87
2. Experiment 89
3. Results and discussion 90
3.1. Angular distributions of the TDCS 90
3.2. Interference effect 94
4. Conclusion 98
Acknowledgments 99
References 99
VI. (e,2e) Study of Two-Centre Interference Effects in the Ionization of N_2 102
Abstract 102
1. Introduction 103
2. Experiment details 104
3. Theory: Molecular distorted wave approach 107
4. Results and discussions 108
4.1. Asymmetric energy sharing 108
2.4. Symmetric energy sharing 112
5. Conclusions 116
Acknowledgments 117
References 117
VII. Low-energy Symmetric Coplanar and Symmetric Non-coplanar (e, 2e) Studies from the $3a_1$ State of H_2O 119
Abstract 119
1. Introduction 120
2. Experimental apparatus 122
3. Theoretical framework 128
4. Results and discussion 129
4.1. Symmetric coplanar kinematics 129
4.2. Symmetric non-coplanar kinematics 130
4.3. Unequal energy sharing, coplanar and perpendicular geometries 131
5. Conclusions 133

Acknowledgments 134

References 134

VIII. Dynamical (e, 2e) Studies of Formic Acid 136

Abstract 136

1. Introduction 137

2. Experimental apparatus 138

3. Theory 139

4. Results and discussion 142

5. Conclusions 149

Acknowledgements 149

References 150

IX. Recent Theoretical Progress in Treating Electron Impact Ionization of Molecules 152

Abstract 152

1. Introduction 153

2. Theory 153

3. Results and discussion 155

3.1. Molecular hydrogen (H_2) 155

3.2. Molecular nitrogen (N_2) 158

3.3. Water (H_2O) 159

3.4. Formic acid ($HCOOH$) 161

5. Conclusions 162

Acknowledgment 162

References 163

X. Search for Interference Effect in Electron Impact ionization of Aligned Hydrogen Molecules 164

Abstract 164

Acknowledgements 173

References 173

XI. Five-fold Differential Cross Sections for Ground-State Ionization of Aligned H_2 by Electron Impact 175

Abstract 175

1. Introduction 176
2. Theoretical framework 178
3. Experimental procedure 180
3.1. Reaction microscope set-up 180
3.2. Obtaining the molecular alignment 181
4. Results and discussion 183
4.1. General dependence of the ionization rate on the alignment 183
4.2. Five-fold differential cross sections 184
5. Conclusion 189
Acknowledgments 189
References 192
SECTION
3. CONCLUSIONS 194
BIBLIOGRAPHY 197
VITA 201

LIST OF ILLUSTRATIONS

Page

Paper I

Figure 1: The experimental geometry. A plane is defined by the detected electrons. The incident-electron gun can move from a coplanar geometry ($\psi = 0^o$) to the perpendicular plane ($\psi = 90^o$), where the angle $\varphi = \theta_a + \theta_b$ is defined. A common point between all planes occurs when $\theta_a = \theta_b = \pi / 2$ 30

Figure 2: Experimental and theoretical DCS data in the perpendicular plane for *He* and H_2 targets, normalized to unity at the experimental maximum. The outgoing energies were $E_a = E_b$ =10 eV in both cases. The results show the significant differences between ionizing atomic and molecular targets, and contrast the effects of using plane and distorted waves to describe the projectile electron. Error bars in the DCS indicate the statistical variation measured over a series of sweeps of the analysers around the detection plane. Horizontal error bars show the estimated angular response of the spectrometer due to the analyser entrance apertures and the incident electron beam pencil angle. The type of collision process noted in this figure is described in Fig. 3. 31

Figure 3: Different mechanisms that may lead to ionization in the perpendicular plane. a, The only mechanism that can occur without nuclear scattering. b, The effect of nuclear scattering followed by a binary collision, leading to peaks at φ ~ 90°, 270°. c, The triple scattering process that leads to a central peak at φ ~ 180° for targets that have a nucleus at the centre of mass. d, The effect of distributing the nuclear charge on a thin shell, in which case the mechanism in c, cannot occur. 33

Figure 4: Averaging of the electronic and nuclear structure of the targets due to experimental constraints which cannot determine the orientation of the molecule. For H_2, the nuclear charge is distributed on a thin shell of diameter 1.4 Bohr radii, whereas for *He* the charge is concentrated at the centre of the target. 35

Figure 5: Change in the calculated ionization DCS for H_2 in the perpendicular plane as a function of the size of the spherically averaged nuclear shell, normalized to unity at the experimental maximum. Error bars are as described in Fig. 2. 37

Figure 6: DCS for ionization of CO_2 in the perpendicular plane normalized to unity at the experimental maximum. A maximum is seen at $\varphi = 180°$, as found for He, in contrast to the results from H_2. This is attributed to the carbon nucleus being at the centre of mass of the molecule, so that spherical averaging produces an oxygen nuclear shell with an extra nuclear target at the centre of the molecule. The scattering process shown in Fig. 3c can then take place from this carbon nucleus. Error bars are as described in Fig. 2. 39

Paper II

Figure 1: The experimental geometry. The incident electron beam makes an angle ψ with respect to the detection plane defined by theanalyzers. ψ=0° defines a coplanar geometry, ψ =90° a perpendicular geometry. The analyzers rotate through angles ξ_1 and ξ_2 as shown. In the current experiments $\xi_1 = \xi_2$. A common normalization point exists for all gun angles when $\xi_1=\xi_2=90°$. 49

Figure 2: (Color online) Triple differential cross sections for the electron-impact ionization of H_2 for equal-energy sharing between the outgoing electrons (E_1=E_2=10 eV). We present cross sections for various values of the gun angle ψ, as a function of the angle ξ, where 2ξ is the angle between the outgoing electrons. The measurements are compared with TDCC calculations and two sets of 3DW calculations; one including a correlation-polarization potential [labeled 3DW (with CP)] and one without this potential [labeled 3DW(no CP)]. Both sets of 3DW calculations are divided by 6.3 to allow a better comparison with the other results. 1 kb=1.0 $\times 10^{-21}$ cm^2; 1 kb/ sr^2 eV $\approx$ 1×10^{-3} a.u. 51

Figure 3: (Color online) Same as Fig. 2, except for unequal energy sharing: E_1=18 eV; E_2=2 eV, for ψ values ranging from 0 to 45 degrees. The 3DW (with CP) cross sections are divided by 3.7 and the 3DW (no CP) cross sections are divided by 4.5 to allow a better comparison with the other results..... 55

Figure 4: (Color online) Same as Fig. 3, for ψ values ranging from 50 to 90 degrees..... 56

Paper III

Figure 1: The experimental geometry. The incident electron beam makes an angle ψ with respect to the detection plane defined by the analysers. The analysers rotate through angles ξ_1 and ξ_2 as shown. In the measurements discussed here, $\xi_1 = \xi_2$. A common normalization point exists for all gun angles when $\xi_1 = \xi_2 = 90°$..... 61

Figure 2: Triple differential cross sections for the electron-impact ionization of helium for three incident electron energies and gun angles as indicated. In all cases, the outgoing electrons have equal energy sharing. The experimental data are compared with TDCC calculations (solid red lines) and with 3DW calculations (dashed green lines) 1.0 kb = 1.0×10^{-21} cm^2. 65

Figure 3: TDCC calculations for the triple differential cross sections for the electron-impact ionization of helium for an incident electron energy of 64.6 eV, at a gun angle of $\psi = 61.5°$, and for equal energy sharing outgoing electrons. A complete TDCC calculation (including $L = 0–9$) is indicated by the solid red line. The various dashed lines show TDCC calculations which include fewer partial wave contributions, as indicated in the caption. 66

Figure 4: TDCC calculations for the same case as figure 2. Here, we show the contributions from individual partial waves (dashed black lines) in each panel up to $L = 8$. The solid red lines signify the contribution from the interference (cross) terms inherent in the coherent sum in equation (1). For example, the red line in the upper right panel shows the contribution from the $L = 0, 1, 2$ cross terms. The vertical dotted lines indicate the position of the minimum in the TDCS in figure 3 67

Figure 5: TDCC and 3DW calculations of the triple differential cross sections for the electron-impact ionization of atomic hydrogen at an incident energy of 33.6 eV, for various gun angles as indicated. The $\psi = 0^{\circ}$ case corresponds to the coplanar geometry..... 70

Figure 6: Triple differential cross sections for the electron-impact ionization of molecular hydrogen at an incident energy of 35.4 eV, for equal energy sharing outgoing electrons. Experimental data are compared with TDCC calculations (thick red line) which are averaged over all molecular orientations and two sets of 3DW calculations. The calculations labeled 3DW (with CP) include a correlation-polarization term, while the calculation labeled 3DW (no CP) omits the correlation-polarization term. Both sets of 3DW calculations are divided by 6.3 to allow a better comparison with other results. The double-dashed purple line indicates the TDCC calculation for a specific molecular orientation ($\theta_N = 50°$; $\varphi_N = 0°$), where it can be seen that a deep interference minimum is predicted..... 71

Paper IV

Figure 1: FDCS for ionization of H_2 using perpendicular plane kinematics. The FDCS are plotted as a function of φ (the angle between the two final state electrons in the detection plane). The energies of the outgoing electrons are shown on the respective plots. The experimental measurements are compared with MDW calculations (the solid curve) and the TDCC calculations (the dashed curve). For each energy, the experimental and theoretical data are normalized to unity at the experimental maximum. 78

Figure 2: The dependence of the FDCS as a function of φ (the angle between the two final state electrons in the detection plane) for various nuclear separations. Both ejected electrons have energy of 1 eV. The MDW calculations are for different nuclear separations R = 0.0, 0.6, 1.0 and 1.4 a_0 as shown. 80

Figure 3: Same as fig. 1 except now the solid curve is the M3DW..... 81

Figure 4: Calculated H_2 FDCS for equal energy sharing with φ = 180° as a function of excess energy. The solid line is the results of the Wannier theory normalized to the M3DW at the lowest energy and the dashed line is the M3DW FDCS. 83

Paper V

Figure 1: (e,2e) TDCS for ionization of *He* (left column) and H_2 (right column), plotted versus ejection angle θ_b, at a fixed scattering angle, θ_a=−6° and the fixed scattering energy, E_a = 500 eV. Panels (a) and (d) E_b = 37 eV; (b) and (e) E_b = 74 eV; (c) and (f) E_b = 205 eV. The incident energy (E_0) is consequently adjusted to fulfil the energy conservation. For *He*, the dashed line represents the results of the CCC calculations. For H_2, the dotted and full lines represent the theoretical results from the FBA–TCC and the M3DW–OAMO models, respectively. Solid circles: experimental data, with one standard deviation statistical error bars. The vertical arrows indicate the momentum transfer direction and its opposite. The insets in the H_2 results represent a zoom on the low intensity recoil region to facilitate comparison. The relative experimental data have been normalized for the best visual agreement with theory. The absolute scale shown is that of the CCC calculations for *He* and that of the FBA–TCC for H_2, both in 10−2 atomic units. The M3DW–OAMO results have been multiplied by 2.5 in (d), 2.8 in (e) and 6.7 in (f). 91

Figure 2: Interference factor, I, predicted by equation (1), plotted versus ejection angle, θ_b, at the ejected electron energies E_b = 37 eV (full line), E_b = 74 eV (dashed line) and E_b = 205 eV (dotted line). The I values are arbitrarily normalized to unity in the region of the binary peak..... 96

Figure 3: Solid circles: the experimental ratio, $\sigma_{e,2e}(H_2)/\sigma_{e,2e}(He)$, of the (e,2e) TDCS for ionization of H_2 relative to that of He, plotted versus the ejection angle θ_b at (a) E_b = 37 eV; (b) E_b = 74 eV; (c) E_b = 205 eV. The full lines represent the predicted interference factor of figure 2. 97

Paper VI

Figure 1: (Color online) Interference factor as a function of ejected electron emission angle, for continuum electron energies of E_0=150 eV, E_s=124.4 eV, E_e=10 eV. 110

Figure 2: (Color online) Binding energy spectrum for N_2. The 3 outermost orbitals (labelled in the figure) are all resolved at the current coincidence energy resolution of 850 meV..... 110

Figure 3: (Color online) TDCS for ionization of the (a) $3\sigma_g$, (b) $1\pi_u$ and (c) $2\sigma_u$ orbitals of N_2. The incident electron energy was 150 eV, the ejected electron energy was 10 eV and the scattered electron angle -15°. The experimental results (circles) are compared with DWBA calculations for the atomic nitrogen 2*s* (a) and 2*p* (b, c) orbitals (solid curve), and the same calculation multiplied by the interference factor (long dashed curve). Also shown is the M3DW calculation for ionization of the $3\sigma_g$ orbital of N_2 (short dashed curve)..... 113

Figure 4: (Color online) TDCS for ionization of the $3\sigma_g$ orbital of N_2. The incident electron energy was 75 eV, the scattered and ejected electron energies 30 eV, with scattered electron angles of (a) -25° and (b) -10°. The present experimental results (circles) are compared to results from new M3DW calculations (solid curve), as well as results from a previous experiment (open squares) [9] and a previously published M3DW calculation (short dashed curve) [24]. 114

Figure 5: (Color online) TDCS for coplanar symmetric ionization of the $3\sigma_g$ orbital of N_2. The incident energy was 75 eV, both outgoing electrons have 30 eV energy and the scattered electron angle was -22°. The M3DW calculations are for different nuclear separations r_0: r_0= 2.14 a_0 (solid curve); r_0= 0.5 a_0 (long dashed curve); and r_0= 0.0 a_0 (short dashed curve)..... 116

Paper VII

Figure 1: Schematic of the scattering geometry, depicting the various angles employed. A *coplanar geometry* (ψ=0°) is defined when all three electrons are in the detection plane. The analyzer angles (ξ_1 and ξ_2) are measured with respect to the projection of the incident electron beam k_0 onto this plane as shown. For non-coplanar geometries the electron gun is lifted out of the plane, and is defined by the angle ψ. ψ=90° is called the *perpendicular geometry*. 123

Figure 2: A typical coincidence binding energy spectrum obtained for H_2O. These data were measured in a coplanar geometry with outgoing electron energies of 20 eV detected at $\xi_1 = \xi_2 = 55°$. The peaks in the spectrum correspond to the three highest orbitals, *i.e.* the $1b_1$, $3a_1$ and $1b_2$ orbitals as labelled. The full line represents a three-Gaussian fit, whereas the dotted lines show the individual Gaussians from this fit, illustrating the degree of separation measured with the current energy resolution. Very little contamination is expected from neighbouring orbitals in the measured TDCS for the $3a_1$ state. 124

Figure 3: Triple differential cross sections for ionisation of the $3a_1$ state of H_2O using coplanar symmetric kinematics (*i.e.* ψ=0° and ξ_1=ξ_1). The energies of the outgoing electrons are shown on the respective plots. The solid line shows results from the Molecular Distorted Wave Born Approximation (MDW) while the dashed line was generated from the Molecular 3-body Distorted Wave Approximation (M3DW). The experimental and theoretical data has been independently normalised to unity at each energy. 126

Figure 4: Triple differential cross sections for the ionisation of the $3a_1$ state of H_2O. These measurements were taken in a series of symmetric non-coplanar geometries with outgoing electron energies of 10 eV. The angle of the electron gun (ψ) is shown on the respective plots. The data and theory are normalised to unity at the peak in the coplanar (ψ=0°) geometry. The data within the remaining plots are normalised at the ξ=90° point (see text for details). 127

Figure 5: Triple differential cross sections for ionisation of the $3a_1$ state of H_2O. Symmetric geometries were adopted for these data with unequal energy sharing kinematics. Both coplanar and perpendicular geometries were utilised. In all plots the excess energy is 20 eV, with the outgoing electron energies as shown. The electron gun angle ψ is also shown on the respective plots. 132

Paper VIII

Figure 1: Experimental triple differential cross section for the 10a′ valence orbital of formic acid (solid circles) as a function of ejected electron scattering angle, compared with M3DW-CPE (solid line) and PWIA (dashed line) calculations. The incident electron energy is 831.6 eV, the projectile scattering angle is 20.5°, and the ejected electron energy is 105 eV. The experimental data and the PWIA results are those of Nixon *et al*. [34]. 142

Figure 2: Measured binding energy spectrum for the outer valence orbital region of formic acid, fitted with a sum of Gaussian functions. 143

Figure 3: Experimental triple differential cross sections for the summed 10a′ and 2a″ valence orbitals of formic acid (solid circles), with E_0=100 eV and E_b=10 eV, compared with M3DW-CPE (solid line) and M3DW (dashed line) calculations for the 10a′ orbital only. The scattered electron detection angles and corresponding momentum transfers are (a) -10°, |K|=0.54au and (b) -15°, |K|=0.74au. 145

Figure 4: Experimental triple differential cross sections for the summed 10a′ and 2a″ valence orbitals of formic acid (solid circles), with E_0=250 eV and E_b=10 eV, plotted against the M3DW-CPE (solid line) and M3DW (dashed line) calculations for the 10a′ orbital only (a, b). Panel (c) includes previous experimental results for the summed $3a_1$+$1b_1$ orbitals for water under the same kinematics [9] (open circles). The scattered electron detection angles and corresponding momentum transfers are (a) -5°, |K|=0.42au, (b) -10°, |K|=0.75au and (c) -15°, |K|=1.11au 147

Figure 5: Molecular structures of (a) formic acid, and (b) water. The centre of mass for each molecule is marked by an *..... 148

Paper IX

Figure 1: TDCS for the electron impact ionization of H_2 for unequal final state energies E_a=18 eV and E_b=2 eV. See text for definition of angles. The measurements are compared with M3DW calculations obtained with and without the correlation-polarization potential..... 156

Figure 2 : TDCS for the electron impact ionization of H_2 for unequal final state energies E_a=18 eV and E_b=2 eV. See text for definition of angles. The measurements are compared with M3DW calculations obtained with and without the correlation-polarization potential..... 157

Figure 3: TDCS for the $3\sigma_g$ state of N_2 with E_0=75.6 eV, E_a=E_b=30 eV and θ_a=22°. The experiment data are compared to two sets of M3DW. The dotted blue line is the M3DW using an old wave-function and the solid red line is the M3DW using an improved wave-function. The experimental data are those of Murray et al. [20]. 158

Figure 4: TDCS for electron impact ionization of H_2O in symmetric coplanar geometry as a function of ξ (2ξ is the angle between the two outgoing electrons). The cross sections are presented for excess energies of 10 eV and 20 eV. 160

Figure 5: Triple differential cross section of ionization of Formic Acid with E_0=100 eV, E_b=10 eV and θ_a=10° as a function of the ejected electron angle. The Experimental measurements represent a sum of the 10a′ and 2a″ states while the M3DW results are for the 10a′ state only. 161

Paper X

Figure 1: (color online) Selected potential curves of H_2 and H_2^+ (after [16, 17]) with illustration of two dissociative ionization channels: Ground-state dissociation (GSD) and autoionization (AI). 166

Figure 2: (color online) Measured kinetic energy released to the fragments of the dissociating H_2^+ ion versus the emitted electron's energy for molecules aligned parallel (left) and perpendicular (right) to the momentum transfer $\vec{q}$. The logarithmic color scales are identical in both images, with black representing the highest count rates. 169

Figure 3: (color online) (a) Geometry of the ionizing collision in the scattering plane spanned by the incoming and scattered projectile momentum vectors. The sketched momentum of the emitted electron is exemplary. (b)–(d) Dependence of the ionization cross section on the emission direction of the protonic fragment. Summed over the whole detected solid angle for the two electrons while the emitted electron energy amounts (b) (3 ± 2) eV, (c) (9 ± 3) eV and (d) (16 ± 4) eV. 170

Figure 4: (color online) Five-fold differential cross sections (5DCS) as a function of the emitted electron's emission angle in the scattering plane. This electron's energy is (3.5 ± 2.0) eV and the projectile scattering angle is (16 ± 4)°. Points represent experimental results, lines model calculations, which is either M3DW(upper panel) or 3C for a helium target multiplied with the interference factor given by [13] (lower panel). For all data shown the molecule is aligned in the scattering plane, at angles of 0° (triangles/dotted line), 45° (circles/dashed line) or 90° (squares/solid line) relative to the momentum transfer $\vec{q}$. Shaded areas represent angular ranges outside the experimental acceptance. 172

Paper XI

Figure 1: Geometry of the ionizing collision. 178

Figure 2: Schematic drawing of the employed reaction microscope. 180

Figure 3: Selected potential curves of H_2 and H_2^+ (after [36,37]) with illustration of two dissociative ionization channels: Ground-state dissociation (GSD) and autoionization (AI). 182

Figure 4: Dependence of the ionization cross-section for H_2 on the angle between the molecular axis and momentum transfer $\vec{q}$. The emitted electron's energy is (3 ± 2) eV (left) and (16 ± 4) eV (right) while the scattering angle varies from (5 ± 2)° (triangles) and (9.5 ± 2.5)° (squares) to (16 ± 4)° (circles). All data sets are normalized to one at their maximum..... 184

Figure 5: Illustration of the molecular alignments inside the scattering plane as considered in figs. 6, 8 and 7. $\varphi_M = 0°$ for all situations depicted. 185

Figure 6: Coplanar 5DCS for molecules aligned in the scattering plane at an angle of 0° (red), 45° (green) and 90° (blue) relative to the momentum transfer $\vec{q}$ (compare fig. 5). The second electron energy is (3.5 ± 2.5) eV while the scattering angle is (a) (5 ± 2) °, (b) (9.5 ± 2.5) ° and (c) (16 ± 4) °. The lines are M3DW calculations. Shaded areas represent angular ranges without experimental acceptance. 186

Figure 7: 5DCS in the plane perpendicular to the incoming beam at a scattering angle of (16 ± 4)° and second electron energy of (3.5 ± 2.0) eV, which are the kinematics of fig. 6 (c). Molecules are aligned in the scattering plane at an angle of 0° (red), 45° (green) and 90° (blue) relative to the momentum transfer $\vec{q}$ (compare fig. 5). 188

Figure 8: Same as figure 6, but at an energy of the second electron of (16 ± 4) eV 190

Figure 9: Illustration of the molecular alignments considered in figure 10. θ = 90° for all situations depicted, i.e. the internuclear axis is always located in the plane normal to $\vec{q}$ 191

Figure 10: Coplanar 5DCS for molecules aligned perpendicular to $\vec{q}$ but with a relative angle towards the scattering plane of 0° (blue), 45° (salmon) and 90° (green) as illustrated in fig. 9. The scattering angle is fixed to (9.5 ± 2.5) ° while the plotted electron's energy is either (a) (3.5 ± 2.5) eV or (b) (16 ± 4) eV. Shaded areas represent angular ranges without experimental acceptance. 191

LIST OF TABLES

Page

Paper VIII

Table 1 : Formic acid binding energies (in eV), with the error in the Gaussian peak position quoted in brackets. 144

1. INTRODUCTION

Many of the everyday processes both natural and man-made are driven by collisions between electrons and atoms and/or molecules. An electron can undergo an elastic collision or it can excite or ionize the atom and/or molecule. The fundamental interaction (the Coulomb force) between the individual particles in the atomic systems is well known, but what is not understood is how a complex target like an atom or molecule interacts with a charged projectile.

Ionization by electron impact is one of the most important collision processes in atomic and molecular physics. It has many applications in astrophysics, lasers, florescence lights, and plasmas. As a result, it is crucial to understand the properties of all collision particles involved in the process. A complete knowledge of the ionization process happens when the energies and the momenta of all of the collision particles are determined. For electron impact ionization, which is referred to as (e, 2e), the projectile (incident electron) collides with a target (either atom or molecule) and ionizes the target. As a result, a bound electron will be ejected from the target and two outgoing electrons will be detected in the final channel. In order to gain information about the (e,2e) ionization process, one measures the fully differential cross section (FDCS) which is proportional to the probability that the two outgoing electrons will be moving in a particular directions with a particular energies after the ionization event.

Theoretical modeling of few-body dynamics such as electron impact ionization is very challenging since the few-body problem is one of the most fundamental unsolved problems in physics. The few-body problem arises from the fact that the Schrödinger equation is not analytically solvable for more than two mutually interacting particles. As a result, for three or more particles, theory must resort to significant modeling efforts using approximations, the validity of which are determined by comparison with experiment.

Electron impact ionization has received a lot of attention from experimental and theoretical work in the past three decades. Therefore, the (e, 2e) collision process has become a powerful tool to investigate the dynamics of the ionization process. Advances on the theoretical side now allow for an essentially exact numerical calculation of one of

the simplest three-body problems – namely electron-impact ionization of hydrogen [1-3]. Single ionization of helium with the ion being left in the ground state can also be treated as a 3-body problem, very good agreement between experiment and theory has been achieved for electron-impact ionization of helium as well [4-7]. However, in general, approximations have to be made. This has led to the development of a number of theoretical models that deal with different targets, impact energies, and geometries. Each model uses different approximations and as a result, the experiments play an important role in verifying the accuracy of theoretical approximations and guiding the calculations.

Electron-impact single ionization of molecules has been extensively studied for 2-3 decades using high energy incident electrons. This work has been summarized by Weigold and McCarthy [8]. It is now well known that, for high energy, the FDCS is proportional to the square of the momentum space wavefunction for the active orbital averaged over all orientations (the so-called Dyson orbital). As a result, the high energy studies, which are normally called EMS (electron momentum spectroscopy), are based on the so-called binary (e, 2e) reaction. These EMS studies have provided a wealth of information about the quality of quantum chemistry calculations of molecular wavefunctions. For high energy, the dynamics of the collision are not important (i.e. the determined Dyson orbital is independent of the incident electron energy).

Experimental measurements of electron impact ionization of molecules for low to intermediate incident electron energy are limited, although there were some experimental papers reported in the 90's. Atoms received more attention, probably due to limited theoretical support for molecular measurements. However, in the last ten years there has been an increase in interest in low energy molecular ionization [9-51]. There are some difficulties in the experimental measurements of the FDCS for molecules. This is mainly due to the difficulties in resolving the different molecular electronic states, since these states are very closely spaced in energy. Theoretical modeling is also limited in calculating the FDCS for molecules due to the complexity needed to describe the cross section. The challenge here is to develop a multi-center wavefunction since molecules have multiple scattering centers and non-spherical wavefunctions while atoms have one scattering center and spherical wavefunctions. Another challenge arises from the fact that the experiments cannot align the molecules before the collision. The traditional (e,

2e) measurements represent an average over all molecular orientations. Therefore, the theories must consider the average of all orientations of the molecules in order to compare the results with the experimental data. This turns out to be a serious problem due to the limitation of present-day computing power.

There exist several theories to calculate the FDCS for molecules. These theories are the first Born approximation (FBA), the plan-wave impulse approximation (PWIA), the distorted-wave impulse approximation (DWIA), the time dependent close coupling method (TDCC), the distorted-wave Born approximation (DWBA), and the molecular three-body distorted-wave approximation (M3DW).

The first Born approximation (FBA) is one of the simplest approximations where the ejected electron is treated as a Coulomb wave while the incident and scattered electrons are treated as plane waves. The FBA is in good agreement with (e, 2e) experiments at high incident electron energies for helium [52]. In 2001, Champion *et al.* [12] used the FBA to study electron-impact ionization of H_2O.

Weck *et al*. [11, 20] developed the first Born approximation two-center continuum (FBA-TCC) approximation with correct boundary conditions in the entrance and exit channels. In the TCC approximation for diatomic molecules, one assumes that the ejected electron is ionized from the proximity of one of the nuclei and the passive electrons completely screen the other nucleus. As a result, the ejected electron interacts with only one nucleus and the projectile electron. In this approach, the incident and scattered electron is represented as plane-waves. This method was quite successful in reproducing the high energy (~4 keV) H_2 absolute experimental data of Chérid *et al.* [53].

The plane-wave impulse approximation (PWIA) developed by McCarthy and co-workers [8, 54-56] has been very successful in the electron momentum spectroscopy (EMS) work for studying molecular structure. Robicheaux [57] introduced an analytical method to treat electron-impact ionization of H_2^+ using a prolate spherical coordinate system. This method is a useful way to assess the experimental data and other approximations for higher incident electron energies. The modified additive rule (MAR) was used for electron-impact ionization of C_2H_6 by Deutch and Becker [58]. The MAR

method obtains molecular ionization cross sections by summing the ionization cross section for each constituent atom with an appropriate atomic weighting factor.

The DWIA is similar to the PWIA except the plane waves are replaced with distorted-waves. Gao *et al.* presented a theoretical calculation using the DWIA approach for incident electron energies between 35.6 eV and 400 eV for electron ionization of N_2 [26]. This approach used a molecular wavefunction, which was averaged over all orientations. The DWIA results were compared to the Rioual *et al.* [59], and Hussey and Murray [17] experiment data. There was reasonable agreement at intermediate to high incident electron energies. However, the agreement worsened at low incident electron energies. Comparing the PWIA and the DWIA, the DWIA gave better agreement with the experimental data mostly at the intermediate energies.

One of the most successful theoretical approaches for electron-impact ionization of more complicated targets is the distorted-wave Born approximation (DWBA). The DWBA treats single ionization of a complex target as a 3-body problem with the effect of the spectator electrons being represented by a spherically symmetric potential which is used in the Schrödinger equation to calculate the continuum wavefunctions for the continuum particles. In the standard DWBA for ionization, the final-state wavefunction is represented as a product of two wavefunctions which contain no mutual electron-electron repulsion (normally called post-collision-interaction). Madison *et al.* [60] reported the very first DWBA calculation for ionization of helium in 1977. The DWBA approach was used by Monzani *et al.* [61] for H_2 where all incoming and outgoing continuum electrons are represented as distorted-waves calculated in a single-center static-exchange potential. This approximation was used to calculate the total cross section for molecules such as N_2, O_2 and CO [62]. Since the wavefunctions used in Born approximation are not exact solutions to the Schrödinger equation, they cannot fully describe all the processes and interactions that can happen during the ionization. There are several modifications which can be used to improve the theoretical FDCS, such as approximating the post collision interaction (PCI), correlation-polarization effects, and electron exchange which are known to be important.

The simplest approach of treating the PCI (the Coulomb interaction between the two electrons) is to multiply the FDCS of the DWBA by the Gamow factor and an

approximation for the ${}_1F_1$ hypergeometric function. Botero and Macek [63] [see also Whelan *et al.* [64, 65]] proposed neglecting the hypergeometric function and just using the Gamow factor. With this approximation, the electron-electron repulsion factors out of the integral and the net effect is to multiply the DWBA amplitude by the Gamow factor. Kheifets *et al*. [66, 67] recently showed that approximating the Coulomb interaction by the Gamow factor significantly improved agreement between experiment and theory for high energy ionization of inert gases particularly at larger scattering angles. Ward and Macek [68] proposed a low energy approximation keeping the hypergeometric function but evaluating it for an average separation between the electrons. We showed recently that this was a good approximation for low energy ionization of molecular hydrogen and water [69, 70].

In 1989, Brauner, Briggs and Klar [71] (to be referred to as BBK) calculated the FDCS using a plane wave for the incident electron and a product of three Coulomb functions – a Coulomb wave for the two continuum electrons in the field of a proton and the Coulomb interaction between the two electrons in the final-state wavefunction (normally called PCI). The BBK results were in better agreement with experiment for electron-impact ionization of atomic hydrogen at lower energies if the PCI was included directly in the final-state wavefunction instead of just the perturbation. Including the PCI in the final-state wavefunction is accomplished by including the Coulomb interaction between the two final-state continuum electrons in the final-state wavefunction. The big advantage of including the electron-electron interaction directly in the final-state wavefunction stems from the fact that any physics contained in the wavefunction is automatically contained to all orders of perturbation theory so the BBK treatment contains the PCI to all orders of perturbation theory.

Jones *et al.* [72] modified the BBK approach by using distorted-waves for the incident electron and the two outgoing electrons along with an electron-electron interaction. This model is called the three-body distorted-wave Born approximation (3DWBA). This approximation was good for calculating the FDCS for intermediate electron energies but failed to predict the position of the binary beak for low incident electron energies. Jones and Madison [73] modified the electron interaction by including a short-range static electron-target interaction for both the initial- and final-state

wavefunctions in order to satisfy the correct asymptotic boundary conditions to reduce the discrepancy of the FDCS at low energies. Inclusion of the final-state electron-electron interaction lead to better agreement with experiment for coplanar asymmetric collisions for small atoms.

For electron-impact ionization of heavier atoms or molecules, it is necessary to use numerical bound state wavefunctions and numerical distorted-waves for the continuum electrons. If one additionally wants to include the final-state electron-electron Coulomb interaction in the final-state, one is forced to perform a full numerical 6-dimensional integral for the T-matrix. Due to the complexity of performing such an integral [74], it was not until 2003 before the first DWBA calculation including the PCI was reported by Prideaux and Madison [75] for ionization of argon and krypton. Prideaux and Madison called the DWBA calculation including the full Coulomb PCI the 3-body distorted-wave (3DW) approximation. The difference in computer time between the DWBA and the 3DW calculations is a few minutes versus a few days on a single processor and this gave good agreement with the experiment data.

Correlation-polarization effects are important particularly for low energy electrons since the charge cloud polarization of the target can create strong static fields. The polarization potential can be added to the static potential used to calculate the incident electron distorted-wavefunction. An approximation for the correlation-polarization potential was given by Perdew and Zunger [76]. The use of the correlation-polarization potential for a small target such as *He* or H_2 yielded good agreement for the FDCS. However, the use of the correlation-polarization potential failed to give good results for the FDCS for heavier atoms and molecules.

Quantum mechanically the two outgoing electrons are indistinguishable, so there is a possibility that electron exchange will be important. This exchange is included in most theories through the exchange amplitude which treats the exchange between the projectile and the ejected electron. Another possible exchange is the exchange between the continuum electron and the passive bound electrons in the target. This can be included as an approximate exchange potential in calculating the wavefunction of the ejected electron.

Gao *et al.* generalized the 3DW approach that was developed for atoms to molecules, which has been labeled as the molecular 3-body distorted-wave approach (M3DW) [27, 28]. Gao *et al*. [28] proposed the orientation averaged molecular orbital (OAMO) approximation in which a molecular orbital is averaged over all orientations. This approximation works well for molecules where the bound valence electrons are in a nearly spherical state of the molecules. To calculate a proper average over all orientations, one should first calculate the FDCS and then average over all orientations of the molecules. This represents a significant computer challenge since a few days are required to get the results for a single orientation. While the OAMO approximation is not good for most molecular states, it has proved to be very successful for a few highly symmetric states for N_2 and H_2 in coplanar geometry, where the incident and outgoing electrons are in the same plane, and the incident energies were about 50 eV and higher [27-39].

The time dependent close coupling (TDCC) approach expands the wavefunctions in terms of partial waves and then solves the time-dependent Schrödinger equation numerically. Colgan *et al.* [47] first applied the TDCC to calculate the FDCS for ionization of atomic hydrogen. Recently, Colgan *et al.* [48, 49] generalized the TDCC method previously used for atoms to calculate the FDCS for ionization of molecular hydrogen and obtained good agreement with the experimental data. This method can be used to calculate the FDCS for aligned H_2 at low incident energies. However, due to the limitation in computing power, the TDCC is not able to calculate (e, 2e) cross sections at high impact energies because a very large number of partial waves are needed to get the solution of the time-dependent Schrödinger equation to converge.

There has been a large amount of interest in diatomic molecules inspired by the possibility of observing an interference effect due to the two molecular centers playing the role of a double slit. Stia *et al*. [19] predicted that, similar to photon scattering, the electron scattering cross section for H_2 could be expressed as the atomic cross section multiplied by an 'interference' factor and the interference factor depends on the molecular separation and the momentum transferred to the residual ion. As a result, the shape of the molecular FDCS was predicted to be different from the shape of the atomic FDCS as modified by the interference factor. Milne-Brownlie *et al*. [36] compared

atomic and molecular H_2 FDCS's and, for the cases they examined, the interference factor predicted that, relative to the binary peak, the molecular recoil peak should be smaller than the atomic recoil peak. This was verified by the experimental data. Consequently, this was interpreted as an observation of double-slit interference effects. In this dissertation, the interference effect for the diatomic molecules H_2 and N_2 will be examined using the M3DW approximation.

As mentioned before, there is presently considerable experimental effort directed towards measuring the FDCS for a specific molecular orientation. However, the experimentalists are facing difficulties in aligning the molecules prior to the collisions. The very first measurement of this type was reported by Takahashi *et al.* [79] in Japan for electron-impact ionization of H_2. However, the statistics were very bad, and only rough qualitative features could be seen from the data. Following this measurement, a measurement was made in Ullrich's group at Heidelberg, Germany for proton-impact ionization of H_2. The results were reported by Dimopoulou *et al.* [80]. Most recently, the FDCS for single ionization of aligned hydrogen molecules was studied by Senftleben *et al.* [81] in Heidelberg, Germany. These measurements were successful for the first time to observe features of the FDCS for different alignment of H_2. The kinematics of the experiment was 200 eV for the incident electron and for a range of scattering angles and scattering energies. On the theoretical side, calculating the FDCS for aligned molecules in a particular orientation is possible without doing the averaging [48]. Consequently, we modified the M3DW to be able to calculate aligned H_2. We were able to calculate wavefunctions that depended on the molecular orientation and we were able to obtain a reasonable agreement with the experimental data of Senftleben *et al.*

In this dissertation, more accurate wavefunctions for the molecular states are used than was previously used by Gao. Gao initially calculated molecular wavefunctions using the computer code GAMESS with a small basis set. However, more recently, we formed a collaboration with C.G. Ning who calculates more accurate wavefunctions using density functional theory. This collaboration allows us to do calculations beyond diatomic molecules and calculate FDCS for larger molecules and for oriented molecules. Consequently, a range of theoretical calculations of the FDCS for molecular targets will be presented. The FDCS will be shown for the simple diatomic molecule H_2 for different

geometries and impact energies. The interference effect and the role of the PCI for energies near the threshold will be also shown. Then the FDCS of the triatomic molecule H_2O will be studied in coplanar and non-coplanar geometries for low impact energies, with both equal and non-equal outgoing electron energies using the improved wavefunction. Additionally, The (e,2e) FDCS for ionization of formic acid at intermediate to high incident electron energies will also be shown and compared to experimental data. Finally, theoretical calculations for aligned H_2 will be presented. These calculations were able to obtain a reasonable agreement with the experimental data.

2. THEORY OF ELECTRON IMPACT IONIZATION

2.1. INTRODUCTION

The process of interest is a collision between the incident electron and a target. There are two types of collisions: elastic and inelastic. In elastic scattering, both particles (the target and the electron) scatter without any change in their internal structure whereas, in inelastic scattering, the target undergoes a change in its internal structure during the collision process. The events for which the target undergoes changes in its internal structure are the ionization and the excitation processes. In the ionization process, an electron is ejected from the target and this dissertation deals with the ionization process.

2.2. IONIZATION PROCESSES

The ionization process occurs when an incident electron collides with a target followed by a removal of one or more electrons from the target. There are many types of ionization processes. The first type is single ionization where the incident electron releases one electron from the target. The second type is multiple ionization where the incident electron removes more than one electron form the target. And finally, there is autoionization in which the incident electron excites two of the outer shell electrons and then the target decays to a lower energy state by emission of one electron so the target will be ionized. However, this work is concerned with single ionization which is normally called an (e, 2e) process in which the kinematics of the incident and two outgoing electrons are known.

2.2.1. Electron Impact Ionization. If X is the target and assumed to be in the ground state, then the direct single electron impact ionization can be expressed as:

$$e_{in}^{-}(E_{in},\vec{k}_{in}) + X \rightarrow X^{+} + e_{a}^{-}(E_{a},\vec{k}_{a}) + e_{b}^{-}(E_{b},\vec{k}_{b}) \qquad (1)$$

where $e_{a(b)}^{-}$ is the scattered (ejected) electron and X^{+} is the ion generated by the collision. The ion motion can be neglected since the ion mass is very large compared to the mass of the electron. The energies E_{in}, E_a, E_b and momenta $\vec{k}_{in}, \vec{k}_a, \vec{k}_b$ are the kinetic energies and the momenta of the incident, scattered, and ejected electrons respectively.

The total energy of the collision must be conserved and therefore the incident energy is equal to:

$$E_{in} = \varepsilon_i + E_a + E_b \tag{2}$$

where ε_i is the ionization potential. The total momentum of the collision is also conserved. Thus

$$\vec{k}_{in} = \vec{k}_a + \vec{k}_b + \vec{P} \tag{3}$$

where $\vec{P}$ is the momentum of the residual ion. This gives the momentum of the residual ion as

$$\vec{P} = \vec{k}_{in} - \vec{k}_a - \vec{k}_b \tag{4}$$

The momentum transferred by the scattered electron is

$$\vec{q} = \vec{k}_{in} - \vec{k}_a \tag{5}$$

The results of these kinds of collisions are typically presented as a cross section.

2.3. DIFFERENTIAL CROSS SECTIONS

In electron impact ionization, the probability for the (e, 2e) process is expressed in terms of a differential cross section. The cross section in general can be defined as the ratio of the number of scattered particles in a given quantum state per unit time and per scatterer to the relative flux of the incident particles with respect to the target [78]. There are different types of cross sections: normally, the total cross section, the singly, doubly, and triply (or fully) differential cross sections. This work will focus on the triply differential cross section.

The singly differential cross section ($d\sigma/dE_a$) describes the energy distribution of the scattered electron. The double differential cross section ($d^2\sigma/d\Omega_a dE_a$) describes the energy and the angular distribution of the scattered electron after the ionization. The fully differential cross section (FDCS) is given by:

$$\frac{d^5\sigma}{d\Omega_a d\Omega_b dE_a} \tag{6}$$

It describes the probability that the two outgoing electrons with energies of E_a and E_b will be found in solid angles $d\Omega_a$ and $d\Omega_b$ after the ionization. This type of cross section

determines all the kinematics of the electrons involved in the ionization processes. The differential cross section is obtained from the square of the transition matrix (T- matrix), multiplied by a factor which includes the momenta of the electrons. The T-matrix will be described elsewhere in this dissertation.

2.4. GENERAL SCATTERING THEORY

Electron collisions in general should be treated using quantum mechanics instead of classical mechanics. For potential scattering the Hamiltonian for the projectile motion (H which is an observable of the system) splits into two parts:

$$H = K + V \tag{7}$$

where K is the kinetic energy operator ($K = \frac{-1}{2}\nabla^2$) and V is the potential energy which represents the interaction between the electron and the target. For every free moving particle, the associated wavefunction is $\psi(\vec{r})$ and its eigenstate is $|\Psi\rangle$. The eigenstates are solutions of the Schrodinger equation

$$(E - H)|\Psi\rangle = 0 \tag{8}$$

Likewise, the wavefunction Φ, which is an eigenstate of K, can be obtained from

$$(E - K)|\Phi\rangle = 0 \tag{9}$$

Consequently, we need to solve the Schrödinger equation:

$$[\frac{-1}{2}\nabla^2 + V(\boldsymbol{r})]\,\psi(\boldsymbol{r}) = E\,\psi(\boldsymbol{r}) \tag{10}$$

where V(r) is the scattering potential and E is the energy of the electron which is given in atomic units by:

$$E = \frac{k^2}{2} \tag{11}$$

By multiplying eqn. (10) by -2 and defining $U(\vec{r}) = 2V(\vec{r})$, we get:

$$[\nabla^2 + k^2 - U(\boldsymbol{r})]\,\psi(\boldsymbol{r}) = 0 \tag{12}$$

If we assume that $V(\vec{r})$ goes to zero faster than $\frac{1}{r}$ as $r \to \infty$, the equation 12 can then be solved numerically. From scattering theory, it can be shown that the desired solution for eqn. (12) should have an asymptotic form [78] given by:

$$\psi(\boldsymbol{r})_{r\to\infty} \to C(e^{i\vec{k}\cdot\vec{r}} + f(k,\theta,\phi)\frac{e^{+ikr}}{r}) \tag{13}$$

where C is a normalization constant which is independent of r, θ and ϕ. The wavefunction for the steady state contains a plane-wave for the incident electron and an outgoing spherical wave for the scattered electron. The function *f* is called the scattering amplitude. The differential cross section is related to the scattering amplitude f by

$$\frac{d\sigma}{d\Omega} = \left|f(k,\Omega)\right|^2 \tag{14}$$

The scattering amplitude depends on the scattering angle and energy of the projectile. If two outgoing electrons are detected, the cross section for (e, 2e) (often-called fully differential cross section) is:

$$\frac{d^5\sigma}{d\Omega_a d\Omega_b dE_a} = \frac{k_a k_b}{k_{in}}\left|f\right|^2 \tag{15}$$

Since the Schrödinger equation more difficult to solve for the three-particle problem, approximations are needed to evaluate the scattering amplitude *f*. To understand these approximations, we will first discuss the Lippmann-Schwinger equation.

2.4.1. The Lippmann-Schwinger Equation. The solution of the wavefunction ψ in eqn. (12) can be obtained using the Lippmann-Schwinger equation, which takes into account the boundary conditions. Eqn. 12 can be rewritten as:

$$[\nabla^2 + k^2]\psi_k(\boldsymbol{r}) = U(\boldsymbol{r})\psi_k(\boldsymbol{r}) \tag{16}$$

The general solution of eqn. (16) is:

$$\Psi_k^{\pm}(\boldsymbol{r}) = \Phi_k(\boldsymbol{r}) + \int G_0^{\pm}(\boldsymbol{r},\boldsymbol{r}')\,U(\boldsymbol{r}')\Psi_k^{\pm}(\boldsymbol{r}')d\boldsymbol{r}' \tag{17}$$

The term $\Phi_k(\mathbf{r})$ is a solution to the homogeneous equation

$$[\nabla^2 + k^2]\Phi_k(\boldsymbol{r}) = 0 \tag{18}$$

This wavefunction is a plane-wave, which is given by:

$$\Phi_k(\boldsymbol{r}) = (2\pi)^{-3/2} \exp(i\boldsymbol{k}\bullet\boldsymbol{r}) \tag{19}$$

The function $G_0^{\pm}(\boldsymbol{r},\boldsymbol{r}')$ in eqn. (17) is the Green's function for an incoming (-) or outgoing (+) wave. Equation (17) for outgoing wave can be written in the symbolic form as:

$$\Psi_k^+ = \Phi_k + G_0^+ U \Psi_k^+ \tag{20}$$

The free particle Green's function G_0^+ satisfies the following equation:

$$[\nabla^2 + k^2] G_0^+(\boldsymbol{r},\boldsymbol{r}') = \delta(\boldsymbol{r}-\boldsymbol{r}') \tag{21}$$

and its solution is :

$$G_0^+(\boldsymbol{r},\boldsymbol{r}') = -\frac{1}{4\pi}\frac{e^{ik|\boldsymbol{r}-\boldsymbol{r}'|}}{|\boldsymbol{r}-\boldsymbol{r}'|} \tag{22}$$

In an integral form we can write

$$G_0^+(\boldsymbol{r},\boldsymbol{r}') = -\frac{1}{(2\pi)^3}\lim_{\varepsilon\to 0^+}\int \frac{e^{i\boldsymbol{k}'\bullet(\boldsymbol{r}-\boldsymbol{r}')}}{k'^2 - k^2 - i\varepsilon} d\boldsymbol{k}' \tag{23}$$

For large r, G_0^+ can be evaluated as:

$$G_0^+(\boldsymbol{r},\boldsymbol{r}') \underset{r\to\infty}{\sim} -\frac{1}{4\pi}\frac{e^{ik\hat{r}\cdot\boldsymbol{r}'}}{r} e^{ikr} \tag{24}$$

where $\hat{\boldsymbol{r}}$ is a unit vector in the direction of the scattered particle and $|\boldsymbol{r}-\boldsymbol{r}'|$ is taken as r. The final momentum vector $\boldsymbol{k}_f$ is equal to $k\hat{\boldsymbol{r}}$ and the initial momentum vector is $\boldsymbol{k}_i$. Substituting eqn. (24) into eqn. (17) we get:

$$\Psi_{ki}^+(\boldsymbol{r}) \underset{r\to\infty}{\sim} \Phi_{ki}(\boldsymbol{r}) - \frac{e^{ikr}}{4\pi r}\int e^{-i\boldsymbol{k}_f\cdot\boldsymbol{r}'} U(\boldsymbol{r}')\Psi_{ki}^+(\boldsymbol{r}')d\boldsymbol{r}' \tag{25}$$

Comparing eqn. (25) with eqn. (13), we find:

$$f(\theta,\phi) = -2\pi^2 \left\langle \Phi_{k_f} \middle| U \middle| \Psi_{k_i}^+ \right\rangle \tag{26}$$

The transition matrix is related to the scattering amplitude where

$$T_{fi} = \left\langle \Phi_{k_f} \middle| U \middle| \Psi_{k_i}^+ \right\rangle \tag{27}$$

2.4.2. Born Approximations. Equation (20) can be solved by iteration. The distorted part of the wavefunction is:

$$\Psi_d(\boldsymbol{r}) = G_0^+ U \Psi_k^+ \tag{28}$$

$$\Psi_d(\boldsymbol{r}) = \int G^+{}_0(\boldsymbol{r},\boldsymbol{r}')\, U(\boldsymbol{r}')\Psi_k^+(\boldsymbol{r}')d\boldsymbol{r}' \tag{29}$$

We can solve eqn. (28) by iteration; we start with the $\Phi_k(\mathbf{r})$ as the zero-order approximation and increase the number of order to produce a sequence of functions. We replace Ψ_k^+ in eqn. (28 or 29) by the initial wavefunction $\Phi_k(\boldsymbol{r})$ which gives the first order correction.

$$\Psi_k^{(1)}(\boldsymbol{r}) = \int G_0^+(\boldsymbol{r},\boldsymbol{r}')\, U(\boldsymbol{r}')\Phi_k(\boldsymbol{r}')d\boldsymbol{r}' \tag{30}$$

Also, replacing Ψ_k^+ by Ψ_1 in (29) to get the second-order correction.

$$\Psi_k^{(2)}(\boldsymbol{r}) = \int G_0^+(\boldsymbol{r},\boldsymbol{r}')\, U(\boldsymbol{r}')\Psi_k^{(1)}(\boldsymbol{r}')d\boldsymbol{r}' \tag{31}$$

Using (30) in (31) gives

$$\Psi_k^{(2)}(\boldsymbol{r}) = \int \int G_0^+(\boldsymbol{r},\boldsymbol{r}')\, U(\boldsymbol{r}')G_0^+(\boldsymbol{r}',\boldsymbol{r}'')\, U(\boldsymbol{r}'')\Phi_k(\boldsymbol{r}'')d\boldsymbol{r}'d\boldsymbol{r}'' \tag{32}$$

We can write eqn. (32) in a simpler form as:

$$\Psi_k^{(2)}(\boldsymbol{r}) = G_0^+ U G_0^+ U \Psi_0 = (G_0^+ U)^2 \Phi_k \tag{33}$$

The general form is given by:

$$\Psi_k^{(n)} = (G_0^+ U)^n \Psi_0 = G_0^+ U \Psi_k^{(n-1)} \tag{34}$$

where Φ_k is the initial wavefunction and n is an integer. We can also write

$$\Psi_k{}^+ = \sum_{n=1}^{\infty} (G_0^+ U)^{n-1} \Phi_k \tag{35 a}$$

This can be also written as:

$$\Psi_k^+ = \Phi_k + G^+ U \Phi_k \tag{35 b}$$

where G^+ is the full Green's function which is given by

$$G^+ = G_0^+ + G_0^+ U G_0^+ + G_0^+ U G_0^+ U G_0^+ + \ldots\ldots \tag{36}$$

eqn. (35 a) is known as the Born series [87]. By substituting the Born series (35 a) into the scattering amplitude (26), we get:

$$f(\theta,\phi) = -2\pi^2 \left\langle \Phi_{k_f} \left| U \right| \sum_{n=1}^{\infty} (G_0^+ U)^{n-1} \Phi_{k_i} \right\rangle = f_{B1} + f_{B2} + f_{B3} + \cdots + f_{Bn} + \cdots \quad (37)$$

and

$$\overline{f}_{Bn} = -2\pi^2 \left\langle \Phi_{kf} \left| U \right| G_0^+ U)^{n-1} \Phi_{k_i} \right\rangle \quad (38)$$

where $\overline{f}_{Bn}$ is the nth Born term and f_{Bn} is the sum of the first n-terms for the Born scattering amplitude which is equal to:

$$f_{Bn} = \sum_{p=1}^{n} \overline{f_{Bp}} \quad (39)$$

2.4.3. First Born Approximation. The first Born approximation (FBA) is often used in collision theory and it is the simplest approach. Using eqn. (37), we obtain the first born term (n=1) in the Born series:

$$f_{B1} = -2\pi^2 \left\langle \Phi_{k_f} \left| U \right| \Phi_{k_i} \right\rangle \quad (40)$$

where the U is the potential and both the incident and final wavefunctions are plane-waves so f_{B1} can be written as:

$$f_{B1} = A\int e^{i\mathbf{k}_i \cdot \mathbf{r}} U(\mathbf{r}) e^{-i\mathbf{k}_f \cdot \mathbf{r}} d\mathbf{r} = A\int e^{i(\mathbf{k}_i - \mathbf{k}_f)\cdot \mathbf{r}} U(\mathbf{r}) d\mathbf{r} = A\int e^{i\mathbf{K}\cdot \mathbf{r}} U(\mathbf{r}) d\mathbf{r} \quad (41)$$

where ***K*** is the momentum of transferred between the incoming and outgoing particle and *A* is a constant coming from all of the normalization constants. Equation (41) shows that the first Born scattering amplitude is the Fourier transform of the potential for elastic scattering. As we saw in eqn. (15), $|f_{B1}|^2$ is proportional to the differential cross section. Note, the interaction potential *U(**r**)* does not include all of the interactions in the collision. However, the FBA is able to obtain good agreement with experimental data for high energies as mentioned in the introduction.

The inclusion of higher order terms in the Born approximation amplitude might improve the agreement with the experiment for intermediate and low energies since the incident electron will interact multiple times with the target. However, including higher terms increases the time and the usage of computing resources. Another disadvantage of this approximation is that the Born series will converge only if the potential does not

support any bound state which is not the case for low energies so this series will diverge for low energies [78].

2.5. DISTORTED WAVE BORN APPROXIMATION

Since the inclusion of higher order terms in the interaction potential gives a diverging series for low and intermediate energies, as an alternative, one can describe the initial and final wavefunction using distorted-waves. The basic idea of the distorted-wave treatment is to break the interaction into two parts. The first part is treated exactly and the second part is handled by perturbation theory. The scattering amplitude in eqn. (26) and the T-matrix in (27) are reformulated in terms of the distorted-wave eigenstates of U rather than plane-waves. We start with the exact T-Matrix for the ionization process which can be written as [78]:

$$T = \left\langle \Psi_f \left| H - H_0 \right| \Phi_i \right\rangle \tag{42}$$

where H is the full Hamiltonian for the system, H_0 is an approximate initial-state Hamiltonian and the wave functions Ψ_f and Φ_i in the T-matrix are eigenfunctions of the two Hamiltonians

$$H \left| \Psi_f \right\rangle = E \left| \Psi_f \right\rangle \tag{43}$$

$$H_0 \left| \Phi_i \right\rangle = E \left| \Phi_i \right\rangle \tag{44}$$

In terms of the physics contained in the T-matrix, any interaction which is included in the calculation of the initial- and final-state wave functions is contained to all orders of perturbation theory for that channel while any interactions contained in the operator $(H - H_0)$ (normally called the perturbation) are contained to first order in perturbation theory. To evaluate the T-matrix, one must choose H_0 and approximate Ψ_f.

One of the most successful approximations for calculating atomic ionization by electron impact has been the first-order distorted-wave Born approximation (DWBA). In the standard DWBA, the initial-state Hamiltonian is chosen to be

$$H_0 = H_{\text{target}} + T_p + U_i \tag{45}$$

where H_{target} is the Hamiltonian for the neutral target with eigenfunctions ψ_{target},

$$H_{target} = -\frac{1}{2}\sum_{i=1}^{n}\nabla_i^2 - \sum_{i=1}^{n}\frac{Z}{r_i} + \sum_{i=1}^{n-1}\sum_{j=i+1}^{n}\frac{1}{|\boldsymbol{r}_i - \boldsymbol{r}_j|} \tag{46}$$

The first term in eqn. (46) is the kinetic energy operator for the target, the second term is the sum of the potential energy of the interaction between the nucleus and the electrons, and the last term is of the sum of the potential energy of the inter-electronic repulsion.

In eqn. (45), T_{p} in is the kinetic energy operator for the projectile and U_i is an initial-state spherically symmetric potential for the projectile-target interaction (normally called the initial-state distorting potential). The initial-state distorting potential consists of the nuclear term plus a spherically symmetric approximation for the interaction between the projectile electron and the target electrons obtained from the quantum mechanical charge density of the target.

$$U_i(r) = U_{ele}(r) + U_{nuc}(r) \tag{47}$$

The initial-state wave function Φ_i can be expressed as a product of the target wave function (molecule in our case) Φ_i and the projectile wave function:

$$\Phi_i = \phi_i \chi_i \tag{48}$$

The initial-state distorted wave χ_i is an eigenfunction obtained from the initial-state distorting potential

$$(T_p + U_i)\,\chi_i = \varepsilon_i\,\chi_i \tag{49}$$

where ε_i is the energy of the incoming projectile. The physics contained in the initial state distorted wave is elastic scattering of the projectile from the neutral target represented by the effective potential U_i. In the normal DWBA, the exact final-state wave function is approximated as a product of wave functions for each of the final three particles

$$\Psi_f \approx \chi_{proj}\,\chi_{eject}\,\psi_{ion} \tag{50}$$

Here ψ_{ion} is the final-state wave function for the ion and the final-state distorted waves χ_{proj} (χ_{eject}) are obtained from the final-state distorting potential U_{ion}

$$(T_p + U_{ion})\,\chi_{proj(eject)} = \varepsilon_{a(b)}\,\chi_{proj(eject)} \tag{51}$$

where $\varepsilon_{a(b)}$ is the energy of the scattered (ejected) electron. The final-state distorting potential U_{ion} consists of the nuclear contribution plus a spherically symmetric approximation for the interaction between the continuum electron and the bound electrons in the ion. The physics contained in the final state distorted wave is elastic scattering of the continuum electron from the final state ion represented by the effective potential U_{ion}. The full Hamiltonian is given

$$H = H_{\text{target}} + T_p + V_i \tag{52}$$

where V_i is the initial state interaction between the projectile and target. Subtracting eqn. (45) from eqn. (52) we obtain:

$$H - H_0 = V_i - U_i \tag{53}$$

and by substituting eqn. (53) and (50) in eqn. (42), the direct-scattering molecular distorted wave Born Approximation (MDW) T-matrix is given by

$$T_{dir}^{MDW} = \left\langle \chi_{proj}\ \chi_{eject}\ \psi_{ion} \left| V_i - U_i \right| \psi_{\text{target}}\ \chi_i \right\rangle \tag{54}$$

As mentioned above, any physics contained in the wavefunctions of the T-matrix is contained to all orders of perturbation theory. For the initial state, the distorted wave χ_i is an eigenfunction of U_i which means that elastic scattering from the nuclei plus elastic scattering from the spherically symmetric effective potential for all the bound electrons is contained to all orders of perturbation theory. Likewise, for the final state, the distorted waves χ_{proj} (χ_{eject}) are eigenfunctions of U_{ion} which means that elastic scattering from the nuclei plus elastic scattering from the spherically symmetric effective potential for the bound electrons in the ion is contained to all orders of perturbation theory. As will be discussed below, in the 3-body approximation, the physics contained in $(V_i - U_i)$ is the non-spherical part of the projectile-active-electron interaction so this is the only physics contained to first order.

The distorted wave Born Approximation (DWBA) has been highly successful in calculating the FDCS for ionization by high-energy electrons. However, as the energy of the electron decreases, the DWBA starts to fail. One source of this failure is an

inadequate treatment of the final-state interaction between the projectile-electron and ejected-electron.

2.6. THREE-BODY DISTORTED WAVE APPROXIMATION

The failure of the DWBA in producing good results for low to intermediate energy electrons encourages theorists to include the interaction between the projectile-electron and ejected-electron in the final state.

As mentioned in the introduction, BBK demonstrated that better agreement with experiment for electron-hydrogen scattering could be achieved for lower incident electron energies by including the final-state projectile-electron interaction in the approximation for the final-state wave function. In the BBK approach, the exact final state for electron-hydrogen scattering is approximated as

$$\Psi_f \approx CW_{proj}\, CW_{eject}\, C_{proj-eject} \tag{55}$$

where CW is a Coulomb wave for an electron in the field of a proton and C is the Coulomb distortion factor which contains the effects of the final-state Coulomb interaction between the projectile and the ejected electron (PCI). The wave function (55) is called the 3C wave function. For heavier atoms or molecules, a generalization of the 3C to the distorted-wave approach is required. The DWBA equivalent of the 3C wave function for the final-state wave function would be

$$\Psi_f \approx \chi_{proj}\, \chi_{eject}\, C_{scat-eject}\, \psi_{ion} \tag{56}$$

Asymptotically this wave function would be a phase-shifted 3C wave function. The wavefunction (56) is called a 3-body distorted wave (3DW) function and this lead to the development of the three body distorted wave approximation. Prideaux and Madison [75] described the theoretical basis for the 3-body distorted wave approximation for ionization of atoms. Then, Gao *et al.* generalized the approach to molecules [27, 29].

One of the attractive features of this wavefunction (56) is that it is an exact asymptotic solution of the three body problem. The direct-scattering 3-body distorted-wave T-matrix with the final-state wave function (56) is given by

$$T_{dir}^{3DW} = \left\langle \chi_{proj}\, \chi_{eject}\, C_{scat-eject}\, \psi_{ion} \left| V_i - U_i \right| \psi_{\text{target}}\, \chi_i \right\rangle \tag{57}$$

The physics contained in 3DW Approximation is the following. The final-state Coulomb interaction between the projectile and a screened nuclear charge, the Coulomb interaction between the ejected-electron and a screened nuclear charge, and the Coulomb interaction between the projectile and ejected-electron are contained to all orders of perturbation theory. For the initial state, the Coulomb interaction between the projectile and a screened nuclear charge for a neutral atom is contained to all orders of perturbation theory. Similar to the DW, the only interaction contained to first order in the 3DW is the initial-state non-spherical projectile-active-electron interaction as will be demonstrated below.

In the DW approach, ionization of more complex targets is treated as a three body problem. In the 3-body approach, the initial-state interaction is approximated as

$$V_i = \frac{1}{r_{ab}} + U_{ion} \tag{58}$$

Here $(\frac{1}{r_{ab}})$ represents the interaction between the projectile electron and the active target electron and U_{ion} is the interaction between the projectile electron and the rest of the target including the nuclei. The initial-state distorting potential is given by

$$U_i = U_a + U_{ion} \tag{59}$$

where U_a is the spherically symmetric interaction potential between the projectile and the active electron. As a result the perturbation is given by

$$V_i - U_i = \frac{1}{r_{ab}} - U_a \tag{60}$$

From eqn. (60), it is seen that the perturbation is the difference between the full interaction between the projectile-active electron and the spherically symmetric approximation for this interaction. Hence the perturbation is the non-spherical part of the projectile-active electron interaction as mentioned above. Since U_a depends only on the radial distance of the projectile $U_a(r_a)$, the perturbation depends only on the coordinates of the projectile and active electron. If we let ξ represent the coordinates of all the passive electrons, the final state ion wave function for the molecule $\psi_{ion}(\xi, \mathbf{R})$ will

depend on ξ and the orientation of the molecule $(\mathbf{R})$, while the initial target wave function $\psi_{\text{target}}(\xi, \mathbf{r}_a, \mathbf{R})$ will depend on both ξ *and* $\mathbf{R}$ and the active electron $\boldsymbol{r_a}$ (we assume that the collision time is sufficiently short on that the final-state orientation is the same as the initial-state orientation). Consequently the integral

$$\left\langle \psi_{ion}(\xi) \middle| \psi_{\text{target}}(\xi, \mathbf{r}_a) \right\rangle = \phi_{Dyson}(\mathbf{r}_a, \mathbf{R}) \tag{61}$$

where $\phi_{Dyson}(\mathbf{r}_a, \mathbf{R})$ is the so-called Dyson orbital which depends on the orientation of the molecule $\mathbf{R}$. Consequently, the direct-scattering molecular 3-body distorted wave (M3DW) T-matrix of eqn. (57) depends on the orientation of the molecule

$$T_{dir}^{M3DW}(\mathbf{R}) = \left\langle \chi_{proj}(\mathbf{r}_a)\, \chi_{eject}(\mathbf{r}_b)\; C_{scat-eject}\,(\mathbf{r}_{ab})\; \left| \frac{1}{r_{ab}} - U_a(r_a) \right| \phi_{Dyson}(\mathbf{r}_a, \mathbf{R})\, \chi_i(\mathbf{r}_b) \right\rangle \tag{62}$$

As mentioned in the introduction, evaluating the DW T-matrix of eqn. (54) takes a few minutes on a single processor while evaluating eqn. (62) can take a few days. Almost all of the experimental data reported so far represents an average over all molecular orientations and the proper way to calculate an average over orientations would be to evaluate eqn. (62) at a sufficiently large number of orientations that a numerically accurate average could be calculated. Due to the excessive computer time required for this process, Gao *et al*. [27] proposed the OAMO (orientation averaged molecular orbital) approximation. The essence of the OAMO approximation is to average the molecular orbitals instead of averaging the cross sections. In this approximation, the calculation of molecular (e, 2e) cross sections reduces to the same level of difficulty as calculating atomic cross sections

$$T_{dir}^{M3DW} = \left\langle \chi_{proj}(\mathbf{r}_a)\, \chi_{eject}(\mathbf{r}_b)\; C_{scat-eject}\,(\mathbf{r}_{ab})\; \left| \frac{1}{r_{ab}} - U_a(r_a) \right| \phi_{Dyson}^{OAMO}(r_a)\, \chi_i(\mathbf{r}_b) \right\rangle \tag{63}$$

where $\phi_{Dyson}^{OAMO}(r_a)$ is the Dyson orbital averaged over all orientations. While the OAMO approximation is not valid for most molecular orbitals, Gao *et al*. [27] showed that it is valid for highly symmetric orbitals as long as the momentum transferred to the ion is less than unity (i.e. near the binary peak).

The spherically symmetric distorting potentials for molecules are calculated similar to the atomic case. The starting point is the molecular charge density for the neutral molecule which is obtained from the Dyson orbitals

$$\rho(\mathbf{r},\mathbf{R}) = \sum_{k=1}^{m} n_k \left| \phi_{Dyson}^{k}(\mathbf{r},\mathbf{R}) \right|^2 \tag{64}$$

where m is the number of orbitals in the molecule, n_k is the occupation number of the orbital, and the density depends on the orientation of the molecule. We initially calculated the Dyson orbitals using the computer code GAMESS with a small basis set. GAMESS is software program that stands for General Atomic and Molecular Electronic Structure System. It can perform a number of general computational chemistry calculations, including Hartree-Fock and density functional theory (DFT). More recently we formed a collaboration with C.G. Ning who calculates more accurate wavefunctions using density functional theory along with the standard hybrid B3LYP [82] functional by means of the ADF 2007 (Amsterdam Density Functional) program [83] with the TZ2P (triple-zeta with two polarization functions) Slater type basis sets. To obtain the spherically symmetric distorting potential, we average eqn. (64) over all orientations to form the average radial charge density.

$$\rho^{ave}(r) = \left\langle \rho(\mathbf{r},\mathbf{R}) \right\rangle \tag{65}$$

where the brackets denote taking an average over all orientations. Similar to atoms, the key ingredient for the M3DW is the electronic charge distribution of the target and the orbital for the active electron. However, very different from atoms, the charge distributions and orbitals cannot be expressed in terms of radial functions and spherical harmonics but rather in terms of a numerical 3-dimensional grid. The spherically symmetric static distorting potential representing the interaction between the projectile-electron and the target molecular electrons is then found in the standard way using the average radial density

$$U_{ele}(r_a) = \left\langle \int \frac{\rho^{ave}(r) d\mathbf{r}}{|\mathbf{r}_a - \mathbf{r}|} \right\rangle \tag{66}$$

where now the brackets denote taking an average over all angular locations for $\mathbf{r}_a$. The initial state static distorting potential is the sum of the electronic contribution plus the nuclear contribution

$$U_{static} = U_{ele} + U_{nuc} \tag{67}$$

Here U_{nuc} is the contribution from the molecular nuclei. Just as we need to average over all orientations to obtain the potential for the molecular electrons, we also need to average over all orientations for the nuclei. Averaging a nucleus over all orientations is equivalent to placing the nuclear charge on a spherical shell which has a radius equal to the distance from the nucleus to the center-of-mass. Consequently, U_{nuc} is a sum of potentials for concentric spheres for each nucleus centered at the center-of-mass.

In addition to the static distorting potential, it is standard practice to add additional terms designed to approximate known important physical effects. Two such effects are exchange distortion (U_E) (effect of continuum electron exchanging with passive electrons), and the correlation-polarization potential U_{CP}.

$$U_i = U_{static} + U_E + U_{CP} \tag{68}$$

For U_E, we use the exchange-distortion potential of Furness and McCarthy [84] (corrected for errors – see Riley and Truhlar [85]). In this approximation, the exchange potential U_E depends on the average molecular charge density

$$U_E(r_a) = 0.5\left[\varepsilon_i - U_{static}(r_a) - \sqrt{\left(\varepsilon_i - U_{static}(r_a)\right)^2 + 8\pi\rho^{ave}(r_a)}\right] \tag{69}$$

One needs to be careful when looking at papers which use the Furness-McCarthy approximation since different definitions of the radial density are often used. For eqn. (69), the integral of the radial density over all space yields the number of electrons in the molecule. Frequently, a radial density is used for which the integral over radius only yields the number of electrons in the target (we used this definition in the past for atoms where the angular dependence is simply a spherical harmonic). The difference is replacing $8\pi\rho^{ave}$ with $2\rho^{ave}$ (see also for example Martinez *et al.* [86]).

For the correlation-polarization potential U_{CP}, we use the approximation of Perdew and Zunger [76] (see also Padial and Norcross [77]).

$$U_{CP}(r) = \begin{cases} v_{co}(r), & r \le r_0 \\ -\dfrac{\alpha_0}{2r^4}, & r > r_0 \end{cases} \tag{70}$$

where v_{co} is the short range correlation potential, α_0 is the dipole polarizability, and r_0 is the intersection between the long range polarization and short range correlation. The correlation potential v_{co} can be expressed as follows:

$$v_{co}(r) \begin{cases} 0.0311 \ln r_s - 0.0584 + 0.00133 r_s \ln r_s - 0.0084 r_s, & r_s < 1 \\ \dfrac{\gamma(1 + \frac{7}{6}\beta_1 r_s^{1/2} + \frac{4}{3}\beta_2 r_s)}{(1 + \beta_1 r_s^{1/2} + \beta_2 r_s)^2}, & r_s \ge 1 \end{cases} \tag{71}$$

where γ, β_1, and β_2 are constants and r_s is the density parameter given by:

$$r_s = \left[3 \Big/ 4\pi \rho^{ave}(r) \right]^{\frac{1}{3}} \tag{72}$$

The final state distorting potential U_{ion} is calculated in the same way as U_i except that the active electron is removed in the calculation of the charge density.

As mentioned in the introduction, including the full final state Coulomb interaction $C_{proj-eject}$ in the wavefunction requires the evaluation of a numerical 6D integral. This factor is given by

$$C_{proj-eject} = e^{\frac{-\pi\gamma}{2}} \Gamma(1 - i\gamma)\ {}_1F_1(i\gamma, 1, -ik_{ab} r_{ab} - i\mathbf{k}_{ab} \bullet \mathbf{r}_{ab}) \tag{73}$$

Here ${}_1F_1$ is a confluent hypergeometric function, $\Gamma(1 - i\gamma)$ is the gamma function, $\mathbf{k}_{ab}$ is the relative momentum between the two outgoing electrons, and γ is the Sommerfeld parameter $\gamma = \dfrac{1}{2k_{ab}}$ which is a measure of the strength of the coulomb interaction between the two electrons.

For lower energies, it has become clear that using the full Coulomb interaction of eqn. (73) tends to overestimate the effect of the PCI. We have found that the low energy

approximation of Ward and Macek [68] often yields very good agreement with experimental data. Ward and Macek introduced the M_{ee} factor which is given by:

$$M_{ee} = N_{ee} \left| {}_1F_1(-iv_{ab}, 1, -2ik_{ab} r_{ab}^{ave}) \right|^2 \tag{74}$$

where N_{ee} ,which called the Gamow factor, is defined as:

$$N_{ee} = \left| e^{\frac{-\pi\gamma}{2}} \Gamma(1 - i\gamma) \right|^2 = \frac{\pi e^{\frac{-\pi}{k_{ab}}}}{k_{ab}(1 - e^{\frac{-\pi}{k_{ab}}})} \tag{75}$$

With

$$v_{ab} = \frac{-1}{|\boldsymbol{k}_a - \boldsymbol{k}_b|} \quad \text{and} \qquad k_{ab} = |\boldsymbol{k}_a - \boldsymbol{k}_b| \tag{76}$$

In the Ward-Macek approximation, one replaces the actual final state electron-electron separation $\mathbf{r}_{ab}$ by an average separation which is given by

$$r_{ab}^{ave} = \frac{\pi^2}{16\,\varepsilon_t} \left(1 + \frac{0.627}{\pi} \sqrt{\varepsilon_t} \ln \varepsilon_t \right)^2 \tag{77}$$

where ε_t is the total energy of the scattered and ejected electrons. Botero and Macek [63] [see also Whelan *et al*. [64]] proposed neglecting the hypergeometric function in eqn. (74) and just using the Gamow factor to approximate $C_{proj-eject}$. Both of these approximations allow one to factor the electron-electron repulsion outside the integral which means that the computational difficulty is reduced to that of a DWBA calculation. The net effect is to multiply the DWBA amplitude by the M_{ee} factor.

$$\frac{d^5\sigma}{d\Omega_a d\Omega_b dE_b} = M_{ee} \frac{d^5\sigma^{MDW}}{d\Omega_a d\Omega_b dE_b} \tag{78}$$

Finally, eqn. (63) is for the direct scattering amplitude. Since one cannot distinguish the projectile electron from the ejected electron, we have to evaluate the exchange amplitude as well

$$T_{exc}^{M3DW} = \left\langle \chi_{proj}(\mathbf{r}_b)\, \chi_{eject}(\mathbf{r}_a)\; C_{scat-eject}(\mathbf{r}_{ab}) \left| \frac{1}{r_{ab}} - U_a(r_a) \right| \phi_{Dyson}^{OAMO}(r_a)\, \chi_i(\mathbf{r}_b) \right\rangle \tag{79}$$

The FDCS for orientated molecules can also be calculated using eqn. (79) if we replace $\phi_{Dyson}(r_a)$ with $\phi_{Dyson}(\mathbf{r}_a, \mathbf{R})$ which depends on molecular orientation. With these

amplitudes, the fully differential molecular 3-body distorted-wave cross section can be obtained from:

$$\frac{d^5\sigma}{d\Omega_a d\Omega_b dE_b} = \frac{1}{(2\pi)^5}\frac{k_a k_b}{k_i}\left(\left|T_{dir}\right|^2 + \left|T_{exc}\right|^2 + \left|T_{dir} - T_{exc}\right|^2\right) \tag{80}$$

I. Atomic and Molecular Signatures for Charged Particle Ionization

Ola Al-Hagan[1], Christian Kaiser[2], Don Madison[1] and Andrew James Murray[2]

[1] *Physics Department, Missouri University of Science and Technology, Rolla, Missouri 65409, USA*

[2]*School of Physics and Astronomy, University of Manchester, Manchester M13 9PL, UK*

Abstract

The way in which atoms and molecules are ionized by the impact of charged particles has important consequences for the behavior of many physical systems, from gas lasers to astrophysical plasmas. Much of our understanding of this process has come from ionization measurements of the energy and angular distribution of electrons ejected in the same plane as the trajectory of the incident ionizing beam. Such studies suggest that the mechanisms governing the ionization of atoms and molecules are essentially the same. But by measuring the electrons ejected from a gas in a plane perpendicular to the incident beam, we show this is not always the case. Experiments and quantum mechanical calculations enable us to construct a remarkably accurate classical picture of the physics of charged-particle ionization. This model predicts that the differences in ionization behaviour arise in molecules that do not have nuclei at their centers of mass.

Introduction

The most sophisticated experiments being carried out at present measure the ionization probability as a function of the outgoing projectile and ejected electron momenta [1-4]. These measurements, called differential cross-sections (DSCs), provide very sensitive tests for theory. Theoretical models for low to intermediate energies (where the ionization probability is highest) must consider many factors, including distortions in the wavefunctions describing the projectile and target, target polarization due to the Coulomb interaction between the incident projectile, nucleus and bound electrons, exchange effects, multiple scattering and post-collision interactions between particles emerging from the reaction. The most sophisticated theories include all of these processes, and compare well to experimental data for atomic targets such as hydrogen [5-7], helium [8], the noble gases [9-13] and alkali and alkali-earth metals [14,15].

A common experimental arrangement is to fix the scattered projectile energy and angular location, and then measure the probability that the ejected electron emerges at different angles in a plane determined by the initial and final momentum of the projectile (called the coplanar scattering plane, $\psi = 0^{o}$ in Fig. 1). These measurements show that there is a large probability for ejecting the target electron in the direction of the projectile momentum change (this is for ionization of s states; for p states, this peak may split into two lobes centred on the direction of momentum change), and a smaller probability that the electron is ejected opposite to this direction [16]. In the first feature, the ejected electron moves in a direction that conserves momentum for the projectile ejected electron system, and so this is attributed to a classical binary collision between these two particles, which is then called the binary peak. The second feature is attributed to a binary collision sending the atomic electron in the direction of momentum transfer, followed by an elastic 180° backscattering from the nucleus. This second feature containing a double collision process is called the recoil peak because the nucleus must recoil to conserve momentum. Binary and recoil peaks are the dominant features in all ionizing collisions, and are found for all projectiles and for all atomic and molecular targets.

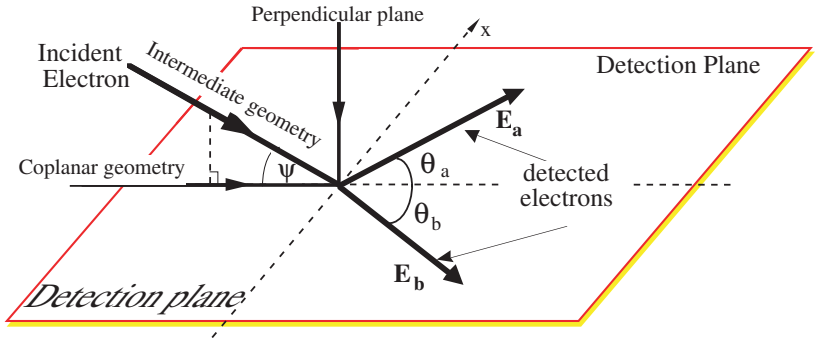

Figure 1: The experimental geometry. A plane is defined by the detected electrons. The incident-electron gun can move from a coplanar geometry ($\psi = 0^o$) to the perpendicular plane ($\psi = 90^o$), where the angle $\varphi = \theta_a + \theta_b$ is defined. A common point between all planes occurs when $\theta_a = \theta_b = \pi / 2$.

1. Experimental arrangement and results

Here, we report an investigation of ionization in a plane perpendicular to the incident beam direction ($\psi = 90^o$ in Fig. 1) using electrons as projectiles and atomic helium and molecular hydrogen as targets. Figure 2 shows the experimental data for electron impact ionization of *He* and H_2 in the perpendicular plane, where the outgoing electron energies are $E_a = E_b = 10$ eV (the incident electron energy is 44.6 eV for *He* and 35.6 eV for H_2). As neutral *He* and H_2 have an equivalent number of protons and electrons, these results markedly contrast the difference in distribution of the constituents that make up these atomic and molecular targets. For *He*, three peaks are observed as a function of the angle $\varphi = \theta_a + \theta_b$ (see Fig. 1), with a large central peak at φ =180° (two electrons leaving back-to-back) and clearly resolved smaller peaks at φ ~ 90° , 270° (the three-lobe atomic helium structure has previously been observed for different kinematics [17]). Similar to *He*, we find peaks in the vicinity of φ ~ 90°, 270° for ionization of H_2. However, instead of a maximum for back-to-back scattering as in *He*, we find a minimum at φ =180°. This difference must be due to either the nuclear configuration of H_2 compared with *He*, or to the different bound-state electron momentum distributions. The data clearly show the sensitivity of measurements in this geometry. It should be noted

that experimental results in a coplanar geometry in this energy regime are very similar for both targets, which means the marked differences between atoms and molecules seen here are not observable in the usual coplanar geometry adopted by most researchers.

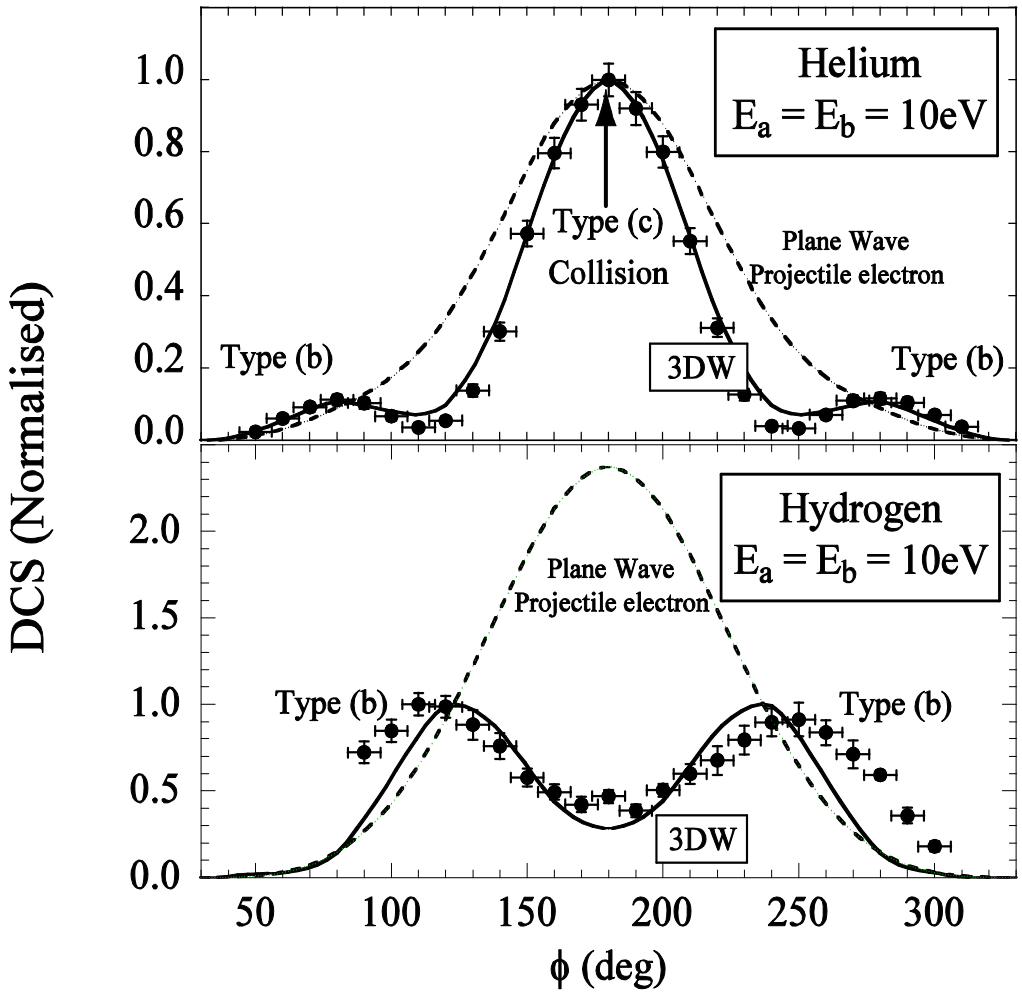

Figure 2: Experimental and theoretical DCS data in the perpendicular plane for *He* and H_2 targets, normalized to unity at the experimental maximum. The outgoing energies were $E_a = E_b = 10$ eV in both cases. The results show the significant differences between ionizing atomic and molecular targets, and contrast the effects of using plane and distorted waves to describe the projectile electron. Error bars in the DCS indicate the statistical variation measured over a series of sweeps of the analysers around the detection plane. Horizontal error bars show the estimated angular response of the spectrometer due to the analyser entrance apertures and the incident electron beam pencil angle. The type of collision process noted in this figure is described in Fig. 3.

2. Possible types of collision

It is instructive to consider classically how the projectile-target interaction can produce ionization into the perpendicular plane. First, consider only binary collisions between the projectile and the target electrons, ignoring the nuclei. If we look at the 180° case, where there is a large difference between atoms and molecules, the two final-state electrons have equal energies and are moving in opposite directions such that the net final-state momentum is zero. This means that, in the initial state, the bound-state electron momentum $\mathbf{k}_{bd}$ would need to be opposite to the initial projectile momentum $\mathbf{k}_{in}$, as shown in Fig. 3a. For back-to-back final-state electron measurements, this is the only process leading to ionization into the perpendicular plane that does not involve the nucleus.

If we include the nucleus in our model, it is possible for the projectile electron to enter the perpendicular plane by first undergoing a small-impact-parameter elastic collision with the nucleus, followed by a classical binary collision with the atomic electron, so that both electrons emerge in the perpendicular plane. In this case, a binary collision will tend to cause the two electrons to emerge at a relative angle of $\varphi \sim 90°$ owing to their equal mass (Fig. 3b). For spherically symmetric targets, scattering into this plane must be symmetric around kin, resulting in peaks at $\varphi \sim 90°, 270°$ as seen for both *He* and H_2.

For this process to produce back-to-back ($\varphi \sim 180°$) electrons, we must have an extra scattering from the nucleus. As small impact parameters are required to bring the projectile into the perpendicular plane (of the order of $0.5a_0$, where $a_0 \sim 0.53$ nm is the Bohr radius), one of the electrons ($\mathbf{k}_a$) may also re-scatter from the nucleus so as to emerge in a direction opposite the other electron ($\mathbf{k}_b$) after the binary collision occurs (Fig. 3c). As this happens on either side of the nucleus with equal probability, a peak centred at $\varphi = 180°$ results. Other second- and higher-order processes involving nuclear scattering may also occur.

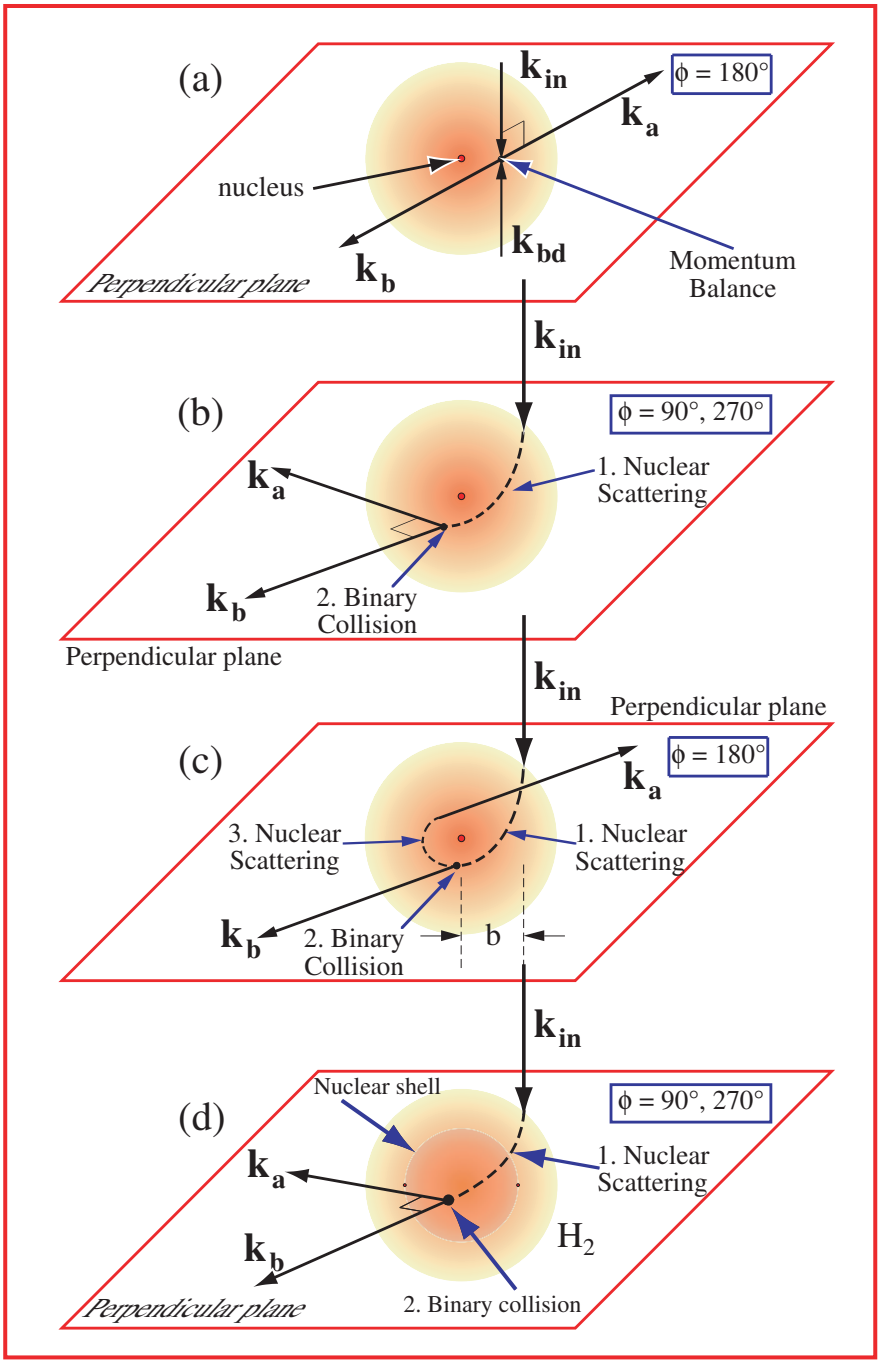

Figure 3: Different mechanisms that may lead to ionization in the perpendicular plane. a, The only mechanism that can occur without nuclear scattering. b, The effect of nuclear scattering followed by a binary collision, leading to peaks at φ ~ 90°, 270°. c, The triple scattering process that leads to a central peak at φ ~ 180° for targets that have a nucleus at the centre of mass. d, The effect of distributing the nuclear charge on a thin shell, in which case the mechanism in c, cannot occur.

3. Quantum mechanical calculation

Although these simple classical pictures are very appealing, atomic and molecular ionization is fundamentally a quantum mechanical process. It is however possible to use quantum mechanics to test these classical ideas. We can calculate the probability of these processes occurring quantum mechanically by evaluating a quantity called the T-matrix, which, in a three-body approximation, is given by:

$$T = \underbrace{\left\langle \chi_{scat}\ \chi_{ej}\ C_{scat-ej} \right|}_{Final\ state} V \underbrace{\left| \varphi_{bound}\ \chi_{in} \right\rangle}_{Initial\ state}$$

The T-matrix is an integral involving the initial and final states of the system and the interaction between the projectile and target (V). The initial state consists of the incoming projectile wave-function (χ_{in}) and the bound state wave-function for the atomic or molecular electron (φ_{bound}) (we use numerical Hartree-Fock wave-functions for either an atom or molecule). The final state consists of the scattered projectile wave-function (χ_{scat}), the ejected electron wave-function (χ_{ej}), and the Coulomb interaction between the scattered projectile and ejected electron ($C_{scat-ej}$) (We use a form first proposed by Ward and Macek[18]). For the calculations presented here, the wave-functions for the free particles (χ) are called *distorted waves*. Distorted waves are solutions of the Schrödinger equation for a spherically symmetric potential representing either the atom or molecule. The important physics contained in the distorted wave is elastic scattering from the target. Consequently, (χ_{in}) is a wave-function representing elastic scattering from a neutral target and (χ_{scat},χ_{ej}) are wave-functions representing elastic scattering from an ion.

As current experiments using molecules do not determine the orientation of the molecule at the time of ionization, an average over all orientations must be made. We approximate this by calculating an elastic scattering potential for molecules obtained by averaging the bound-state electron charge density over all orientations, and by averaging the two nuclei over all orientations. For H_2, the two protons are separated by $1.4a_0$, and so we approximate averaging over all molecular orientations by assuming the nuclear charge of +2 is uniformly distributed on a spherical shell with a radius of $0.7a_0$

(see Fig. 4). The approximate form of the T-matrix we use is called the three-body distorted wave (3DW) model [19, 20]. The 3DW results for ionization of *He* and H_2 are compared to experiment in Fig. 2. As the data are not absolute, experiment and theory are each scaled to unity at their highest value. The agreement between experiment and theory is clearly very good.

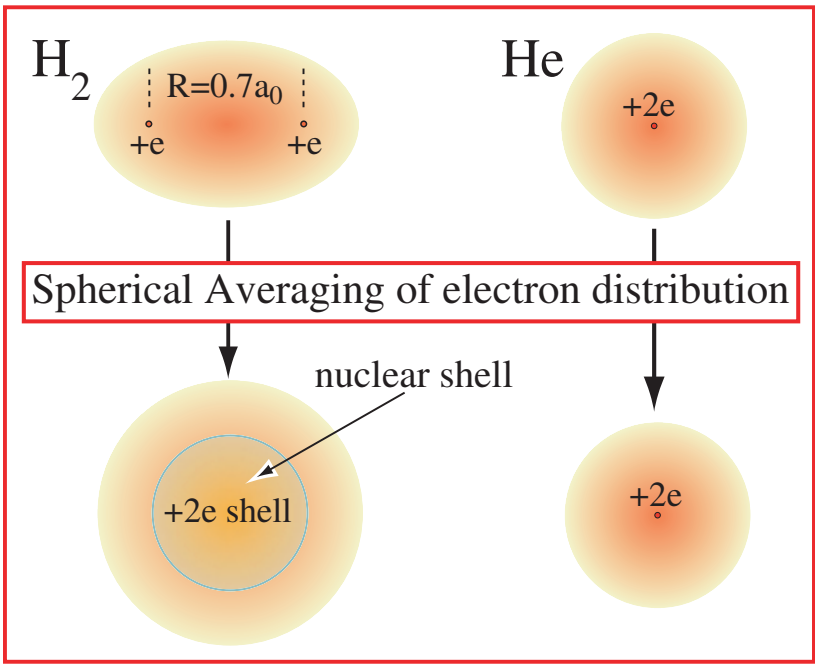

Figure 4: Averaging of the electronic and nuclear structure of the targets due to experimental constraints which cannot determine the orientation of the molecule. For H_2, the nuclear charge is distributed on a thin shell of diameter 1.4 Bohr radii, whereas for *He* the charge is concentrated at the centre of the target.

4. Using quantum mechanics to identify collision types

The key objective of this work is to understand the underlying physical effects producing both similarities and differences between atomic and molecular targets. There are two components to the theoretical calculation – the bound state wave-functions (ϕ_{bound}) and wave-functions describing the electrons in the continuum (χ). If the mechanism in figure 3a is the main contributor to the maximum at $\varphi \sim 180°$ for *He* and

also produces the minimum in H_2, this must be due to the bound state wave-functions, since they contain the initial-state momentum distributions $\mathbf{k_{bd}}$ of the bound electrons. To determine the importance of the momentum distribution in H_2, we repeated the H_2 calculation by replacing the molecular H_2 wavefunction (ϕ_{H_2}) with a *He* wavefunction (ϕ_{He}) (leaving everything else unchanged for the molecule). The result of these calculations again produced a minimum at $\varphi = 180°$. This clearly indicates that the mechanism in Fig. 3a is not the primary source of the differences between *He* and H_2 at this angle. The result of these calculations again produced a minimum at $\varphi = 180°$. This clearly indicates that the mechanism in Fig. 3a is not the primary source of the differences between *He* and H_2 at this angle.

The mechanisms shown in Fig. 3b,c both require elastic scattering from the target. As noted above, the free-particle distorted waves we use are elastic scattering wavefunctions from the target. A wavefunction that does not contain elastic scattering from the target is a free-particle plane wave. Consequently, we can determine the effect of elastic scattering of the projectile from the target by replacing (χ_{scat}, χ_{ej}) by plane waves. The results of these calculations are also shown in Fig. 2, where it is seen that elastic scattering of the projectile from the target produces the peaks near 90° and 270° for both H_2 and *He*. The 90° and 270° peaks for *He* have been observed previously for different kinematics [17], and Zhang *et al.* [21] carried out a detailed study for ionization of *He* into the perpendicular plane. They proposed this method for identifying the physical mechanisms of the collision. We hence conclude that the mechanism in Fig. 3b is responsible for these outlying structures in both atomic *He* and molecular H_2 targets and speculate that these features are generic for atomic and molecular targets.

5. Nuclear distribution causes the difference

The most striking observation is the difference seen at $\varphi = 180°$. The source of this feature must lie in the difference between elastic scattering wavefunctions for atoms and molecules, as distorted waves give a peak for *He* and a minimum for H_2. Given that these wavefunctions contain elastic scattering from the bound-state electrons as well as elastic scattering from the nuclei, we investigated the electronic and nuclear contributions

individually and found the important difference lies in the treatment of the nuclei (described as a point charge for *He* and a thin spherical shell of charge for H_2, as discussed above).

To investigate the importance of the size of the nuclear shell for H_2, calculations were repeated with the shell size reducing from R = $0.7a_0$ to a point charge (while keeping the electronic component unchanged). The marked changes in the predicted results are seen in Fig. 5. As the shell diameter decreases, the minimum at $\varphi = 180°$ becomes deepest at $0.5a_0$, after which a maximum appears, which is largest for a point charge (R=$0.0a_0$). The H_2 results are then very similar to that for *He* when the nuclear charge is concentrated at a single point, indicating that the distance between the nuclei

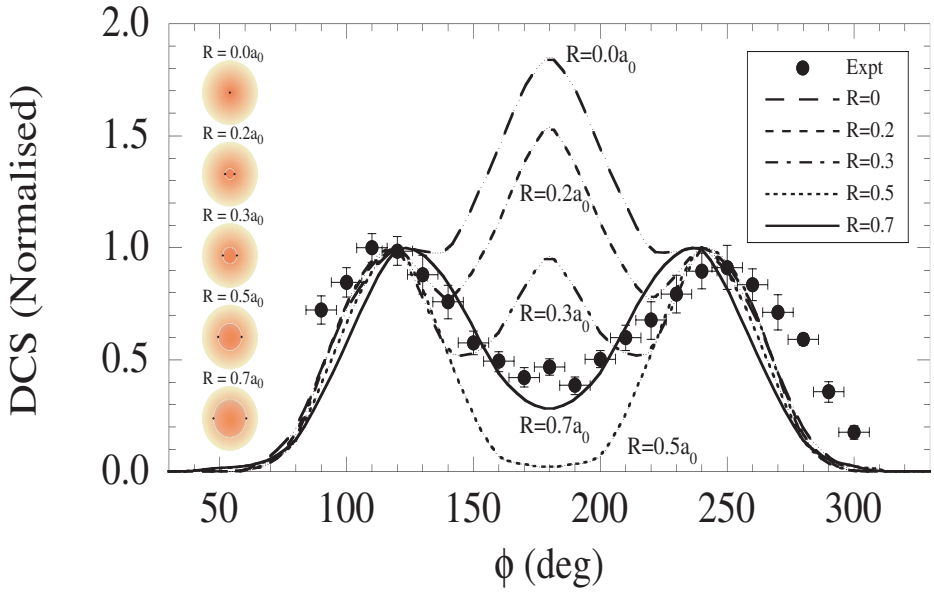

Figure 5: Change in the calculated ionization DCS for H_2 in the perpendicular plane as a function of the size of the spherically averaged nuclear shell, normalized to unity at the experimental maximum. Error bars are as described in Fig. 2.

has a critical role in determining the ionization probability for back-to-back scattering. We also carried out a similar calculation for *He*. In this case, we replaced the point charge with a charge of +2 on a sphere of increasing size while leaving everything else the same. Again, we found that the maximum at 180° quickly developed into

a minimum. It is therefore clear that the 180° minimum stems from the separated nuclei in the molecule.

The effect of shell size on the peak at $\varphi = 180°$ indicates this feature is dominated by the processes shown in Fig. 3c,d. If classical Rutherford scattering theory is used to equate the impact parameter b with scattering angle, it is found that $b=0.4a_0$-$0.6a_0$ is required to elastically scatter into the perpendicular plane for the present kinematics. For *He*, the projectile (or ejected) electron following the binary collision is then close to the nucleus so it has a strong attraction to the point nucleus, and preferentially backscatters elastically as in Fig. 3c. For H_2, the electrons are mostly inside the spherical shell at the time of the binary collision (Fig. 3d), so experience no attractive force that would produce a peak at $\varphi = 180°$. For binary collisions within the shell, the Coulomb force from the nuclei is zero, so the electrons will then leave at a mutual angle $\varphi \sim 90°$.

The question arises of why there is a peak at 180° for *He* resulting from backscattering from the nucleus when all scattering angles should be equally likely. This is of course true only if all impact parameters are equally likely. However, for the present kinematics following the binary collision, the electrons have energy ~10 eV and an impact parameter between $0.4a_0$ and $0.6a_0$. Again using Rutherford scattering from a point charge, the resulting scattering angles range from 150° to 160° for these values. As there is an equal probability of left and right scattering, the resulting signal will be distributed between ±150° centred around $\varphi = 180°$, as is observed.

Although these classical descriptions of ionization aid in explaining the differences between *He* and H_2 and highlight the importance of the nuclear configuration, the fully quantum mechanical calculation is of course needed to accurately describe the data. It is intriguing to note that the nuclear configuration has such a crucial role in the observed structures in the perpendicular plane, whereas it has almost no role for the binary and recoil peaks seen in a coplanar geometry (where most previous measurements have been made).

6. Generalizing the model to larger molecules

The minimum in the cross-section for 180° scattering in the perpendicular plane found for H_2 has been attributed here to the fact that the binary collisions are taking place

in a force-free region inside a spherical shell of charge. This spherical shell of charge resulted from averaging over all molecular orientations. The present results suggest that a minimum would be found for any diatomic molecule or perhaps for any molecule that does not have a nucleus located at the centre of mass. Conversely, molecules that have a nucleus at the centre of mass might then be expected to act in a similar way to an atom. To test this conjecture, experimental results for ionization of the $1\pi_g$ state of CO_2 in the perpendicular plane are presented in Fig. 6, where it is seen that we find a broad maximum at 180° instead of a minimum. Consequently, these results strongly suggest that molecules that have no nuclei at the centre of mass will have a minimum for back-to-back scattering and molecules that have a nucleus at the centre of mass will have a maximum, as is found for atoms.

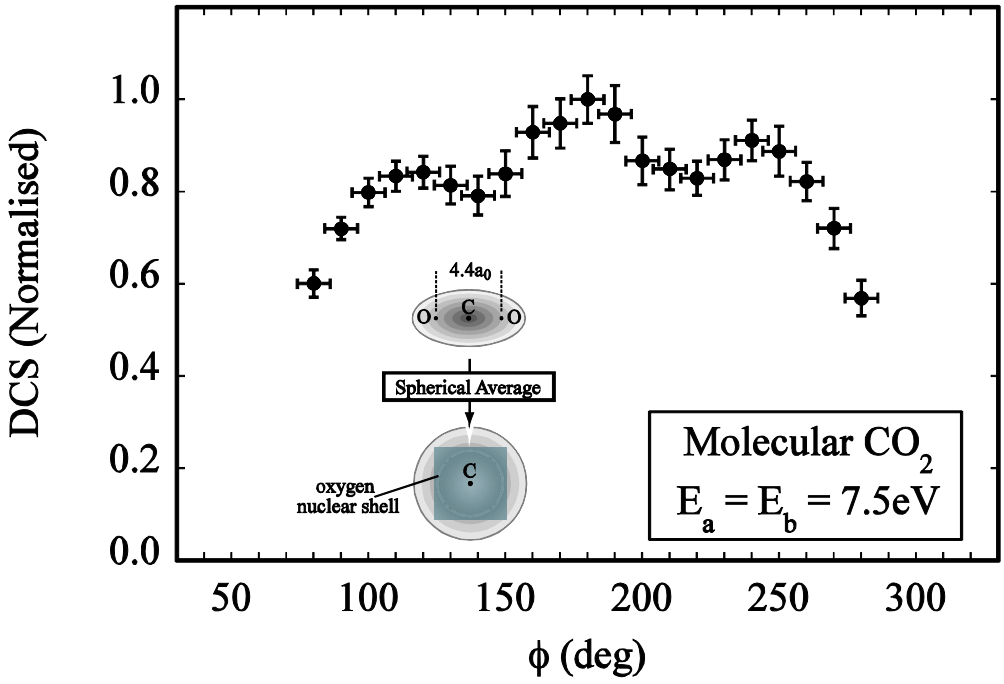

Figure 6: DCS for ionization of CO_2 in the perpendicular plane normalized to unity at the experimental maximum. A maximum is seen at $\varphi = 180°$, as found for He, in contrast to the results from H_2. This is attributed to the carbon nucleus being at the centre of mass of the molecule, so that spherical averaging produces an oxygen nuclear shell with an extra nuclear target at the centre of the molecule. The scattering process shown in Fig. 3c can then take place from this carbon nucleus. Error bars are as described in Fig. 2.

Acknowledgements

We thank the EPSRC (UK) for supporting these experiments, and the NSF for support of the theoretical work under grant No. PHY-0757749.

Author contributions

O.A.-H. and D.M. carried out the theoretical calculations for this work, whereas C.K. and A.M. carried out the experimental investigations that are presented.

References

[1] Dürr, M., Dimopoulou, C., Najjari, B., Dorn, A. & Ullrich, J. Three-dimensional images for electron-impact single ionization of *He*: Complete and comprehensive (e,2e) benchmark data. *Phys. Rev. Lett.* **96**, 243202 (2006).

[2] Casagrande, E. M. S. et al. New coplanar (e,2e) experiments for the ionization of *He* and Ar atoms. *J. Electron Spectrosc. Relat. Phenom.* **161**, 27-30 (2007).

[3] Lower, J. R., Bellm, S. & Weigold, E. An improved double-toroidal spectrometer for gas phase (e,2e) studies. *Rev. Sci. Instrum.* **78**, 111301 (2007).

[4] Deharak, B. A. & Martin, N. L. S. An out-of-plane (e, 2e) spectrometer using a movable electron gun. *Meas. Sci. Tech.* **19**, 015604 (2008).

[5] Bray, I. & Stelbovics, A. Explicit demonstration of the convergence of the close-coupling method for a Coulomb three-body problem. *Phys. Rev. Lett.* **69**, 53-56 (1992).

[6] Rescigno, T. N., Baertschy, M., Isaacs, W. A. & McCurdy, C. W. Collisional breakup in a quantum system of three charged particles. *Science* **286**, 2474-2479 (1999).

[7] Colgan, J., Pindzola, M. S., Robicheaux, F. J., Griffin, D. C. & Baertschy, M. Time-dependent close-coupling calculations of the triple-differential cross section for electron-impact ionization of hydrogen. *Phys. Rev.* A **65**, 042721 (2002).

[8] Bray, I., Fursa, D. V. & McCarthy, I. E. Convergent close-coupling method for electron scattering on helium. *J. Phys.* B **27**, L421-L425 (1994).

[9] Murray, A. J. & Read, F. H. Evolution from the coplanar to the perpendicular plane geometry of helium (e,2e) differential cross sections symmetric in scattering angle and energy. *Phys. Rev.* A **47**, 3724_3732 (1993).

[10] Murray, A. J. & Read, F. H. Low energy (e, 2e) differential cross section measurements on neon from the coplanar to the perpendicular plane geometry. *J. Phys.* B **33**, L297-L302 (2000).

[11] Rasch, J., Whelan, C. T., Allan, R. J., Lucey, S. P. & Walters, H. R. J. Strong interference effects in the triple differential cross section of neutral-atom targets. *Phys. Rev.* A **56**, 1379-1383 (1997).

[12] Stelbovics, A. T., Bray, I., Fursa, D. V. & Bartschat, K. Electron-impact ionization of helium for equal-energy-sharing kinematics. *Phys. Rev.* A **71**, 052716 (2005).

[13] Milne-Brownlie, D. S., Foster, M., Gao, J., Lohmann, B. & Madison, D. H. Young-type interference in (e, 2e) ionization of H_2. *Phys. Rev. Lett.* **96**, 233201 (2006).

[14] Murray, A. J. (e, 2e) ionization studies of alkaline-earth-metal and alkali-earth-metal targets: Na, Mg, K, and Ca, from near threshold to beyond intermediate energies. *Phys. Rev*. A **72**, 062711 (2005).

[15] Srivastava, M. K., Kumar, R. C. & Srivastava, R. Coplanar doubly symmetric (e, 2e) process on sodium and potassium. *Phys. Rev.* A **74**, 064701 (2006).

[16] Schulz, M. et al. Three-dimensional imaging of atomic four-body processes. *Nature* **422**, 48-50 (2003).

[17] Murray, A. J., Woolf, M. B. J. & Read, F. H. Results from symmetric and non-symmetric energy sharing (e, 2e) experiments in the perpendicular plane. *J. Phys.* B **25**, 3021-3036 (1992).

[18] Ward, S. J. & Macek, J. H. Wave functions for continuum states of charged fragments. *Phys. Rev.* A **49**, 1049-1056 (1994).

[19] Gao, J., Peacher, J. L. & Madison, D. H. An elementary method for calculating orientation-averaged fully differential electron-impact ionization cross sections for molecules. *J. Chem. Phys* **123**, 204302 (2005).

[20] Gao, J., Madison, D. H. & Peacher, J. L. Distorted wave born and three-body distorted wave born approximation calculations for the fully differential cross section for electron impact ionization of nitrogen molecules. *J. Chem. Phys*. **123**, 204314 (2005).

[21] Zhang, X., Whelan, C. T. & Walters, H. R. J. Energy sharing (e,2e) collisions ionisation of helium in the perpendicular plane. *J. Phys.* B **23**, L173-L178 (1990).

II. Triple Differential Cross Sections for the Electron-Impact Ionization of H_2 Molecules for Equal and Unequal Outgoing Electron Energies

J. Colgan, [1] O. Al-Hagan, [2] D. H. Madison, [2] C. Kaiser, [3] A. J. Murray, [3] and M. S. Pindzola[4]

[1]*Theoretical Division, Los Alamos National Laboratory, Los Alamos, New Mexico 87545, USA*

[2]*Department of Physics, Missouri University of Science and Technology, Rolla, Missouri 65409, USA*

[3]*School of Physics and Astronomy, University of Manchester, Manchester M13 9PL, United Kingdom*

[4]*Department of Physics, Auburn University, Auburn, Alabama 36849, USA*

Abstract

A comprehensive theoretical and experimental investigation of the triple differential cross sections arising from the electron-impact ionization of molecular hydrogen is made, at an incident electron energy of 35.4 eV, for cases where the outgoing electrons have equal and unequal energies, and for a range of experimental geometries. Generally, good agreement is found between two theoretical approaches and experiment, with the best agreement arising for intermediate geometries with large gun angles and for the perpendicular geometry.

1. Introduction

Studies of the electron-impact ionization of one- and two electron systems have provided a wealth of information about the role of electron-electron correlation, polarization, and three-body effects in the ionization process [1]. As experimental techniques such as recoil-ion momentum spectroscopy and multi-electron coincidence detection have become ever more sophisticated, the triple differential cross sections (TDCSs) for electron-impact ionization have been measured for a wide variety of electron angles and energies, and now for many different targets (see for example [2–10]). Recent theoretical progress in several non-perturbative approaches now mean that good agreement with measurement for a variety of kinematical conditions exists. For example, for the electron-impact ionization of atomic hydrogen, theory and experiment are in excellent agreement for all possible differential cross sections [11–16], and for the ionization of helium [17–20] a somewhat similar situation exists.

This progress has spurred recent measurements of the TDCS arising from ionization of the hydrogen molecule [21–23], which have mainly been made at quite high incident electron energies, in order to test perturbative plane-wave and distorted-wave theoretical approaches [24]. Other distorted-wave approaches employing an average over all molecular orientations have been used to examine the TDCS arising from the ionization of N_2 and H_2 [25–30]. Some of these theoretical approaches have also been extended to examine the triple differential cross sections arising from the electron-impact ionization of the hydrogen molecule at much lower incident energies (35.4 eV), where the correlation between the electrons can be expected to play a more prominent role. For example, recent distorted-wave [31] and time dependent close-coupling (TDCC) [32] calculations have found good agreement with measurements for the TDCS from ionization of H_2 for equal-energy sharing of the outgoing electrons.

In this paper, we present further comparisons of these approaches with measurements made using the Manchester experimental apparatus [2,3,33] at an incident electron energy of 35.4 eV, and present calculations and measurements of the TDCS for *unequal*-energy-sharing conditions for the outgoing electrons. In the following section we give outlines of the two theoretical approaches (molecular distorted-wave theory and time-dependent close-coupling theory) used to compute the TDCS. This is followed by a

brief overview of the experimental setup used in the measurements presented here. We then discuss in detail the results and comparisons between theory and experiment. We end with a short conclusion.

2. Theoretical approach

2.1. 3DW theory

The three-body distorted-wave (3DW) model has been described elsewhere [25–29], so only a brief outline of the theory will be presented. The TDCS for 3DW is given by

$$\frac{d^3\sigma}{d\Omega_a d\Omega_b dE_b} = \frac{1}{(2\pi)^5}\frac{k_a k_b}{k_i}|T|^2, \quad (1)$$

where $\vec{k}_i$, $\vec{k}_a$, and $\vec{k}_b$ are the wave vectors for the initial, scattered, and ejected electrons, respectively. The scattering amplitude is given by

$$T = \left\langle \chi_a^-(\vec{k}_a, \mathbf{r}_1)\chi_b^-(\vec{k}_b, \mathbf{r}_2) C_{scat-eject}(r_{12}^{ave}) | V - U_i | \phi_j^{OA}(\mathbf{r}_2)\chi_i^+(\vec{k}_i, \mathbf{r}_1) \right\rangle, \quad (2)$$

where $\boldsymbol{r}_1$ and $\boldsymbol{r}_2$ are the coordinates of the incident and the bound electrons, χ_i, χ_a and χ_b are the distorted waves for the incident, scattered, and ejected electrons, respectively, and $\phi_j^{OA}(\boldsymbol{r}_2)$ is the initial bound-state wavefunction which is the orientation-averaged molecule wavefunction for H_2 [27]. The factor $C_{scat-eject}(r_{12}^{ave})$ is the average Coulomb-distortion factor and V is the initial-state interaction potential between the incident electron and the neutral molecule.

The molecular distorted waves are calculated using a spherically averaged distorting potential as described previously [25–29]. The Schrödinger equation for the incoming electron wavefunction is given by

$$(T + U_i - \frac{k_i^2}{2})\chi_i^+(\vec{k}_i, \boldsymbol{r}) = 0, \quad (3)$$

where T is the kinetic-energy operator. The initial-state distorting potential U_i contains three components $U_i = U_S + U_E + U_{CP}$, where U_S is the initial-state spherically symmetric static potential, U_E is the exchange potential of Furness and McCarthy [34], which approximates the effect of the continuum electron exchanging with the bound electrons in

the molecule, and U_{CP} is the correlation-polarization potential of Perdew and Zunger [35,36]. The static potential U_S has two parts, the electronic potential V_{ele} (r) and the nuclear potential V_{nuc} (r),

$$U_s(r) = V_{ele}(r) + V_{nuc}(r). \tag{4}$$

Here $V_{ele}(r)$ is obtained by taking a spherical average of the interaction of the projectile electron with the molecular electrons using a numerical Hartree-Fock charge distribution calculated for the molecular electrons. The nuclear potential $V_{nuc}(r)$ is the interaction between the incident electron and two protons separated by 1.4a0, averaged over all orientations. This spherical average places a charge of +2 uniformly distributed on a sphere of radius 0.7a0. The final-state distorted waves are calculated in the same manner except that the charge distribution for an ion is used to calculate the distorting potentials.

In previous works for higher incident energy electrons [23,27,30], the full Coulomb-distortion factor $C(r_{12})$ was used in the T matrix [Eq. (2)], where r_{12} is the actual relative electron-electron separation which ranges from 0 to infinity in the evaluation of the T-matrix integral. However, for lower energies of interest in this study, it became clear that using $C(r_{12})$ overestimated the effect of the final-state electron-electron repulsion, normally called the postcollision interaction (PCI). Consequently, we have used the Ward-Macek average C factor [37], which gave better agreement with the experimental results.

2.2. Time-dependent close-coupling method

The TDCC technique [38] is also used to obtain the triple differential cross sections for the ionization of H_2. This approach has been used previously to obtain total cross sections for electron-impact ionization of H_2^+ [39] and H_2 [40], and was recently shown to produce good agreement for triple differential cross sections for equal-energy sharing [32]. We expand the total electronic wavefunction for the two outgoing electrons as products of four-dimensional radial angular functions and rotational functions [39] using

$$\Psi^M(\vec{r}_1, \vec{r}_2, t) = \sum_{m_1, m_2} \frac{P^{l_0 MS}_{m_1 m_2}(r_1, \theta_1, r_2, \theta_2, t)}{r_1 r_2 \sqrt{\sin\theta_1}\sqrt{\sin\theta_2}} \Phi_{m_1}(\phi)\, \Phi_{m_2}(\phi), \tag{5}$$

where $M = m_1+m_2$ and $\Phi(\phi) = \frac{e^{i\phi m}}{\sqrt{2\pi}}$ in center-of-mass spherical polar coordinates. The angular reduction of the time dependent Schrödinger equation then yields a set of time dependent close-coupled partial differential equations given by

$$i\frac{\partial P^{l_0 MS}_{m_1 m_2}(r_1,\theta_1,r_2,\theta_2,t)}{\partial t} = T_{m_1 m_2}(r_1,\theta_1,r_2,\theta_2)P^{l_0 MS}_{m_1 m_2}(r_1,\theta_1,r_2,\theta_2,t) + \sum_{m_1' m_2'} V^{M}_{m_1 m_2, m_1' m_2'}(r_1,\theta_1,r_2,\theta_2)P^{l_0 MS}_{m_1 m_2}(r_1,\theta_1,r_2,\theta_2,t), \quad (6)$$

where detailed expressions for the single-particle operators $T_{m_1 m_2}(r_1,\theta_1,r_2,\theta_2)$ and the two-particle coupling operator $V^{M}_{m_1 m_2, m_1' m_2'}(r_1,\theta_1,r_2,\theta_2)$ can be found in [40]. The single particle operator includes a Hartree-Slater potential term which defines the interaction with the nonionized (frozen) electron. This potential term includes a direct and local exchange potential [40].

The initial condition at time t=0 for the radial angular functions is given by

$$P^{l_0 MS}_{m_1 m_2}(r_1,\theta_1,r_2,\theta_2,t=0) = \sqrt{\frac{1}{2}}[P_{1s_0}(r_1,\theta_1)G_{k_0 l_0 M}(r_2,\theta_2)\delta_{m_1,0}\delta_{m_2,M} + (-1)^S G_{k_0 l_0 M}(r_1,\theta_1)P_{1s_0}(r_2,\theta_2)\delta_{m_1,M}\delta_{m_2,0}], \quad (7)$$

where S is the total spin of the two-electron pair, and the Gaussian wave packet $G_{k_0 l_0 M}$ is a function of the incident energy $k_0^2/2$ and the incident angular momentum l_0. The radial angular orbitals $P_{nlm}(r,\theta)$ are obtained through diagonalization of the one-electron Hamiltonian [40]. The time-dependent close-coupled equations described by Eq. [6] are then propagated in time for each value of M, S, and l_0, until the interaction is complete. As previously discussed [39], an implicit algorithm is used for efficient time evolution.

After propagation to a suitable time T, probabilities for ionization may be obtained [40] by projection onto bound wavefunctions and appropriate subtraction from unity. An alternative approach is to project directly onto suitable products of H_2^+ continuum functions using

$$P^{l_0 MS}_{l_1 m_1 l_2 m_2}(k_1,k_2,T) = \int dr_1 \int d\theta_1 \int dr_2 \int d\theta_2 P^{*}_{k_1 l_1 |m_1|}(r_1,\theta_1) P^{*}_{k_2 l_2 |m_2|}(r_2,\theta_2) \times P^{l_0 MS}_{m_1 m_2}(r_1,\theta_1,r_2,\theta_2,T), \tag{8}$$

where $P_{klm}(r,\theta)$ are appropriately normalized H_2^+ continuum functions. This latter approach allows triple differential cross sections to be computed [32] using

$$\frac{d^3\sigma}{dE_1 d\Omega_1 d\Omega_2} = \frac{\pi}{4k_0^2}\frac{1}{k_1 k_2}\sum_S (2S+1)\int dk_1 \int dk_2 \times \delta\left(\alpha - \tan^{-1}\left[\frac{k_2}{k_1}\right]\right)\left|M\right|^2, \tag{9}$$

where k_1 and k_2 are the outgoing electron momenta (ejected into solid angles $\Omega_{1,2}$). For diatomic molecules, where the z axis is defined along the internuclear direction and the in-coming electron beam is oriented at angles (θ_k,ϕ_k) with respect to the z axis,

$$M = \sum_{l_0}\sum_{M=-l_0}^{+l_0} i^{l_0} Y^{*}_{l_0 M}(\theta_k,\phi_k) \sum_{l_1,l_2}\sum_{m_1 m_2} (-i)^{l_1+l_2} e^{i(\sigma_{l_1}+\sigma_{l_2})} \times P^{l_0 MS}_{l_1 m_1 l_2 m_2}(k_1,k_2,T) Y_{l_1 m_1}(\hat{k}_1) Y_{l_2 m_2}(\hat{k}_2) \delta_{m_1+m_2,M}. \tag{10}$$

In Eq. (10), $Y_{lm}(\hat{k})$ is a spherical harmonic, and σ_l is the Coulomb phase shift. Our TDCS expression defined by Eqs. (9) and (10) is given in the molecular frame. To compare with experiment, a transformation must be made into the Laboratory frame. Singly differential cross sections in outgoing electron energy may also be extracted if necessary. Our calculations were performed using a 384×32×384×32 lattice for the $(r_1,\theta_1,r_2,\theta_2)$ spherical polar coordinates, with a uniform mesh spacing of Δr=0.2 a.u. and $\Delta\theta$ =0.031 25π, for all l_0 ,M values from 0 to 6, and for S=0,1. The wavefunctions for $-M$ values were assumed equal to those for $+M$ values, which was confirmed by several explicit calculations for selected $-M$ values. The ranges of l_0 ,M employed were found to be sufficient to converge all the TDCS presented here, although larger values may be required to fully converge TDCS at larger incident energies. Since the orientation of the molecule with respect to the incoming electron gun angle is *unknown*, we compute the TDCS for all possible molecular angles (θ_N,ϕ_N) (which are the angles made by the molecule with respect to the z axis in the Laboratory frame, where in the Laboratory

frame the z axis is defined by the incoming electron-beam direction) and then average over these to compare with the measurements.

3. Experimental setup

The apparatus used to collect these data has been well documented [41,42] and so will only be described briefly here. The electron source is comprised of an unselected energy electron gun which uses two electrostatic lenses to focus a collimated electron beam onto the interaction region. The energy of the incident electron beam can be changed from ~20 eV to 300 eV, while maintaining a beam angle of zero degrees and a pencil angle of ±2°. Typical electron beam currents used in these experiments ranged from 200 to 1000 nA, as detected on a Faraday cup. The electron energy analyzers are of a hemispherical design, the input to these analyzers being focused onto the interaction region using a three-element cylindrical electrostatic lens with an acceptance angle of ±3°. Electrons of the correct selected energy are detected and amplified using X719BL channel electron multipliers, whose output is fed to ORTEC 473A constant fraction discriminators (CFDs) via Philips scientific 6954 preamplifiers. The output NIM pulses from the CFDs are fed to an ORTEC time-to-amplitude converter (TAC), one output being time delayed so as to produce a coincidence signal within the timing window of the TAC. The output from the TAC feeds a multichannel analyzer (MCA) which accumulates the correlated coincidence counts from the experiment.

The two electron analyzers are located on separate turntables inside the vacuum system so as to rotate around a detection plane with angles ξ_1 and ξ_2, as shown in Fig. 1. The electron gun can also be moved through an angle ψ with respect to the detection plane. When ψ=0° the electron gun lies in the detection plane which is referred to as a *coplanar geometry*, whereas when ψ=90° the incident electron beam is orthogonal to the detection plane, referred to as the *perpendicular geometry*. A common point occurs between all geometries when ξ_1=ξ_2=90°, and this allows all data to be normalized to this common reference point at any given energy.

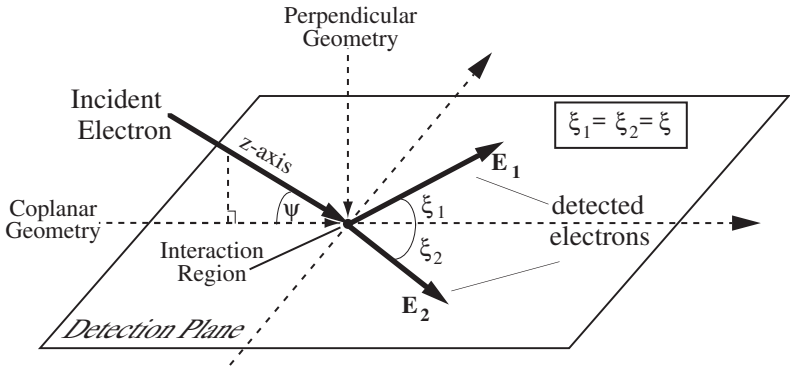

Figure 1: The experimental geometry. The incident electron beam makes an angle ψ with respect to the detection plane defined by theanalyzers. ψ=0° defines a coplanar geometry, ψ =90° a perpendicular geometry. The analyzers rotate through angles ξ_1 and ξ_2 as shown. In the current experiments $\xi_1 = \xi_2$. A common normalization point exists for all gun angles when $\xi_1=\xi_2=90°$.

The interaction region must be precisely positioned at the center of rotation of the analyzers and the electron gun. This is facilitated using laser diodes to accurately define the axes of these components, which are adjusted using custom built in-vacuum translators [43,44]. The molecular hydrogen beam effuses from a 1 mm diameter platinum-iridium needle located ~6 mm from the interaction region which rotates with the electron gun. The background pressure inside the chamber is 2×10^{-7} torr, which increases to 1.2×10^{-5} torr while the experiment is operating. Typical electron counts from the analyzers range from 20 to 2 kHz depending on the angles of the analyzers and gun, whereas the coincidence count rates range from ~2 Hz to ~0.01 Hz.

The experiments proceed by selecting a gun angle ψ, then moving the analyzers to a given angle $\xi_1=\xi_2=\xi$ before collecting data (typically for 2000 s at each angle). The analyzers are then moved to new angles, and the experiment is repeated until the analyzers have covered the available detection plane. The possible detection angles are limited by the physical size of the analyzers, electron gun, and Faraday cup. The experiment continues for a set gun angle ψ until the statistical variation in the accumulated data is small. This may take up to 20 sweeps of the detection plane, depending upon the coincidence count rates. Once a set of data is accumulated for a given geometry, the gun is moved to a new angle and the process is repeated. All data

are then placed on a common scale by equating the results at the common normalization point given by $\xi_1=\xi_2=90°$.

Control of the experiment is facilitated using custom designed control software which not only adjusts the angles of the detectors and gun, but also optimizes the signal by computer controlling the voltages on the analyzers and electron gun [45]. In this way the experiment automatically adjusts for any long term drifts in the operating conditions of the apparatus over the several weeks required for data accumulation.

4. Results and discussion

4.1. Equal-energy sharing

We begin our discussion by presenting, in Fig. 2, TDCS for ionization of H_2 for equal-energy-sharing outgoing electrons. A selection of these results has previously been presented [31, 32]. We compare the experimental data to TDCC calculations and two 3DW calculations: one including a correlation-polarization potential (CP) [labeled 3DW (with CP)] and one without [labeled 3DW (no CP)]. The relative measurements are normalized to the absolute TDCC calculations at $\psi = \xi = 90°$, and the common point which exists at $\xi = 90°$ for all ψ values (confirmed in all the calculations) allows the measurements to be relatively normalized. This choice of normalizing the measurements to the TDCC calculations at $\psi=\xi=90°$ gives best overall fit to the complete data set. In all the results presented below, the 3DW calculations have been scaled (as specified in the figure captions) to the TDCC to provide an equivalent shape and relative magnitude comparison with experimental data. The need for such a scaling is not unexpected as distorted-wave approaches often differ significantly from measurements of the total ionization cross section [40] at low and intermediate incident energies.

The most obvious trend from the comparisons in Fig. 2 is that experiment and theory are in good agreement when considering the shape of the TDCS for large ψ values. In particular, the TDCC and 3DW (with CP) calculations are in very good agreement with experiment for the perpendicular geometry ($\psi = 90°$). This trend persists as ψ decreases down to 45°, with the 3DW (with CP) calculations predicting a binary peak at slightly larger ξ values than found in the experiment and TDCC calculations. The 3DW (no CP) calculations also compare reasonably well with experiment for ψ values

from 45° to 90°, but are perhaps not in as good agreement as the 3DW (with CP) calculations.

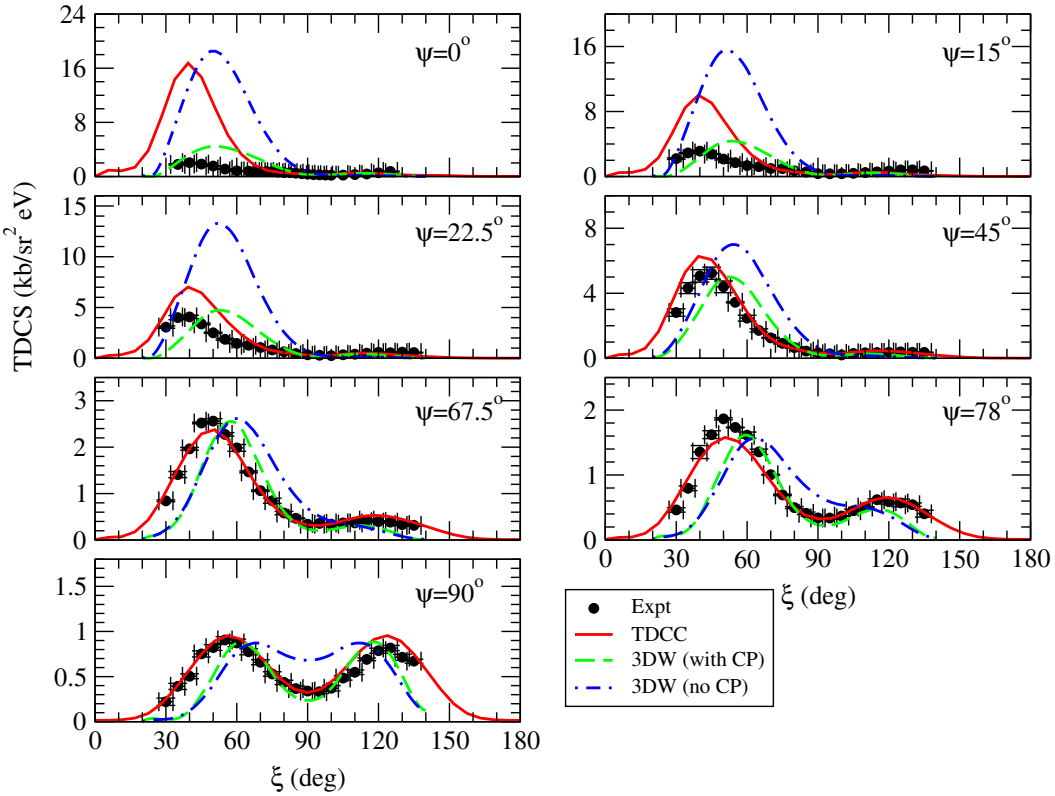

Figure 2: (Color online) Triple differential cross sections for the electron-impact ionization of H_2 for equal-energy sharing between the outgoing electrons (E_1=E_2=10 eV). We present cross sections for various values of the gun angle ψ, as a function of the angle ξ, where 2ξ is the angle between the outgoing electrons. The measurements are compared with TDCC calculations and two sets of 3DW calculations; one including a correlation-polarization potential [labeled 3DW (with CP)] and one without this potential [labeled 3DW(no CP)]. Both sets of 3DW calculations are divided by 6.3 to allow a better comparison with the other results. 1 kb=1.0 $\times 10^{-21}$ cm^2; 1 kb/sr^2 eV $\approx 1\times 10^{-3}$ a.u.

For lower ψ values, the agreement between experiment and all the calculations worsens, with poorest agreement arising for the coplanar ψ =0° case. The 3DW (with CP) calculations are in best agreement with the relative magnitude of the experiment, but

again predict binary peak positions at larger ξ values than found experimentally. The TDCC calculations find a similar binary peak position compared to experiment, but predict a much larger TDCS than found experimentally. The 3DW (no CP) calculations have a similar binary peak position compared to the 3DW (with CP) calculations, but, like the TDCC calculations, predict a much larger relative TDCS.

We note also that the experimental data indicate that the largest cross section is found for the ψ=45° case, which is also found in the 3DW (with CP) calculations. However, the TDCC calculations and the 3DW (no CP) calculations both predict that the largest cross section is found in the coplanar geometry. This might suggest that inclusion of the correlation-polarization potential may change the magnitude of the TDCC calculations, but tests show that inclusion of this potential in the TDCC calculations makes almost no difference to the resulting TDCS. Previous experiments [2,3] and calculations [19] which examined the TDCS from *He* at similar energies and geometries also found that the largest cross section is in the coplanar geometry.

It is difficult to understand why the TDCC calculations should be in such poor agreement with experiment for small ψ values, but in good agreement for larger ψ values. The perpendicular geometry exhibits the smallest cross section, yet displays the best agreement between theory and experiment. Also, the TDCC calculations for each ψ are made from the same set of amplitudes, and so should have the same set of convergence properties, and so it might be expected that the level of agreement would be similar for each ψ angle. The ability to inter-normalize the set of experimental data using the common point at ξ=90° also rules out any potential problem with normalization of the measurements or in the calculations. One tentative explanation for the discrepancy between experiment and theory found at low ψ values is that, for coplanar geometries, the molecules may be significantly more aligned (with respect to the incoming electron beam) than for near-perpendicular geometries. TDCC calculations for the coplanar case and for molecules oriented along the electron beam [32] do predict a smaller cross section than in the average case. However, it is not at all obvious why the molecules would align with the incident electron beam in the coplanar geometry, but not in out-of-plane geometries, since there are no deliberate mechanisms for alignment of the molecules in the experiment. However we do note that recent experiments on proton scattering from

H_2 suggest preferential orientation of the molecule parallel to the beam direction for large scattering angles [46].

The 3DW calculations are also in closer agreement with the measurements in the perpendicular plane. To scatter into the perpendicular plane, the projectile must undergo a very close collision with the nuclei at small impact parameters [31]. This type of scattering dominates in the perpendicular plane, but is less important as the coplanar geometry is approached, where polarization and exchange effects become relatively more important. The 3DW method treats the projectile-nuclear scattering exactly for the model potential, and so shows good agreement with the measurements made in the perpendicular plane. On the other hand, the 3DW method treats polarization and exchange more approximately, which may explain why poorer agreement exists as the coplanar geometry is approached. The TDCC approach treats exchange between the outgoing electrons in an exact manner, but only treats the exchange with the bound electron approximately (via a local exchange approximation). Although we have found that inclusion of a static polarization term makes little difference, we have not explored the effects of dynamic (time-dependent) polarizability of the core. Such considerations may also explain the discrepancies which exist for the coplanar geometry.

It is also instructive to compare the TDCS found for *He* at similar outgoing electron energies to those presented in Fig. 2. In the *He* case, measurements made using the same apparatus [2,3] were previously shown to be in good agreement with convergent close-coupling calculations [19] and are also in good agreement with TDCC and 3DW calculations [47]. The differences between the TDCS from *He* and from H_2 for the perpendicular geometry have already been discussed in detail [31], and indicate how the TDCS is influenced by the positioning of a nucleus at the center of mass (as in atoms or molecules such as CO_2) compared to diatomic molecules such as H_2. For intermediate geometries, the positions of the binary and recoil peaks are similar for *He* and H_2, but the recoil peak is generally suppressed more in the H_2 case. This is most clearly demonstrated in the coplanar geometry, where almost no recoil peak is found experimentally or theoretically for H_2, but in the *He* case the recoil peak has a similar magnitude compared to the binary peak.

4.2. Unequal-energy sharing

Unequal-energy-sharing TDCS (with one electron having 18 eV and the other 2 eV of the available outgoing energy) are presented in Figs. 3 and 4 for a variety of gun angles ψ. Examining the asymmetric energy sharing case is instructive as it breaks the "doubly symmetric" conditions found for these measurements at equal-energy sharing. Figures 3 and 4 show a similar trend to that found for equal-energy sharing: the best agreement between theory and experiment is found for large ψ values. The TDCC calculations find a binary peak position slightly closer to the experimental position as compared to the 3DW calculations. The agreement between theory and experiment worsens at lower ψ values, but the discrepancies are perhaps not as great as for the equal energy-sharing case. For the coplanar and low-ψ geometries, the TDCC and 3DW calculations predict somewhat different binary peak positions, although the measurements are such that it is difficult to gauge which set of calculations are in best agreement with the data. The large differences in magnitude of the TDCS are also not as evident for the unequalenergy- sharing case. We also observe that the TDCC calculations predict extra structure in the TDCS for low ψ values, which are not found in the measurements or the 3DW calculations.

The TDCC calculations again find the largest cross section for the coplanar geometry. The experimental data indicates that the largest cross section is found at around ψ =45°, although this may be somewhat ambiguous since the measurements could not be made at low enough ξ values to fully map out the binary peak position for low ψ values. However, the 3DW (with CP) calculations also find a maximum for ψ =45°, although the drop in the TDCS as ψ is decreased is gradual.

5. Conclusions

We have presented a joint experimental and theoretical study of the triple differential cross sections arising from the electron-impact ionization of H_2 at an incident electron energy of 35.4 eV. Results have been presented for both equal (E_1=E_2=10 eV) and unequal (E_1=18 eV, E_2=2 eV) energy sharings, for a variety of experimental geometries, for cases where the molecular orientation is unknown.

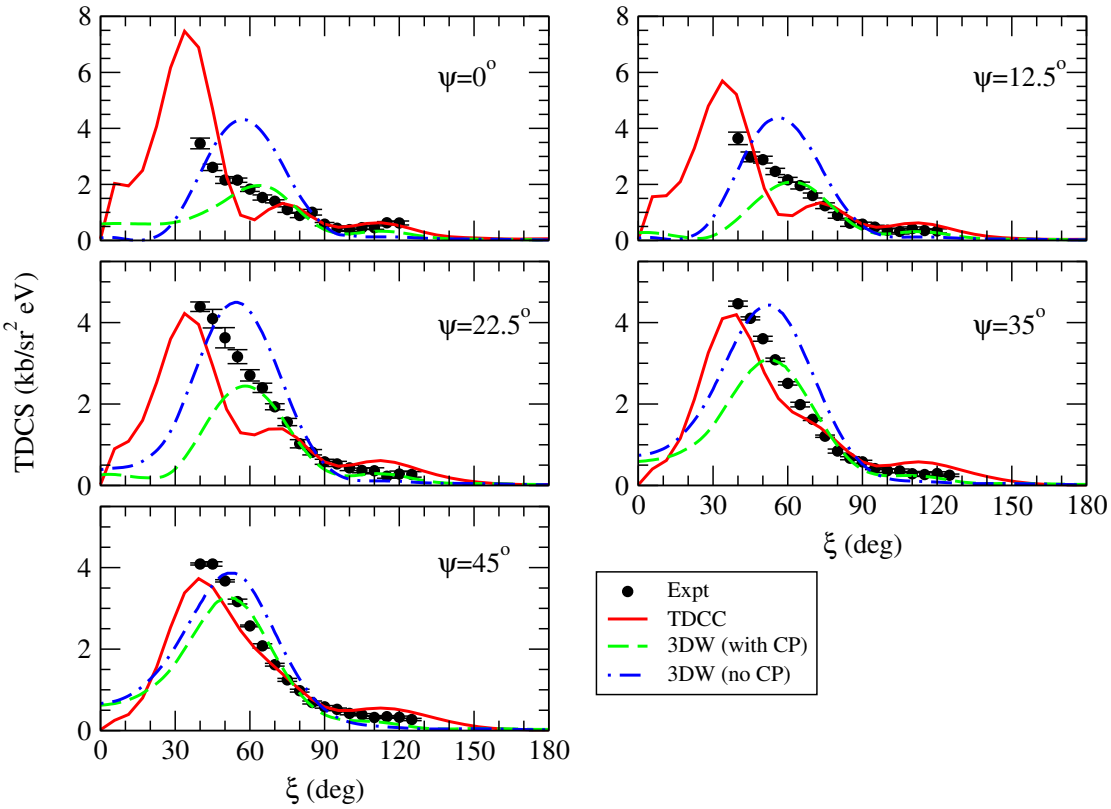

Figure 3: (Color online) Same as Fig. 2, except for unequal energy sharing: E_1=18 eV; E_2=2 eV, for ψ values ranging from 0 to 45 degrees. The 3DW (with CP) cross sections are divided by 3.7 and the 3DW (no CP) cross sections are divided by 4.5 to allow a better comparison with the other results.

We find that time-dependent close-coupling (TDCC) calculations and molecular distorted-wave (3DW) calculations give good agreement with measurements for large gun angle values, and especially for the perpendicular geometry. At lower gun angles, and for the coplanar geometry, the agreement between experiment and theory is not as satisfactory. In the 3DW calculations, inclusion of a correlation-polarization potential was found to improve the agreement with experiment, but inclusion of this potential did not alter the TDCC calculations.

In future work, we hope to measure cross sections from molecules oriented with respect to the electron beam. These measurements will test recent predictions of the TDCS for ionization from oriented molecules [32], and may also shed some light on the

discrepancies which exist between theory and experiment for the coplanar geometry TDCS as discussed here.

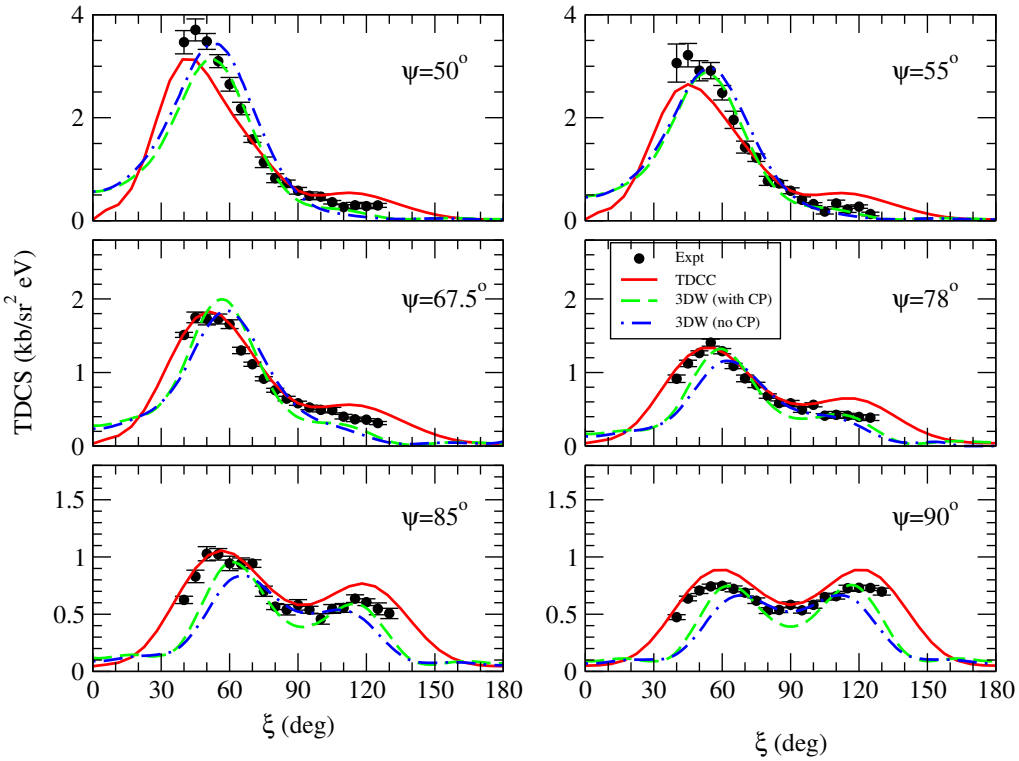

Figure 4: (Color online) Same as Fig. 3, for ψ values ranging from 50 to 90 degrees.

Acknowledgements

The Los Alamos National Laboratory is operated by Los Alamos National Security, LLC for the National Nuclear Security Administration of the U.S. Department of Energy under Contract No. DE-AC5206NA25396. A portion of this work was performed through DOE and NSF grants to Auburn University. Computational work was carried out at the NCCS in Oak Ridge, TN, and through a LANL Institutional Computing Resources grant. A portion of this work was done under National Science Foundation under Grant No. PHY- 0757749, and we acknowledge the EPSRC (U.K.) for additional support to C.K

References

[1] E. Weigold and I. E. McCarthy, *Electron Momentum Spectroscopy* _Kluwer, Dordrecht, (1999).

[2] A. J. Murray, M. B. J. Woolf, and F. H. Read, J. Phys. B **25**, 3021 (1992).

[3] A. J. Murray and F. H. Read, J. Phys. B **26**, L359 (1993).

[4] J. Roder, M. Baertschy, and I. Bray, Phys. Rev. A **67**, 010702(R) (2003).

[5] J. Röder, H. Ehrhardt, C. Pan, A. F. Starace, I. Bray, and D. V. Fursa, Phys. Rev. Lett. **79**, 1666 (1997).

[6] A. J. Murray and F. H. Read, Phys. Rev. A **63**, 012714 (2000).

[7] J. G. Childers, K. E. James, M. Hughes, I. Bray, M. Baertschy, and M. A. Khakoo, Phys. Rev. A **68**, 030702(R) (2003).

[8] J. G. Childers, K. E. James, I. Bray, M. Baertschy, and M. A. Khakoo, Phys. Rev. A **69**, 022709 (2004).

[9] M. Dürr, C. Dimopoulou, B. Najjari, A. Dorn, and J. Ullrich, Phys. Rev. Lett. **96**, 243202 (2006).

[10] M. Dürr, C. Dimopoulou, A. Dorn, B. Najjari, I. Bray, D. V. Fursa, Z. Chen, D. H. Madison, K. Bartschat, and J. Ullrich, J. Phys. B **39**, 4097 (2006).

[11] T. N. Rescigno, M. Baertschy, W. A. Isaacs, and C. W. Mc- Curdy, Science **286**, 2474 (1999).

[12] M. Baertschy, T. N. Rescigno, W. A. Isaacs, X. Li, and C. W. McCurdy, Phys. Rev. A **63**, 022712 (2001).

[13] I. Bray, Phys. Rev. Lett. **89**, 273201 (2002).

[14] I. Bray, K. Bartschat, and A. T. Stelbovics, Phys. Rev. A **67**, 060704(R) (2003).

[15] J. Colgan and M. S. Pindzola, Phys. Rev. A **74**, 012713 (2006).

[16] I. Bray, J. Phys. B **33**, 581 (2000).

[17] I. Bray, D. V. Fursa, J. Röder, and H. Ehrhardt, J. Phys. B **30**, L101 (1997).

[18] S. Rioual, J. Röder, B. Rouvellou, H. Ehrhardt, A. Pochat, I. Bray, and D. V. Fursa, J. Phys. B **31**, 3117(1998).

[19] A. T. Stelbovics, I. Bray, D. V. Fursa, and K. Bartschat, Phys. Rev. A **71**, 052716 (2005).

[20] J. Colgan, M. S. Pindzola, G. Childers, and M. A. Khakoo, Phys. Rev. A **73**, 042710 (2006).

[21] M. Takahashi, N. Watanabe, Y. Khajuria, Y. Udagawa, and J. H. D. Eland, Phys. Rev. Lett. **94**, 213202 (2005).

[22] D. S. Milne-Brownlie, M. Foster, J. Gao, B. Lohmann, and D. H. Madison, Phys. Rev. Lett. **96**, 233201 (2006).

[23] E. M. Staicu-Casagrande, A. Naja, F. Mezdari, A. Lahmam- Bennani, P. Bolognesi, B. Joulakian, O. Chuluunbaatar, O. Al- Hagan, D. H. Madison, D. V. Fursa, and I. Bray, J. Phys. B **41**, 025204 (2008).

[24] C. R. Stia, O. A. Fojón, P. F. Weck, J. Hanssen, and R. D. Rivarola, J. Phys. B **36**, L257 (2003).

[25] J. Gao, D. H. Madison, and J. L. Peacher, J. Chem. Phys. **123**, 204314 (2005).

[26] J. Gao, D. H. Madison, and J. L. Peacher, Phys. Rev. A **72**, 020701_R) (2005).

[27] J. Gao, D. H. Madison, and J. L. Peacher, J. Phys. B **39**, 1275 (2006).

[28] J. Gao, D. H. Madison, and J. L. Peacher, Phys. Rev. A **72**, 032721(2005).

[29] J. Gao, J. L. Peacher, and D. H. Madison, J. Chem. Phys. **123**, 204302(2005).

[30] C. Kaiser, D. Spieker, J. Gao, M. Hussey, A. Murray, and D. H. Madison, J. Phys. B **40**, 2563 (2007).
[31] O. Al-Hagan, C. Kaiser, D. Madison, and A. J. Murray, Nat.Phys. **5**, 59 (2008).
[32] J. Colgan, M. S. Pindzola, F. Robicheaux, C. Kaiser, A. J. Murray, and D. H. Madison, Phys. Rev. Lett. **101**, 233201(2008).
[33] A. J. Murray, J. Phys. B **38**, 1999 (2005).
[34] J. B. Furness and I. E. McCarthy, J. Phys. B **6**, 2280 (1973).
[35] J. P. Perdew and A. Zunger, Phys. Rev. B **23**, 5048 (1981).
[36] N. T. Padial and D. W. Norcross, Phys. Rev. A **29**, 1742 (1984).
[37] S. J. Ward and J. H. Macek, Phys. Rev. A **49**, 1049 (1994).
[38] M. S. Pindzola *et al.*, J. Phys. B **40**, R39 (2007).
[39] M. S. Pindzola, F. Robicheaux, and J. Colgan, J. Phys. B **38**, L285 (2005).
[40] M. S. Pindzola, F. Robicheaux, S. D. Loch, and J. P. Colgan, Phys. Rev. A **73**, 052706 (2006).
[41] A. J. Murray and F. H. Read, Phys. Rev. Lett. **69**, 2912 (1992).
[42] A. J. Murray and F. H. Read, Phys. Rev. A **47**, 3724 (1993).
[43] A. J. Murray, Meas. Sci. Technol. **14**, N72 (2003).
[44] A. J. Murray, M. J. Hussey, and A Venables, Meas. Sci. Technol. **16**, N19 (2005).
[45] A. J. Murray, B. C. H. Turton, and F. H. Read, Rev. Sci. Instrum. **63**, 3346 (1992).
[46] J. S. Alexander, A. C. Laforge, A. Hasan, Z. S. Machavariani, M. F. Ciappina, R. D. Rivarola, D. H. Madison, and M. Schulz, Phys. Rev. A **78**, 060701(R) (2008).
[47] J. Colgan *et al.* (unpublished).

III. Deep Interference Minima in Non-coplanar Triple Differential Cross Sections for the Electron-Impact Ionization of Small Atoms and Molecules

J Colgan[1], O Al-Hagan[2], D H Madison[2], A J Murray[3] and M S Pindzola[4]

[1] *Theoretical Division, Los Alamos National Laboratory, NM 87545, USA*

[2] *Physics Department, Missouri University of Science and Technology, Rolla, MO 65409, USA*

[3] *School of Physics and Astronomy, University of Manchester, Manchester M13 9PL, UK*

[4] *Department of Physics, Auburn University, Auburn, AL 36849, USA*

Abstract

The time-dependent close-coupling method and a distorted-wave approach are used to explore deep minima discovered in the non-coplanar triple differential cross sections for the electron-impact ionization of helium. This phenomenon has been well studied experimentally but so far has not been investigated by a non-perturbative theoretical approach. We find that our time-dependent calculations reproduce very well the experimental minima, and that the distorted-wave calculations also confirm this phenomenon. Further investigations reveal that the minima appear to be due to deep destructive interference between the partial-wave contributions which make up the cross sections. We also show that similar minima may be found in triple differential cross sections arising from the electron-impact ionization of atomic and molecular hydrogen.

1. Introduction

Investigations of the electron-impact ionization of small atoms and molecules (commonly known as (e, 2e) processes) continue to further our knowledge of the nature of the three-body Coulomb dynamics inherent in the final state of this process [1]. In recent years, significant progress has been made on the theoretical side, with several theories demonstrating excellent agreement with a variety of experimental data yielding multiple differential cross sections for ionization of H [2–7] and *He* [8–11], for a variety of outgoing electron geometries and kinematics, and from near threshold to relatively high impact energies [12, 13].

Experimental investigations of (e, 2e) processes in small atoms have been underway for several years, since the earliest pioneering measurements (see, e.g., [14]). A variety of multiple coincidence techniques, together with more sophisticated optimization and computer control of the electron spectrometers, have allowed precise measurements to be conducted over a wider range of electron angles and kinematics [12, 15, 16, 17, 18]. Recently, several of these techniques have been extended to investigate (e, 2e) processes in small molecules at low incident energies, with corresponding theoretical progress now showing reasonable agreement with these new measurements [19–22].

An outstanding puzzle in some of the earlier (e, 2e) measurements [16, 17] was the presence of an unexpected deep and sharp minimum in the triple differential cross sections (TDCS) measured from helium out of the coplanar geometry. The minimum was observed in the 'doubly symmetric' geometry pioneered by the Manchester group and shown in figure 1. The doubly symmetric label refers to the equal energies of the outgoing electrons and the same angle (ξ) made by the outgoing electrons with respect to the axis defined by the incident electron beam. The minimum in the TDCS was most clearly observed for measurements made with an incident electron energy of 64.6 eV (where the outgoing electrons have equal energies of 20 eV), and for a gun angle of ψ = 67.5° (where the gun angle is the angle between the incident electron beam and the detection plane as shown in figure 1). Although the TDCS often is relatively small between the two usual forward and backward scattering peaks, it is not expected to go to zero, as was observed experimentally. Minima were also found to be present for other

incident electron energies, and for a neon target ionized from the 2s shell [23, 24]. These minima are unexpected because their positions do not correspond to the 'usual' dips in the TDCS.

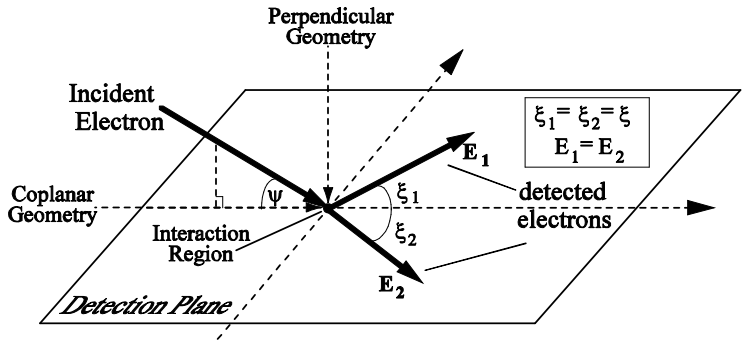

Figure 1: The experimental geometry. The incident electron beam makes an angle ψ with respect to the detection plane defined by the analysers. The analysers rotate through angles ξ_1 and ξ_2 as shown. In the measurements discussed here, $\xi_1 = \xi_2$. A common normalization point exists for all gun angles when $\xi_1 = \xi_2 = 90°$.

For example, there is usually a (near) zero in the TDCS for the geometries where both electrons leave along the same direction (due to Coulomb repulsion between the equal energy electrons), and in double photoionization differential cross sections, zeros in the cross section have long been identified as due to selection rules governing the two-electron ejection. The minima observed in the (e, 2e) experiments did not seem to be associated with any known selection rule, and a selection rule argument seemed even more unlikely since the angular position of the minima changed with the incident energy of the electron. Early distorted-wave approaches to the (e, 2e) problem [25] had difficulty reproducing this minimum, but modified 3C (three- Coulomb product wavefunctions) calculations [26, 27], and later modified distorted-wave approaches [24] showed that the TDCS minimum could be ascribed to interference between the various terms which make up the *T*-matrix. However, these calculations predicted slightly different minima positions than observed experimentally, and also predicted that no

minima should be observed for (e, 2e) ionization measurements from atomic hydrogen targets.

2. Theoretical approach

In this communication, we explore the minimum in the TDCS from helium. The time-dependent close-coupling (TDCC) [28] method and a three-body distorted-wave (3DW) approach [29, 30] are used to compute the TDCS for a variety of electron energies. TDCC calculations are seen to predict minima in the TDCS in very good agreement with previous measurements. Further investigations also find that, within our partial wave formulation of the (e, 2e) scattering problem, the minimum is due to deep destructive interference between the various partial waves which contribute to the cross section. We also find that the minimum found for helium can also be seen in TDCS from atomic hydrogen (although this is weaker than in helium) and from molecular hydrogen (when the TDCS is considered from a molecule at a fixed orientation with respect to the scattering geometry).

The time-dependent close-coupling theory as applied to electron-impact ionization has previously been well described [11, 28]. The central idea is the propagation of the time dependent Schrodinger equation for the two outgoing electrons with the interaction between the two electrons treated in full. The remaining electron (in the case of helium and molecular hydrogen) is frozen, and its interaction with the outgoing electrons is represented through direct and local exchange potential terms.

In the TDCC approach, the triple differential cross section for electron-impact ionization of helium is given by

$$\frac{d^3\sigma}{dE_1 d\Omega_1 d\Omega_2} = \frac{\pi}{4k_0^2}\frac{1}{k_1 k_2}\sum_S (2S+1)\int dk_1 \int dk_2$$

$$\times\delta\left(\alpha - \tan^{-1}\left[\frac{k_2}{k_1}\right]\right)\left|\sum_L i^L\sqrt{2L+1}\right.$$

$$\times\sum_{l_1 l_2}(-i)^{l_1+l_2} e^{i(\sigma_{l_1}+\sigma_{l_2})} e^{i(\delta_{l_1}+\delta_{l_2})} P_{l_1 l_2}^{LS}(k_1,k_2)$$

$$\times \sum_{m_1,m_2} C^{l_1 l_2 L}_{m_1 m_2 0} Y_{l_1 m_1}(\hat{k}_1) Y_{l_2 m_2}(\hat{k}_2) \Bigg|^2 , \qquad (1)$$

where the incident electron energy is $k_0^2/2, \alpha$ is the angle in the hyperspherical plane between the two outgoing momenta vectors k_1 and k_2, $Y_{lm}(\hat{k})$ is a spherical harmonic, $C^{l_1 l_2 l_3}_{m_1 m_2 m_3}$ is a Clebsch–Gordan coefficient, and σ_l and δ_l are Coulomb and distorted-wave phase shifts, respectively. Integration of the TDCS over all electron angles and energies recovers the total ionization cross section, where we remember that multiplication by the initial state occupation number is also required (which is 2 for *He* and H_2). The function $P^{LS}_{l_1 l_2}(k_1, k_2)$ is formed by projecting the final two electron radial wavefunction (after propagation to a time *T*) $P^{LS}_{l_1 l_2}(r_1, r_2, t = T)$ onto the one-electron continuum orbitals via

$$P^{LS}_{l_1 l_2}(k_1, k_2) = \iint P_{k_1 l_1}(r_1) P_{k_2 l_2}(r_2) \times P^{LS}_{l_1 l_2}(r_1, r_2, t = T) dr_1 dr_2 , \qquad (2)$$

where the $P_{kl}(r)$ are box normalized continuum orbitals. We note that, for this highly symmetric geometry, only singlet terms in the expansion in equation (1) contribute to the TDCS. The TDCC calculations discussed below were performed in a similar manner to previously published calculations [11], where details of the numerics of the calculation may be found.

The three-body distorted-wave (3DW) approach to electron-impact ionization of atoms and molecules has been described in detail previously [22, 29–32]. The scattering amplitude is given by

$$T = \left\langle \chi_a^-(\vec{k}_a, \boldsymbol{r}_1) \chi_b^-(\vec{k}_b, \boldsymbol{r}_2) C_{scat-eject}(r_{12}^{ave}) \middle| V - U_i \middle| \phi_j(\boldsymbol{r}_2) \chi_i^+(\vec{k}_i, \boldsymbol{r}_1) \right\rangle , \qquad (3)$$

where distorted-waves χ are used to represent the incident (*i*), scattered (*a*) and ejected (*b*) electrons. The initial bound-state wavefunction is φ_j ; for *He*, a Hartree–Fock wavefunction is used, and for H_2, an orientation-averaged molecular wavefunction is used [33]. The factor $C_{scat-eject}(r_{12}^{ave})$ is the average Coulomb-distortion factor [34], *V* is the initial state interaction potential between the incident electron and the neutral atom or molecule, and U_i is the initial state distorting potential. In the 3DWcalculations presented below for H_2, we present two different sets of calculations, one of which contains a

correlation–polarization potential [35, 36] (labeled with CP) and one without this potential (labeled no CP). Inclusion of this potential was found to make a noticeable difference to the H_2 calculations, but made very little difference to the *He* calculations also presented here.

3. Results and discussions

In figure 2, we compare previous experimental measurements [17] with TDCC and 3DW calculations, where the measurements are normalized to the absolute TDCC calculations. The measurements presented here were all made using the Manchester computer-controlled and computer optimized apparatus, have been fully described previously [15–18] and so will not be discussed again here. We note that, for some of these energies, convergent close-coupling (CCC) calculations also show good agreement with these experimental data [10]. The TDCC calculations are in excellent agreement with the measurements, and the TDCC calculations and experiment clearly display the strong minima in the TDCS. The 3DW calculations for incident energies of 44.6 and 54.6 eV also find the strong minima in the TDCS, although this method predicts the minima position at a slightly different angle than experiment or the TDCC calculations. Puzzlingly, the 3DW calculations at 64.6 eV do not show a minimum, although the cross section does dip in the region of the experimental minimum. The ψ value for which the minima are deepest appears to decrease as the incident energy is increased (subsequent TDCC calculations for E = 64.6 eV find a deeper minimum when ψ = 61.5°, although there are no measurements at this angle). The ξ angle at which the minima appear also increases as the incident energy increases. The TDCC calculations and experiment also agree extremely well as to the position and heights of the forward and backward peaks in the TDCS.

To further analyse the source of the minima in the TDCS, in figure 3 we present TDCC calculations at ψ = 61.5° (the angle at which the minimum was found to be deepest). The full TDCC calculations in this energy range include partial waves up to L = 9 in the expansion in equation (1). Figure 3 shows TDCC calculations which have been truncated at various L values as indicated. Interestingly, it is not until partial waves

L = 2 and higher are included that the TDCS minimum begins to appear. We also note that by L = 6 the cross section is already well converged at this energy.

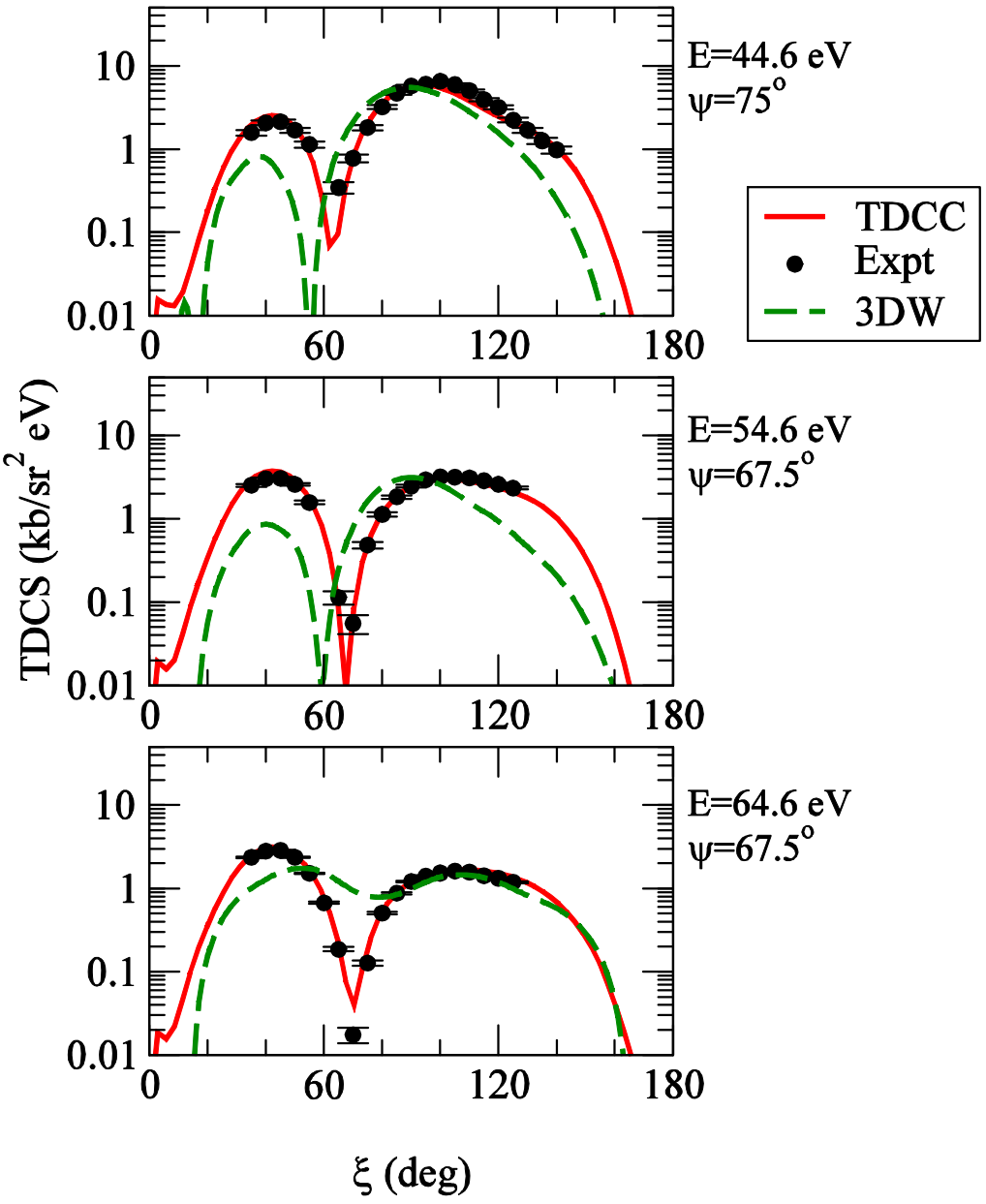

Figure 2: Triple differential cross sections for the electron-impact ionization of helium for three incident electron energies and gun angles as indicated. In all cases, the outgoing electrons have equal energy sharing. The experimental data are compared with TDCC calculations (solid red lines) and with 3DW calculations (dashed green lines) 1.0 kb = 1.0×10^{-21} cm^2.

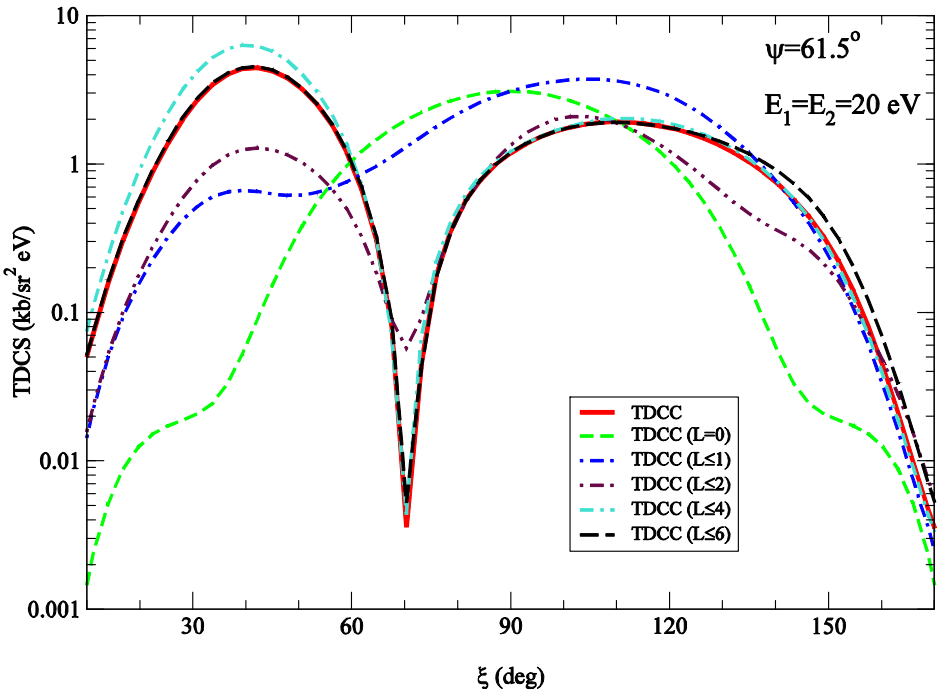

Figure 3: TDCC calculations for the triple differential cross sections for the electron-impact ionization of helium for an incident electron energy of 64.6 eV, at a gun angle of $\psi = 61.5°$, and for equal energy sharing outgoing electrons. A complete TDCC calculation (including $L = 0$–9) is indicated by the solid red line. The various dashed lines show TDCC calculations which include fewer partial wave contributions, as indicated in the caption.

We can further examine the TDCC calculations by considering the contributions from individual partial waves, as shown by the dashed lines in each panel of figure 4. The black dashed lines show the contributions from each partial wave from $L = 0$ to $L = 8$. The red solid lines show the contribution from the cross terms (or interference terms) which arise in the coherent sum over L in equation (1). For example, the red solid line in the upper middle panel shows the cross term contribution between the partial waves $L = 0$ and $L = 1$. The total cross section can be recovered from this figure by summing each individual partial wave contribution (all black dashed lines) and the final red solid line (lower right panel), which represents the cross term contribution between all partial waves. It is immediately obvious that it is the *interference* between the partial waves which causes the minima in the TDCS (the dotted vertical line indicates the position of

the minima in the total TDCS). The individual (or direct) partial wave contributions are significant for L = 0–2 and contribute strongly in the region from $\xi \sim 60$ to 120°. The interference terms, however, *destructively* contribute to the TDCS in this region, and as more partial waves are included, the destructive term is enhanced. This explains the findings of figure 3; when contributions from L = 0, 1 only are included, the positive contribution from the direct terms is much larger than the destructive interference term, so that no minima is found. However, as more partial waves are included, the destructive contribution becomes larger, leading eventually to the deep minima observed in the full calculations and as found experimentally.

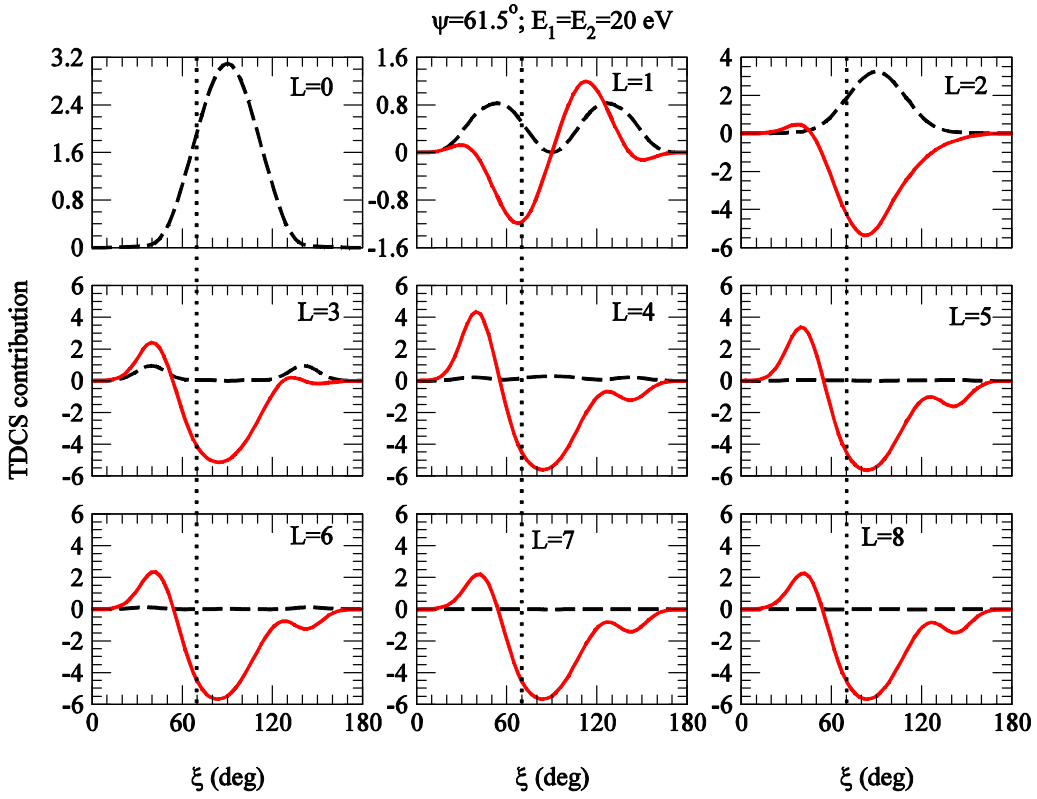

Figure 4: TDCC calculations for the same case as figure 2. Here, we show the contributions from individual partial waves (dashed black lines) in each panel up to L = 8. The solid red lines signify the contribution from the interference (cross) terms inherent in the coherent sum in equation (1). For example, the red line in the upper right panel shows the contribution from the L = 0, 1, 2 cross terms. The vertical dotted lines indicate the position of the minimum in the TDCS in figure 3

Similar investigations for the other incident energies presented in figure 2 reach the same conclusion: that it is the deep destructive interference between the contributing partial waves in the sum in equation (1) which causes the observed minima in the TDCS. Our findings are consistent with the conclusions of previous 3C calculations [26, 27] that destructive interference is the cause of the TDCS minima. However, in the previous 3C formulation [27], it was stated that the interference is manifested between the various terms which make up the T-matrix, and that the decisive contribution which gives rise to the minima was the interference due to the T_3 term (which represents the initial scattering off the passive (frozen) electron). In the quite different TDCC approach, in which the initial wavefunction is expanded over partial waves, the destructive contribution arises from interference between the partial wave contributions. However, our 3DW approach, which only includes the T_1 term (scattering off the ionized electron), also finds a clear minimum in the TDCS (the 3DW approach uses orthogonal wavefunctions and so the T_2 term, representing the scattering off the nucleus, is automatically zero). Yet the minimum in the TDCS found in the 3DW calculations clearly *cannot* be due to interference between the various terms which constitute the T-matrix, since only one term *(T_1)* exists in our 3DW approach. Berakdar and Briggs [27] also stated that, since in (e, 2e) experiments from atomic hydrogen no T_3 term exists (since there is no passive electron), the deep minima should not be observed. Their 3C calculations of the TDCS for (e, 2e) from atomic hydrogen found a weak minimum at low ψ values. We have now also undertaken TDCC and 3DW calculations of the TDCS for (e, 2e) on atomic hydrogen, as shown in figure 5, although at a different incident energy than [27]. We find that a fairly sharp minimum does exist, which is also most evident for low ψ values close to the coplanar geometry. At this energy sharing ($E_1 = E_2 = 10$ eV), the minimum TDCS does not reach zero, but does reach the lowest value of the TDCS near $\xi = 0°$, where the TDCS is very small due to electron–electron repulsion. Similar investigations as for the helium case reveal that the minimum in this atomic hydrogen case is also due to deep destructive interference between the various partial-wave contributions.

As a final demonstration of the minimum in the TDCS, we consider in figure 6 the TDCS from electron-impact ionization of molecular hydrogen at a gun angle of 67.5°, again for equal energy sharing outgoing electrons with $E_1 = E_2 = 10$ eV. Comparisons

with experiment (where the molecular orientation is unknown) and theoretical TDCC and 3DW calculations (averaged over all molecular orientations) have previously been published [21, 22].

As a final demonstration of the minimum in the TDCS, we consider in figure 6 the TDCS from electron-impact ionization of molecular hydrogen at a gun angle of 67.5°, again for equal energy sharing outgoing electrons with $E_1 = E_2 = 10$ eV. Comparisons with experiment (where the molecular orientation is unknown) and theoretical TDCC and 3DW calculations (averaged over all molecular orientations) have previously been published [21, 22]. In figure 6, it is again seen that the agreement between the averaged TDCC calculations and the measurements is excellent, and that the 3DW calculations also are in reasonable agreement with experiment. No minima are observed in the experimental data for randomly oriented molecules. However, by analyzing TDCC calculations at various fixed molecular orientations, minima in the TDCS *can* be observed. For example, in figure 6, TDCC calculations at a molecular orientation of $\theta_N = 50°$; $\varphi_N = 0°$ (where the angles refer to the orientation of the molecule with respect to the z-axis, where the z-axis is defined by the incoming electron beam) find a sharp minimum at a scattering angle ξ around 75°. Since measurements of the TDCS from molecules in which the orientation is known have not yet been made, these calculations represent a prediction for which experimental verification would be highly desirable.

In summary, we have explored the minima in the TDCS first found by (e, 2e) experiments on helium. TDCC and 3DW calculations are in excellent agreement with experiment for helium and reproduce the experimental minima position and depth very well. Analysis of the TDCC calculations finds that the minima appear due to deep destructive interference between the various contributing partial waves which are included in the TDCC calculations. We also demonstrate that a minimum can be observed in the TDCS from atomic hydrogen (although the minima are somewhat weaker than in the helium case). We also find, for the first time, that a minimum is predicted in the TDCS from molecular hydrogen, although only if consideration is made of the TDCS from a molecule with a specific orientation.

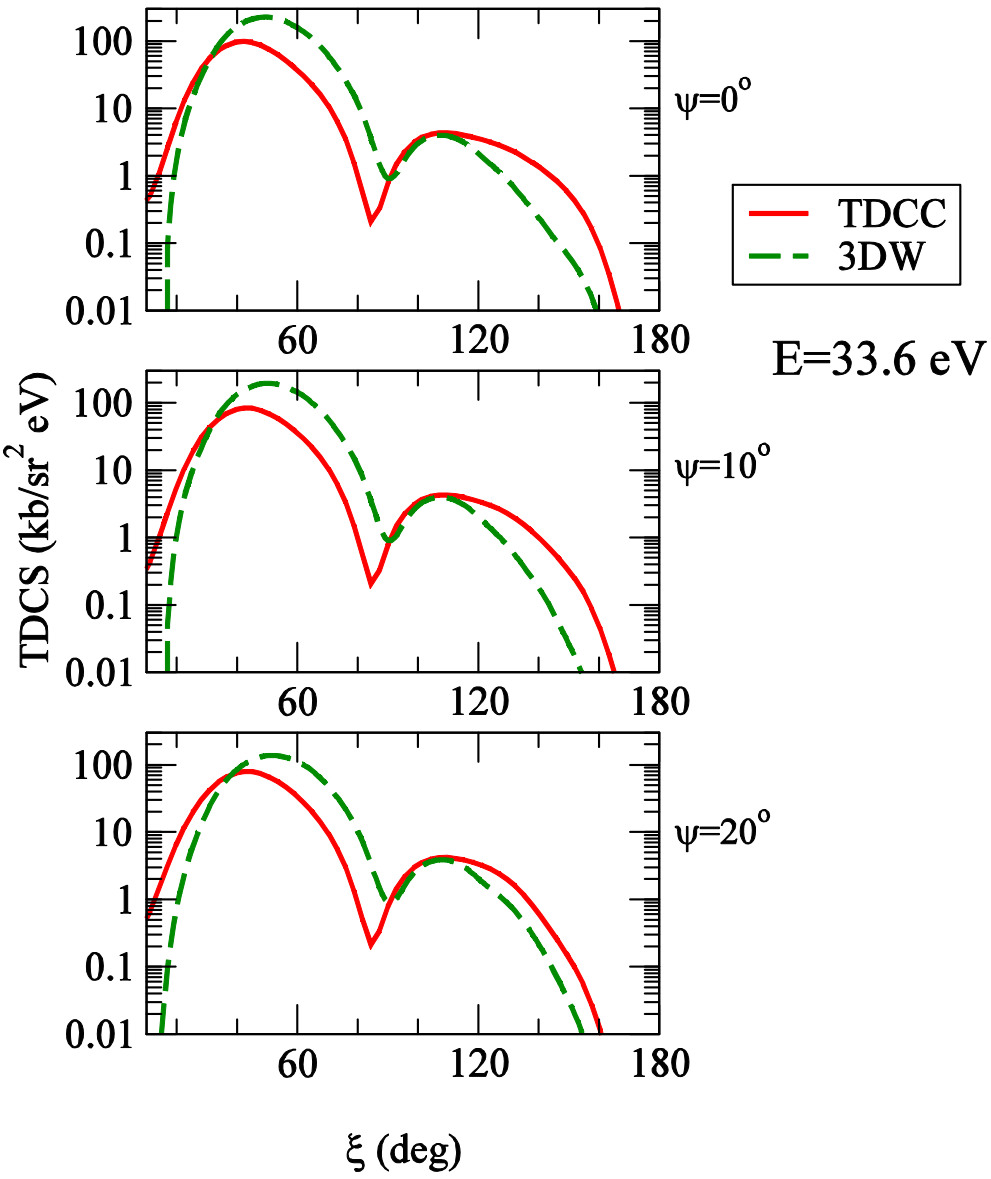

Figure 5: TDCC and 3DW calculations of the triple differential cross sections for the electron-impact ionization of atomic hydrogen at an incident energy of 33.6 eV, for various gun angles as indicated. The $\psi = 0^{\circ}$ case corresponds to the coplanar geometry.

Some outstanding questions still remain with regard to the deep minima phenomena. In particular, there is no theoretical guideline as to *where* the minima in the TDCS will occur, i.e. at which specific geometry, such as the selection rules derived for zeros in the TDCS for double photoionization [37]. Although it seems clear that the

minima are due to interference effects, there is as yet no obvious physical argument as to why this interference should occur for these particular geometries. However, we have demonstrated that the TDCS minima first observed over 15 years ago appear to be a *general* feature of (e, 2e) studies for the specialized symmetric geometries under consideration, and so it would be extremely interesting to investigate this phenomenon further in more complicated systems [23].

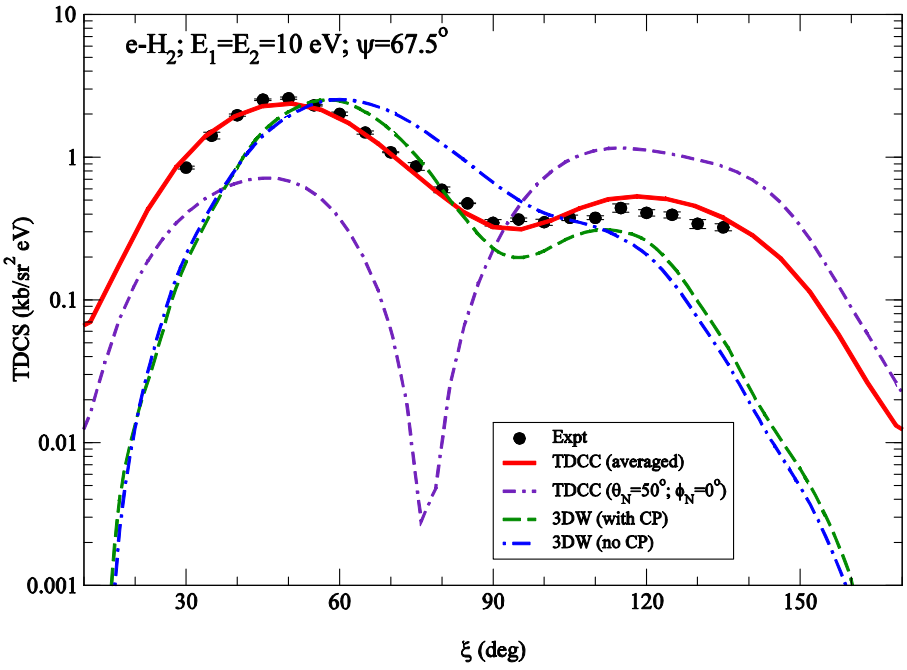

Figure 6: Triple differential cross sections for the electron-impact ionization of molecular hydrogen at an incident energy of 35.4 eV, for equal energy sharing outgoing electrons. Experimental data are compared with TDCC calculations (thick red line) which are averaged over all molecular orientations and two sets of 3DW calculations. The calculations labeled 3DW (with CP) include a correlation-polarization term, while the calculation labeled 3DW (no CP) omits the correlation-polarization term. Both sets of 3DW calculations are divided by 6.3 to allow a better comparison with other results. The double-dashed purple line indicates the TDCC calculation for a specific molecular orientation ($\theta_N = 50°$; $\varphi_N = 0°$), where it can be seen that a deep interference minimum is predicted.

Acknowledgments

The Los Alamos National Laboratory is operated by Los Alamos National Security, LLC for the National Nuclear Security Administration of the US Department of Energy under contract no: DE-AC5206NA25396. A portion of this work was performed through DOE and NSF grants to Auburn University. Computational work was carried out at NERSC, in Oakland, CA, and through a LANL Institutional Computing Resources award. A portion of this work was done under National Science Foundation grant no: PHY-0757749, and we acknowledge the EPSRC (UK) for supporting the experimental program in the UK.

References

[1] Weigold E and McCarthy I E 1999 Electron Momentum Spectroscopy (Dordrecht: Kluwer)
[2] Rescigno T N, Baertschy M, Isaacs W A and McCurdy C W *1999 Science* **286** 2474
[3] Baertschy M, Rescigno T N, Isaacs W A, Li X and McCurdy C W 2001 *Phys. Rev.* A **63** 022712
[4] Bray I 2000 *J. Phys.* B: *At. Mol. Opt. Phys*. **33** 581
[5] Bray I 2002 *Phys. Rev. Lett.* **89** 273201
[6] Bray I, Bartschat K and Stelbovics A T 2003 *Phys. Rev*. A **67** 060704
[7] Colgan J and Pindzola M S 2006 *Phys. Rev*. A **74** 012713
[8] Bray I, Fursa D V, R¨oder J and Erhardt H 1997 *J. Phys*. B*: At. Mol. Opt. Phys*. **30** L101–8
[9] Rioual S, R¨oder J, Rouvellou B, Erhardt H, Pochat A, Bray I and Fursa D V 1998 *J. Phys.* B: *At. Mol. Opt. Phys*. **31** 3117
[10] Stelbovics A T, Bray I, Fursa D V and Bartschat K 2005 *Phys. Rev.* A **71** 052716
[11] Colgan J, Pindzola M S, Childers G and Khakoo M 2006 *Phys. Rev*. A **73** 042710
[12] D¨urr M, Dimopoulou C, Najjari B, Dorn A and Ullrich J 2006 *Phys. Rev. Lett*. **96** 243202
[13] D¨urr M, Dimopoulou C, Dorn A, Najjari B, Bray I, Fursa D V, Chen Z, Madison D H, Bartschat K and Ullrich J 2006 *J. Phys.* B: *At. Mol. Opt. Phys*. **39** 4097–111
[14] Erhardt H, Jung K, Knoth G and Schlemmer P 1986 *Z. Phys.* D **1** 3
[15] Murray A J, Woolf M B J and Read F H 1992 *J. Phys*. B: *At. Mol. Opt. Phys*. **25** 3021
[16] Murray A J and Read F H 1993 *J. Phys*. B: *At. Mol. Opt. Phys*. **26** L359–65
[17] Murray A J and Read F H 1993 *Phys. Rev*. A **47** 3724
[18] Murray A J, Read F H and Bowring N J 1997 *J. Phys*. B: *At. Mol. Opt. Phys*. **30** 387
[19] Murray A J 2005 *J. Phys*. B: *At. Mol. Opt. Phys*. **38** 1999
[20] Al-Hagan O, Kaiser C, Madison D H and Murray A J 2008 *Nature Phys*. **5** 59

[21] Colgan J, Pindzola M S, Robicheaux F, Kaiser C, Murray A J and Madison D H 2008 *Phys. Rev. Lett*. **101** 233201
[22] Colgan J, Al-Hagan O, Madison D H, Kaiser C, Murray A J and Pindzola M S 2009 *Phys. Rev*. A **79** 052704
[23] Murray A J and Read F H 2000 *Phys. Rev.* A **63** 012714
[24] Rasch J, Whelan C T, Allen R J, Lucey S P and Walters H R J 1997 *Phys. Rev.* A **56** 1379
[25] Zhang X, Whelan C T and Walters H R J 1990 *J. Phys*. B: *At. Mol. Opt. Phys*. **23** L173
[26] Berakdar J and Briggs J S 1994 *Phys. Rev. Lett*. **72** 3799
[27] Berakdar J and Briggs J S 1994 *J. Phys*. B: *At. Mol. Opt. Phys.* **27** 4271
[28] Pindzola M S et al 2007 *J. Phys*. B: *At. Mol. Opt. Phys*. **40** R39
[29] Prideaux A and Madison D H 2003 *Phys. Rev*. A **67** 052710
[30] Gao J, Madison D H and Peacher J L 2005 *J. Chem. Phys*. **123** 204314
[31] Gao J, Madison D H and Peacher J L 2005 *Phys. Rev.* A **72** 032721
[32] Gao J, Madison D H and Peacher J L 2005 *J. Phys*. B: *At. Mol. Opt. Phys*. **39** 1275
[33] Gao J, Madison D H and Peacher J L 2005 *J. Chem. Phys*. **123** 204302
[34] Ward S J and Macek J H 1994 *Phys. Rev*. A **49** 1049
[35] Perdew J P and Zunger A 1981 *Phys. Rev*. B **23** 5048
[36] Padial N T and Norcross D W 1984 *Phys. Rev*. A **29** 1742
[37] Maulbetsch F and Briggs J S 1995 *J. Phys.* B: *At. Mol. Opt. Phys*. **28** 551

IV. Electron Impact Ionization Cross Sections of H_2 for Low Energy Outgoing Electrons from 1 eV to 10 eV

Ola Al-Hagan[1], A. J. Murray[2], C. Kaiser[2], J. Colgan[3], and D. H. Madison[1]

[1]*Physics Department, Missouri University of Science and Technology, Rolla, MO 65409,USA*

[2]*School of Physics and Astronomy, Photon Science Institute, University of Manchester, Manchester M13 9PL, UK*

[3]*Theoretical Division, Los Alamos National Laboratory, New Mexico 87545, USA*

Abstract

Theoretical and experimental fully differential cross sections are presented for electron-impact ionization of molecular hydrogen in a plane perpendicular to the incident beam direction. The experimental data exhibit a maximum for 1 eV electrons detected 180° apart, and a minimum for 10 eV electrons. We investigate the different physical effects which cause back-to-back scattering and demonstrate that, over the energy range from 10 eV to 1 eV, a direct transition is observed from a region where Wannier threshold physics is essentially unimportant, to where it completely dominates.

Low electron energy (near threshold) ionization has been studied for atoms over the years and it is now well understood [1-3]. There have been several experiments and theories reported for near threshold ionization for hydrogen [4], helium [5], and heavier inert gasses [6], and the agreement between the experiment and theory is generally very good. By contrast, (e, 2e) studies for ionization of molecules at low energies has received relatively little attention until recently. Current models are now in reasonable agreement with experimental data for H_2 providing an understanding of the collision dynamics under the conditions used in the experiments [7-9]. These collisions provide direct information about the importance of three-body effects including electron-electron correlation, polarization, and multiple collisions in the ionization process.

Al-Hagan *et al*. [7] compared experimental and theoretical (e, 2e) results for ionization of H_2 and He (having the same number of electrons and protons) in a plane perpendicular to the incident beam direction (the *perpendicular plane*). The experimental measurements were performed with both final state electrons having 10 eV energy and the fully differential cross section (FDCS) was measured as a function of the relative angle between outgoing electrons. The experiments found that both H_2 and He had peaks in the cross sections at relative angles around 90° and 270°. In contrast, for back-to-back scattering at 180°, helium showed a very strong peak (the largest cross section) while H_2 had a very small minimum. It was demonstrated that the 90° and 270° peaks for both H_2 and He resulted from elastic scattering of the projectile from the target into the perpendicular plane, followed by a binary collision between projectile and target electrons. Since the binary collision occurs between particles with equal mass and energy, the mutual angle between the electrons is then 90° (or 270°). This process occurs for both atomic and molecular targets. For helium, it was shown that the large maximum resulted from one of the scattered electrons being very close to the nucleus, so that it elastically backscattered at 180° from the point nuclei. For the case of H_2, the electron-electron collision occurs *between* the two hydrogen nuclei where on average the net attractive force cancels, resulting in almost no backscattering and hence a minimum at 180°.

We have now extended the (10 eV, 10 eV) measurements for H_2 in the perpendicular plane to lower equal energy pairs down to (1 eV, 1 eV). We discovered

that the deep 180° *minimum* for (10 eV,10 eV) became decreasingly shallow as the energy lowered, and eventually developed into a *peak* at 180° for (1 eV,1 eV). The purpose of this paper is to identify the physical effects responsible for the minimum changing into a maximum. We show that at 1 eV the maximum is *not* related to nuclear scattering as was the case for 10 eV He, but rather is due to final state electron-electron repulsion (normally called post collision interaction (PCI)).

This finding is reminiscent of the Wannier law which predicts that at threshold, the electrons will emerge at 180° due to PCI. An interesting and unresolved question concerns the range of validity for the Wannier threshold law, and we show here that this starts to break down for electrons with energy (0.5 eV, 0.5 eV). However, we are close enough to this region at (1 eV, 1 eV) so that PCI is still dominant for the FDCS. Martinez et al [10] very recently showed that PCI was not dominant for these same energies for atomic targets, so this finding appears to be a phenomena associated with molecules. To our knowledge, this is the first direct observation of the transition from Wannier physics to non-threshold physics for fully differential cross sections of H_2. Surprisingly, the dominance of PCI becomes unimportant very quickly after 1 eV, and is found to be of no consequence for back-to-back scattering by 10 eV.

The apparatus used for the experimental studies in Manchester has been described in detail elsewhere [8, 9, 11]. Briefly, the spectrometer is fully computer controlled and computer optimized, and can access geometries from coplanar to the perpendicular plane. All results presented here were carried out in the perpendicular plane using an unselected energy electron gun and hemispherical energy analyzers to detect scattered and ejected electrons. The energy resolution was ~1 eV, and the angular resolution around ±3°. Different electron beam currents were used at each energy so as to optimize the coincidence signal to noise ratio, so all results are re-normalized to unity at the peak of the data for comparison to theory.

The molecular distorted wave Born approximation (MDW) has been presented previously [12] so only a short summary is presented here. The FDCS for the MDW is given by:

$$\frac{d^5\sigma}{d\Omega_a \Omega_b dE_b} = \frac{2}{(2\pi)^5}\frac{k_a k_b}{k_i}|T|^2 \qquad (1)$$

where $\vec{k}_i$, $\vec{k}_a$, and $\vec{k}_b$ are wave vectors for the initial, scattered and ejected electrons. The T-matrix is given by:

$$T^{MDW} = \left\langle \chi_a^-(\vec{k}_a, \mathbf{r}_1)\chi_b^-(\vec{k}_b, \mathbf{r}_2) \mid V - U_i \mid \phi_j^{OA}(\mathrm{r}_2)\chi_i^+(\vec{k}_i, \mathbf{r}_1) \right\rangle \qquad (2)$$

where $\mathbf{r}_1$, $\mathbf{r}_2$ are coordinates of the incident and bound electrons, χ_i, χ_a, and χ_b are distorted waves for the incident, scattered, and ejected electrons respectively, and $\phi_j^{OA}(r_2)$ is the initial bound-state wave-function approximated by the orientation averaged molecular wave-function. The initial state interaction V is the potential between the incident electron and neutral molecule, and U_i is a spherically symmetric molecular potential used to calculate the initial-state distorted wave for the incident electron $\chi_i^+(\vec{k}_i, \mathbf{r}_1)$. The final state is approximated as a product of distorted waves for the two continuum electrons which are calculated as with the initial state, except the spherically symmetric static distorting potential of the molecular ion is used instead of U_i.

The molecular three-body distorted wave approximation (M3DW) [13,14] is similar to the MDW except an electron-electron Coulomb repulsion factor is included in the final state wavefunction. Here we adopt the Ward-Macek average Coulomb-distortion factor between the two final state electrons [15]. When the Coulomb interaction is included in the final state wavefunction, PCI is included to all orders of perturbation theory and when only included in the perturbation, PCI is included only to first order.

The time-dependent close-coupling (TDCC) approach to electron-impact ionization of H_2 has also been described in detail previously [8,9]. For small impact electron energies, fewer partial waves are usually required than at higher impact energies, but the spatial grids required to fully converge the calculation may become very large. Since the TDCC calculations must also be run for each impact energy separately, the computational cost associated with deriving the required amplitudes for each energy is considerable. We therefore only present TDCC calculations for three outgoing energies, as detailed below.

Figure 1 compares experimental and theoretical FDCS for electron-impact ionization of H_2 for the case of equal final state electron energies in the perpendicular plane.

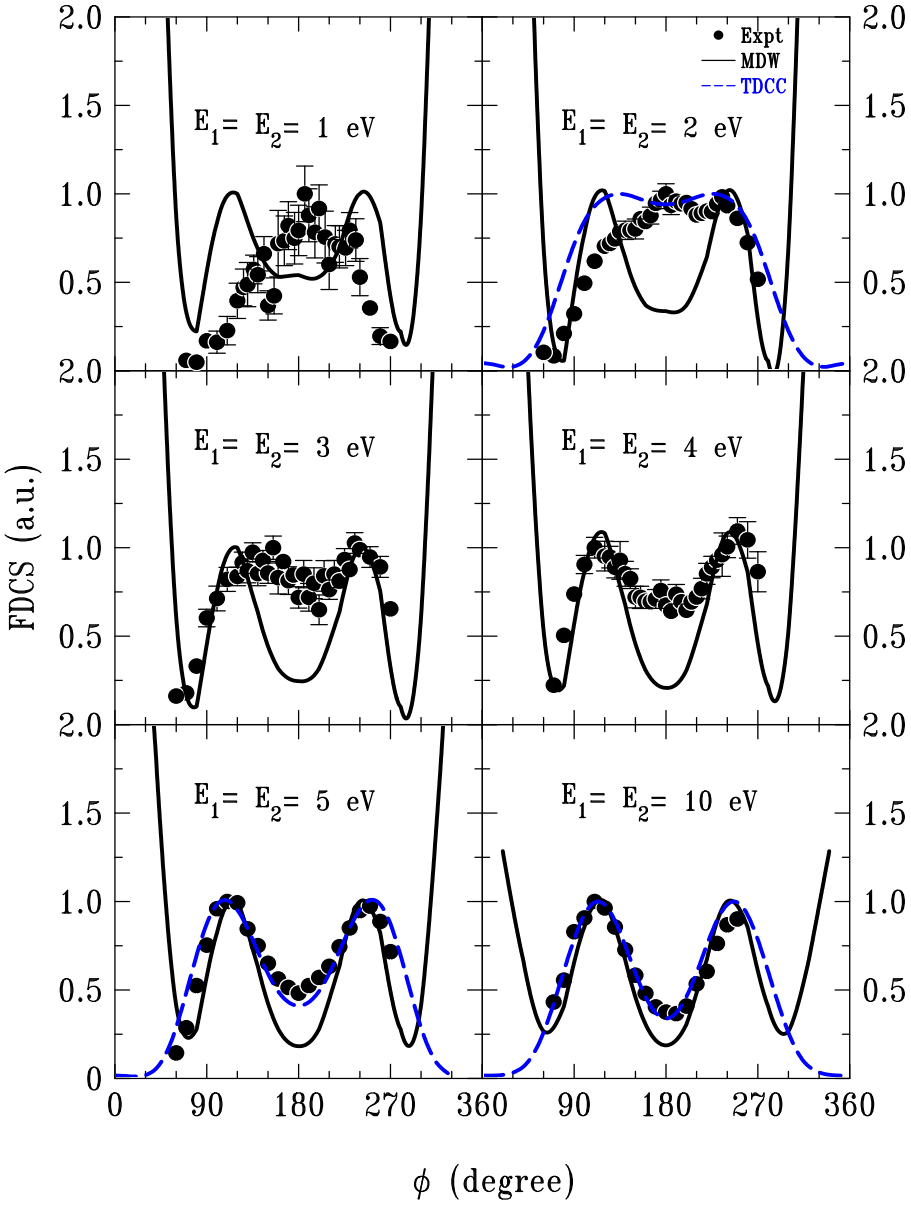

Figure 1: FDCS for ionization of H_2 using perpendicular plane kinematics. The FDCS are plotted as a function of φ (the angle between the two final state electrons in the detection plane). The energies of the outgoing electrons are shown on the respective plots. The experimental measurements are compared with MDW calculations (the solid curve) and the TDCC calculations (the dashed curve). For each energy, the experimental and theoretical data are normalized to unity at the experimental maximum.

The data are compared with MDW and TDCC theories, both theory and experiment being normalized to unity as noted above. The TDCC results are presented only where the two electrons have energies of 2 eV, 5 eV and 10 eV respectively. The shape of the experimental data changes dramatically as the energy decreases. The binary scattering peaks at 90° and 270° and minimum at 180° for 10 eV electrons becomes a single 180° maximum at 1 eV. Agreement between experiment and both calculations is good at 10 eV for the angular range of the experimental measurement. We would note, however, that the MDW predicts unphysically large cross sections for small and large angular separations. Since 0^o (or 360^o) scattering corresponds to two equal energy electrons travelling in the same direction, it is clear that these cross sections should be very small as the TDCC predicts. For the MDW, as the energy decreases, there is a minimum at 180° for all energies. Although the MDW 180° minimum becomes less shallow with decreasing energy, disagreement between experiment and theory increases with decreasing energy, the MDW predicting a minimum at 1 eV in contrast to the data. It is important to note that Martinez et al. [10] found very good agreement with the comparable 1 eV data for He using the atomic equivalent of the MDW so the MDW is good for atoms at this energy but not molecules! The lowest energy calculated using the TDCC theory was at 2 eV, and the TDCC still exhibits a shallow minimum at this energy while the data indicates a maximum at 180°.

To investigate the physical effects causing the change in shape of the FDCS as the energy decreases, we tested the importance of both nuclear scattering and electron-electron interactions. In [7] we investigated the effect of nuclear scattering for electron impact ionization of H_2 in the perpendicular plane where the two outgoing electrons had 10 eV. For this case, we demonstrated that the 180° minimum in H_2 became a maximum when the two nuclei were brought together to form a point charge while the electronic distribution was left unchanged. Consequently, we decided to see if nuclear scattering could be causing the peak in the data at 1 eV. In figure 2, MDW results are presented where the size of the nuclear separation is reduced from 1.4 a_0 to a point charge, keeping everything else unchanged. It is clear that reducing the spacing of the nuclear separation to a point charge caused the 180° minimum to become deeper, so these results do not support the idea that the 180° peak results from nuclear scattering.

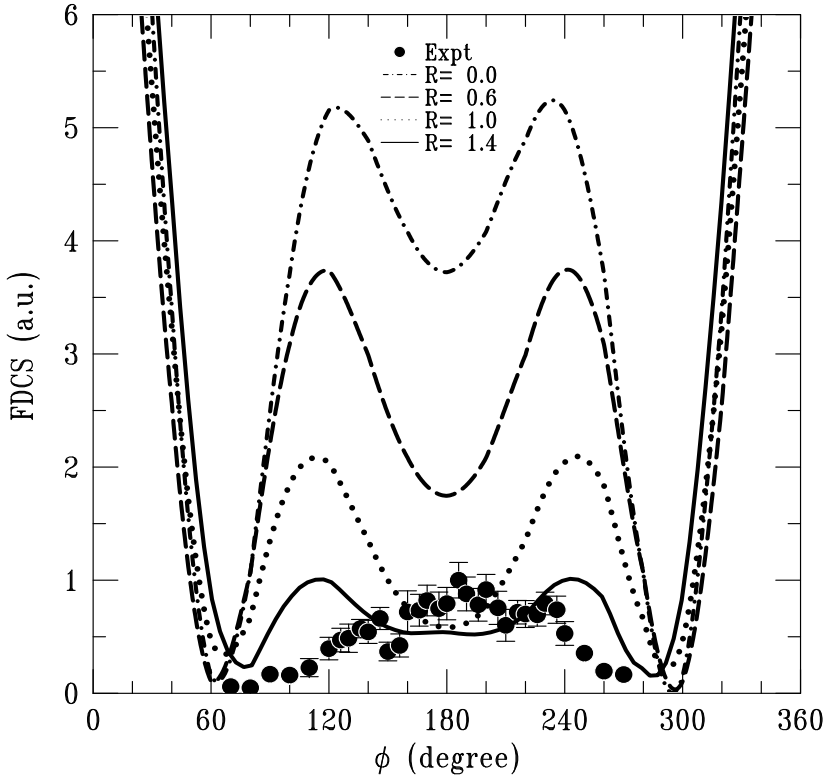

Figure 2: The dependence of the FDCS as a function of φ (the angle between the two final state electrons in the detection plane) for various nuclear separations. Both ejected electrons have energy of 1 eV. The MDW calculations are for different nuclear separations R = 0.0, 0.6, 1.0 and 1.4 a_0 as shown.

For further investigation, we added PCI to our theory to study the importance of electron-electron interactions near threshold. The Coulomb interaction in M3DW is included in the final state wavefunction, so PCI is included to all orders of perturbation theory. Figure 3 shows the data compared with the M3DW approach as well as the TDCC method. As before, theory and experiment are normalized to unity at the experimental maximum. The agreement between experiment and the M3DW is now much improved. The 180° minimum for the M3DW decreases with lowering energy in fairly good agreement with experiment, and the minimum at 2 eV is now much closer to the TDCC results. Although the experiment indicates a slight peak at 180°, a shallow minimum

would nevertheless lie within the statistical uncertainty of the experiment. Also, the theoretical calculations have not been convoluted over the experimental uncertainty in energy around ± 1 eV which could also explain the small difference with theory at this energy. It is clear that inclusion of PCI is important at all energies, but it becomes much more important when both final state electrons have 1 eV energy, since PCI turns the minimum into a maximum, and the binary peaks are eliminated.

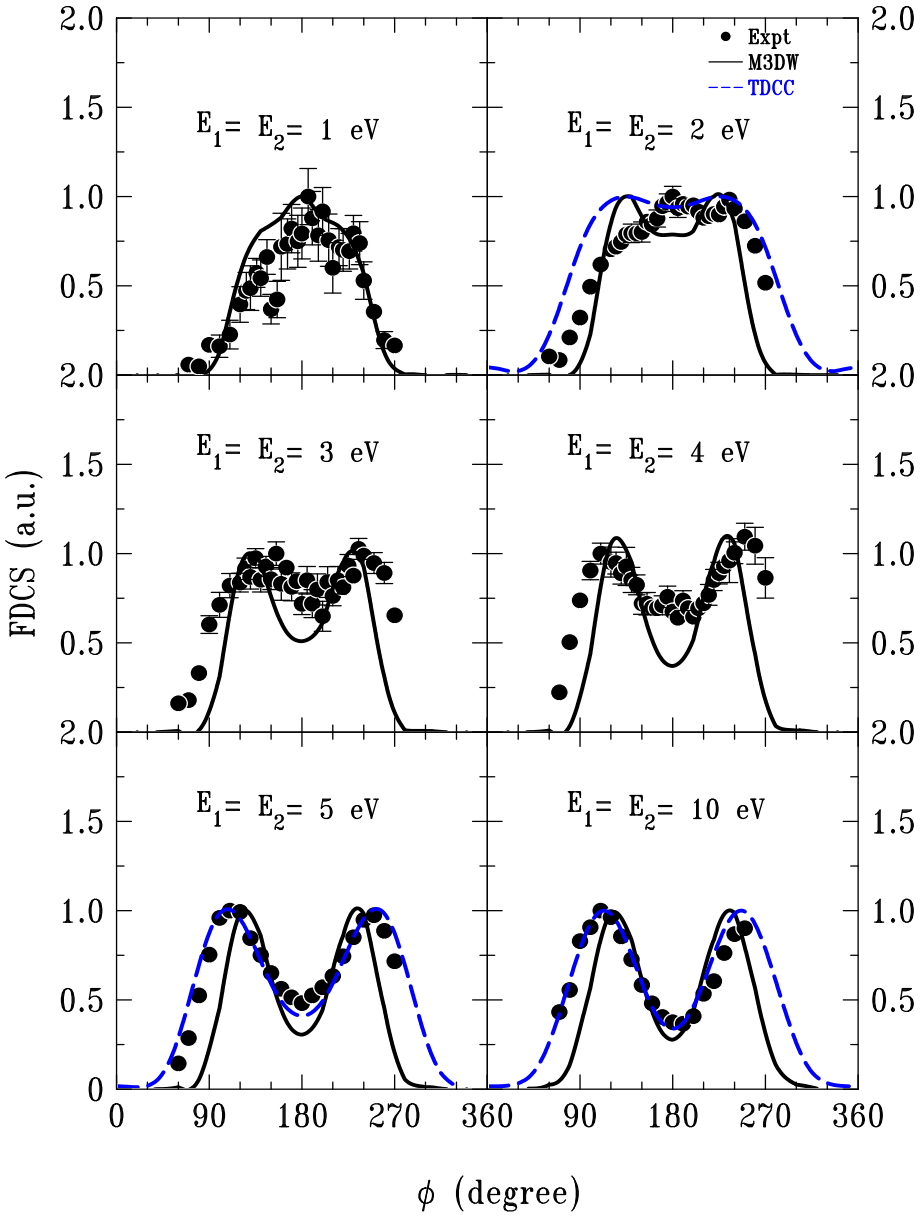

Figure 3: Same as fig. 1 except now the solid curve is the M3DW.

As noted, Al-Hagan *et al.* [7] showed that PCI did not produce a peak for back-to-back scattering at 10 eV, but rather that the minimum resulted from the binary collision occurring between the two H_2 nuclei where the net attractive force producing electrons at 180° cancels on average. What is seen here is a transition from the case where PCI is *unimportant* at 10 eV, to the case where PCI becomes *dominant* at 1 eV. This can be understood since the outgoing electrons have more time to interact as the energy decreases, and hence PCI forces the outgoing electrons to emerge at a mutual angle of 180°. However, it is surprising that this transition happens so quickly over a small range of energies

The dominance of PCI at 1 eV reminds us of the Wannier threshold law. The problem of threshold ionization has been extensively studied and is now well understood [16-18]. The first theory of near threshold breakup given by Wannier [16] was extended by Peterkop and Rau, the Wannier-Peterkop-Rau (WPR) threshold law predicting that the fully differential cross section for (e,2e) ionization of hydrogen should satisfy $FDCS \propto E_{ex}^{-0.373}$ [1,2,17,18] where E_{ex} is the excess energy. This law has recently been confirmed by accurate numerical calculations for electron-hydrogen scattering [3, 4]. If we adopt a simple double atom model for molecular hydrogen, threshold ionization of H_2 should follow the same law. Figure 4 shows the excess-energy dependence of the FDCS for H_2 in the near threshold energy region for backscattering at 180°. The solid line is the WPR theory normalized to the M3DW at the lowest energy and the dashed curve is the M3DW calculation. Clear differences occur only for excess energies above 1 eV (i.e. each electron has 0.5 eV energy) and significant deviations from the Wannier region are clear at higher energies.

For the case of E_1=E_2=1 eV, the M3DW is within ~20% of the WPR curve indicating that PCI is still the dominant process producing a maximum for 180° scattering. For E_1=E_2=2 eV (4 eV excess energy), the M3DW is about 50% below the WPR curve and both M3DW and TDCC theories predict a minimum. This means that the strength of PCI is significantly reduced, and by 10 eV excess energy PCI is of little consequence. As a final note, the WPR theory also predicts the FDCS should have a

Gaussian angular distribution centered around 180°. From fig. 3 for E_1=E_2=1 eV, we see that both experiment and theory have a Gaussian-like distribution around this angle, which is consistent with Wannier theory.

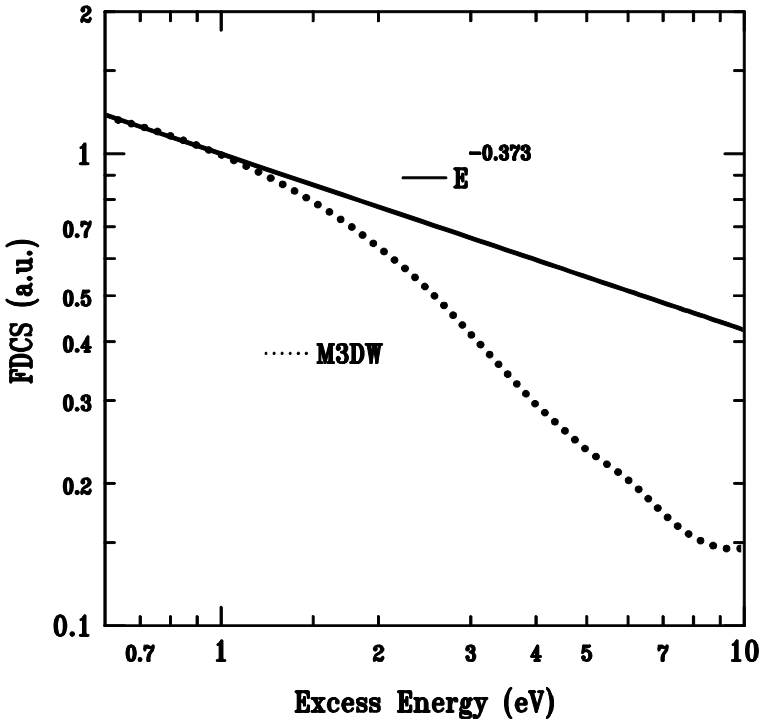

Figure 4: Calculated H_2 FDCS for equal energy sharing with φ = 180° as a function of excess energy. The solid line is the results of the Wannier theory normalized to the M3DW at the lowest energy and the dashed line is the M3DW FDCS.

We can also compare and contrast the Wannier region for atomic hydrogen with the current molecular case. Previous studies [1] have shown that the Wannier region for atomic hydrogen extends to an excess energy of around 3.3 eV. In the molecular hydrogen case, the Wannier region has a lesser extent of about 2 eV (as indicated by figure 4). This can be understood by remembering that the molecular hydrogen wavefunction is more extended in space than the atomic hydrogen wavefunction, even though the two systems have similar binding energies. Wannier theory relies on classical

scaling, where the distances r are replaced by r* scaled by the excess energy E of the system: r = r*/E. If a universal r* is assumed to control the range of the Wannier region in energy, then E = r*/r. Inserting r = R_i with i = m or a for molecule and atom respectively, yields $E_m < E_a$ since $R_m > R_a$. This explains why the threshold region for molecular hydrogen is smaller in energy than for atomic hydrogen.

In conclusion, we have compared experimental data with TDCC and M3DW calculations in the perpendicular plane for cases where the outgoing electrons have equal energies ranging from 1 eV to 10 eV. The data for 10 eV exhibits peaks at 90° and 270° and a minimum at 180°. We had previously shown that the 90° and 270° peaks result from elastic scattering of the projectile from the target into the perpendicular plane followed by a classical binary collision between the projectile and target electrons. For the minimum at 180°, it was shown that PCI is unimportant at this energy, and that the electron-electron collision occurs between the nuclei where the net attractive force cancels on average, so that there is almost no 180° scattering.

The new data presented here reveal that the shape of the FDCS completely changed from two peaks centered at 90° and 270°, to a single peak at 180° as the electron energy approaches threshold. We investigated the physical effects causing this change and found that PCI changes from being unimportant at 10 eV to being the dominant physical process at 1 eV. For the lowest energy, the FDCS has a Gaussian shape centered on 180° as is predicted by the WPR threshold law. Although theory indicates that the minimum measured energies are not quite low enough for the threshold law to hold strictly, they are nonetheless close enough for the Wannier model to provide the dominant physics. It should be noted that the FDCS for helium at the same outgoing electron energies also displays a dominant single peak at 180° as seen here, and that the side lobes are also eliminated. This shows that as PCI dominates the interaction, the target structure becomes decreasingly important.

Acknowledgements

We would like to thank one of the Referee's for suggesting the energy dependence explanation for molecules. This work was supported by the University of Manchester and the US National Science Foundation under Grant. No. PHY-0757749.

OAH would also like to thank the Saudi Ministry of Higher Education and King Abdullah Bin Abdul-Aziz Scholarship program for funding. The Los Alamos National Laboratory is operated by Los Alamos National Security, LLC for the National Nuclear Security Administration of the U.S. Department of Energy under Contract No. DE-AC5206NA25396.

References

[1] J. M. Rost, *Phys. Rev. Lett.* **72**, 1998 (1994).
[2] J. Röder *et al*, *Phys. Rev. Lett.* **79**, 1666 (1997).
[3] P. L. Bartlett and A. T. Stelbovics, *Phys. Rev. Lett.* **93,** 233201 (2004).
[4] J. F. Williams *et al, Phys Rev. Lett.* **96,** 123201 (2006).
[5] S**.** Cvejanovic and F H Read *J. Phys. B*. **7**, 14 (1974).
[6] J. F. Williams *et al*, *Phys. Rev. A* **71**, 052709 (2005).
[7] O. Al-Hagan *et al, Nat. Phys.* **5,** 59 (2008).
[8] J. Colgan *et al, Phys. Rev. Lett*. **101**, 233201 (2008).
[9] J. Colgan *et al, Phys. Rev*. A **79,** 052704 (2009).
[10] J.M. Martinez *et al*, *J. Phys*. B **41**, 065202 (2008).
[11] J. Gao *et al, J. Chem. Phys*. **124**, 194306 (2006).
[12] S. Jones and D. H. Madison, *Phys. Rev*. A **62**, 042701 (2000).
[13] J. Gao *et al*, *J. Chem. Phys*. **123**, 204302 (2005).
[14] J. Gao *et al*, *J. Chem. Phys*. **123**, 204314 (2005).
[15] S. J. Ward and J. H. Macek, *Phys. Rev*. A **49,** 1049 (1994).
[16] G. H. Wannier, *Phys. Rev*. **90**, 817 (1953).
[17] R. Peterkop*, J. Phys*. B **4**, 513 (1971).
[18] A. R. P Rau, *Phys. Rev*. A **4,** 207 (1971); *Phys. Rep* **110,** 369 (1984).

V. (e,2e) Ionization of Helium and the Hydrogen Molecule: Signature of Two-Centre Interference Effects

E M Staicu Casagrande[1,2], A Naja[1,2], F Mezdari[1,2], A Lahmam-Bennani[1,2], P Bolognesi[3], B Joulakian[4], O Chuluunbaatar[5], O Al-Hagan[6], D H Madison[6], D V Fursa[7] and I Bray[7]

[1] *Universit´e Paris-Sud 11, Laboratoire des Collisions Atomiques et Mol´eculaires (LCAM), Bˆat. 351, 91405 Orsay Cedex, France*

[2] *CNRS-LCAM (UMR 8625), Bˆat. 351, 91405 Orsay Cedex, France*

[3] *CNR-IMIP, Area della Ricerca di Roma 1, CP 10, 00016 Monterotondo Scalo, Italy*

[4] *Universit´e Paul Verlaine-Metz, Laboratoire de Physique Mol´eculaire et des Collisions, ICPMB (FR 2843), 1 rue Arago, 57078 Metz Cedex 3, France*

[5] *Joint Institute for Nuclear Research, Dubna, Moscow Region 141980, Russia*

[6] *Department of Physics, University of Missouri-Rolla, Rolla, Missouri 65409, USA*

[7] *ARC Centre for Excellence for Antimatter-Matter Studies, Curtin University of Technology, GPO Box U1987, Perth, WA 6845, Australia*

Abstract

Relative (e,2e) triply differential cross sections (TDCS) are measured for the ionization of the helium atom and the hydrogen molecule in coplanar asymmetric geometry at a scattered electron energy of 500 eV and ejected electron energies of 205, 74 and 37 eV. The *He* experimental results are found to be in very good agreement with convergent close-coupling calculations (CCC). The H_2 experimental results are compared with two state-of-the-art available theoretical models for treating differential electron impact ionization of molecules. Both models yield an overall good agreement with experiments, except for some intensity deviations in the recoil region. Similar (e, 2e) works were recently published on H_2 with contrasted conclusions to the hypothesis that the two H nuclei could give rise to an interference pattern in the TDCS structure. Murray (2005 *J. Phys. B: At. Mol. Opt. Phys.* **38** 1999) found no evidence for such an effect, whereas Milne-Brownlie *et al* (2006 *Phys. Rev. Lett.* **96** 233201) reported its *indirect* observation.

In this work, based on a *direct* comparison between experimental results for *He* and H_2, we observe an oscillatory pattern due to these interference effects, and for the first time the destructive or constructive character of the interference is observed, depending on the de Broglie wavelength of the ejected electron wave. The experimental finding is in good agreement with the theoretical prediction by Stia *et al* (2003 *J. Phys. B: At. Mol. Opt. Phys.* **36** L257).

1. Introduction

Over the past two decades, the field of electron impact single ionization (SI) of simple one- and two-electron atoms (*H* and *He*) has reached a degree of maturity such that sophisticated theoretical models (e.g. the exterior complex scaling ECS [1] or the convergent close-coupling CCC [2] methods) can now accurately predict the behaviour of the triple, *fully* differential cross section (TDCS) for wide ranges of the kinematical parameters (energies and vector momenta). Thus, the interest has now moved to the study of more complex, multi-electron atomic or molecular targets where the situation is by far more challenging. In particular, a renewed interest has emerged for the (e,2e) studies of the dynamics of molecular ionization, both experimentally [3–7] and theoretically [8–14]. This has led to the development of theoretical approaches meant to deal with the description of the molecular ionization processes, the most sophisticated ones being probably the first Born approximation (FBA)– two centre continuum (TCC) approximation with correct boundary conditions in the entrance and exit channels [9]and the molecular three-body distorted wave approximation (M3DW) coupled with an orientation averaged molecular orbital approximation (OAMO) [13, 14]. During the course of these developments, considerable interest has been raised by the possibility of observing, in the case of diatomic molecules, quantum mechanical interference effects resulting from the coherent superposition of the scattered waves from the two atomic centres [15]. These Young-type interference effects have been considered for many years in the photon ionization of H_2 [16, 17]. They were recently theoretically predicted by Stia *et a*l [18] and by Gao *et al* [19] for electron impact ionization of molecular hydrogen and molecular nitrogen, respectively. Their observation was reported in *double* differential cross section (DDCS) measurements for heavy, multicharged ion impact on

H_2 [20–22] and for fast (2.4 keV) electron impact on D_2 [23]. The question of their observation in *fully* differential cross sections was recently addressed by two groups in (e,2e) TDCS measurements (we note a speculative mention made by Jung *et al* [24] to explain the low coincidence rates in the recoil peak as being due to destructive interferences). First, at Manchester University, Murray [5] found no evidence of such effects in 'low' energy (<100 eV) electron impact ionization of H_2. Subsequently, Murray *et al* [6] reported a similar investigation on the$N_2(3\sigma_g)$ state, where they discuss the possibility of the existence of an interference peak in the vicinity of the backscattering angles, as predicted in [19]. However, they could not definitely prove it as the experimental data did not cover the angular range of the expected peak. Later on, Milne-Brownlie *et al* [3] at Griffith University reported the observation of Young-type interference effects in (e,2e) ionization of H_2 at an intermediate incident energy of 250 eV. The observable result is partial intensity suppression in the recoil peak compared with the binary one. The contrasted conclusions from these works on such an important matter called for and warranted a new investigation, in order to contribute to the understanding of such fundamental phenomenon.

Thus, in order to resolve the above-mentioned contrast, we have undertaken a newest of measurements similar (though not fully identical) to the case studied by Milne-Brownlie *et al* [3]. These authors used coplanar asymmetric geometry with an electron impact energy E_0 = 250 eV, ejected electron energies E_b = 10, 20 and 50 eV and a scattering angle for the fast electron θ_a=−15°. Under these kinematics, the interference effect is predicted to always result in a suppression of the recoil intensity with respect to the binary one. In contrast, we use the higher energies, E_0 ~ 600 to 700 eV, the ejected electron energies E_b = 37, 74 and 205 eV and the smaller scattering angle θ_a = −6°. Under these kinematics, the effect of the interference process is predicted (see below) to reduce the relative intensity of the recoil peak at the two lowest ejected energies and to increase it at the largest one. Hence, the new data allow a more stringent test of the theoretical prediction. Moreover, though we use in the present work, as was done in [3], comparison of the H_2 and the *He* TDCS, we will see below that our approach does not rely at all on any calculated TDCS neither for H_2 nor for *He*, as was the case in [3], but it

solely relies on the ratio of our measured triple differential cross sections for both targets. Hence, the new data allow a more *direct* test of the theoretical prediction.

2. Experiment

The experimental set-up currently in use in Orsay, whose main characteristic is the combination of three high-efficiency, multi-angle toroidal electrostatic energy analysers, has been described in detail elsewhere [25]. The experimental procedure is identical to that reported in [7]. Briefly, an incident electron beam collides with the gas jet formed at the collision centre. A coplanar geometry is used, where all electrons are observed in the collision plane defined by the incident and scattered momentum vectors $\mathbf{k_0}$ and $\mathbf{k}_a$, respectively. The 'slow' ejected electrons (designated with an index 'b' for convenience) are multi-angle analysed in a double toroidal analyser, with the energies E_b = 205, 74 and 37 eV and over the angular ranges θ_b=20–160° and 200–340°, where 0° is defined by the incident beam direction. In the offline analysis, the total θ_b angular range is divided into sectors of width $\Delta\theta_b$ = 5°. The 'fast', forward-scattered electron (indexed 'a') is collected by the third toroidal analyser [25] at the scattered energy E_a = 500 eV. In the present work, the a electron is simultaneously observed at two symmetrical angles, θ_a=+(6° ±0.25°) and–(6° ±0.25°), as set by input slits at the entrance to the electrostatic lenses associated with the toroidal analyser. The incident energy (E_0) is consequently adjusted to fulfill the energy conservation requirement for the target under study, $E_0 = E_a + E_b$ + IP, where IP is its ionization potential (24.6 eV for *He* and 15.5 eV for H_2). As an example, for the helium target and for the case E_b = 74 eV, the corresponding momentum transfer value is $K = 0.88 \pm 0.02$ au and the momentum transfer direction is $\theta_K = 46° \pm 1°$.

Due to the low coincidence rate, especially at the highest ejection energy, the spectrometer was operated at the reduced coincidence energy resolution [26], ΔE_{coin} ~ ±2.5 eV. This value did not allow resolving the final ionic state of the hydrogen molecule.

Finally, we note that the *He* (e,2e) experiments were performed *under exactly the same experimental conditions* as those used for H_2 (except for a slight change in incident energy, due to the difference in their IP), so that we can readily determine the ratio of the measured TDCS for both targets.

3. Results and discussion

The discussion of the results is organized in two parts. First, the measured angular distributions for *He* and H_2 are compared with calculated results from state-of-the-art theoretical models. The *He* results are used to validate our procedure, while the molecular results allow to pin-point successes (at the binary peak region) and deficiencies (at the recoil peak region) of the models. Second, the behaviour of the ratio of the *measured* TDCS for both targets is confronted to the theoretical prediction in [3] which allows interpreting this behaviour in terms of molecular two-center interference effects.

3.1. Angular distributions of the TDCS

The experimental results for the TDCS distribution for ionization of *He* are shown in figures 1(a)–(c) for the three investigated ejected electron energies, whereas figures 1(d)– (f) show the similar results for ionization of H_2. The data are compared with calculated results obtained using the convergent close coupling (CCC) method [2] for the helium atom, and using two state-of-the-art available approaches for the molecular target. Note that for each angular distribution, the relative experimental data have been independently normalized to the absolute scale given by theory, as explained in the figure caption.

The CCC calculations are performed separately for each incident energy. Due to the vastly different energies of the outgoing electrons and large incident energy on the single ground state, exchange needs not be included. For the kinematics considered, the Born approximation is reasonably accurate with a distorted wave Born approximation yielding further improvement. In such cases the close-coupling formalism converges with increasing basis sizes, N_l, relatively rapidly and we simply need to ensure sufficient number of angular momenta l for the ejected electron and L for the scattered electron. We find that $l \leq 5$ is sufficient for the smaller ejected energies and $l \leq 7$ required for the 205 eV case. With increasing incident energy we require larger L, which ranges from 30 to 50. Lastly, the CCC calculations presented were performed in the frozen-core approximation which keeps one of the *He* electrons fixed, as a He^+ 1s orbital.

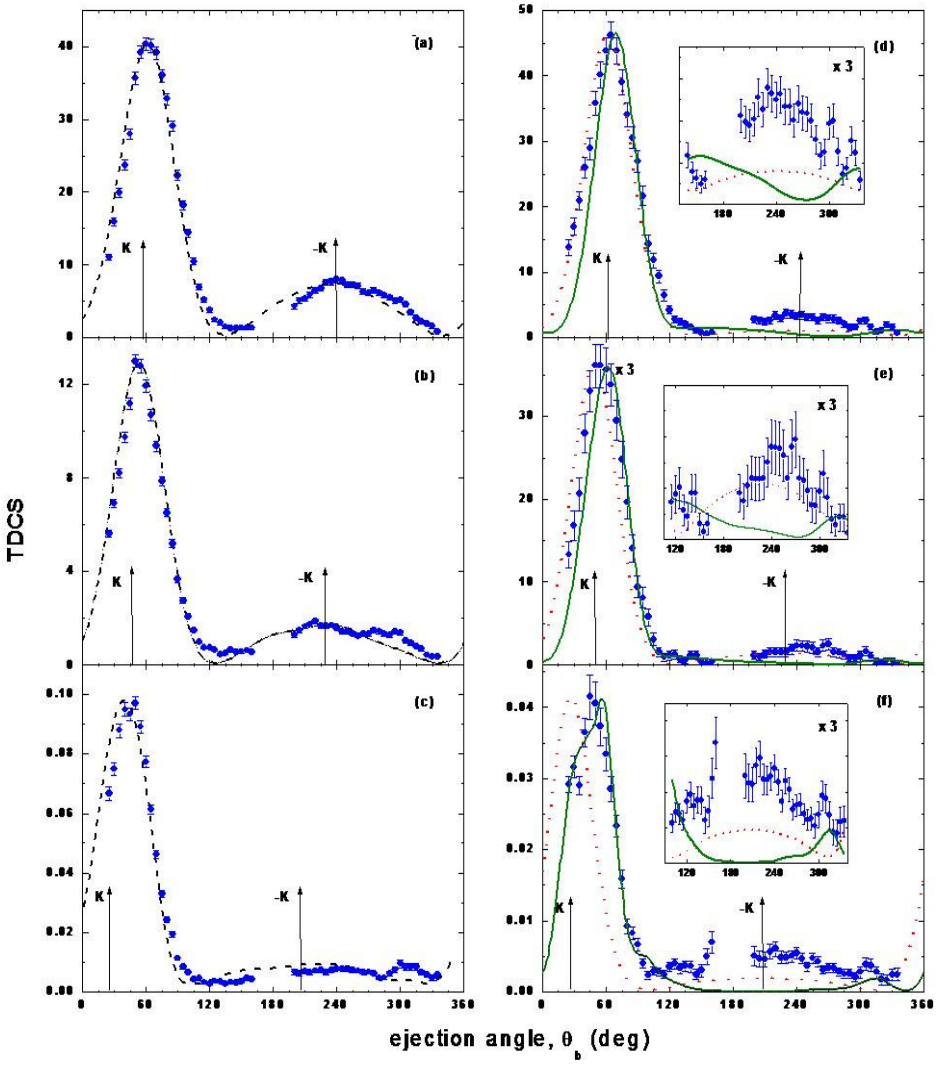

Figure 1: (e,2e) TDCS for ionization of *He* (left column) and H_2 (right column), plotted versus ejection angle θ_b, at a fixed scattering angle, θ_a=−6° and the fixed scattering energy, E_a = 500 eV. Panels (a) and (d) E_b = 37 eV; (b) and (e) E_b = 74 eV; (c) and (f) E_b = 205 eV. The incident energy (E_0) is consequently adjusted to fulfil the energy conservation. For *He*, the dashed line represents the results of the CCC calculations. For H_2, the dotted and full lines represent the theoretical results from the FBA–TCC and the M3DW–OAMO models, respectively. Solid circles: experimental data, with one standard deviation statistical error bars. The vertical arrows indicate the momentum transfer direction and its opposite. The insets in the H_2 results represent a zoom on the low intensity recoil region to facilitate comparison. The relative experimental data have been normalized for the best visual agreement with theory. The absolute scale shown is that of the CCC calculations for *He* and that of the FBA–TCC for H_2, both in 10−2 atomic units. The M3DW–OAMO results have been multiplied by 2.5 in (d), 2.8 in (e) and 6.7 in (f).

We checked that relaxing this approximation by adding more configurations, significantly improved the quality of the ground state, but had no substantial effect on the ionization cross sections presented.

The first theoretical model used for H_2 is based on a first Born approximation (FBA) in which the two-centre continuum (TCC) approximation with correct boundary conditions in the entrance and exit channels [10] is applied. Special care is taken in the description of the slow ejected electron in the field of the residual diatomic ion by a two-center Coulomb function, which has given [27] excellent results compared to those obtained by the exact solutions of the two-centre Schr¨odinger equation in prolate spheroidal coordinates [28]. Here, the relatively fast incident and the scattered electrons are described by plane waves. For the initial and final state bound electrons the wavefunctions given in [9] are used. Owing to the high incident energy and the large difference in energies of the outgoing electrons, exchange effects between these electrons are not expected to be significant and hence were not included.

The second model used for H_2 is the molecular three-body distorted wave (M3DW) approximation coupled with an orientation-averaged molecular orbital (OAMO) approximation [13, 14]. The M3DW–OAMO is a two-centre approach in which all three continuum electron wavefunctions are represented by distorted waves calculated on a spherically symmetric potential obtained from the Hartree–Fock charge distribution for H_2 averaged over all molecular orientations. For the incoming electron, the neutral charge density is used and for the two final state electrons the ionic charge density is used. The nuclear contribution to the distorting potential is equivalent to the potential of a thin metal spherical shell of radius $0.7a_0$ containing a total charge of 2. The polarization and correlation potential of Perdew and Zunger [29] and the Furness–McCarthy [30] exchange-distortion potential are added to the static Hartree–Fock distorting potential. The electron–electron Coulomb factor is included in the final state wavefunction which means that the final state post-collision interaction (PCI) between the two continuum electrons is included to all orders of perturbation theory. In the OAMO approximation, an orientation averaged molecular orbital is used for the initial-state wavefunction. The OAMO approximation has been shown to be valid for ionization of H_2 as long as the momentum transferred to the residual ion is less than unity [31].

Here again, exchange was not included due to the large energy difference of the outgoing electrons.

We first comment on the *He* (e,2e) results in figures 1(a)–(c). It is nowadays a well established fact that at high and intermediate impact energy the ionization process is very well described by the CCC method. Indeed, the agreement between experiments and theory is very good at the three considered energies, both in the shape of the distributions and in the position of the binary lobes. The small deviations seen in the recoil region might at least partly be of the statistical nature (the count rates being there rather small), reflecting the difficulty involved in performing measurements of processes characterized by low cross sections. The CCC results show a shift of the binary lobe of some 10◦ from the momentum transfer direction (θ_K), and so do our data, though at the highest energy the CCC theory yields a slightly smaller shift than experiments. These observations are consistent with known trends for *He* [32, 33], where peak shifts away from θ_K direction are to be expected whenever the first Born approximation is not sufficiently accurate. We thus believe that the experiments are free from any significant error or artefact. Our experimental procedure can thus be applied with good confidence to the other target studied here, since the H_2 data were obtained *under exactly the same experimental conditions* as those used for *He*.

For H_2, figures 1(d)–(f), the comparison between experiments and theory is less satisfactory, with a somehow better agreement reached by the FBA–TCC model with respect to the M3DW–OAMO at the two lowest energies, while the M3DW–OAMOis doing better in describing the binary peak at the highest energy. The shape of the binary lobes is essentially correctly reproduced by both model calculations. For the highest ejected-electron energy (figure 1(f)), we note that the M3DW–OAMO predicts a shoulder on the low angle side of the binary peak, which might possibly be also present in the experimental data though the statistics do not allow to be more affirmative. The origin of this shoulder was found to be mostly due to final state elastic scattering of the projectile electron from the target. However, both models predict a too small recoil intensity (except for the FBA-TCC at 74 eV), or even the absence of a recoil lobe in the M3DW–OAMO results. Since the recoil peak corresponds to the largest momentum transferred to the ion, the incorrect behaviour of the M3DW– OAMO in the region of the recoil peak

most likely stems from the breakdown of the OAMO approximation, as also discussed in [7]. Moreover, as expected FBA–TCC predicts a binary lobe aligned with the momentum transfer direction, θ_K, being a first Born model. The M3DW–OAMO includes final state PCI between the two continuum electrons, whose effect is to rotate the lobes in the backward direction. However, the effect seems to be overestimated, the M3DW–OAMO shift of the binary lobe from the **K**-direction being larger than the about 10◦ measured shift (the latter is similar to the observed and the CCC-calculated shift for *He* in figures 1(a)–(c)).

We note that both theoretical models (TCC and M3DW) were recently found [7] to be less successful in describing (e,2e) experiments on N_2 under very similar kinematics as the present ones, a failure which thus must be attributed to the difficulty of describing the more complex nitrogen molecule. On the other hand, the TCC model behaved very well [9] in describing high energy (~ 4.1 keV) (e,2e) processes on H_2 [34], so that its deficiencies here must be attributed at least in part to the different impact energy regime (~ 600 eV in this work) where non-first-Born effects are expected to start playing a role.

3.2. Interference effect

At first glance, the TDCS distributions obtained for *He* and H_2 (figure 1) may look very similar as far as the shape of the lobes is concerned. However, a closer inspection shows that the recoil peak in H_2 is substantially smaller than that in *He*, relative to the height of the binary peak, for the cases E_b = 74 and 37 eV, whereas the recoil peak in H_2 is larger than that in *He* for the case at E_b = 205 eV. This recoil intensity suppression on the one side and enhancement on the other side in the molecular case is attributed to Young-type interference effects, and is the subject of the discussion in this section.

In their theoretical investigation of the (e,2e) single ionization of H_2, Stia *et al* [18] (see also an earlier derivation by Dal Cappello *et al* [35]), have shown that the angular distribution of the ejected electrons exhibits interference structures arising from the coherent emission from the two molecular centres. Moreover, they predicted that these interference structures should be observed even in the TDCS distribution from non-oriented molecules (as is the case in the present study). They showed that, provided a two-effective-centre description is used, the TDCS distribution for molecular hydrogen,

$\sigma_{e2e}(H_2)$, can be expressed as twice the TDCS distribution of the one-centre atomic hydrogen, σ_{e2e}(H), modulated by an interference factor, I, that is:

$$\sigma_{e2e}(H_2) = 2 * \sigma_{e2e}(H) * I$$

where I is given by

$$I = 1 + \frac{\sin(q\rho)}{q\rho} \qquad (1)$$

Here, $\mathbf{q}$ is the momentum imparted to the recoiling ion, $\mathbf{q} = \mathbf{k_0} - \mathbf{k_a} - \mathbf{k_b}$, and ρ is the equilibrium internuclear distance of the H_2 molecule, ρ = 1.4 au [36]. In other words, the ratio $\sigma_{e2e}(H_2)$ / $2*\sigma_{e2e}(H)$ should display the same oscillatory behaviour as the I factor. This is the basic idea of the present study. However, instead of using twice the atomic hydrogen cross section, we have used *He* cross section (an equivalent two-electron-single centre atom), hence comparing the ratio $R = \sigma_{e2e}(H_2) / \sigma_{e2e}(He)$, to I. We emphasize that this procedure does not rely on any theoretical calculations neither for *He* nor for H_2, as was the case in [3]. The whole argument hinges on the behaviour of the recoil peak relative to the binary one and does not need any support from the theoretical calculations presented above, which anyway fail to properly predict the recoil intensity.

The interference factor, I, is plotted in figure 2 as a function of the ejected electron angle, θ_b, for the kinematics of the present experiments. As expected, the factor I has an oscillatory behaviour, passing through a maximum at θ_b angles I the vicinity of 50–60◦, that is close to the maximum of the binary peak as observed in figure 1. Our cross section measurements are obtained on a relative scale, and so is their ratio, R, to which I should be compared. Hence, we arbitrarily normalized the I values to unity in the region of the binary peak. We note that, for the ejected electron energies E_b = 37 and 74 eV, the I factor passes through a minimum in the angular range where the recoil peak is at maximum, i.e. at θ_b angles in the vicinity of 230–240°. The secondary maximum observed in this angular range for the 37 eV case is too small to be meaningful for the present discussion. But a remarkable fact is that for the ejected electron energy E_b = 205 eV, the I factor displays a maximum in the recoil region instead of a minimum. Consequently, we might expect the recoil peak to be diminished in H_2 (with respect to that of the *He* atom) for the two lowest energies, and in contrast to be enhanced in the

case of the highest E_b value. This is exactly the analogue of Young-type double slit interference effects, which might be either destructive or constructive at a given scattering angle, depending on the ratio λ/ρ, where λ is the light (here ejected electron) de Broglie wavelength and ρ is the distance between the two slits (here the two nuclei). We note that for the three considered energies, the ejected electron wavelength λ varies between 1.6 and 3.8 au, that is λ is close to the 'inter-slit distance' ρ = 1.4 au, which is the condition of the existence of interference effects.

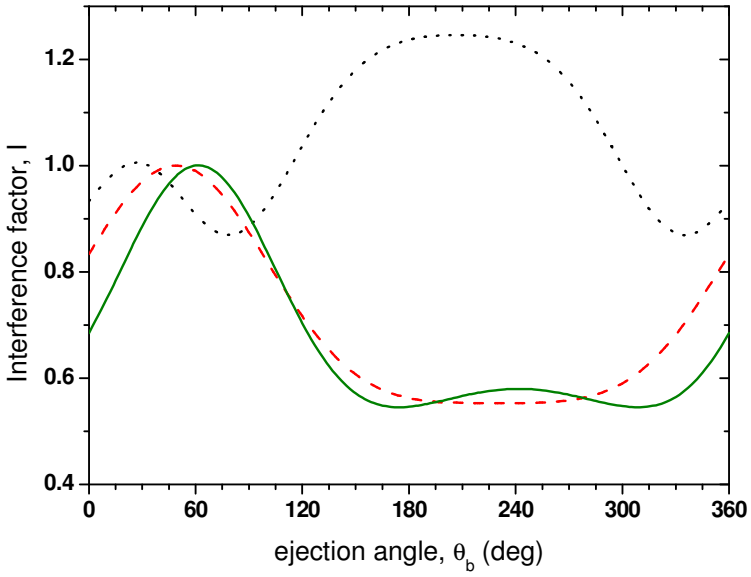

Figure 2: Interference factor, I, predicted by equation (1), plotted versus ejection angle, θ_b, at the ejected electron energies E_b = 37 eV (full line), E_b = 74 eV (dashed line) and E_b = 205 eV (dotted line). The I values are arbitrarily normalized to unity in the region of the binary peak.

In figures 3(a)–(c), the experimental ratio $R = \sigma_{e,2e}(H_2)/\sigma_{e,2e}(He)$ is plotted as a function of the ejected electron angle, θ_b, for the three ejection energies considered in the present experiments. Comparison is made with the interference factor, I. Qualitative good agreement is seen in the three cases between R and I, in spite of the large error bars due to the fact that, in certain angular ranges, we are taking the ratio of two small quantities, and considering the approximations made in the Stia *et al*'s model. Figures

3(a) and (b) clearly show a suppression of the recoil peak intensity with respect to the binary one, while figure 3(c), where E_b = 205 eV, displays its prominent enhancement. In figures 3(b) and (c) the effect is more pronounced in the experiments than in the theoretical prediction, but the effect is qualitatively the same. The reasonably good agreement of the experimental results with the predictions of Stia *et al* [18] suggests that the present observations can be ascribed to the destructive (E_b = 37, 74 eV) or constructive (E_b = 205 eV) interference effects arising from the two-centre nature of H_2. We note that, to our best knowledge, this is the first time that both the destructive and constructive characters of the interference process are simultaneously observed in the same (e,2e) experiments.

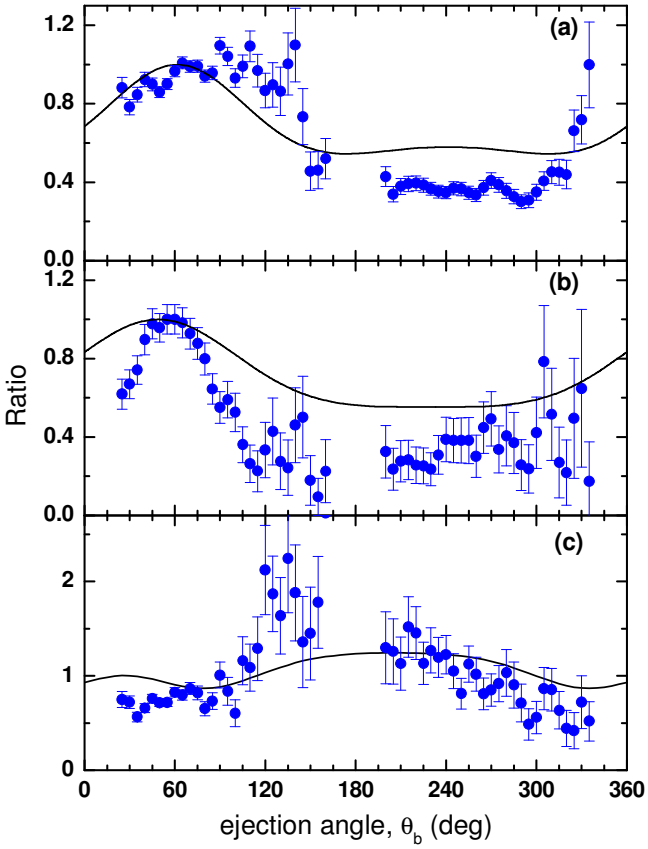

Figure 3: Solid circles: the experimental ratio, $\sigma_{e,2e}(H_2)/\sigma_{e,2e}(He)$, of the (e,2e) TDCS for ionization of H_2 relative to that of He, plotted versus the ejection angle θ_b at (a) E_b = 37 eV; (b) E_b = 74 eV; (c) E_b = 205 eV. The full lines represent the predicted interference factor of figure 2.

It might be tempting to attribute the peak observed at about 60° in the experimental ratio of figure 3(b) to the broader initial state momentum distribution in *He* with respect to H_2 which results in a larger width of the *H*e binary peak. However, such interpretation implies that a similar peak should be observed at the three considered energies, which is not the case. Rather, our measured peak is in qualitative agreement with the Stia *et al*'s predicted interference factor, which does not depend on the target momentum distribution. We thus believe that the origin of this peak is mostly of a geometrical/kinematical nature, as is the factor *I*.

The reduction of the recoil peak relative to the binary one observed in figures 3(a) and (b) might have other plausible explanations. For example, the recoil peak is known to be very sensitive to the properties of the initial target state. Since it involves elastic backscattering of the ejected electron from the target core, the more diffuse nuclear charge in H_2 compared to *H*e might result in a reduction of the recoil peak. Alternatively, the interaction between the faster electron and the target core might also contribute to a reduction of the molecular recoil peak. However, our argument above is based on the simultaneous observation of a reduction *and* an enhancement of the recoil peak, and we think that there is no way that a diffuse nuclear charge or any alternative argument might yield to an enhanced recoil peak for H_2. It would certainly be interesting to investigate the role of the different electron charge distributions or nuclear charge distributions, but this would not be a meaningful task here since the molecular models considered do not even get the recoil peak correctly described.

Similarly, our analysis relies, as was done in [3], on the assumption that the interference term, *I*, can be compared to the ratio of the TDCS for H_2 to that for *He* instead of twice that of atomic hydrogen. Although this assumption might be questionable, the good agreement achieved with the Stia *et al* [18] ratio factor provides further support for the validity of this approach.

4. Conclusion

Relative (e,2e) TDCS for ionization of the H_2 molecule at ~ 600 eV incident energy are reported. Similar data obtained for the ionization of *He* are found to be in good agreement with the well-established CCC results, thus providing a validation of our

experimental procedure. The H_2 results are compared with the most elaborate available molecular calculations. Reasonable agreement is found between measured and calculated distributions in the binary region. However, clear discrepancies are observed between theories and experiments, in particular, (i) for the position of the binary lobes, which calls for a proper treatment of second-order effects in the theories and (ii) for the intensity distribution in the recoil region which calls for a better modelling of the interaction with the nucleus. These discrepancies demonstrate the need for further development of the theoretical models in order to accurately describe the ionization process, even for the simplest molecular target, H_2.

Our H_2 data were analysed in a *direct* comparison with the *He* ones, showing a diminution or an enhancement of the recoil intensity with respect to the binary one, in the molecular case. Though the reduction of the recoil intensity could have several plausible explanations, the simultaneous observation of a reduction and an enhancement depending on the ejected electron de Broglie wavelength supports on the one hand the interpretation of these effects as being the signature of the presence of interference effects as theoretically predicted in [18] and experimentally observed in [3], while on the other hand bringing further indication by showing the destructive or constructive character of these interferences.

Acknowledgments

AN acknowledges a doctoral grant from the 'Agence Universitaire de la Francophonie' (AUF). PB thanks the Universit´e de Paris-Sud XI for a 'Professeur Invit´e' position. DHM would like to thank the US National Science Foundation grant PHY-0456528 for providing funding for the theoretical work carried out in Rolla.

References

[1] Rescigno T N, Baertschy M, Isaacs W A and McCurdy C W 1999 *Science* **286** 2474
[2] Bray I, Fursa D V, Kheifets A and Stelbovics A T 2002 *J. Phys. B: At. Mol. Opt. Phys.* **35** R117
[3] Milne-Brownlie D S, Foster M, Gao J, Lohmann B and Madison D H 2006 *Phys. Rev. Lett.* **96** 233201
[4] Kaiser C, Spieker D, Gao J F, Hussey M, Murray A and Madison D H 2007 *J. Phys. B: At. Mol. Opt. Phys.* **40** 2563–76

[5] Murray A J 2005 *J. Phys. B: At. Mol. Opt. Phys.* **38** 1999
[6] Murray A J, Hussey M J, Gao J F and Madison D H 2005 *J. Phys. B: At. Mol. Opt. Phys.* **39** 3945
[7] Naja A, Staicu Casagrande E M, Lahmam-Bennani A, Nekkab M, Mezdari F, Joulakian B, Chuluunbaatar O and Madison D H J 2007 *J. Phys. B: At. Mol. Opt. Phys.* **40** 3775–83
[8] Weck P, Fojon O A, Hanssen J, Joulakian B and Rivarola R D 2001 *Phys. Rev.* A **63** 042709
[9] Weck P, Fojon O A, Joulakian B, Stia C R, Hanssen J and Rivarola R 2002 *Phys. Rev.* A **66** 012711
[10] Stia C R, Foj´on O A, Weck P F, Hanssen J, Joulakian B and Rivarola R D 2002 *Phys. Rev.* A **66** 052709
[11] Champion C, Hanssen J and Hervieux P A 2001 *Phys. Rev.* A **63** 052720
[12] Champion C, Hanssen J and Hervieux P A 2002 *Phys. Rev.* A **65** 022710
[13] Gao J F, Madison D H and Peacher J L 2005 *Phys. Rev.* A **72** 020701(R)
[14] Gao J F, Madison D H and Peacher J L 2005 *J. Chem. Phys.* **123** 204314
[15] Barrachina R O 2007 *Radiat. Phys. Chem.* **76** 375–9
[16] Cohen H D and Fano U 1966 *Phys. Rev.* **150** 30–3
[17] Walter M and Briggs J 1999 *J. Phys. B: At. Mol. Opt. Phys.* **32** 2487–501
[18] Stia C R, Foj´on O A, Weck P F, Hanssen J and Rivarola R D 2003 *J. Phys. B: At. Mol. Opt. Phys.* **36** L257
[19] Gao J F, Madison D H and Peacher J L 2005 *Phys. Rev.* A **72** 032721 (R)
[20] Stolterfoht N *et al* 2001 *Phys. Rev. Lett.* **87** 023201
[21] Deepankar M, Kadhane U, Singh Y P, Tribedi L C, Fainstein P D and Richard P 2004 *Phys. Rev. Lett.* **92** 153201
[22] Stolterfoht N, Sulik B, Skogvall B, Chesnel J Y, Fr´emont F, Hennecart D, Cassimi A, Adoui L, Hossain S and Tanis J A 2004 *Phys. Rev.* A **69** 012701
[23] Kamalou O, Chesnel J Y, Martina D, Hanssen J, Stia C R, Foj´on O A, Rivarola R D and Fr´emont F 2005 *Phys. Rev.* A **71** 010702
[24] Jung K, Schubert E, Paul D A L and Ehrhardt H 1975 *J. Phys. B: At. Mol. Phys.* **8** 1330–7
[25] Catoire F, Staicu Casagrande E M, Lahmam-Bennani A, Duguet A, Naja A, Ren X G, Lohmann B and Avaldi L 2007 *Rev. Sci. Instrum.* **78** 013108
[26] Dupr´e C, Lahmam-Bennani A and Duguet A 1991 *Meas. Sci. Technol.* **2** 327
[27] Chuluunbaatar O, Joulakian B, Tsookhuu K and Vinitsky S I 2004 *J. Phys. B: At. Mol. Opt. Phys.* **37** 2607–16
[28] Serov V V, Joulakian B, Derbov V L and Vinitsky S I 2005 *J. Phys. B: At. Mol. Opt. Phys.* **38** 2765–73
[29] Perdew J P and Zunger A 1981 *Phys. Rev.* B **23** 5048–79
[30] Furness J B and McCarthy I E 1973 *J. Phys. B: At. Mol. Phys.* **6** 2280
[31] Gao J F, Madison D H and Peacher J L 2006 *J. Phys. B: At. Mol. Opt. Phys.* **39** 1275
[32] Lahmam-Bennani A 1991 *J. Phys. B: At. Mol. Opt. Phys.* **24** 2401
[33] Ehrhardt H, Jung K, Knoth G and Schlemmer P 1986 *Z. Phys.* D **1** 3–32
[34] Ch´erid M, Lahmam-Bennani A, Duguet A, Zurales R W, Lucchese R R, Dal Cappello M C and Dal Cappello C 1989 *J. Phys. B: At. Mol. Opt. Phys.* **22** 3483

[35] Dal Cappello M C, Dal Cappello C, Tavard C, Ch´erid M, Lahmma-Bennani A and Duguet A 1989 *J. Phys. France* **50** 207–17
[36] Huber K P and Herzberg G 1979 *Molecular Spectra and Molecular Structure: IV. Constants of Diatomic Molecules* (Princeton, NJ: Van Nostrand Reinhold) p 250

VI. (e,2e) Study of Two-Centre Interference Effects in the Ionization of N_2

L.R. Hargreaves[1], C. Colyer[1], M.A. Stevenson[1], B. Lohmann[1], O. Al-Hagan[2], D.H. Madison[2], and C.G. Ning[3]

[1]*ARC Centre of Excellence for Antimatter-Matter Studies, The University of Adelaide, Adelaide, SA, 5005, Australia*

[2]*Department of Physics, Missouri University of Science and Technology, Rolla, Missouri 065409, USA*

[3]*Department of Physics and Key Laboratory of Atomic and Molecular NanoSciences of MOE, Tsinghua University, Beijing 100084, People's Republic of China*

Abstract

A number of previous studies have suggested the possibility of two-centre interference effects in the single ionization of diatomic molecules such as H_2 and N_2. While interference effects have been successfully observed in the ionization of H_2, to date evidence for interference in N_2 ionization has yet to be conclusively demonstrated. This study presents triply differential cross sections for electron impact ionization of N_2, measured using the (e,2e) technique. The data is probed for signatures of two-centre interference effects. Evidence for interference manifesting in the cross sections is observed.

1. Introduction

The problem of single ionization of diatomic molecules by particle impact has received significant attention from atomic and molecular physicists in recent years, due to the possibility of observing two-centre interference effects. Such interference can be considered analogous to a `Young's double-slit' type effect, with the two atomic centres (the slits) acting as localized sources of coherent electron emission. Understanding of interference phenomena is critical to any theoretical description of dual-nature quantum objects such as electrons, and is therefore fundamental to a thorough understanding of collision-induced reactions.

If particle impact ionization of diatomics can indeed lead to interference effects, then an obvious question is how such effects can be observed in an experiment. The method generally employed by experimentalists has been to measure ionization cross sections (probabilities) for diatomic molecules, as a function of either the ionising or ejected particle's momentum, and look for structures which could be interpreted as indicative of two-centre effects. Several early experimental studies into this problem studied the doubly differential cross sections (DDCS) of H_2 [1-4] and D_2 [5] ionization by heavy ion (H_2) and electron (D_2) impact. Oscillatory structures in the DDCS (the probability of a collision yielding an electron with momentum $\boldsymbol{k_e}$ as a function of the incident particle momentum $\boldsymbol{k_0}$) were observed and interpreted by the authors as evidence of two-centre interference. Alexander *et* al. [6] recently investigated a different type of DDCS – one in which the scattered projectile momentum k_s is determined instead of the ejected electron momentum $\boldsymbol{k_e}$ and they found that this type of DDCS was much more sensitive to two-centre interference effects for proton-impact ionization of H_2.

Several studies [7-10] have also considered the possibility of observing interference effects in triply differential cross sections (TDCS), using the (e,2e) technique. An (e,2e) measurement requires the detection of both the ionising and ejected electron, in time coincidence. Hence, the TDCS represents the probability of a collision yielding both an ejected electron with momentum $\boldsymbol{k_e}$ AND a scattered electron with momentum $\boldsymbol{k_s}$, again as a function of $\boldsymbol{k_0}$. By the above definition the DDCS is determined by the integration of the TDCS over the momentum of one of the two final state continuum particles. Since

integration often masks scattering effects, several authors [8,9] have suggested that interference effects may show stronger signatures in a TDCS than in a DDCS. Indeed, evidence of two-centre effects has already been observed in (e,2e) measurements of H_2 ionization [8,10], by comparing molecular and equivalent atomic TDCS.

Here, TDCS results from an (e,2e) study of N_2 ionization are presented, with emphasis placed on examining the results for two-centre interference. As a heavier target than H_2, with a correspondingly larger cross section, N_2 may be expected to show an even stronger signature of interference than H_2 [9]. The theoretical study of Gao *et. al.* [7] supports interference effects in N_2 ionization, finding a pronounced oscillatory structure in the backward angle scattering of the coplanar symmetric energy-sharing TDCS, which was attributed by the authors to two-centre effects. The experimental results of Murray *et. al.* [9] also showed some limited evidence of two-centre interference in the symmetric energy-sharing regime for N_2.

To look for two-centre interference effects, the strategies of both previous studies have been employed here. Firstly, the TDCS's of N_2 were measured and compared with theoretical TDCS results for the kinematically equivalent atomic nitrogen TDCS. The kinematics for these measurements were very similar to those employed by Milne-Brownlie *et. al.* [8], with the energy-sharing between the two outgoing electrons being highly asymmetric. The second approach employed has been to probe the TDCS in the symmetric energy-sharing regime to try and observe evidence of the oscillation predicted by Gao *et. al.* [7]. As well as the additional measurements, improved theoretical calculations of the N_2 TDCS, employing the molecular three-body distorted wave (M3DW) approach, under both kinematics are presented.

2. Experiment details

The apparatus used for the present measurements has been described extensively in a prior publication [11] and so only an overview is given here. A collimated electron beam of the desired energy was produced by a standard electron gun, comprising a tungsten filament electron emission source and a 5-element, cylindrical geometry lens stack. The energy of the electron beam could be varied between 0 – 2000 eV, with an energy width around 0.5 eV full-width-half-maximum (FWHM). This electron beam

intersected a molecular nitrogen beam formed by the effusive flow of nitrogen gas through a stainless steel capillary (diameter 0.7 mm, length 20 mm). The interaction region was thus formed by the volume overlap of the electron and gas beams. Two identical electron energy analyzers, mounted on independently rotatable turntables, collected electrons emerging from the interaction region. Electrons entering an analyzer were transported and focussed, again by cylindrical geometry lenses, into a hemispherical energy selector which filtered the electrons according to their energy. Electrons with energies ranging from 2 eV up to the incident energy could be selectively detected, with a total system energy resolution of around 0.75 eV. Electrons which passed through the selector impacted on a channel electron multiplier (CEM). The output pulses from the two CEMs were registered and analysed by standard fast timing electronics and coincidence circuitry.

Measurements in the present study were conducted using an asymmetric, coplanar geometry. Under such geometry, the two outgoing electrons and the incident electron are in the same plane but the emission angle of the two outgoing electrons, each with respect to the incident, are different to one another. During a measurement, one electron energy analyzer was held at a fixed detection angle, typically between -15° – -25° with respect to the incident beam direction, while the other was scanned repeatedly over the accessible angular region until sufficient statistical precision was obtained in the data. The scanned analyzer could access electron emission angles between 35° – 135° (the forward scattering angle or 'binary' collision region) and 225° – 285° (the backward scattering angle or 'recoil' collision region), again with respect to the incident beam. The angular range accessible by the scanned electron energy analyzer was limited by the positions of the stationary analyzer and fixed electron gun. Data was accumulated for periods ranging between several days to one week per scan, depending on signal levels

To measure the TDCS in the either the binary or recoil region, the stationary analyzer was positioned at either -15° and +15°, respectively, with respect to the incident electron beam (where the negative angle denotes that the stationary analyzer is on the opposite side of the election beam to the scanned analyzer). Moving the stationary analyzer symmetrically about 0° then in effect changed the ejected electron detection angle from θ_e to $360°-\theta_e$, allowing the distribution of the TDCS in the binary or recoil

region to be measured. This technique also allowed the relative magnitudes of the binary to recoil scattering to be determined, with an uncertainty of no more than 35%, by comparing the magnitude of the scattering signal between any two points in the binary and recoil region. In addition, the binary/recoil scattering ratios were cross-checked using a new 'mixed flow technique', which is presently being developed by the Adelaide group. The new technique compares the coincident scattering signal from the test gas with that from a control gas (helium), and in principle enables the absolute magnitude of the TDCS to be determined. In this study however, the use of the new technique has been restricted to cross checking the binary/recoil ratios determined by the more conventional method outlined above and all cross sections reported are on a relative scale. In all cases both techniques yielded the same results to within their respective uncertainties. The full details of the new technique will reported in a forthcoming publication.

To establish the kinematics for a given measurement, the incident and ejected electrons' energy were chosen and the scattered electron energy determined by energy conservation, ie.,

$$E_s = E_0 - E_e - \varepsilon \tag{1}$$

where E_0, E_s and E_e are respectively the incident, scattered and ejected electron energies and ε is the ionization potential of the orbital under study. The incident energies used in the present study were less than 150 eV, and the ejected electron energies less than 30 eV. In the case of asymmetric energy-sharing measurements, the stationary electron energy analyzer registers the faster of the two outgoing electrons, which is conventionally designated the scattered electron.

To ensure apparatus effects did not manifest in the measured cross sections, prior to each scan a test measurement using a helium target was performed under *identical* kinematics to the intended nitrogen measurement, save for an adjustment of either the incident or scattered energy to account for helium's different ionization potential. The results of the helium measurements were compared with convergent close-coupling (CCC) calculations [12], which were taken as benchmarked in this energy range [13]. In all instances the helium TDCS distribution was in excellent accord with the CCC results.

3. Theory: Molecular distorted wave approach

The M3DW approximation has been presented elsewhere [14-16] so only a brief overview will be presented here. The M3DW TDCS is given by

$$\frac{d^5\sigma}{d\Omega_a d\Omega_b dE_b} = \frac{1}{(2\pi)^5}\frac{k_a k_b}{k_i}\left(|T_{dir}|^2 + |T_{exc}|^2 + |T_{dir} - T_{exc}|^2\right), \quad (2)$$

where $\vec{k}_i$ is the initial state wave vector, $\vec{k}_a$ ($\vec{k}_b$) is the wave vector for the scattered (ejected) electron, and the direct and exchange amplitudes are T_{dir} and T_{exc} respectively,

$$T_{dir} = \left\langle \chi_a^-(\vec{k}_a, \mathbf{r}_1)\chi_b^-(\vec{k}_b, \mathbf{r}_2)C_{scat-eject}(r_{12})\,|\,V - U_i\,|\,\phi_j^{OA}(\mathbf{r}_2)\chi_i^+(\vec{k}_i, \mathbf{r}_1)\right\rangle, \quad (3)$$

$$T_{exc} = \left\langle \chi_a^-(\vec{k}_a, \mathbf{r}_2)\chi_b^-(\vec{k}_b, \mathbf{r}_1)C_{scat-eject}(r_{12})\,|\,V - U_i\,|\,\phi_j^{OA}(\mathbf{r}_2)\chi_i^+(\vec{k}_i, \mathbf{r}_1)\right\rangle. \quad (4)$$

In eqns. (3) and (4), $\mathbf{r}_1$ ($\mathbf{r}_2$) is the co-ordinate of the incident (bound) electron, χ_i, χ_a and χ_b and are the distorted waves for the incident, scattered, and ejected electrons respectively, $C_{scat\text{-}eject}$ is the Coulomb interaction between the scattered projectile and ejected electron, and ϕ_j^{OA} is the orientation-averaged molecular orbital (OAMO) [14] for the initial bound state wavefunction of the molecule generated from multi-center molecular orbitals. The molecular wavefunction was calculated using density functional theory (DFT) along with the standard hybrid B3LYP [17] functional by means of the ADF 2007 (Amsterdam Density Functional) program [18] with the TZ2P (triple-zeta with two polarization functions) Slater type basis sets. The potential V is the initial state interaction between the projectile and the neutral molecule, and U_i is the initial-state spherically symmetric distorting potential which is used to calculate the initial-state distorted wave χ_i.

The Schrödinger equation for the incoming electron wave-function is given by:

$$(T + U_i - \frac{k_i^2}{2})\chi_i^+(\vec{k}_i, \mathbf{r}) = 0\,, \quad (5)$$

where T is the kinetic energy operator, and the '+' superscript on $\chi_i^+(\vec{k}_i, \mathbf{r})$ indicates outgoing wave boundary conditions. The initial state distorting potential contains three components $U_i = U_S + U_E + U_{CP}$, where U_S is the initial state spherically symmetric static potential. The static potential is composed of an electronic part and a nuclear part. The electronic part is calculated from the molecular charge density obtained from the

numerical orbitals averaged over all angular orientation. The nuclear part is obtained by averaging the two N_2 nuclei over all orientations (the spherical averaging of the two nuclei places a charge of +14 uniformly distributed on a sphere of radius $1.07a_0$). The exchange-distortion potential U_E is that of Furness and McCarthy (corrected for sign errors) [19], and U_{CP} is the correlation-polarization potential of Perdew and Zunger [20] (see also Padial and Norcross [21]).

The two final channel distorted waves are obtained from a Schrödinger equation similar to Eq. (5):

$$(T + U_f - \frac{k_{a(b)}^2}{2})\chi_{a(b)}^{-}(\vec{k}_{a(b)}, \mathbf{r}) = 0 . \qquad (6)$$

Here $U_f = U_I + U_E + U_{CP}$ where U_I is the final state spherically symmetric static distorting potential for the molecular ion which is calculated using the same procedure as U_S except that the active electron is removed from the charge distribution.

The present M3DW model is an improvement over previously published M3DW results for N_2 [9]. In the earlier results, a very simple N_2 wavefunction and a crude polarization potential with a cut-off parameter were employed. Here, the polarization potential with a cut-off parameter has been eliminated and replaced with the Perdew-Zunger correlation-polarization potential and improved N_2 orbital calculations have been used.

4. Results and discussions

4.1. Asymmetric energy sharing

Under an asymmetric scattering geometry, the TDCS can be viewed as containing two distinct scattering regions. The TDCS in the binary region, located between ejected electron angles of 0° and 180°, describes the direct 'knock out' of a bound electron by the incident electron. The recoil region TDCS, corresponding to ejected electron angles between 180° and 360°, arises due to a secondary, elastic collision between the ejected electron and the target nucleus. The relationship between the TDCS in the binary and recoil regions is an important consideration when considering signatures of two-centre interference.

Here, the approach of Milne-Brownlie *et. al.* [8] and and Staicu Casagrande *et al.* [10] has been employed. Both studies were based on the work of Stia *et al* [22], who showed that the TDCS for H_2 ionization could be approximated as:

$$TDCS_{H_2} = 2I \times TDCS_H, \tag{7}$$

where I is the 'interference factor', which describes the two-centre interference. The interference factor is given by:

$$I = 1 + \frac{\sin(|\boldsymbol{\chi}||\boldsymbol{\rho}_0|)}{|\boldsymbol{\chi}||\boldsymbol{\rho}_0|}, \tag{8}$$

where ρ_0 is the equilibrium inter-nuclear separation, 1.07Å for N_2, and $\boldsymbol{\chi}$ is:

$$\boldsymbol{\chi} = \boldsymbol{k}_s - \boldsymbol{k}_e - \boldsymbol{k}_0. \tag{9}$$

Milne-Brownlie *et. al*. and Staicu Casagrande *et. al.* compared the measured TDCS for H_2 with theoretical calculations of the TDCS for H, H_2 and He, and with experimental measurements of the TDCS for He, and concluded that there was evidence for interference in the cross section for H_2, based on the predictions of equation (7).

When plotted as a function of the ejected electron emission angle (figure 1), the interference factor shows a two-fold enhancement of the TDCS in the binary collision region. That is, one would expect that the binary peak for N_2 ionization is four times bigger than the equivalent atomic cross section, rather than simply twice as big due to the additional scattering centre. However, as the measured cross sections are not on an absolute scale, an increase in the binary peak due to interference could not be verified by this method. However, while the interference factor enhances the TDCS in the binary region, its effect in the recoil region is to suppress the TDCS somewhat (by a factor of 0.8). Hence, by measuring the TDCS and comparing the magnitudes of the binary and recoil scattering, two-centre interference effects should manifest as a suppression of the recoil peak, relative to the binary, when compared with the atomic binary-to-recoil ratio. Note that while Stia *et. al.* derived this approximation only for the case of H_2, one might expect that a similar analysis would hold, at least qualitatively, in the case of N_2 ionization.

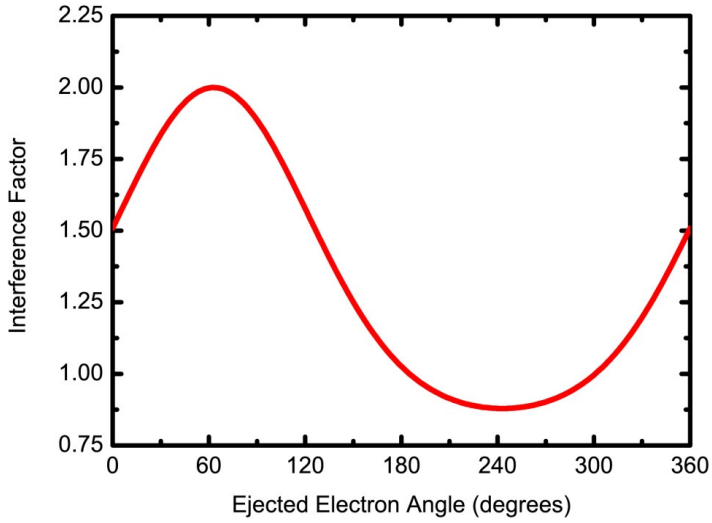

Figure 1: (Color online) Interference factor as a function of ejected electron emission angle, for continuum electron energies of E_0=150 eV, E_s=124.4 eV, E_e=10 eV.

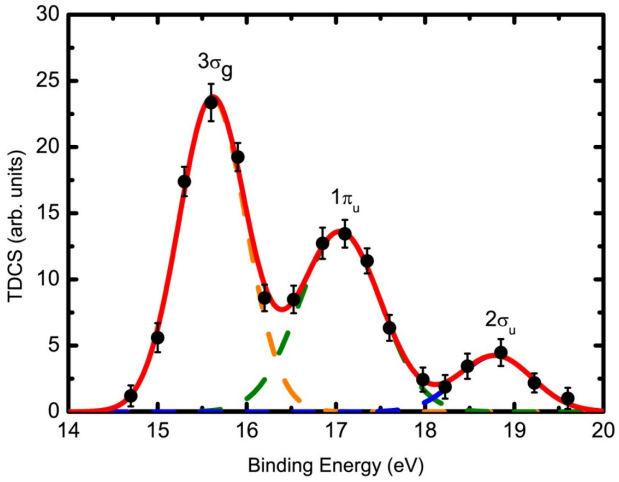

Figure 2: (Color online) Binding energy spectrum for N_2. The 3 outermost orbitals (labelled in the figure) are all resolved at the current coincidence energy resolution of 850 meV.

TDCS measurements were made for ionization of the three outermost orbitals of N_2, the $3\sigma_g$, $1\pi_u$ and $2\sigma_u$ orbitals, all of which were resolved with the present coincidence energy resolution (figure 2). The incident electron energy was set at 150 eV and the ejected electron energy 10 eV. The measured results for each orbital are presented figure 3, together with a calculated, kinematically equivalent, *atomic* nitrogen TDCS and the same atomic TDCS multiplied by the interference factor. All three data sets have been normalised together at the binary maximum. The atomic TDCS have been calculated using the distorted-wave Born approximation (DWBA) code of McCarthy [23].

In figure 3, the experimental data for the three molecular orbitals are compared with the DWBA calculations for the atomic orbitals with the most similar momentum distribution. The two *u*-type molecular orbitals have been compared to the TDCS for an atomic 2*p*-orbital, due to the presence of a node in both orbital momentum distributions (in fact, the $2\sigma_u$ orbital is actually an *s*-orbital hybrid). Similarly the experimental results for the $3\sigma_g$ molecular orbital, a *p*-orbital hybrid, have been plotted against an atomic 2*s*-orbital calculation since both these orbitals' momentum distributions do not contain a node. Also note that the molecular continuum-electron energies were used when calculating the atomic cross sections. In effect this means that the atomic orbitals were prescribed the same ionization potential as the molecular nitrogen orbitals, rather than their physical ionization potential. This approach ensured the experimental and theoretical results were kinematically identical.

As discussed, multiplying the atomic calculations by the interference factor decreases the magnitude of the cross section in the recoil region, relative to the binary region. Across all three orbitals considered, the modification of the atomic calculation by the interference factor significantly improves the description of the experimental data, compared to the unmodified calculation. Indeed, the $1\pi_u$ and $2\sigma_u$ experimental results are in overall excellent agreement with the modified atomic calculations, in both the binary and recoil regions. The $3\sigma_g$ data shows slightly less good agreement, with the location of the binary peak in the molecular cross section shifted with respect to the atomic calculation. Nonetheless, the binary/recoil ratio is certainly better described by the modified DWBA calculation than the straight atomic calculation. As discussed, this

behaviour is consistent with the influence of two-centre interference on the TDCS, and hence all three data sets can be interpreted as showing evidence of interference effects.

In addition to the DWBA results, results from an M3DW calculation for *molecular* nitrogen are included in figure 1(a) for the $3\sigma_g$ orbital. The M3DW approach inherently incorporates two-centre interference due to the two-centre distorting potentials and wavefunctions employed in the calculations. The new M3DW result is in significantly better agreement with the experimental data in terms of the position and width of the binary peak, but predicts a stronger recoil peak than is observed in the experimental data and in terms of the binary/recoil ratio, is in poorer agreement with the experiment than either of the modified or unmodified atomic calculations. In light of the good accord between the M3DW and experimental data for H_2 [8] in the recoil region, under very similar kinematics, the disparity observed here is somewhat surprising and not fully understood at this time.

2.4. Symmetric energy sharing

TDCS measurements were made for the $3\sigma_g$ orbital of N_2 (figure 4) using an incident energy of 75.6 eV and equal scattered and ejected energies of 30 eV. Measurements were made at two different scattered electron angles, -25° and -10° degrees. The measurements at a scattering angle of -25° essentially repeat the kinematics considered in Murray *et. al.* [9], while the data at -10° probes the kinematics considered in the theoretical study of Gao *et. al.* [7]. In addition to the measurements, new M3DW calculations at both scattered electron angles are presented.

The -25° kinematics was previously considered, both experimentally and theoretically, by Murray *et. al.* [9,24]. The earlier theoretical data employed an older M3DW approach using an elementary N_2 wavefunction and a polarization potential with a cut-off parameter. The earlier M3DW results showed a large peak in the cross section, centred on 110°, in addition to the normal binary and recoil structures. This peak was presented as possible evidence of two-centre interference, as the same approach predicted no evidence of a similar structure in the atomic TDCS under equivalent kinematics [7].

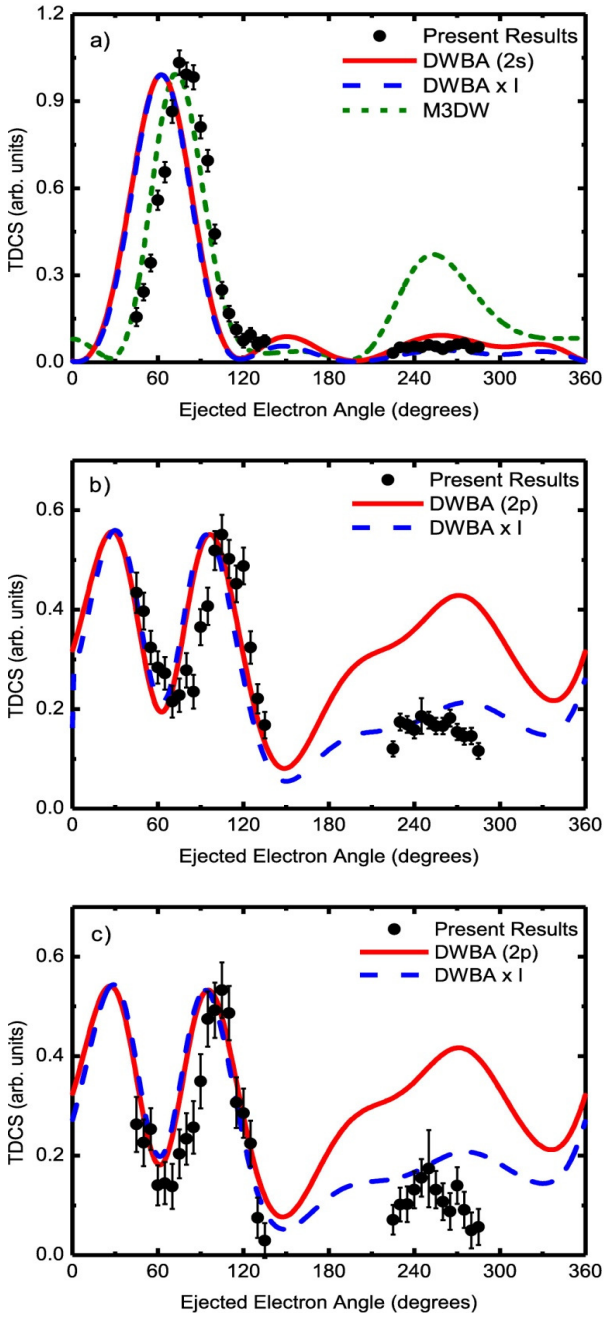

Figure 3: (Color online) TDCS for ionization of the (a) $3\sigma_g$, (b) $1\pi_u$ and (c) $2\sigma_u$ orbitals of N_2. The incident electron energy was 150 eV, the ejected electron energy was 10 eV and the scattered electron angle -15°. The experimental results (circles) are compared with DWBA calculations for the atomic nitrogen 2*s* (a) and 2*p* (b, c) orbitals (solid curve), and the same calculation multiplied by the interference factor (long dashed curve). Also shown is the M3DW calculation for ionization of the $3\sigma_g$ orbital of N_2 (short dashed curve).

The experimental results showed a slight increase in the TDCS in the backward scattering region which was interpreted by the authors as *possible* evidence for the interference structure. However, the location of the peak was significantly shifted and much smaller in magnitude that predicted by the theory and overall the agreement between the experimental and theoretical data was poor. In view of the significant discrepancy in the previous results, this kinematic regime has been further explored here.

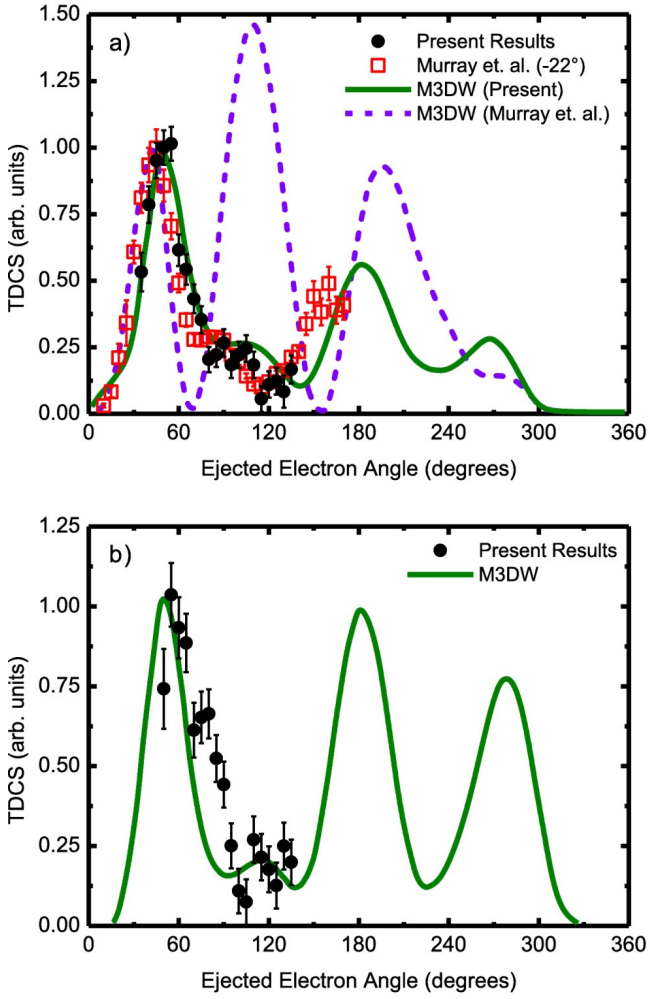

Figure 4: (Color online) TDCS for ionization of the $3\sigma_g$ orbital of N_2. The incident electron energy was 75 eV, the scattered and ejected electron energies 30 eV, with scattered electron angles of (a) -25° and (b) -10°. The present experimental results (circles) are compared to results from new M3DW calculations (solid curve), as well as results from a previous experiment (open squares) [9] and a previously published M3DW calculation (short dashed curve) [24].

The present results at θ_s = -25° are presented in figure 4(a), together with the data of Murray *et. al.* [9,24] and results from the present improved M3DW calculation. Clearly, the two experimental results and the new theoretical data are all in excellent accord, apart from a slight shift in the location of the binary peak. This apparent shift is a result of the slightly different scattering angle considered by Murray *et. al.* (θ_s = -22°). The improved M3DW calculation also retains the three peaks seen in the earlier calculation: a binary peak at 50°, recoil peak at 270° and 'interference' peak at 180°. The magnitude of the interference peak is significantly reduced in the new calculation, which overall is in excellent agreement with both sets of experimental results. Unfortunately, the 180° peak lies outside of the angular range of the experimental apparatus in its current configuration, and so the present experimental results do not offer any new insights into this feature.

The experimental results at a scattering angle of θ_s = -10° (figure 4(b)) are also in generally good agreement with the M3DW calculation. In this instance, there is a small discrepancy in the location of the binary peak, with the calculation locating this peak at too small an ejection angle by around 5°. An interference peak is again predicted in the vicinity of 180° and with a somewhat stronger intensity than in the θ_s = -25° TDCS, relative to the binary peak. Again, the peak lies outside of the accessible range of the apparatus.

Gao et al. [7] interpreted the peak at 180° as a double-slit interference pattern resulting from electrons back-scattering from two separated N_2 nuclei. Since this simple classical picture would suggest that the 180° peak is determined solely by the nuclear separation and not the electronic distribution, the dependence of the cross section on the nuclear separation was examined for a fixed electronic distribution. In fig. 5, M3DW results for the TDCS at a scattering angle of -22° (normalised together at the binary maximum) are presented where the size of the nuclear separation is reduced from 2.14 a_0 to a point charge while keeping everything else unchanged. If the 180° peak is due to backscattering from two separate nuclei, the peak should reduce in magnitude as the nuclei are brought closer together and disappear completely when the distance between the nuclei is reduced to a point charge [25]. However, as is clear from figure 5, the results do not bear out such behaviour. The peak persists even when the nuclear

separation reduces to a point charge and the magnitude minimises at 0.5 a_0, before increasing again with further reduction in nuclear separation. Therefore, the present results do not support the original suggestion of Gao *et al*. [7] that the 180° peak is a Young-type interference resulting from nuclear scattering. On the other hand, it certainly represents interference of some type between amplitudes and is supported by the existing experimental data.

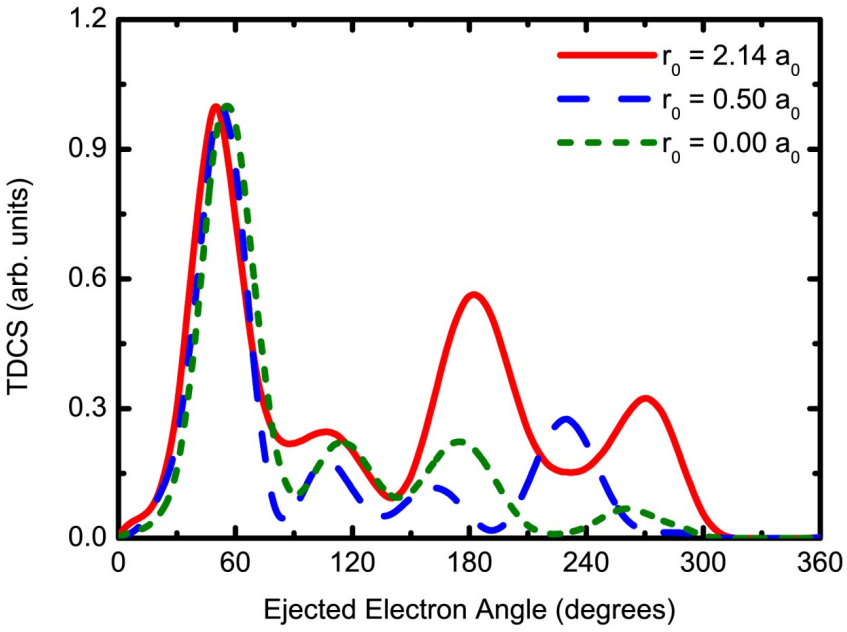

Figure 5: (Color online) TDCS for coplanar symmetric ionization of the $3\sigma_g$ orbital of N_2. The incident energy was 75 eV, both outgoing electrons have 30 eV energy and the scattered electron angle was -22°. The M3DW calculations are for different nuclear separations r_0: r_0= 2.14 a_0 (solid curve); r_0= 0.5 a_0 (long dashed curve); and r_0= 0.0 a_0 (short dashed curve).

5. Conclusions

TDCS data for ionization of N_2 molecules have been presented and examined for signatures of two-centre interference effects. The current data considers two different approaches for detecting two-centre interference. For higher energies and asymmetric kinematics, the molecular recoil peak is suppressed compared to theoretical atomic recoil peaks in accordance with the two-centre predictions. For lower energy symmetric

collisions, the present results are in very good agreement with previous experimental measurements and the improved M3DW results. The M3DW predicts a peak at 180^0 scattering which had previously been interpreted as a double scattering interference peak. Although this angular range is not accessible to the present measurements, the 180° peak is consistent with earlier measurements. However, model calculations with different nuclear separations suggest that this peak does not result from electron scattering from two separate nuclei. Consequently, the present results suggest that two centre effects can be seen in the ratio of recoil peak to binary peak but that other peak structures predicted by the theory are probably due to some other type of interference which is yet to be determined.

Acknowledgments

This work was supported by the Australian Research Council under a Centre of Excellence Scheme and the American NSF under grant number 0757749. CGN would like to acknowledge the support of the National Natural Science Foundation of China under contract No. 10704046 and OA-H would like to acknowledge the support of the Saudi Ministry of Higher Education's King Abdullah Bin Abdul-Aziz Scholarship.

References

[1]N. Stolterfoht *et. al.*, *Phys. Rev. Lett.* **87**, 023201 (2001)
[2]N. Stolterfoht *et. al.*, *Phys. Rev. A* **69**, 012701 (2004)
[3]D. Mishra *et. al., Phys. Rev. Lett.* **92,** 153201 (2004)
[4]D. Akoury *et al.*, *Science* **318**, 949 (2007); N. Stolterfoht *et al.*, *Phys. Rev. A* **67**, 030702(R) (2003); D. Misra *et al*., *Phys. Rev. A* **74**, 060701(R) (2006)
[5]O. Kamalou, J.-Y. Chesnel, D. Martina, J. Hanssen, C.R. Stia, O.A. Fojon, R. D. Rivarola and F. Fremont, *Phys. Rev. A* **71**, 010702(R) (2005)
[6]J. S. Alexander, A. C. Laforge, A. Hasan, Z. S. Machavariani, M. F. Ciappina, R. D. Rivarola, D. H. Madison and M. Schulz, *Phys. Rev. A* **78**, 060701(R) (2008)
[7]J. Gao, D.H. Madison and J.L. Peacher, *Phys. Rev. A* **72**, 032721 (2005)
[8]D.S. Milne-Brownlie, M. Foster, J. Gao, B. Lohmann and D.H. Madison, *Phys. Rev. Lett* **96**, 233201 (2006)
[9] A.J. Murray, M.J. Hussey, J. Gao, and D.H. Madison, *J. Phys. B* **39**, 3945 (2006)
[10] E. M. Staicu Casagrande, A. Naja, A. Lahmam-Bennani, A.S. Kheifets, D.H. Madison and B. Joulakian, *J. Phys.: Conf. Ser.* **41**, 012016 (2008)
[11] M.A. Haynes and B. Lohmann, *J. Phys. B* **33**, 4711 (2000)
[12] I. Bray, private communiciaton

[13] M. Dürr, C. Dimopoulou, B. Najjari, A. Dorn and J. Ullrich, *Phys. Rev. Lett.* **96,** 243202 (2006)
[14] J. Gao, J. L. Peacher and D. H. Madison, *J. Chem. Phys.* **123**, 204302 (2005)
[15] J. Gao, D. H. Madison and J. L. Peacher, *J. Chem. Phys* **123**, 204314 (2005)
[16] J. Gao, D. H. Madison and J. L. Peacher, *J. Phys. B* **39**, 1275 (2006)
[17] C. Lee, W. Yang and R. G. Parr, *Phys. Rev. B* **37**, 785 (1988)
[18] C. F. Guerra et al., *Theor. Chem. Acta* **99**, 391 (1998)
[19] J. B. Furness and I. E. McCarthy, *J. Phys. B* **6**, 2280 (1973)
[20] J. P. Perdew and A. Zunger, *Phys. Rev. B* **23**, 5048 (1981)
[21] N. T. Padial and D. W. Norcross, *Phys. Rev. A* **29**, 1742 (1984)
[22] C.R. Stia, O.A. Fojon, P.F. Weck, J. Hanssen and R.D. Rivarola, *J. Phys. B* **36**, L257 (2003)
[23] I. E. McCarthy, *Aust. J. Phys.* **48**, 1, (1989)
[24] A.J. Murray, M.J. Hussey, C. Kaiser, J. Gao and D.H. Madison, *Journal of Electron Spectroscopy and Related Phenomena.* **161**, 11-16 (2007)
[25] O. Al-Hagan, C. Kaiser, D. Madison and A. J. Murray, *Nature Physics* **5**, 59 (2008)

VII. Low-energy Symmetric Coplanar and Symmetric Non-coplanar (e, 2e) Studies from the $3a_1$ State of H_2O

Kate L Nixon[1], Andrew James Murray[1], Ola Al-Hagan[2], Don H Madison[2] and Chuangang Ning[3]

[1] *School of Physics and Astronomy, Photon Science Institute, University of Manchester, Manchester M13 9 PL, UK*

[2] *Department of Physics, Missouri University of Science and Technology, Rolla, MO 65409 USA*

[3] *Department of Physics and Key Laboratory of Atomic and Molecular NanoSciences of MOE, Tsinghua University, Beijing 100084, People's Republic of China*

Abstract

Experimental and theoretical results are presented for electron impact ionization of water in the energy regime from near threshold to intermediate energies. Results were taken in symmetric coplanar and non-coplanar geometries, with both equal and non-equal outgoing electron energies. The models approximate the random orientation of the target using a spherical averaging of the wavefunction prior to the collision, using sophisticated distorted wave Born calculations that include post-collisional interactions in first order and to all orders of perturbation theory. The calculations predict the data most accurately at the lowest energy studied (4 eV above threshold) in a coplanar symmetric geometry, whereas the comparison between theory and experiment is generally marginal for higher energies and for non-coplanar geometries.

1. Introduction

Water is one of the most abundant molecules on earth. It is a relatively simple molecule and has attracted much attention over the years. The human body, and other biological material comprise ~80% water, which makes water an ideal test case to investigate processes occurring in the body. As an example, energy deposition and angular distributions resulting from electron collisions with water are used in charged particle track structure analyses to model radiation damage in biological samples [1]. These models are an active area of research since the observation that high-energy radiation that is used to treat cancers also liberates many low-energy electrons, causing additional damage to cell DNA [2]. These low-energy electrons have an effect over a much wider volume than the targeted cancer site. Knowledge of the collision dynamics of low energy electrons with biological systems is hence needed, so as to develop robust models of these processes. As a starting point, these biological systems are approximated as H_2O molecules.

(e, 2e) studies can be used to fully characterize the collision dynamics of electron impact ionization. In such experiments the energy and momenta of the outgoing electrons are measured, giving a fivefold-differential cross section. Despite this, only two experimental studies of electron impact ionization of H_2O at energies where the collision dynamics are important have been reported. The first used incident energies of ~250 eV in an asymmetric coplanar configuration [3]. The second concentrated on the highest occupied molecular orbital (HOMO) at lower energies, i.e. <100 eV [4]. Consequently, only a limited number of theoretical investigations have been reported for incident energies below 300 eV [5]. Alternatively, (e, 2e) studies of H_2O at higher energies conducted under electron momentum spectroscopy conditions have been used to study the electronic structure of this chemically important molecule [6, 7], and these structure results are used to inform the models for lower energy collisions.

At incident energies less than ~200 eV, the collision dynamics are strongly influenced by effects including post collision interactions, target polarization, distortions in the wavefunctions for the participating electrons and multiple collisions. In this regime these processes must be considered on an equal basis, and so the complexity of the interactions means that theoretical studies have mainly been limited to atomic targets.

Current models are now at the stage where they yield reasonable agreement with experimental data for a range of atoms, implying a good understanding of the collision dynamics under the conditions used in the experiments, and these models are now being extended to low-energy (e, 2e) collisions from molecules.

Molecular targets provide a significant challenge to theory due to their distributed nuclei. This contrasts to atoms which have a single nuclear scattering centre, and which can hence be described using a spherical basis. Molecular wavefunctions are generally not spherical, the nuclei within the molecule providing multiple scattering centres. A key challenge in modelling electron collisions with molecules is hence in developing an accurate multi-centred wavefunction. A further challenge arises since the experiments cannot, at present, align the molecules prior to the collision; therefore, the models must consider the random orientation of the targets for accurate comparison with experiment. This becomes a computationally intensive problem, and so approximations are usually made to allow these calculations to become tractable.

Recently, experiments studying simple diatomic targets including H_2 and N_2 [8–12] have provided benchmark data to assess the performance of the new models that are being developed. The majority of data were recorded in a coplanar geometry, where the incident and two outgoing electrons are all in the same plane, and were conducted at a higher incident energy than the studies presented here. By contrast the apparatus at Manchester can also access *non-coplanar* geometries, and so has provided additional data to further test these models. Studies on more complex molecules at low energies are more limited, with only two measurements for CO_2 being reported [13, 14]. In this case no theoretical data were available for comparison with experiment.

H_2O has five molecular orbitals: $1a_1$, $2a_1$, $1b_2$, $3a_1$ and $1b_1$ (HOMO). The symmetry of the $2p_y$ oxygen atomic orbital, representing the lone pair of electrons on the oxygen atoms, prevents it from hybridizing with the H atomic orbital, leaving the molecular $1b_1$ HOMO orbital essentially atomic like, and therefore symmetric. In a previous study the groups at Manchester and Missouri investigated the $1b_1$ (HOMO) state of H_2O in coplanar kinematics [4]. However, the orientation averaged molecular orbital used in the theoretical calculation is not a good approximation for that state given the cancellations due to the orbital symmetry. By contrast, the $3a_1$ orbital of interest in this

paper is involved in the *O–H* bonding and has a charge density distribution that is distorted from that of a symmetric atomic-like orbital. The molecular orbital used in the model therefore should not suffer from the same cancellation problem during the orientational averaging procedure. Thus, a comparison here between the theoretical predictions and the experimentally measured results should provide a much better assessment of the current models of the collision dynamics.

The remainder of this paper is presented in four sections. A brief description of the apparatus used to measure the differential cross sections is given in section 2, where experimental considerations necessary to obtain good quality data are highlighted. Section 3 outlines the techniques used to generate the theoretical predictions. Both experimental and theoretical data are presented and discussed in section 4. Section 4.1 shows symmetric coplanar data, 4.2 gives symmetric non-coplanar data and section 4.3 shows data collected in both coplanar and perpendicular symmetric geometries with unequal energy sharing. Finally, section 5 draws conclusions from this investigation, and outlines future directions.

2. Experimental apparatus

The experimental triple-differential cross sections (TDCS) presented in section 4 were measured in the (e, 2e) apparatus at the University of Manchester. This apparatus is fully computer controlled and computer optimized, allowing it to operate continuously without user intervention. Full details of this spectrometer have been given previously [15–17] and so only a brief description is given here, with details pertinent to this study. The spectrometer can be operated in a 'standard' coplanar geometry where the momenta of all three electrons (the incident and two outgoing electrons) are within the same detection plane ($\psi = 0°$, figure 1). The electron gun can also rotate out of the detection plane, ($0° < \psi < 90°$) to access non-coplanar geometries, with $\psi = 90°$ being termed the *perpendicular geometry*. The two outgoing electron analysers rotate independently in the detection plane as shown. The analyser angles, ξ_1 and ξ_2, are referenced to the incident electron beam direction. In this study the analysers were always kept in a symmetric configuration, i.e. $\xi_1 = \xi_2 = \xi$.

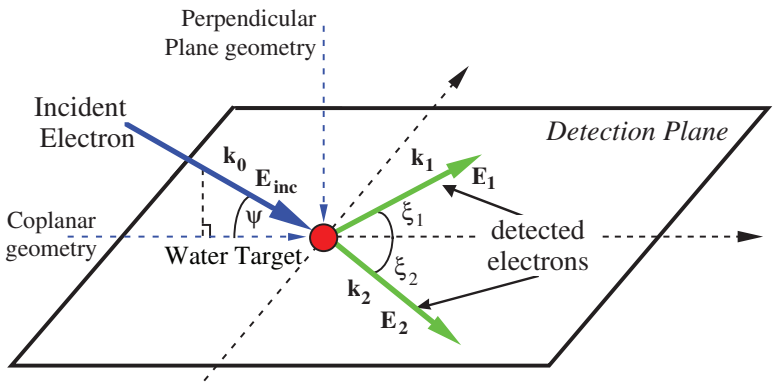

Figure 1: Schematic of the scattering geometry, depicting the various angles employed. A *coplanar geometry* (ψ=0°) is defined when all three electrons are in the detection plane. The analyzer angles (ξ_1 and ξ_2) are measured with respect to the projection of the incident electron beam k_0 onto this plane as shown. For non-coplanar geometries the electron gun is lifted out of the plane, and is defined by the angle ψ. ψ=90° is called the *perpendicular geometry*.

The power supplies for the electrostatic lenses in the electron gun and the electron analysers are fully computer controlled and computer optimized. This feature allows for automated tuning of the spectrometer optics at regular intervals, with the analysers being re-optimized each time they move to a new angle ξ. The energy of the spectrometer was re-calibrated at the start of each new kinematic arrangement, by measuring the coincidence binding energy spectrum. Here, the coincidence count rates as a function of incident energy are measured by scanning the incident electron beam energy (see figure 2). The coincidence energy resolution obtained with this apparatus was typically ~1.3 eV, which is sufficient toresolve the H_2O $3a_1$ orbital from those at higher and lower binding energies, as shown in figure 2. Over the course of this study the binding energy spectra were recorded for various energies and geometries, and it is estimated that contamination from neighbouring orbitals was always less than 10%, and is more typically in the range of 0.5%. The angular resolution of the apparatus is estimated as ±3°, based on geometric considerations of the electrostatic lenses at those energies.

The distilled water sample used to provide the molecular target beam was contained within a 50 mm diameter 100 mm long stainless steel vessel sealed by a CF-70

flange to a 6.35 mm swagelok fitting. The vessel was connected to the scattering chamber via 6.35 mm copper tubing.

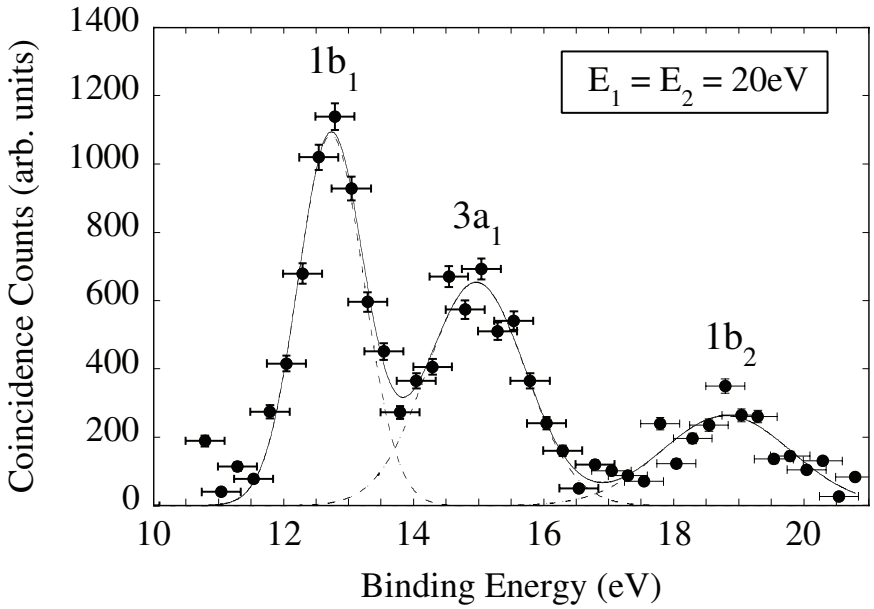

Figure 2: A typical coincidence binding energy spectrum obtained for H_2O. These data were measured in a coplanar geometry with outgoing electron energies of 20 eV detected at $\xi_1 = \xi_2 = 55°$. The peaks in the spectrum correspond to the three highest orbitals, *i.e.* the $1b_1$, $3a_1$ and $1b_2$ orbitals as labelled. The full line represents a three-Gaussian fit, whereas the dotted lines show the individual Gaussians from this fit, illustrating the degree of separation measured with the current energy resolution. Very little contamination is expected from neighbouring orbitals in the measured TDCS for the $3a_1$ state.

A needle valve at the entrance to the scattering chamber controlled the flow of target H_2O vapour into the interaction region. The sample vessel and gas handling line were held at a constant temperature of 50 °C throughout data collection, so as to create sufficient driving pressure for the target beam. Several freeze-pump-thaw cycles were performed using a salted ice slurry bath, to remove dissolved gas impurities from the water prior to admission into the scattering chamber. The purity of the target beam was verified with a Spectra VacScan mass spectrometer fitted to the scattering chamber.

Typical operational ratios of H_2O to N_2 were >25:1, and it was observed that the partial pressure of N_2 did not change appreciably from the background value when the needle valve was opened. This indicates that anH_2O target molecular beam of high purity was created, as confirmed from binding energy spectral studies. The purity of this beam was monitored regularly using the mass spectrometer throughout this study. The background pressure within the scattering chamber was set to 1.1×10^{-5} torr during operation, and was found to remain constant throughout all data runs, in contrast to the observations of Milne-Brownlie *et al* [3] during their studies.

During these experiments we observed an unusual behaviour of the tungsten hairpin filament used as the incident electron source. Over time the emission current from the filament dramatically increased, when a constant current was delivered to the filament. This increase in emission current was often more than a factor of 2 within a 24 h period. To ensure constant incident electron beam current throughout the measurements as required, the filament current was hence also placed under computer control. To facilitate this, the current measured by the Faraday cup located on the opposite side of the interaction region to the electron gun was monitored by the computer control software, and the current through the filament adjusted to maintain a beam current of 300 nA throughout data collection. To illustrate the scale of these changes, over the duration of this work (~ 5 months) the filament current required to produce a beam current of 300 nA reduced from 2.1 A at commencement of these studies to less than 1.0 A. Previous measurements in this spectrometer also observed this effect [4], but did not find any explanation. In the present study we also measured the coincidence energy resolution from ionization of helium, and found that this did not change, indicating that the temperature of emission remained approximately constant. The reason for the steadily decreasing filament current is hence unknown at this time.

The first set of data presented in section 4.1 employ coplanar kinematics where the outgoing electron energies and polar angles of both analysers are the same, i.e. $E_1 = E_2$ and $\xi_1 = \xi_2$. Differential cross-section (TDCS) measurements using incident energies of 4 eV, 10 eV, 20 eV and 40 eV above the ionization potential of the $3a_1$ state (IP ~15 eV) over an angular range of 35–125° are presented in figure 3, along with the

corresponding theoretical predictions. Section 4.2, and figure 4, shows data taken for symmetric kinematics where both outgoing electron energies are 10 eV. For these data sets the angle of the electron gun is varied from the standard coplanar geometry ($\psi = 0°$), through to $\psi = 90°$ for the perpendicular geometry. Finally, unequal energy sharing kinematics were investigated (figure 5) as discussed in section 4.3. Here, the angles of the analysers were equal, $\xi_1 = \xi_2$; the incident electron energy was 20 eV above the ionization threshold and the energies of the outgoing electrons were set to be *unequal*. The first set of data used $E_1 = 18$ eV and $E_2 = 2$ eV, while the second used $E_1 = 15$ eV and $E_2 = 5$ eV. Data were measured only for coplanar and perpendicular geometries, over angular ranges from 22.5° to 130° and 35° to 140° respectively.

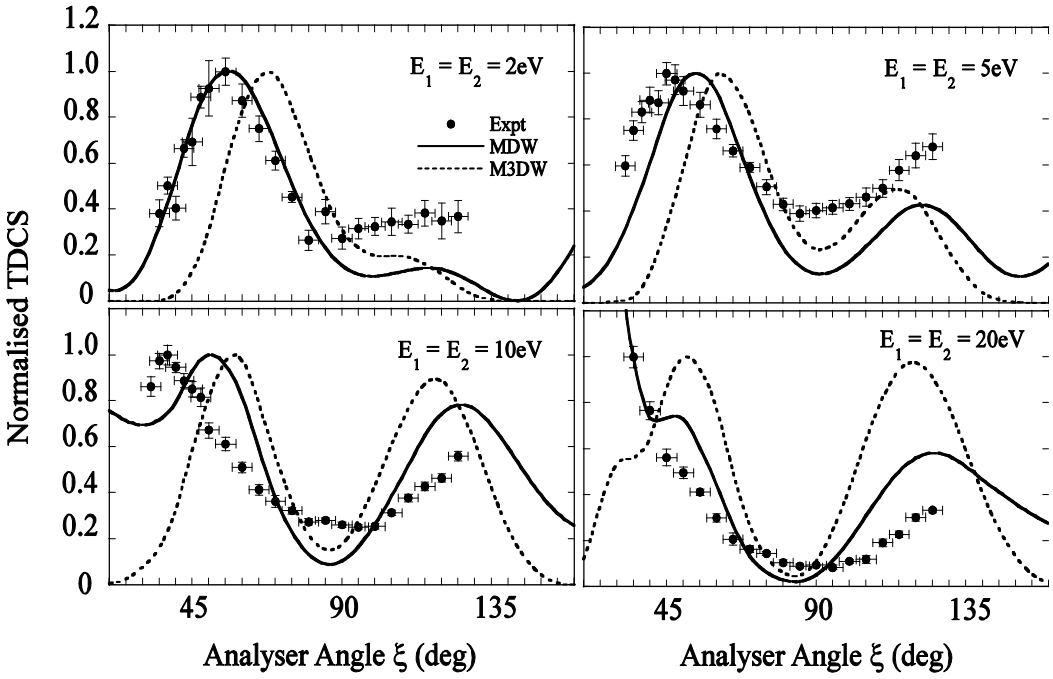

Figure 3: Triple differential cross sections for ionisation of the $3a_1$ state of H_2O using coplanar symmetric kinematics (*i.e.* ψ=0° and ξ_1=ξ_1). The energies of the outgoing electrons are shown on the respective plots. The solid line shows results from the Molecular Distorted Wave Born Approximation (MDW) while the dashed line was generated from the Molecular 3-body Distorted Wave Approximation (M3DW). The experimental and theoretical data has been independently normalised to unity at each energy.

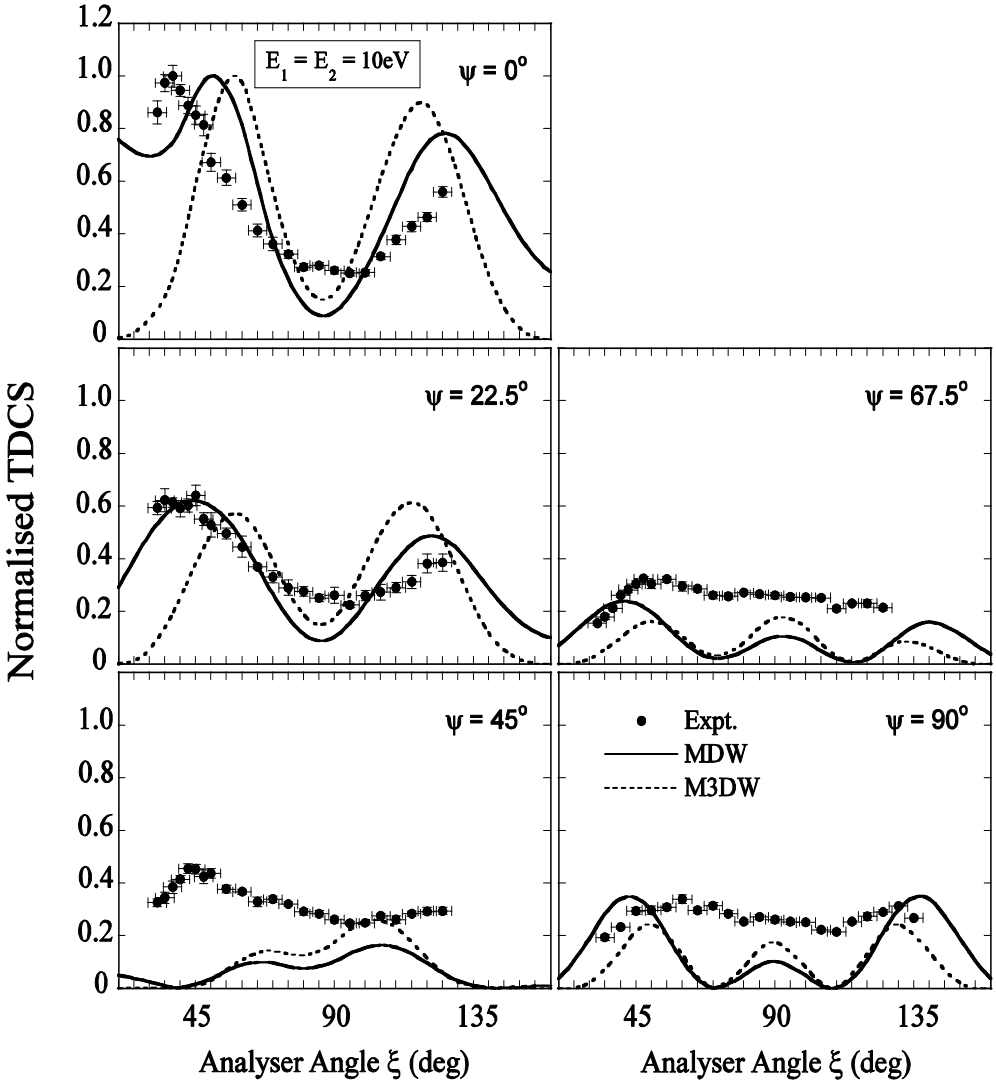

Figure 4: Triple differential cross sections for the ionisation of the $3a_1$ state of H_2O. These measurements were taken in a series of symmetric non-coplanar geometries with outgoing electron energies of 10 eV. The angle of the electron gun (ψ) is shown on the respective plots. The data and theory are normalised to unity at the peak in the coplanar (ψ=0°) geometry. The data within the remaining plots are normalised at the ξ=90° point (see text for details).

All data presented here were taken using a constant chamber pressure and constant beam current as noted above. The data were normalized to a collection time of 1000 s for each measurement, and up to 30 angular sweeps of the detection plane were

used to produce statistically significant results. The data presented in figures 3–5 were then averaged over these sweeps, and the uncertainties in the measurements determined from the complete set of data for each scattering angle.

3. Theoretical framework

The molecular 3-body distorted wave (M3DW) approximation has been presented in previous publications [18–20] so only a brief outline of the theory will be given. The triple-differential cross section (TDCS) for the M3DW is given by:

$$\frac{d^5\sigma}{d\Omega_a \Omega_b dE_b} = \frac{2}{(2\pi)^5}\frac{k_a k_b}{k_i}|T|^2 \qquad (1)$$

where $\vec{k}_i$, $\vec{k}_a$, and $\vec{k}_b$ are the wave vectors for the initial, scattered and ejected electrons, respectively. The amplitude is given by:

$$T = \left\langle \chi_a^-(\vec{k}_a, \mathbf{r}_1)\chi_b^-(\vec{k}_b, \mathbf{r}_2) C_{scat-eject}(\mathbf{r}_{12}^{ave}) \middle| V - U_i \middle| \phi_j^{OA}(\mathbf{r}_2)\chi_i^+(\vec{k}_i, \mathbf{r}_1) \right\rangle \quad (2)$$

where r_1 and r_2 are the coordinates of the incident and the bound electrons, χ_i,χ_a, and χ_b are the distorted waves for the incident, scattered, and ejected electrons respectively, and $\phi_j^{OA}(\boldsymbol{r}_2)$ is the initial bound-state wavefunction which is approximated as the orientation averaged molecular wavefunction for the molecular orbital of interest. The molecular wavefunction was calculated using density functional theory (DFT) along with the standard hybrid B3LYP [21] functional by means of the ADF 2007 (Amsterdam Density Functional) program [22] with the TZ2P (triple-zeta with two polarization functions) Slater-type basis sets. The factor $C_{scat-eject}(r_{12}^{ave})$ is the Ward-Macek average Coulomb-distortion factor between the two final-state electrons [23], *V* is the initial state interaction potential between the incident electron and the neutral molecule and U_i is a spherically symmetric distorting potential which is used to calculate the initial-state distorted wave for the incident electron $\chi_i^+(\vec{k}_i, \mathbf{r}_1)$.

The Schr¨odinger equation for the incoming electron wavefunction is given by

$$(T + U_i - \frac{k_i^2}{2})\chi_i^+(\overrightarrow{k_i}, r) = 0 \qquad (3)$$

where T is the kinetic energy operator and the '+' superscript on $\chi_i^+(\vec{k}_i, \mathbf{r}_1)$ indicates outgoing wave boundary conditions. The initial state distorting potential contains three components $U_i = U_s + U_E + U_{CP}$, where U_s is the initial state spherically symmetric static potential which is obtained from the molecular charge density averaged over all angular orientations, U_E is the exchange potential of Furness–McCarthy (corrected for sign errors) [24] which approximates the effect of the continuum electron exchanging with the passive bound electrons in the molecule and U_{CP} is the correlation polarization potential of Perdew and Zunger [25, 26].

The final state for the system is approximated as a product of distorted waves for the two continuum electrons times the average Coulomb-distortion factor. The final state distorted waves are calculated as for the initial state except that the final state spherically symmetric static distorting potential for the molecular ion is used for U_s . The molecular distorted wave Born approximation (MDW) is the same calculation as the M3DW except that the post-collision-interaction (PCI) factor $C_{scat-eject}(r_{12}^{ave})$ is not included in the calculations.

4. Results and discussion

4.1. Symmetric coplanar kinematics

The experimental data recorded here are not measured on an absolute scale and so to compare experiment and theory both are normalized to a maximum intensity of unity at each energy, as shown in figure 3. The experimental data show the typical characteristics expected from measurements such as these. There is a strong peak at forward scattering angles (ξ <90°) and a peak at backward scattering angles (ξ >90°). The overall shape of the TDCS measured at corresponding energies in a previous study of the $1b_1$ state [4] are qualitatively similar; however, the $1b_1$ state shows a second peak in the forward region emerging at higher energies that is not observed in the $3a_1$ state measured here. Milne-Brownlie *et al* [3] also noted that these two outer-most orbitals have a similar structure using different kinematical conditions to those used here.

As the energy of the outgoing electrons is lowered, it would be expected that the Coulomb repulsion between the outgoing electrons should play an increasingly important

role, driving the electrons apart. This repulsion is normally called the post-collision interaction (PCI). PCI would cause the forward peak to shift towards $\xi = 90°$ as is seen in the data. PCI would also be expected to shift the backward peak towards $\xi = 90°$, although this cannot be confirmed in the data as the peak is beyond the angular range measured in this experiment. This trend is much clearer in the present data compared to that from the $1b_1$ state measured at higher energies [4]. The only difference between the two theoretical calculations shown in the figure is that M3DW contains PCI to all orders of perturbation theory while MDW only has PCI to first order, and it is clearly seen that PCI shifts the forward and backward peaks towards $\xi = 90°$ as would be expected. However, it appears that PCI is too strongly represented in the M3DW since the peak positions of the MDW are closer to the experimental data.

Interestingly, the best agreement between experimental data and theory is at the lowest energy, where the experimental data and MDW model are in excellent agreement for the forward peak. This agreement diminishes as the energy increases, which is unexpected since the MDW model is usually more accurate at higher energies.

4.2. Symmetric non-coplanar kinematics

A key advantage of the spectrometer in Manchester is the ability to measure data for kinematics in non-coplanar geometries. Non-coplanar measurements were hence taken here with both outgoing electrons having an energy of 10 eV. As seen in figure 1, the geometry adopted in this spectrometer provides a common normalization point ($\xi_1 = \xi_2 = 90°$) for all gun angles ψ, which allows ALL data at a given energy to be referenced to a common point. For the current measurements, the data at $\psi = 0°$ have been normalized to a maximum intensity of unity, as before. The value of the TDCS at $\xi = 90°$ is then used to re-normalize the remaining data. For the corresponding theoretical model, the coplanar TDCS has also been normalized to unity for both MDW and M3DW models. This scaling factor is then applied to all subsequent data sets at the various gun angles.

The experimental data in figure 4 show a clear trend indicating that the forward and backward peaks diminish in magnitude as the angle of the electron gun increases from $\psi = 0°$ to 90°. The TDCS measured in the perpendicular plane is almost constant

over all angles ξ, which is very different to what is observed for atomic targets. The data contrast strongly with the theoretical predictions for the larger gun angles ψ, where the theories predict significantly more structure than is seen in the data. The progression in both models shows a decrease in cross section from $\psi = 0°$ to 45°, after which the intensity once again increases. Neither model accurately predicts the results that have been obtained experimentally.

The results found here are in strong contrast to what we have found earlier for H_2 [27]. For that case, excellent agreement between theory and experiment was found for the perpendicular plane and the agreement was not nearly as satisfactory in the scattering plane ($\psi = 0°$), yet here we find better agreement in this plane than the perpendicular plane. Also Al-Hagan *et al* [27] predicted that molecules which have nuclei at the centre of mass should have a TDCS with three peaks at 45°, 90° and 135° in the perpendicular plane. The 45° and 135° peaks would be a result of elastic scattering of the projectile with the target bringing the projectile into the perpendicular plane followed by a binary electron–electron collision. The 90° peak should result from elastic scattering of the projectile with the target bringing the projectile into the perpendicular plane, followed by binary electron-electron collision, and finally a 180° backscattering of one of the electrons from the nuclei at the centre of mass. While this prediction was verified for CO_2, here for H_2O theory is consistent with the prediction while experiment shows almost no structure at all for the perpendicular plane.

4.3. Unequal energy sharing, coplanar and perpendicular geometries

The final kinematic configuration investigated here used symmetric geometries and 20 eV excess energy as above; however, in this case the data are for *unequal* energy sharing between the outgoing electrons. The data were only taken for coplanar ($\psi = 0°$) and perpendicular plane ($\psi = 90°$) geometries, so as to contrast differences in these two extremes. Figures 5(a) and (b) reproduce the data in figure 3 at these angles when E_1 = 10 eV and E_2 = 10 eV, figures 5(c) and (d) show data for E_1 = 5 eV and E_2 = 15 eV, while figures 5(e) and (f) show results for E_1 = 2 eV and E_2 = 18 eV. The theoretical calculations using theM3DW and MDW models are also shown, where once again the data and theory have been normalized to unity at the peak in the coplanar geometry.

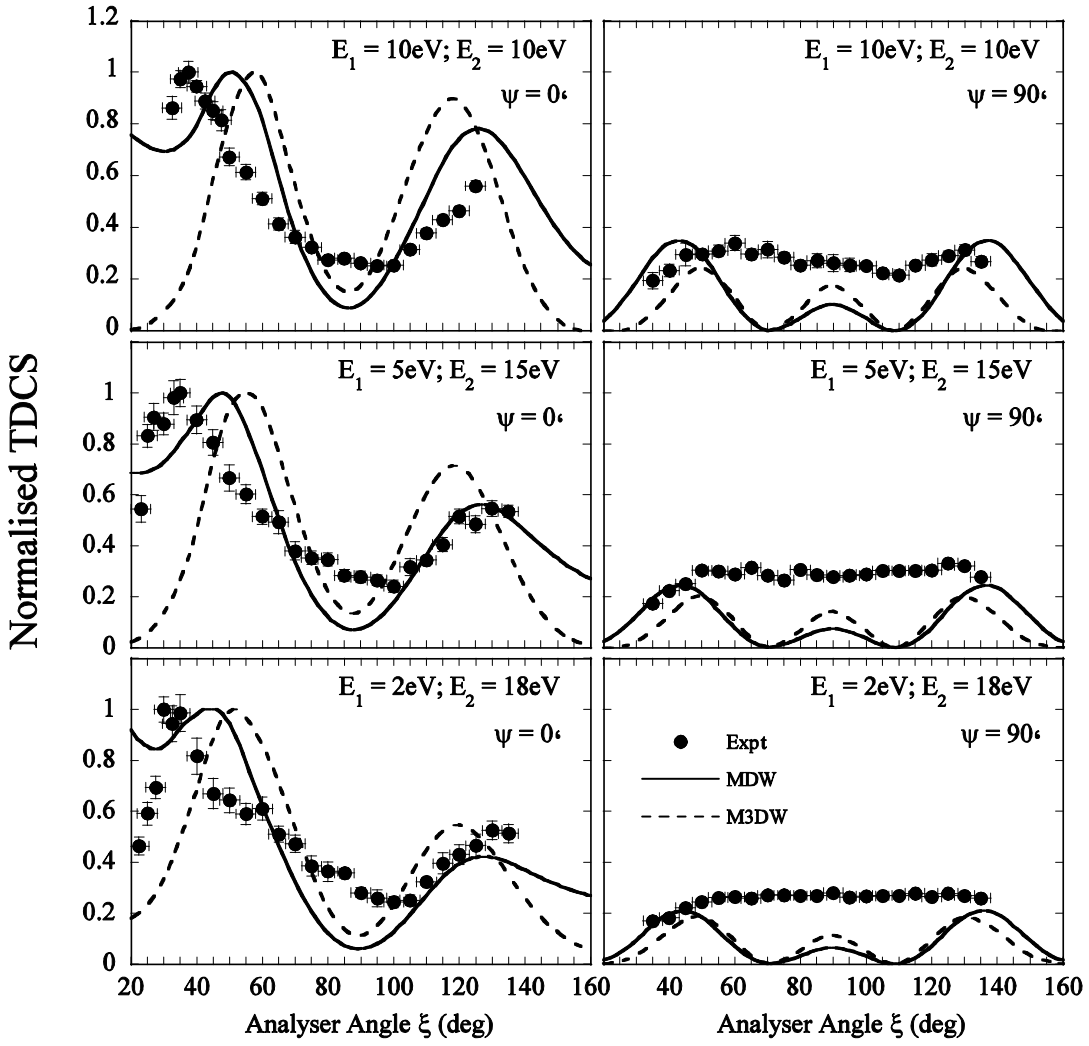

Figure 5: Triple differential cross sections for ionisation of the $3a_1$ state of H_2O. Symmetric geometries were adopted for these data with unequal energy sharing kinematics. Both coplanar and perpendicular geometries were utilised. In all plots the excess energy is 20 eV, with the outgoing electron energies as shown. The electron gun angle ψ is also shown on the respective plots.

The key differences that can be seen in these data for the coplanar geometry are that the forward peak moves to a smaller angle as the energy asymmetry increases, as might be expected from post-collisional interactions. Again for the backward peak, there is not enough data to see this effect at high angles. There also appears to be a narrowing

in the main forward peak as the asymmetry increases, with a new shoulder appearing around $\xi = 60°$. The minimum around 90° in this geometry does not change substantially as the energy sharing changes.

The M3DW and MDW calculations in the coplanar geometry predict the relative magnitudes of the forward and backward peaks for the highest asymmetry, but again the MDW is in better agreement with the experimental peak positions, which is surprising. The position of the minimum is predicted well in all cases, however not the relative magnitude.

In the perpendicular plane the experimental cross section becomes almost completely featureless at the highest asymmetry, although none of the data show any significant structure. This contrasts markedly with the calculations, which predict clear triple peaks in the perpendicular plane that change magnitude only marginally with the asymmetry. The magnitude of the data for equal energy sharing is approximated by the calculation, but this agreement is less satisfactory as the asymmetry increases.

5. Conclusions

Experimental (e, 2e) data for the ionization of water at low energies in both coplanar and non coplanar geometries have been compared with state of the art theoretical results derived from distorted wave models. The theory models the molecules in a spherically averaged basis to allow for the random orientation of the target in the experiments, and considers the effects of post-collisional interactions.

Agreement between theory and experiment is mixed, and rather surprisingly gives best results at low energies, where it might be expected that the approximations are least accurate. The results using the full M3DWmodel (which includes PCI to all orders) appear to overestimate the effects of PCI compared to the MDW theory which only includes PCI to first order. This is particularly seen for coplanar symmetric data 4 eV above threshold, where the forward peak is reproduced more accurately using the MDW calculation.

For non-coplanar measurements the comparison between theory and experiment becomes poorer as the gun angle increases, in contrast to previous results from H_2 which show the opposite trend. This discrepancy is seen both for equal energy and for

non-equal energy data, which have been taken in coplanar and perpendicular geometries. The experimental results for both equal and non-equal energy sharing in the perpendicular plane show almost no structure, whereas the theoretical calculations predict that three clearly defined lobes should be seen.

It is clear from these results that significant discrepancies remain between the models and the experimental data for this important target. These differences may be arising from the approximations made in calculating the spherically averaged wavefunction input to the model, as are used to emulate the random orientation of the targets in the experiment. The results clearly highlight the need for both experiment and theory to provide more exacting data. From the experimental side, it is clearly important to orient the target prior to the collision occurring, whereas theory needs to perform more exacting calculations using a fixed molecular axis, before summing over all possible orientations of the targets so as to yield accurate comparison to experiment. We are considering techniques to try to solve these experimental difficulties, and are investigating the computational challenges that must be overcome to provide more exact theoretical results. It is hoped that in the near future improvements will be forthcoming in both areas, so that robust models of these more complex molecular targets can be derived.

Acknowledgments

This work was supported by the University of Manchester and the US National Science Foundation under grant. No PHY-0757749. KLN would like to thank the British Council for funding under the research exchange programme, and the Royal Society for a Newton International Fellowship. Also, OAH would like to thank the Saudi Ministry of Higher Education's King Abdullah Bin Abdul-Aziz Scholarship for funding. CN would like to acknowledge the support of the National Natural Science Foundation of China under contract no 10704046.

References

[1] Munoz A, Blanco F, Garcia G, Thorn P A, Brunger M J, Sullivan J P and Buckman S J 2008 *Int. J. Mass Spectrom.* **277** 175

[2] Boudaiffa B, Cloutier P, Hunting D, Huels M A and Sanche L 2000 *Science* **287** 1658

[3] Milne-Brownlie D S, Cavanagh S J, Lohmann B, Champion C, Hervieux P A and Hanssen J 2004 *Phys. Rev.* A **69** 032701
[4] Kaiser C, Spieker D, Gao J F, Hussey M, Murray A and Madison D H 2007 *J. Phys.* B **40** 2563
[5] Champion C, Hanssen J and Hervieux P A 2002 *Phys. Rev.* A **65** 022710
[6] Bawagan A O, Brion C E, Davidson E R and Feller D 1987 *Chem. Phys.* **113** 19
[7] Dixon A J, Dey S, McCarthy I E, Weigold E and Williams G R J 1977 *Chem. Phys.* **21** 81
[8] Staicu Casagrande E M *et al* 2008 *J. Phys.* B **41** 025204
[9] Colgan J, Al-Hagan O, Madison D H, Kaiser C, Murray A J and Pindzola M S 2009 *Phys. Rev.* A **79** 052704
[10] Milne-Brownlie D S, Foster M, Gao J F, Lohmann B and Madison D H 2006 *Phys. Rev. Lett.* **96** 233201
[11] Murray A J, Hussey M J, Gao J F and Madison D H 2006 *J. Phys.* B **39** 3945
[12] Naja A, Staicu Casagrande E M, Lahmam-Bennani A, Nekkab M, Mezdari F, Joulakian B, Chuluunbaatar O and Madison D H 2007 *J. Phys.* B **40** 3775
[13] Hussey M J and Murray A J 2005 *J. Phys.* B **38** 2965
[14] Lahmam-Bennani A, Staicu Casagrande E M and Naja A 2009 *J. Phys.* B **42** 235205
[15] Murray A J, Turton B C H and Read F H 1992 *Rev. Sci. Instrum.* **63** 3346
[16] Murray A J and Read F H 1993 *Phys. Rev.* A **47** 3724
[17] Murray A J and Cvejanovic D 2003 *J. Phys.* B **36** 4875
[18] Gao J F, Madison D H and Peacher J L 2005 *J. Chem. Phys.* **123** 204314
[19] Gao J F, Madison D H and Peacher J L 2005 *Phys. Rev.* A **72** 032721
[20] Gao J F, Peacher J L and Madison D H 2005 *J. Chem. Phys.* **123** 204302
[21] Lee C T, Yang W T and Parr R G 1988 *Phys. Rev.* B **37** 785
[22] Guerra C F, Snijders J G, te Velde G and Baerends E J 1998 *Theo. Chem. Acc.* **99** 391
[23] Ward S J and Macek J H 1994 *Phys. Rev.* A **49** 1049
[24] Furness J B and McCarthy I E 1973 *J. Phys.* B **6** 2280
[25] Perdew J P and Zunger A 1981 *Phys. Rev.* B **23** 5048
[26] Padial N T and Norcross D W 1984 *Phys. Rev.* A **29** 1742
[27] Al-Hagan O, Kaiser C, Madison D H and Murray A J 2009 *Nature Phys.* **5** 59

VIII. Dynamical (e, 2e) Studies of Formic Acid

C J Colyer[1], M A Stevenson[1], O Al-Hagan[2], D H Madison[2], C G Ning[3] and B Lohmann[1]

[1] *ARC Centre of Excellence for Antimatter-Matter Studies, The University of Adelaide, Adelaide, SA 5005, Australia*

[2] *Department of Physics, Missouri University of Science and Technology, Rolla, Missouri 65409, USA*

[3] *Department of Physics and Key Laboratory of Atomic and Molecular NanoSciences of MOE, Tsinghua University, Beijing 100084, People's Republic of China*

Abstract

We present triply differential cross sections for the electron impact ionization of the outer valence orbitals of formic acid (*CHOOH*) by 100 eV and 250 eV incident electrons. The experiments were performed under asymmetric kinematics, in which the outgoing ejected electron had an energy of 10 eV, over a range of momentum transfers. The experimental results are compared with theoretical calculations carried out using the sophisticated M3DW model, both with and without correlation-polarization-exchange terms included.

1. Introduction

Electron impact ionization is a fundamental process which is important in a wide range of physical phenomena. The most complete information about this process is obtained by detecting the incident electron, after it has been scattered by the ionization event, and the electron ejected from the target, in time coincidence (the (e,2e) technique). If the energies and momenta of the incident and outgoing electrons are all specified, this yields a measure of the triple differential cross section (TDCS). The study of electron impact ionization of atomic targets using this technique can be considered a mature field [1], however this is not the case for molecular targets. The experimental difficulties associated with TDCS measurements for molecular targets arise from the limits on the ability of the experiment to resolve different molecular orbitals which can, depending on the molecular configuration of the target, be quite closely spaced in energy. Nevertheless, TDCS measurements which probe the dynamics of the collision process are available for a number of molecules ranging from simple diatomics such as H_2 [2-5] and N_2 [6-8] to more complicated molecules such as H_2O [9-10], CO_2 [11], C_2H_2 [12] and N_2O [13]. Electron Momentum Spectroscopy (EMS) studies which use the coincidence technique to obtain structure information are more numerous, and extend to more complex molecules [14].

There is considerable interest in the dynamics of the ionization process in interactions of ionizing radiation with biological matter. In the last decade, experimental studies have indicated that secondary particles produced by the primary ionizing particle can play a significant role in radiation damage to DNA [15]. In the ionization process, large numbers of secondary electrons with comparatively low energies (0-20 eV) are liberated, which then interact with biomolecules such as sugars [16-17], water [18], and the DNA and RNA bases [19-21]. Water in particular has recently been the focus of several theoretical [22-24] and experimental [9-10] dynamical (e, 2e) investigations, with a view to quantifying the interaction of electrons with biological matter using water as an approximation for living tissue. The primary focus of the present study is to further understand this electronic interaction using smaller biomolecules, such as formic acid, as a model for the components of larger biological systems.

Most famously known for its role in the venom of ants and bees, formic acid is the simplest organic acid and is thought to play a key role in the formation of larger biologically relevant molecules such as acetic acid and glycine. It was detected in the interstellar medium [25] and constitutes, together with glycine, one of the simplest building blocks of more complicated biological systems [26]. To date, the majority of experimental studies of this molecule involving electron impact have been of dissociative electron attachment [27-29] while elastic and vibrationally inelastic differential scattering measurements have appeared more recently [30-31]. The structure of formic acid has been rigorously probed by three EMS studies [32-34] where the latter study constituted the first EMS study of the formic acid monomer without contributions from the dimer. To the authors' best knowledge, no dynamical studies exist for formic acid.

In this paper, we present measurements of the TDCS for electron impact ionization of gas phase formic acid molecules. We compare the experimental results with distorted wave calculations of the TDCS. Where possible, the experimental data are also compared to previous experiments performed on water by Milne-Brownlie *et al.* [9] under the same kinematics.

2. Experimental apparatus

This study has been conducted in a conventional (e, 2e) spectrometer, operating in the coplanar asymmetric geometry. The apparatus has been described in detail previously [35]. Briefly, the spectrometer consists of an electron gun and two hemispherical electron energy analysers, all mounted in-plane and perpendicular to the target gas jet. The electron gun consists of six cylindrical electrostatic lens elements, incorporating a thoriated tungsten filament as the source, with a resultant electron beam energy width of approximately 0.5 eV FWHM. The hemispherical analysers are preceded by five cylindrical electrostatic lens elements and are mounted on independently rotatable turntables, concentric with the interaction region. Electrons exiting the analysers are detected by channel electron multipliers, and via the use of fast-timing electronics, can be determined to originate from the same event. The coincidence energy resolution of the system is approximately 1.2 eV FWHM.

The formic acid vapour target enters the interaction region via a 0.69mm stainless steel capillary. The vapour is obtained from a liquid sample held in a glass vial, of 98% stated purity (Sigma-Aldrich, Australia), and further purified via several freeze-pump-thaw cycles. The vapour is a mixture of monomers and dimers whose ratio is a function of temperature and driving pressure. At higher temperatures, the extra kinetic energy serves to break up most of the dimers into monomers. It was demonstrated in ref. [33] that at temperatures in excess of 120°C, the target is composed of greater than 99% monomers. As a result, the beam-forming needle is held at approximately 135°C, while the associated gas handling system and vacuum chamber are heated to approximately 75°C and 50°C respectively to prevent condensation.

In asymmetric kinematics, the fast outgoing electron is usually referred to as the scattered electron whilst the slow outgoing electron is termed the ejected electron. This geometry implies that the scattered electron energy analyser be held at a fixed forward angle while the ejected electron energy analyser is rotated in the scattering plane. Also, the scattered electron energy E_a is generally much larger than the ejected electron energy E_b. Through energy conservation the incident electron energy can be determined.

$$E_0 = E_a + E_b + \varepsilon_i, \tag{1}$$

where E_0 is the incident electron energy and E_i is the binding energy of the orbital in question. From conservation of momentum the recoil ion momentum, **p**, can be obtained.

$$\boldsymbol{P} = \boldsymbol{k}_0 - \boldsymbol{k}_a - \boldsymbol{k}_b \tag{2}$$

where $\mathbf{k}_0$ is the incident electron momentum, $\mathbf{k}_a$ is the scattered electron momentum and $\mathbf{k}_b$ is the ejected electron momentum.

The momentum transferred to the target, **K**, can then be defined.

$$\boldsymbol{K} = \boldsymbol{k}_0 - \boldsymbol{k}_a . \tag{3}$$

3. Theory

The details of the molecular three-body distorted wave (M3DW) approximation have been presented elsewhere [36-38] so only a brief overview will be presented here. The M3DW TDCS is given by

$$\frac{d^5\sigma}{d\Omega_a d\Omega_b dE_b} = \frac{1}{(2\pi)^5}\frac{k_a k_b}{k_i}\left(|T_{dir}|^2 + |T_{exc}|^2 + |T_{dir} - T_{exc}|^2\right), \quad (4)$$

where $\vec{k}_i$ is the initial state wave vector, $\vec{k}_a$ ($\vec{k}_b$) is the wave vector for the scattered (ejected) electron, and the direct and exchange amplitudes are T_{dir} and T_{exc} respectively:

$$T_{dir} = \left\langle \chi_a^-(\vec{k}_a, \mathbf{r}_1)\chi_b^-(\vec{k}_b, \mathbf{r}_2) C_{scat-eject}(r_{12}) | V - U_i | \phi_j^{OA}(\mathbf{r}_2)\chi_i^+(\vec{k}_i, \mathbf{r}_1)\right\rangle \quad (5)$$

$$T_{exc} = \left\langle \chi_a^-(\vec{k}_a, \mathbf{r}_2)\chi_b^-(\vec{k}_b, \mathbf{r}_1) C_{scat-eject}(r_{12}) | V - U_i | \phi_j^{OA}(\mathbf{r}_2)\chi_i^+(\vec{k}_i, \mathbf{r}_1)\right\rangle. \quad (6)$$

In eqns. 5 and 6, $\mathbf{r}_1$ ($\mathbf{r}_2$) is the co-ordinate of the incident (bound) electron, χ_i, χ_a, and χ_b are the distorted waves for the incident, scattered, and ejected electrons respectively, $C_{scat-eject}$ is the Coulomb interaction between the scattered projectile and ejected electron, and ϕ_j^{OA} is the orientation-averaged molecular orbital (OAMO) [36] for the initial bound state wavefunction of the molecule generated from molecular orbitals. The molecular wavefunction was calculated using density functional theory (DFT) along with the standard hybrid B3LYP [39] functional by means of the ADF 2007 (Amsterdam Density Functional) program [40] with the TZ2P (triple-zeta with two polarization functions) Slater type basis sets. In the next section, experimental results will be shown for the sum of the 10a′ and 2a″ valence orbitals of formic acid. Unfortunately the OAMO approximation is not valid for the 2a″ orbital since the average is zero for this symmetry. Consequently, we are able to calculate results for the 10a′ orbital only. The potential V is the initial state interaction between the projectile and the neutral molecule, and U_i is the initial-state spherically symmetric distorting potential which is used to calculate the initial-state distorted wave χ_i.

The initial state molecular distorted waves are calculated using a spherically symmetric distorting potential U_i. The Schrödinger equation for the incoming electron wave-function is given by:

$$(T + U_i - \frac{k_i^2}{2})\chi_i^+(\vec{k}_i, \mathbf{r}) = 0, \quad (7)$$

where T is the kinetic energy operator, and the '+' superscript on $\chi_i^+(\vec{k}_i, \mathbf{r})$ indicates outgoing wave boundary conditions. The initial state distorting potential contains three

components $U_i = U_S + U_E + U_{CP}$, where U_S is the initial state spherically symmetric static potential which is calculated from the molecular charge density obtained from the numerical orbitals averaged over all angular orientations, U_E is the exchange-distortion potential of Furness and McCarthy [41], and U_{CP} is the correlation-polarization potential of Perdew and Zunger [42] (see also Padial and Norcross [43]).

The two final channel distorted waves are obtained from a Schrödinger equation similar to eqn. (7)

$$(T + U_f - \frac{k_{a(b)}^2}{2})\chi_{a(b)}^{-}(\vec{k}_{a(b)}, \mathbf{r}) = 0. \qquad (8)$$

Here $U_f = U_I + U_E + U_{CP}$ where U_I is the final state spherically symmetric static distorting potential for the molecular ion which is calculated using the same procedure as U_S except that the active electron is removed from the charge distribution. Two calculations have been performed – one excluding $U_E + U_{CP}$ which we label M3DW and one including $U_E + U_{CP}$ which we label M3DW-CPE.

An idea of the quality of our OAMO wavefunction can be achieved by comparing theory and experiment at higher incident electron energies where kinematics will play a minor role. Nixon *et al.* [34] reported an EMS study of formic acid which differentiated between the 10a′ and 2a″ orbitals for an incident electron energy of 831.6 eV. Figure 1 compares the present M3DW-CPE results with the Nixon *et al*. [34] measurements and the theoretical PWIA (Plane Wave Impulse Approximation) results reported in the paper. In the PWIA, the cross section is directly proportional to the square of the molecular wavefunction averaged over all orientations. The PWIA calculation used the B3LYP/TZVP molecular wavefunction [34] while we used B3LYP/TZ2P. We checked and these two wavefunctions produced essentially identical results for the M3DW-CPE. Whereas we use the OAMO approximation, the PWIA performs a proper average over molecular orientations without making approximations. Consequently, the difference between the two theoretical curves in figure 1 represents the effects of the OAMO approximation plus the difference between using the plane wave impulse approximation and the distorted wave Born approximation (DWBA). Arguably, the M3DW-CPE results are in better overall agreement with the experimental data which would be

understandable from the point of view that, if kinematics are important, the DWBA should be better than the PWIA and 800 eV is low enough an energy that kinematics might start playing a role. However, for this to be true, the OAMO approximation would also have to be valid. Consequently, the good agreement between the M3DW-CPE and the high energy experiment shown in figure 1 indicates that the OAMO approximation is reasonably good for the 10a′ state.

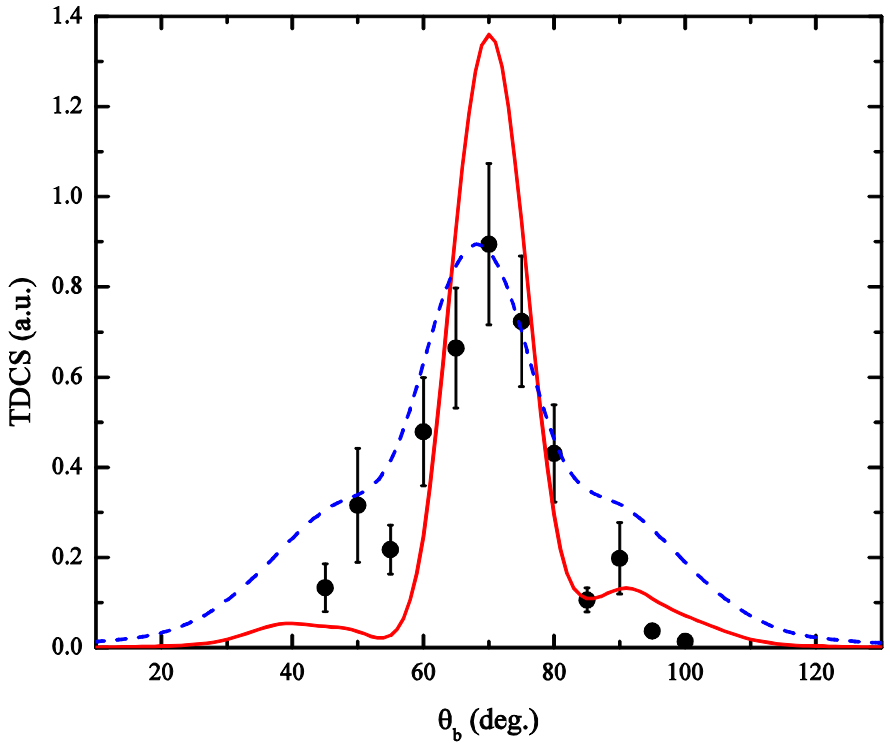

Figure 1: Experimental triple differential cross section for the 10a′ valence orbital of formic acid (solid circles) as a function of ejected electron scattering angle, compared with M3DW-CPE (solid line) and PWIA (dashed line) calculations. The incident electron energy is 831.6 eV, the projectile scattering angle is 20.5°, and the ejected electron energy is 105 eV. The experimental data and the PWIA results are those of Nixon *et al*. [34].

4. Results and discussion

The experiments were performed at two incident electron energies; a lower value of 100 eV and a higher value of 250 eV. In both cases the ejected electron energy was chosen to be 10 eV. Figure 2 shows a coincidence binding energy spectrum of the outer

valence region of formic acid, where the incident and ejected electron energies are fixed at 250 eV and 10 eV respectively, while the scattered electron energy is scanned across a range of energies. The detection angles for the scattered and ejected electrons were chosen to be -5° and 90° respectively. This sets the ejected electron detection angle 30° larger than the momentum transfer direction so that contributions from both s-type and p-type orbitals would be evident. The outer valence region of formic acid consists of seven molecular orbitals: five in the molecular plane (a′) and two out of the molecular plane (a″) [32]. All seven orbitals can be partially resolved, however due to the limited coincident energy resolution of the apparatus and the intensity of each orbital under the chosen kinematics, not all orbitals can be completely separated.

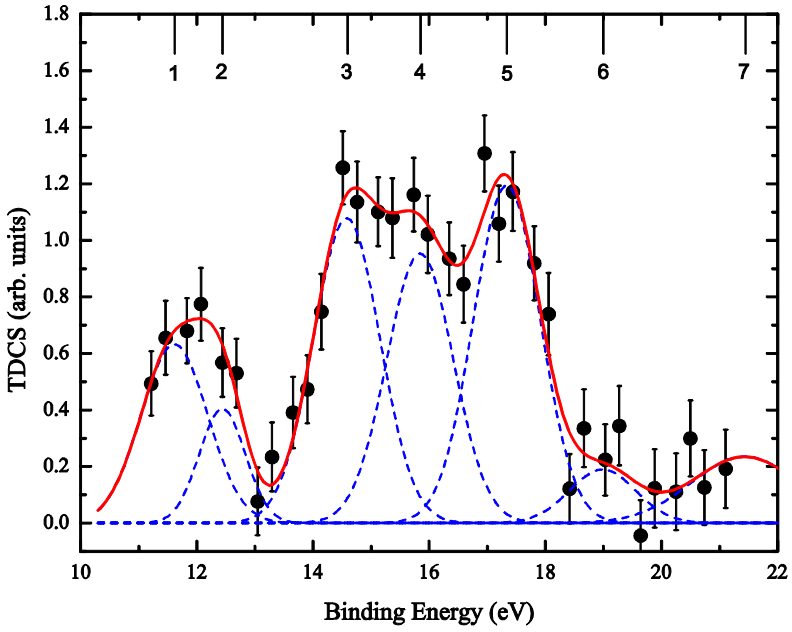

Figure 2: Measured binding energy spectrum for the outer valence orbital region of formic acid, fitted with a sum of Gaussian functions.

Table 1 shows the binding energy of each orbital, as well as the assignments and energies as determined via EMS [33] and photoelectron spectroscopy (PES) [44]. Here we present angular distributions for the summed outermost valence orbitals (10a′+2a″). Examination of the momentum density probability distributions for the 10a′ and 2a″ orbitals presented

in [32] indicates that, for all scattering angles considered here, one may expect the contribution of the 10a′ orbital to be considerably larger than that of the 2a″ orbital at ejected electron angles around 60° and the contributions to be approximately equal at angles around 120°.

Table 1 : Formic acid binding energies (in eV), with the error in the Gaussian peak position quoted in brackets.

Orbital	Present Results	EMS[33]	PES[44]
10a′	11.6 (6)	11.5	11.5
2a″	12.5 (4)	12.65	12.6
9a′	14.6 (6)	14.7	14.8
1a″	15.8 (6)	15.8	15.8
8a′	17.3 (6)	17.15	17.1
7a′	19.0 (6)	17.9	17.8
6a′	21.5 (9)	22	22

Figures 3(a) and 3(b) show the experimental results for the summed 10a′ and 2a″ orbitals, compared to theoretical results for the 10a′ orbital only for the TDCS of the formic acid monomer at an incident energy of 100 eV and an ejected electron energy of 10 eV, for scattered electron angles of -10° and -15° respectively. The angular distributions can be divided into two regions, the binary region ranging from 0° to 180°, and the recoil region which ranges from 180° to 360°. The binary region is so named because structure here arises from single binary collisions. Depending upon the kinematics, the TDCS in the binary region may contain strong signatures of the orbital structure [45]. In contrast, the recoil structure arises from processes whereby the ejected electron produced by an initial binary collision undergoes subsequent recoil scattering from the target nucleus. As the experimental data are not on an absolute scale, they have been normalized to the M3DW-CPE calculation so as to give the best visual fit in the recoil region.

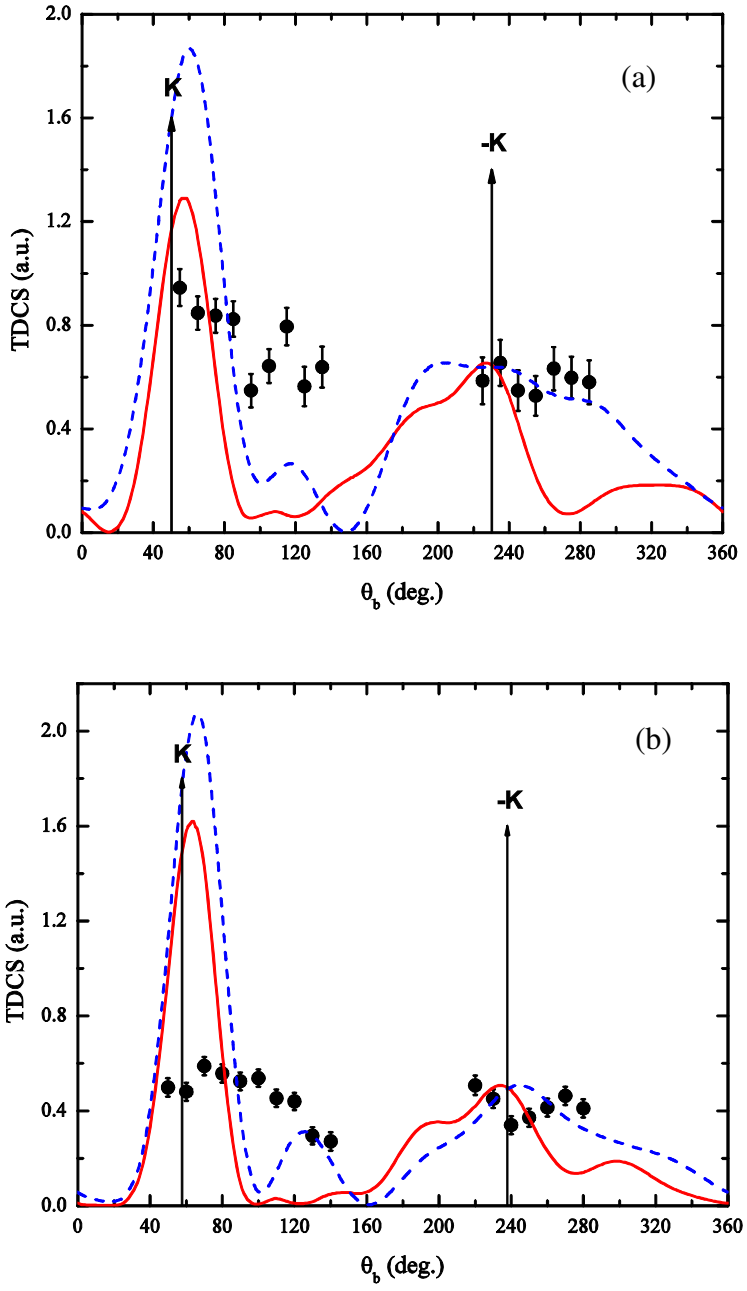

Figure 3: Experimental triple differential cross sections for the summed 10a′ and 2a″ valence orbitals of formic acid (solid circles), with E_0=100 eV and E_b=10 eV, compared with M3DW-CPE (solid line) and M3DW (dashed line) calculations for the 10a′ orbital only. The scattered electron detection angles and corresponding momentum transfers are (a) -10°, |K|=0.54au and (b) -15°, |K|=0.74au.

We have used the recoil region for the normalisation since, from the work of Bharathi *et al.* [32], it is known that the shape and width of the binary peak will be strongly affected by the 2a′ state, which is not included in the theory. It is evident from the relative size of the peaks in the binary and recoil regions that a large amount of interaction between the ejected electron and the target nucleus is present at these energies. The M3DW and M3DW-CPE calculations achieve reasonable qualitative agreement with the experimental results in Figures 3(a) and 3(b), but tend to predict a larger and sharper binary peak than is observed in the experiment. The simpler M3DW agrees well with the shape of the recoil peak; the addition of the CPE terms improves the binary peak to recoil peak ratio but appears to worsen the shape agreement in the recoil region. However, since the theoretical calculation is for the 10a′ orbital only while the experiment is summed 10a′+2a″, it is difficult to evaluate the accuracy of the theory. For example, the fact that the M3DW gives the best agreement with the shape of the recoil peak may be fortuitous since it is quite possible that the M3DW-CPE gives the correct shape and the additional width of the peak comes from the 2a″ orbital. The additional experimental structure in the binary peak for angles between 90°-120° very likely originates from the 2a″ orbital. Although the details of the cross section will undoubtedly be different for our kinematics, we believe this proposition is again supported by an examination of the momentum density profiles reported by Bharathi *et al*. [32]. Plotting their momentum profiles against ejected electron angle, and summing the profiles, indicates that the resultant cross section is enhanced in the region from 90°-120°, compared with the cross section for only the 10a′ orbital.

Figures 4(a)-4(c) present the TDCS for electron impact ionization of formic acid with 250 eV incident electrons, measured for 10 eV ejected electrons. Results are presented for three scattering angles; (a) -5° (b) -10° and (c) -15°. Results for the experimentally determined TDCS for ionization of the summed$1b_1$+$3a_1$ valence orbitals for H_2O [9] under the same kinematics as figure 4(c) are also presented in that figure. Immediately clear is the difference in the relative size of the binary and recoil peaks at an incident energy of 250 eV when compared to the lower energy case. As the scattered electron angle changes from -5° to -10° to -15°, the magnitude of the recoil peak relative to the binary peak decreases significantly, in contrast to the case in figure 3, where the

binary/recoil ratio is approximately constant as the scattering angle is changed from -10° to -15°. The relative magnitude of the recoil peak compared to the binary peak at a scattering angle of -15° (figure 4) is in stark contrast to the data from [9] for H_2O, which under the same conditions produces a recoil peak approximately 4 times greater. In a recent study [46], out of plane TDCS measurements for H_2 and He were compared, and

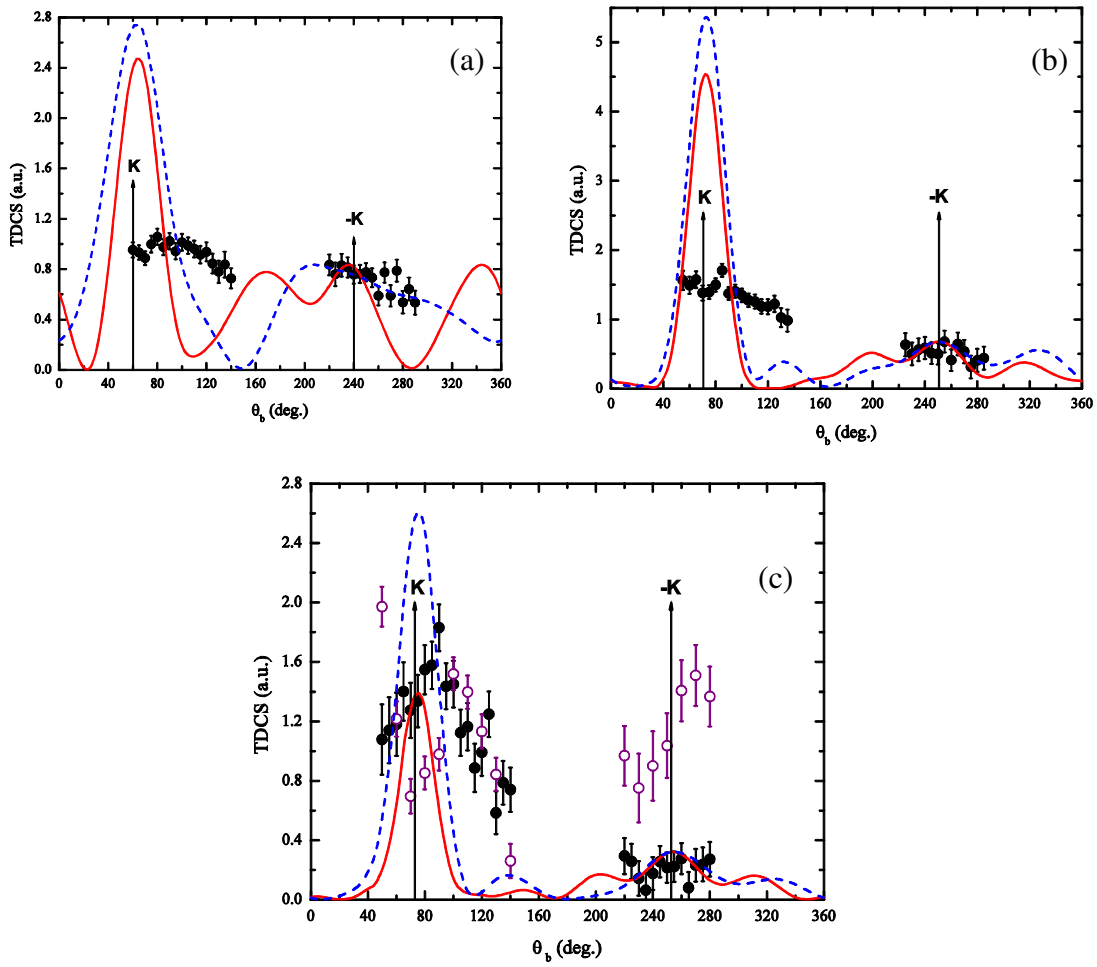

Figure 4: Experimental triple differential cross sections for the summed 10a′ and 2a″ valence orbitals of formic acid (solid circles), with E_0=250 eV and E_b=10 eV, plotted against the M3DW-CPE (solid line) and M3DW (dashed line) calculations for the 10a′ orbital only (a, b). Panel (c) includes previous experimental results for the summed $3a_1$+$1b_1$ orbitals for water under the same kinematics [9] (open circles). The scattered electron detection angles and corresponding momentum transfers are (a) -5°, |K|=0.42au, (b) -10°, |K|=0.75au and (c) -15°, |K|=1.11au.

through the use of state-of-the-art theory, certain structures were determined to arise from recoil interactions; the magnitude of these structures could be increased by minimising the internuclear separation of H_2 to the extent that it represents the localised single centre nuclear charge of helium. In light of this, it seems reasonable to suggest that this lack of recoil interaction in formic acid may be attributed to the molecule's polycentric nature and thus the lack of nuclear charge at the centre of mass, as opposed to the water molecule which has a single oxygen nucleus at its centre (see figure 5). In comparison with the theoretical calculations, the M3DW again predicts quite well the shape of the recoil peaks in all cases, and there is also improved agreement with the M3DW-CPE in this region, especially at the larger momentum transfers. The relative size of the binary and recoil peaks is still predicted better by the M3DW-CPE, but both calculations still do not predict the size and shape of the binary peak, except in figure 3(c), where the M3DW-CPE successfully predicts the correct relative magnitudes of the binary peak and the recoil peak, and the sharper binary peak observed at this larger momentum transfer more closely resembles the peak predicted by the calculation. The sharper binary peak for these kinematics made be indicative of a smaller contribution from the 2a″ orbital.

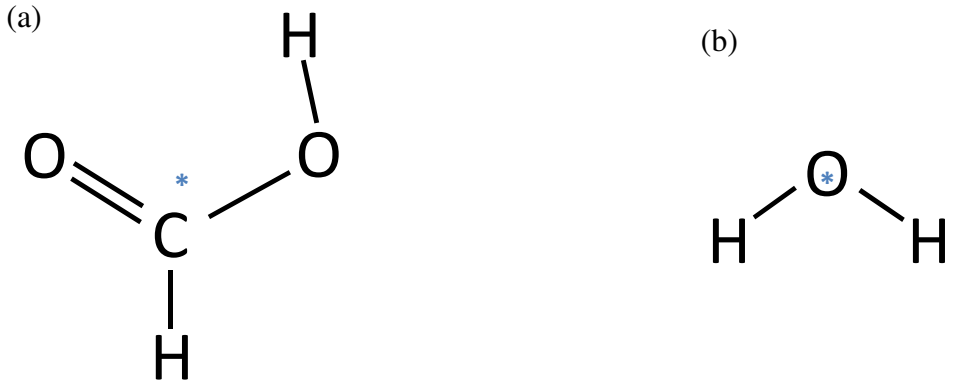

Figure 5: Molecular structures of (a) formic acid, and (b) water. The centre of mass for each molecule is marked by an *.

5. Conclusions

The present paper constitutes the first dynamical (e, 2e) study for the formic acid molecule. The measured binding energies and orbital assignments are in good agreement with the available EMS and PES data. Experimental cross sections for the formic acid monomer exhibit a significant change in binary peak shape as the scattering angle is varied, and a ratio between the recoil peak magnitude and binary peak magnitude which is much smaller than that observed for ionization of water under the same kinematics. The theoretical calculations for the 10a′ state exhibit very good agreement with EMS cross sections measured for higher incident electron energies. This indicates that the OAMO approximation is reasonably good for this state. However, the agreement between theory and the present experimental results summed over the 10a′ and 2a″ states is not very good, particularly in the binary region, and this is most likely due to the 2a″ contribution. The M3DW results are in reasonable agreement with the summed experimental cross sections in the recoil region which seems odd since the M3DW-CPE would be expected to be better. However, this may be fortuitous again due to the 2a″ contribution. Reasonable agreement between experiment and theory was found for the higher incident energy and largest scattering angle which suggests that the 2a″ contribution might be small for this case. This is the first time that the M3DW method has been applied to a large molecule such as this. We are encouraged by the good agreement that was found with the 10a′ EMS measurements and the opportunity to compare the performance of these calculations would be enhanced by further experimental data for the individual, as opposed to summed orbitals.

Acknowledgements

This work was supported by the Australian Research Council Centre of Excellence for Antimatter-Matter Studies and the American NSF under grant number 0757749. The author CGN would like to acknowledge the support of the National Natural Science Foundation of China under contract No. 10704046, and author OA-H would like to acknowledge the support of the Saudi Ministry of Higher Education's King Abdullah Bin Abdul-Aziz Scholarship. We are grateful to K. Nixon for providing the EMS data in numerical form.

References

[1] Lahmam-Bennani A 1991 *J. Phys. B: At. Mol. Opt. Phys.* **24** 2401
[2] Jung K *et al* 1975 *J. Phys. B: At. Mol. Opt. Phys.* **8** 1330
[3] Cherid M *et al* 1989 *J. Phys. B: At. Mol. Opt. Phys.* **22** 3483
[4] Milne-Brownlie D S *et al* 2006 *Phys. Rev. Lett.* **96** 233201
[5] Gao J *et al* 2006 *J. Chem. Phys.* **124** 194306
[6] Avaldi L *et al* 1992 *J. Phys. B: At. Mol. Opt. Phys.* **25** 3551
[7] Murray A J *et al* 2006 *J. Phys. B: At. Mol. Opt. Phys.* **39** 3945
[8] Naja A *et al* 2007 *J. Phys. B: At. Mol. Opt. Phys.* **40** 3775
[9] Milne-Brownlie D S *et al* 2004 *Phys. Rev.* A **69** 032701
[10] Kaiser C *et al* 2007 *J. Phys. B: At. Mol. Opt. Phys.* **40** 2563
[11] Hussey M J and Murray A J 2005 *J. Phys. B: At. Mol. Opt. Phys.* **38** 2965
[12] Avaldi L, Camilloni R and Stefani G 1990 *Phys. Rev.* A **41** 134
[13] Cavanagh S J and Lohmann B 1999 *J. Phys. B: At. Mol. Opt. Phys.* **32** L261
[14] Weigold E and McCarthy I E 1999 *Electron Momentum Spectroscopy* (New York: Kluwer /Plenum)
[15] Boudaiffa B *et al* 2000 *Science* **287** 1658
[16] Ptasinska S *et al* 2004 *J. Chem. Phys.* **120** 8505
[17] Colyer C J *et al* 2007 *New J. Phys.* **9** 41
[18] Varella M T D N *et al* 1999 *J. Chem. Phys.* **111** 6396
[19] Huels M A *et al* 1998 *J. Chem. Phys.* **108** 1309
[20] Denifl S *et al* 2003 *Chem. Phys. Lett.* **377** 74
[21] Hanel G *et al* 2003 *Phys. Rev. Lett.* **90** 188104
[22] Champion C 2003 *Phys. Med. Biol.* **48** 2147
[23] Champion C *et al* 2006 *Phys. Rev.* A **73** 012717
[24] Champion C, Hanssen J and Hervieux P A 2001 *Phys. Rev.* A **63** 052720
[25] Irvine W M *et al* 1989 *Astrophys. J.* **342** 871
[26] Gutowski M, Skurski P and Simons J 2000 *J. Am. Chem. Soc.* **122** 10159
[27] Pelc A *et al* 2002 *Chem. Phys. Lett.* **361** 277
[28] Pelc A *et al* 2003 *Vacuum* **70** 429
[29] Prabhudesai V S *et al* 2005 *Chem. Phys. Lett.* **405** 172
[30] Vizcaino V *et al* 2006 *New J. Phys.* **8** 85
[31] Allan M 2006 *J. Phys. B: At. Mol. Opt. Phys.* **39** 2939
[32] Bharathi S M *et al* 1990 *J. Electron Spectrosc. Relat. Phenom.* **53** 51
[33] Nixon K L *et al* 2008 *Chem. Phys. Lett.* **451** 18
[34] Nixon K L, Lawrance W D and Brunger M J 2009 *Chem. Phys. Lett.* **474** 23
[35] Lohmann B, Meng X-K and Keane M 1992 *J. Phys. B: At. Mol. Opt. Phys.* **25** 5223
[36] Gao J, Peacher J L and Madison D H 2005 *J. Chem. Phys.* **123** 204302
[37] Gao J, Madison D H and Peacher J L 2005 *J. Chem. Phys.* **123** 204314
[38] Gao J, Madison D H and Peacher J L 2006 *J. Phys. B: At. Mol. Opt. Phys.* **39** 1275
[39] Lee C, Yang W and Parr R G 1988 *Phys. Rev.* B **37** 785
[40] Guerra C F *et al* 1998 *Theor. Chem. Acc.* **99** 391
[41] Furness J B and McCarthy I E 1973 *J. Phys. B: At. Mol. Phys.* **6** 2280
[42] Perdew J P and Zunger A 1981 *Phys. Rev.* B **23** 5048

[43] Padial N T and Norcross D W 1984 *Phys. Rev.* A **29** 1742
[44] von Niessen W, Bieri G and A° sbrink L 1980 *J. Electron Spectrosc. Relat. Phenom.* **21** 175
[45] Ehrhardt H *et al* 1986 *Z. Phys.* D **1** 3
[46] Al-Hagan O *et al* 2009 *Nat. Phys.* **5** 59

IX. Recent Theoretical Progress in Treating Electron Impact Ionization of Molecules

[1]Ola Al-Hagan, Chuangang Ning[2], Kate Nixon[3], Andrew Murray[3], Christopher Colyer[4], Mark Stevenson[4], Birgit Lohmann[4] and Don Madison[1]

[1]Department of Physics, Missouri University of Science & Technology, Rolla, MO 65409, USA

[2]Department of Physics and Key Laboratory of Atomic and Molecular NanoSciences of MOE, Tsinghua University, Beijing 100084, People's Republic of China

[3]School of Physics & Astronomy, University of Manchester, Manchester M13 9PL, United Kingdom

[4]ARC Centre for Antimatter-Matter Studies, University of Adelaide, Adelaide, SA 5005, Australia

Abstract

(e,2e) ionization differential cross sections are presented for several molecules. We will compare experimental results with theoretical calculations using the molecular three body distorted wave (M3DW) approximations for H_2 , N_2 , H_2O and Formic Acid (FA) using better wave-function for the molecules than we had in previous works. Generally, good agreement is found between the M3DW approach and experiments.

1. Introduction

There has been impressive progress in the area of theoretical treatments of charge particle collisions with atoms and molecules in the last decade. There have been many (e, 2e) studies for ionization of atoms and this area is now fairly mature. There have been some experimental and theoretical studies performed for the (e, 2e) processes with molecular targets but most of these studies have been performed either for high incident energies or for small molecules [1-4]. Most recently, low to intermediate incident energies have been reported for relatively simple molecular systems [5-6]. For these cases the dynamics of the ionization collisions become important and therefore more sophisticated models are needed to get good agreement with the experimental data.

In this paper, we will use the molecular three-body distorted wave (M3DW) approximation method coupled with the orientation averaged molecular orbital (OAMO) approximation. We apply this treatment to calculate the triple differential cross section (TDCS) for a variety of electron angles and energies for H_2, N_2, H_2O and $HCOOH$ (Formic Acid - FA) using better wave-function for the molecules than we had in previous works.

2. Theory

The molecular 3-body distorted wave (M3DW) approximation has been presented by our group in previous publications [7-9] so only a brief outline of the theory will be presented. The triple differential cross section (TDCS) for the M3DW is giving by:

$$\frac{d^5\sigma}{d\Omega_a \Omega_b dE_b} = \frac{1}{(2\pi)^5}\frac{k_a k_b}{k_i}\left|T\right|^2 \qquad (1)$$

where $\vec{k}_i$, $\vec{k}_a$, and $\vec{k}_b$ are the wave vectors for the initial, scattered and ejected electrons. The amplitude is given by:

$$T = \left\langle \chi_a^-(\vec{k}_a, \mathbf{r}_1)\chi_b^-(\vec{k}_b, \mathbf{r}_2) C_{scat-eject}(r_{12}) \mid V - U_i \mid \phi_j^{OA}(\mathbf{r}_2)\chi_i^+(\vec{k}_i, \mathbf{r}_1)\right\rangle \qquad (2)$$

where r_1 and r_2 are the coordinates of the incident and the bound electrons, χ_i, χ_a, and χ_b are the distorted waves for the incident, scattered, and ejected electrons respectively, and $\phi_j^{OA}(r_2)$ is the initial bound-state wave-function which is approximate as the orientation

averaged molecular wave-function for the molecular orbital of interest. The molecular wavefunction was calculated by Ning using density functional theory (DFT) along with the standard hybrid B3LYP [10] functional by means of the ADF 2007 (Amsterdam Density Functional) program [11] with the TZ2P (triple-zeta with two polarization functions) Slater type basis sets. The present molecular wave-functions are better than the ones we used in previous works. The factor $C_{scat-eject}(r_{12})$ is the Coulomb-distortion factor between the two final state electrons, V is the initial state interaction potential between the incident electron and the neutral molecule, and U_i is a spherically symmetric distorting potential which used to calculate the initial-state distorted wave for the incident electron $\chi_i^+(\vec{k}_i, \mathbf{r}_1)$.

The molecular distorted waves are calculated using a spherically averaged distorting potential as described in previous works [7-9]. The Schrödinger equation for the incoming electron wave-function is given by:

$$(T + U_i - \frac{k_i^2}{2})\chi_i^+(\vec{k_i}, r) = 0 \qquad (3)$$

where T is the kinetic energy operator. The initial state distorting potential contains three components $U_i = U_s + U_E + U_{CP}$, where U_s is the initial state spherically symmetric static potential which is obtained from the molecular charge density averaged over all angular orientations, U_E is the exchange potential of Furness-McCarthy [12] which approximates the effect of the continuum electron exchanging with the passive bound electrons in the molecule, and U_{CP} is the correlation-polarization potential of Perdew and Zunger [13,14].

The final state for the system is approximated as a product of distorted waves for the two continuum electrons times the average Coulomb-distortion factor. The final state distorted waves are calculated as the initial state except that the final state spherically symmetric static distorting potential for the molecular ion which is used for U_s.

3. Results and discussion

3.1. Molecular hydrogen (H_2)

Our recent study using the M3DW method yielded good agreement with the experimental measurements for triply differential cross sections (TDCS) for ionization of both H_2 and *He* by electron impact in a plane perpendicular to the incident beam direction with symmetric final state energies [15]. Figures 1 and 2 contain a comparison between our calculations and some recent experimental data [16] for ionization of H_2 taken by Andrew Murray and Christian Kaiser at Manchester University. The Manchester apparatus is designed such that the angle between the incident beam direction and the detection plane (defined as ψ) can be varied. The scattering plane corresponds to ψ=0° and the perpendicular plane corresponds to ψ=90°. The TDCS results in figures 1 and 2 are plotted as a function of the half-angle between the two final state electrons in the detection plane (i.e. 2ξ is the angle between the electrons in the detection plane). For low incident electron energies, we have found that using the full Coulomb-distortion factor $C(r_{12})$ in M3DW calculations overestimates the effect of the final state electron-electron repulsion, normally called the post collision interaction (PCI), while the Ward-Macek average C-factor $C(r_{12}^{ave})$ [17] yields better agreement with experimental data so we have used the Ward-Macek approximation.

Although the experimental data are not absolute, only one normalization factor is needed for the different ψ angles and we have chosen to normalize experiment to theory for ψ=90°. Two different M3DW calculations are presented – one including the correlation polarization potential and one excluding it. As can be seen from figures 1 and 2, there is good agreement between the experiment and the theory for large values of ψ especially in the perpendicular plane when the correlation-polarization potential is included. At low ψ values, the agreement between the experiment and the theory is not as satisfactory. The largest experimental cross sections for both equal (E_a=E_b=10 eV) and unequal (E_a=18 eV, E_b=2 eV) energy sharing were not in the scattering plane but rather in a plane where ψ =45°. The M3DW also predicts the largest cross sections for the 45° plane if correlation and polarization is included in the calculations.

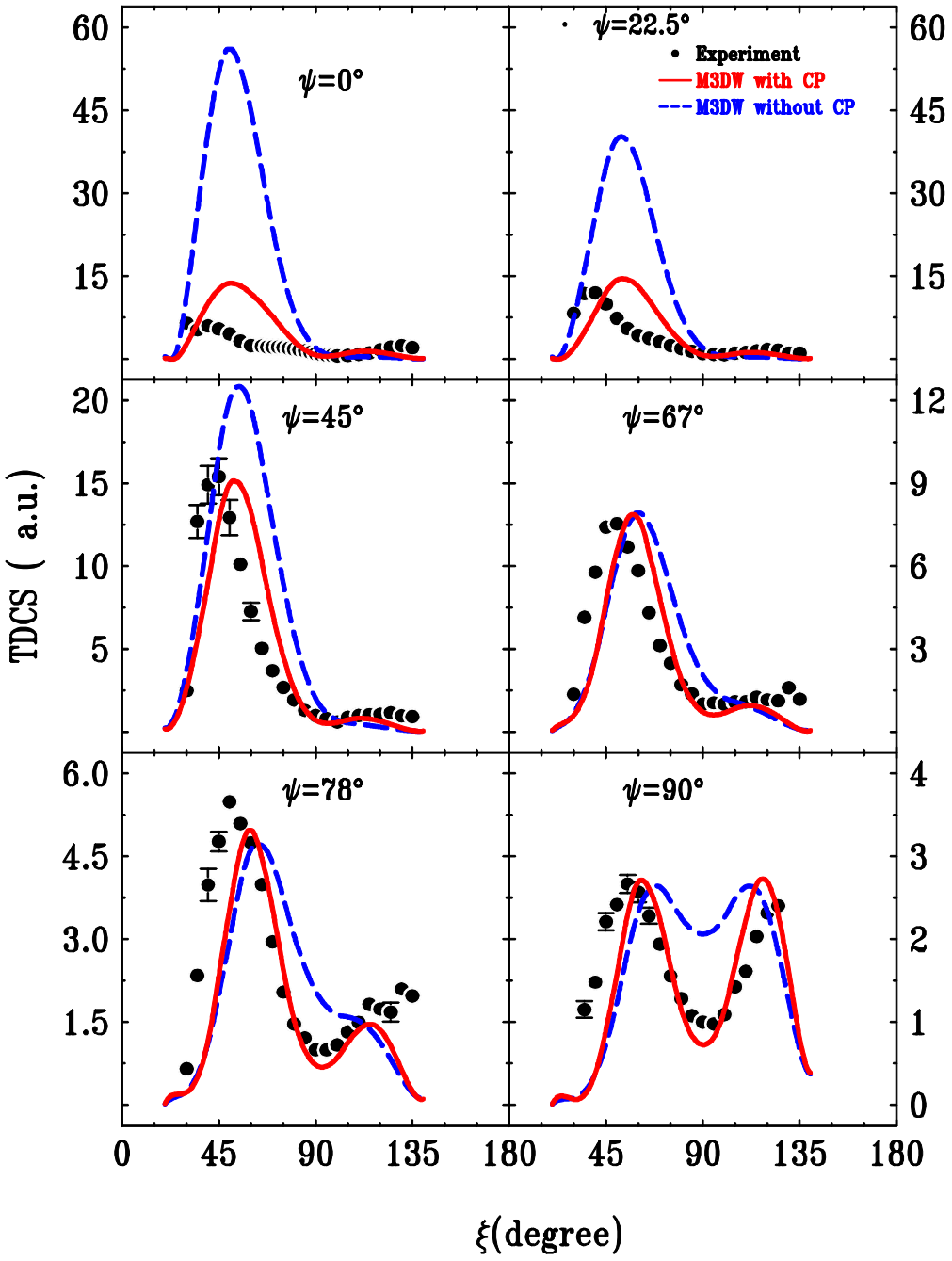

Figure 1: TDCS for the electron impact ionization of H_2 for unequal final state energies E_a=18 eV and E_b=2 eV. See text for definition of angles. The measurements are compared with M3DW calculations obtained with and without the correlation-polarization potential.

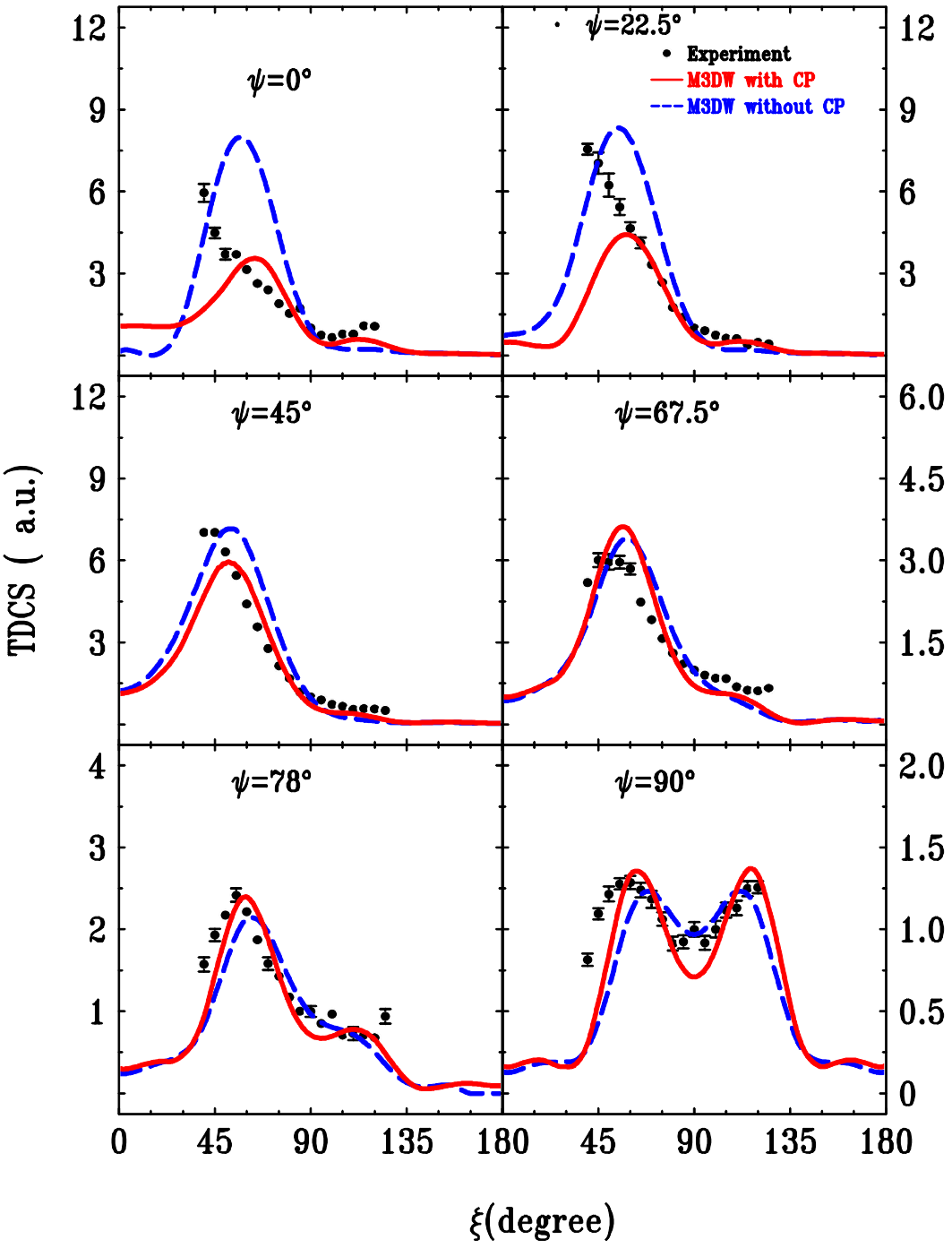

Figure 2 : TDCS for the electron impact ionization of H_2 for unequal final state energies E_a=18 eV and E_b=2 eV. See text for definition of angles. The measurements are compared with M3DW calculations obtained with and without the correlation-polarization potential.

3.2. Molecular nitrogen (N_2)

N_2 measurements are of particular interest due to the possibility of observing the effects of 2-center Young's-type interference terms in the cross sections [18]. Gao et al. [19] predicted a very strong Young's type interference effect for ionization of the $3\sigma_g$ state of N_2 for small projectile scattering angles when the ejected electron comes out at 180° (i.e. the backward beam direction) but this prediction is yet to be verified experimentally. This prediction resulted from a M3DW calculation using a polarization potential containing arbitrary cut-off parameters and a fairly elementary molecular orbital. We repeated these calculations using the M3DW method with an improved correlation-polarization potential [13-14] and improved molecular orbitals. The M3DW with the improved polarization potential and original molecular orbital is shown as the blue dotted line in figure 3 and the agreement with experiment improved but there was a predicted peak near 100° which is not seen in the experimental results. Then we did

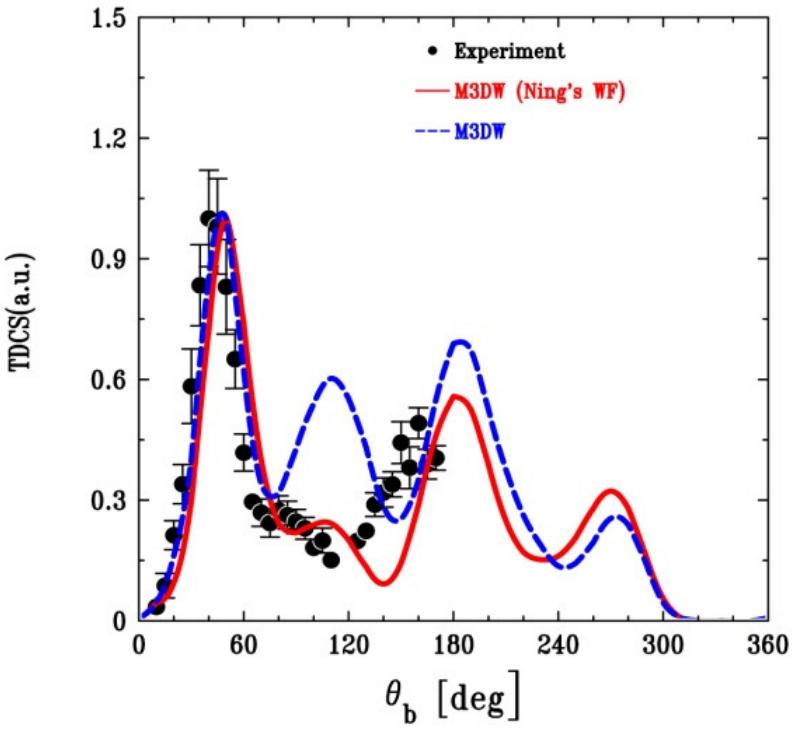

Figure 3: TDCS for the $3\sigma_g$ state of N_2 with E_0=75.6 eV, E_a=E_b=30 eV and θ_a=22°. The experiment data are compared to two sets of M3DW. The dotted blue line is the M3DW using an old wave-function and the solid red line is the M3DW using an improved wave-function. The experimental data are those of Murray et al. [20].

another M3DW calculation and this time we used a better wave- function calculated by Ning. The M3DW with Ning's wave-function is shown also as the solid red line. As can be seen from figure 3, the new calculation is in even better agreement with experimental data and the theory still predicts a Young's type interference peak around 180°. Since the agreement between theory and the experiment is fairly good, we are encouraged to think that the predicted 180° peak may be real. Until now, the existing experimental data is inconclusive concerning the existence of Young's interference effects for N_2.

3.3. Water (H_2O)

A couple years ago we compared the results of the M3DW method with experimental results for ionization of the $1b_1$ state of H_2O [21] and we found qualitative agreement with experiment but the results were somewhat disappointing. We now believe that the disappointing results stemmed from the OAMO being invalid for the $1b_1$ state. Kate Nixon and Andrew Murray have very recently measured triple differential cross sections for low incident energy electron-impact ionization of the $3a_1$ molecular state of H_2O and the OAMO approximation should be much better for this state. They used the same experimental apparatus as for H_2. Figure 4 shows the experimental and theoretical TDCS for H_2O in the symmetric coplanar geometry with excess energy of 10 eV and 20 eV.

There is a relatively good agreement between the experimental data and the M3DW (including the correlation-polarization potentials) and the DWBA calculations which is the same calculation as the M3DW except the PCI term is not included in the calculations. The DWBA without PCI has unphysically large cross sections for 20 eV excess energy when the two electrons leave the collisions in the same direction and this is a common failure of the DWBA. The agreement between experiment and theory found here for the $3a_1$ state is better than we previously found for the $1b_1$ state indicating that the OAMO approximation is much better for this state.

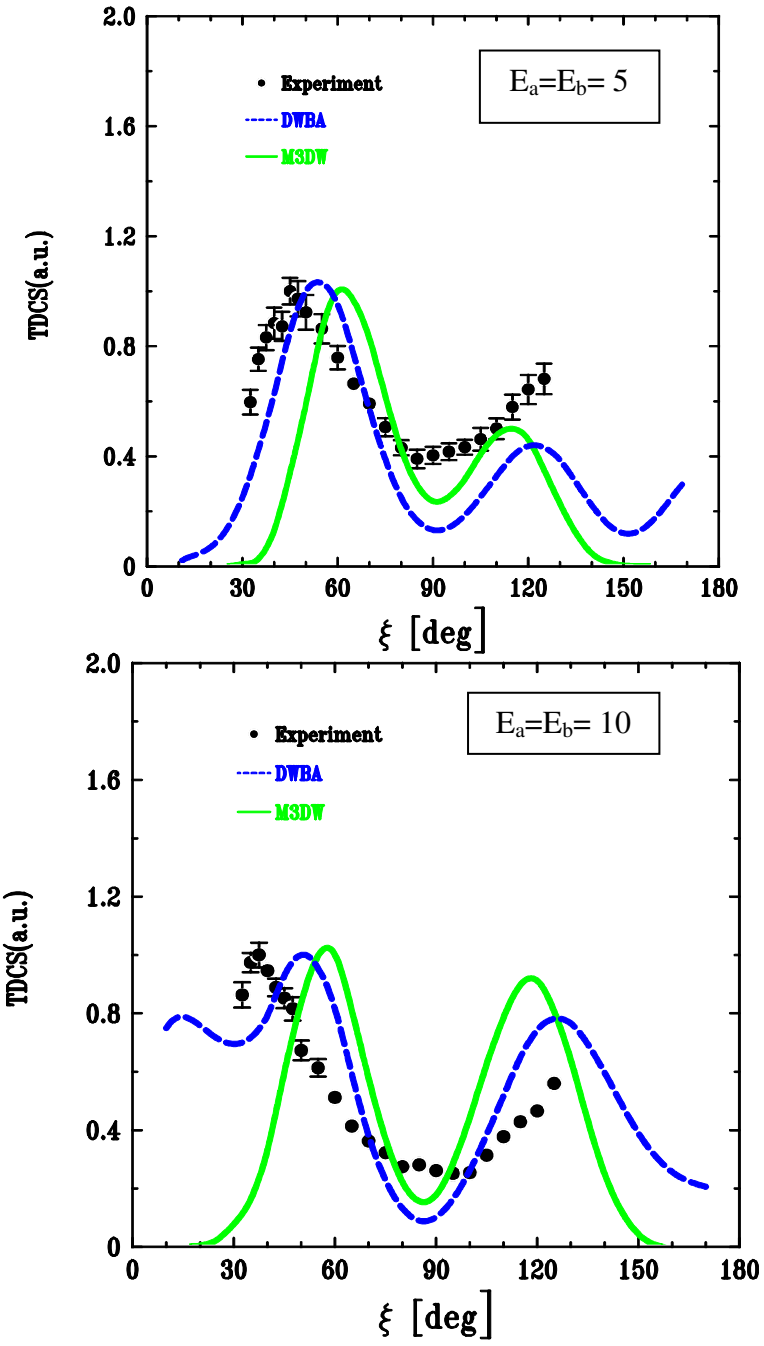

Figure 4: TDCS for electron impact ionization of H_2O in symmetric coplanar geometry as a function of ξ (2ξ is the angle between the two outgoing electrons). The cross sections are presented for excess energies of 10 eV and 20 eV.

3.4. Formic acid (*HCOOH*)

Birgit Lohmann's group at the ARC Center of Excellence for Antimatter-Matter studies at the University of Adelaide, Australia have recently measured (e,2e) ionization differential cross sections ionization of formic acid (*HCOOH*) for an incident electron energy of 100 eV and an ejected electron energy of 10 eV. This is a planar molecule with carbon near the center of mass which is of biological interest. The HOMO (highest occupied molecular orbital) is the 10a′ (ionization potential of 11.6 eV) and the next state is the 2a″ (ionization potential of 12.45 eV) and these two states cannot be resolved in the experiment so the experimental data represent a sum of the 10a′ and 2a″ states. Unfortunately the OAMO approximation is not valid for the 2a″ state so we can only calculate results for the 10a′ HOMO state.

Figure 5 shows a comparison between the experimental data and the M3DW results without the correlation-polarization potential. The experimental data have been

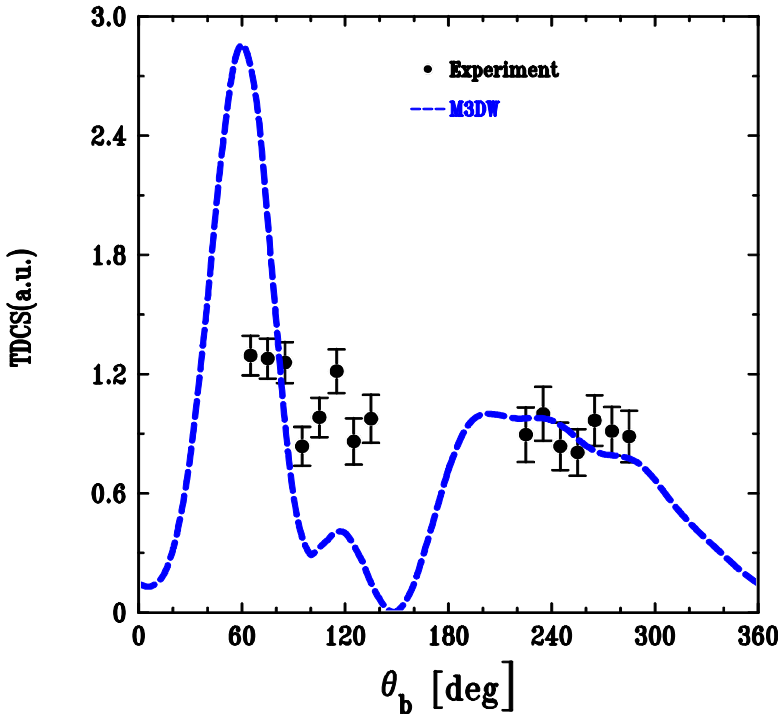

Figure 5: Triple differential cross section of ionization of Formic Acid with E_0=100 eV, E_b=10 eV and θ_a=10° as a function of the ejected electron angle. The Experimental measurements represent a sum of the 10a′ and 2a″ states while the M3DW results are for the 10a′ state only.

normalized to theory in the recoil region. Although the M3DW agrees well with the shape of the recoil peak, the theory predicts a larger and more pronounced binary peak than found in the experimental data. Since the effect of the 2a″ is unknown, it would be highly desirable to have experimental results which resolved the 10a′ state to ascertain how well the M3DW works for a larger molecule such as this.

5. Conclusions

In this paper, we presented TDCS for electron impact ionization of different molecules and compared the experimental results with the M3DW. Overall the theory is in reasonably good agreement with the experiments. Including the correlation polarization potential in the M3DW improved the agreement with the experiment for H_2, N_2, and H_2O. Replacing our old wave-function with Ning's wave-function has also improved the agreement with experiment for N_2 (the H_2 results did not change). We looked at two larger molecules – water and formic acid. We found better agreement with experiment for the $3a_1$ state of H_2O than we had previously found for the $1b_1$ state. For formic acid, we found good agreement with the shape of the recoil peak but not the binary peak. However, the experimental data represented a sum of the 10a′ and 2a″ states while we were only able to calculate results for the 10a′ state so validity of the M3DW method using OAMO for large molecules has not been adequately tested.

Acknowledgment

This work supported by the National Science Foundation under Grant. No. PHY-0757749 and the Australian Research Council Centre of Excellence for Antimatter-Matter Studies and the American NSF Also, we acknowledge the British Council for funding Kate Nixon, the University of Manchester for funding Christopher Kaiser, and the Saudi Ministry of Higher Education's King Abdullah Bin Abdul-Aziz Scholarship for funding Ola Al-Hagan. The author Chuangang Ning would like to acknowledge the support of the National Natural Science Foundation of China under contract No. 10704046.

References

[1] McCarthy I E and Weigold E 1976 *Phys. Rep.* C **27** 275.
[2] McCarthy I E and Weigold E 1988 *Rep.Prgo. Phys*. **51** 299.
[3] Stia C R,Fojon O A, Weck P F, Hanssen J, joulakian B J, and Rivarola R D 2002 *Phys. Rev.* A **66** 052709.
[4] Gao J, Madison D H, and Peacher J L 2006 *J. Phys.* B **39** 1275.
[5] Milne-Brownlie D S,Cavanagh S J, Lohmann B, Champion C, Hervieux P A, and Hanssen J 2004 *Phys. Rev*. A **69** 032701.
[6] Murray A J, 2005 *J. Phys.* B **38** 1999.
[7] Gao J, Madison D H, Peacher J L 2005 *J. Chem. Phys.* **123** 204314.
[8] Gao J, Madison D H, Peacher J L 2005 *Phys. Rev.* A **72** 032721.
[9] Gao J, Madison D H, Peacher J L 2005 *J. Chem. Phys*. **123** 204302.
[10] C. Lee, W. Yang, and R. G. Parr 1988 Phys. Rev. B **37**, 785.
[11] C. F. Guerra *et al.* 1998 Theor. Chem. Acc. **99**, 391.
[12] Furness J B and McCarthy I E 1973 *J.Phys. B* **6** 2280.
[13] Perdew J P and Zunger A 1981 *Phys. Rev.* B **23** 5048.
[14] Padial N Tand Norcross DW 1984 *phys. Rev*. A **29** 1742.
[15] Al-Hagan O, Kaiser C, Madison D H, and Murray A J 2008 *Nat. Phys* **5** 59.
[16] Colgan J, Al-Hagan O, Madison D H ,Kaiser C, Murray A J and Pindzola M S 2009 *Phys. Rev.* A **79** 052704.
[17] Ward S J and Macek J H 1994 *Phys. Rev*. A **49** 1049.
[18] Stia C R, Fojon O A, Weck P F, Hanssen J and Rivarola R D 2003 *J. Phys.* B **36** L257.
[19] Gao J, Madison D H and Peacher J L 2005 Phys. Rev. A **72** 032721.
[20] Murray A J, Hussey M J, Gao J, and Madison D H 2006 *J. Phys* B **39** 3945.
[21] Kaiser C, Spieker D, Gao J, Hussey M, Murray A J, and Madison D H 2007 *J. Phys. B: At. Mol. Opt. Phys*. **40** 2563.

X. Search for Interference Effect in Electron Impact ionization of Aligned Hydrogen Molecules

A Senftleben[1], T Pfl¨uger1, X Ren[1], O Al-Hagan[2], B Najjari[1],
D Madison[2], A Dorn[1] and J Ullrich[1]

[1] *Max-Planck-Institut f¨ur Kernphysik, Saupfercheckweg 1, 69117 Heidelberg, German*
[2] *Department of Physics, Missouri University of Science & Technology, Rolla, MO USA 65409*

Abstract

Five-fold differential cross sections (5DCS) for electron impact ionization of a diatomic molecule have been explored experimentally as a function of molecular alignment. Using H_2 as a test system we exploited dissociative ionization by 200 eV electrons to deduce the alignment of the internuclear axis. Ground-state ionization and autoionization are discussed. 5DCS are investigated for the direct channel and found to be in good agreement with M3DW calculations discarding at the same time a simple two-center interference model discussed recently in literature.

The complex dynamics of molecular ionization by energetic electron impact, also known as the (e, 2e) reaction, has been widely studied during the last decades. Its understanding is of paramount importance for fields such as radiation tumor therapy, the physics and chemistry of planetary atmospheres, near-stellar clouds or reactive plasmas. In general, a projectile electron knocks out a bound electron from the target leading to at least three fragments in the final state, two electrons and one ion. Especially the simple diatomic hydrogen molecule was intensely studied for a wide range of electron energies. Much research was dedicated to total cross sections and their dependence on the alignment which is given by the relative angle between the internuclear axis and the incoming electron beam [1–3]. On the other hand, detailed studies on the final-state electron characteristics were performed for a wide range of kinematic settings [4–9]. However, the ultimate experiment exploring five-fold differential cross sections (5DCS), thus capturing the full kinematics simultaneously with controlling the molecular alignment has not been realized up to now, even though efforts have been made to do so [10–12].

On the theoretical side, 5DCS have been investigated recently [13–15], finding a distinct dependence of the electron scattering dynamics on the alignment. Some of the observed features, especially unexpected minima in the angular spectra were attributed to interference effects, either as a consequence of the two-center nature of H_2 [13] or by coherent superposition of partial waves [15]. Traces of two-center interference were predicted even for three-fold differential cross sections (3DCS) measured with randomly aligned molecules. Evidence for their experimental observation was reported at impact energies above 500 eV [8] and at 250 eV [6], but excluded in investigations below 100 eV [7]. Thus, the subject has been discussed controversially, calling for the most stringent test of the interference hypotheses that can only be provided by alignment-dependent 5DCS.

In this work, 5DCS are presented for 200 eV electrons colliding with hydrogen molecules which can be ionized above 15.4 eV. The general geometry of such a reaction is displayed in fig. 3 (a). In most cases, the incoming projectile will lose a relatively small amount of energy ΔE. Additionally, it will be deflected by a small angle θ_{e1}. The momentum vectors of the projectile before and after the collision define the scattering

plane, which also contains the momentum $\vec{q}$ transferred onto the target. But the molecular alignment and the momentum of the emitted electron $\vec{p}_{e2}$ are not bound to this plane.

In our current experiment, the long standing shortage of experimental 5DCS has been overcome by determining the alignment of the internuclear axis from dissociation of the residual H_2^+ ion in the wake of the ionizing collision. Dissociation as investigated her can take two distinct reaction pathways which are illustrated in the potential curves diagram of fig. 1. On the one hand, it is possible to populate the vibrational continuum of

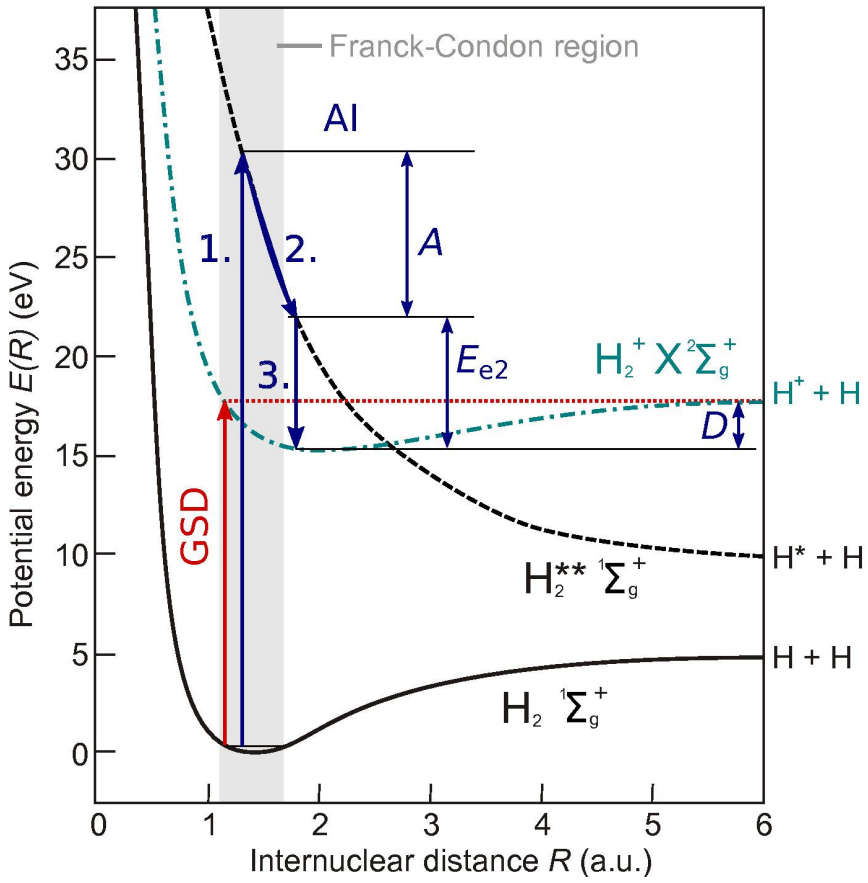

Figure 1: (color online) Selected potential curves of H_2 and H_2^+ (after [16, 17]) with illustration of two dissociative ionization channels: Ground-state dissociation (GSD) and autoionization (AI).

the H_2^+ ground state. This channel is called ground-state dissociation (GSD). The second process is autoionization (AI) which proceeds in three steps: First, a doubly excited state of the neutral molecule is populated. Only the lowest-lying of these is shown in fig. 1, but there is 3 an infinite number of such levels. All of them are repulsive within the Franck-Condon region accessible from the ground state. Consequently, the excited molecule starts to dissociate (second step) where the two nuclei gain a sum kinetic energy of A. As long as the ionic ground state lies energetically lower, spontaneous autoionization is possible in the third step. Thereby, the emitted electron gains the energy E_{e2} equal to the difference of the two potential curves at the current internuclear separation R. The residual H_2^+ ion can be stable if A is smaller than the dissociation energy D. Otherwise, the ion will fragment into a proton and a neutral hydrogen atom with a kinetic energy release (KER) of A – D.

Deducing the molecular alignment from the emission direction of dissocation fragments implies the validity of the axial recoil approximation [18], which is fulfilled if the H_2^+ ion fragments faster than it rotates. Using the method suggested by Wood et al [19] we have verified for the dissociation processes relevant here that the alignment can be determined with an uncertainty of ±20◦ or less for kinetic energy releases above 0.13 eV. The set-up used to measure protons as well as the two final state electrons is an advanced reaction microscope purpose-built to study ionization by low and medium energetic electrons as described in previous works [20, 21]. Briefly, a pulsed electron beam from a thermal source is crossed with a jet of cold hydrogen gas created by super sonic expansion. Beam and target densities are kept low enough such that ionization will occur in less than every tenth shot. Charged collision products are accelerated and guided by well-defined electric and magnetic fields towards two position and time sensitive detectors. From this, three-dimensional momentum vectors of all particles can be calculated. Different to previous works the detector collecting ions has been significantly enlarged and additionally moved closer to the reaction point to increase the acceptance of energtic fragments stemming from dissociation. Furthermore, this structure needed to employ a central bore to allow the incoming beam to pass. This was realized with specially designed hexagonal delay line anode [22] constructed around a

beam tube and, thus, requiring a sophisticated method to read out the position information similar to that described by [23]. It should be noted that neutral fragments are not detected. Since the dissociation of the H_2^+ ion leads to one H atom, its momentum has to be derived through momentum conservation. With the electric and magnetic field settings used we have been able to detect protons emerging from dissociation of H_2^+ over the complete solid angle for a kinetic energy release of up to 1 eV.

The two dissociation channels can be distinguished experimentally through the KER of the heavy fragments, which is derived by doubling the measured energy of the proton, and the emitted electron's energy E_{e2}, as illustrated in fig. 2. This method was demonstrated in ion impact ionization of H_2 [24] where the experimental values were compared to calculated energies. In electron impact studies, channel-selective KER distributions have also been extensively studied and well understood [2, 25, 26]: While GSD is the overwhelmingly dominating channel at KERs close to zero its relative contribution rapidly drops below the AI rate around 1 eV. Therefore, in the energy range studied in this work, it is not possible to separate the two processes through KER alone. To understand the channel-dependent behavior of E_{e2} we are going to take a look at energy conservation for our reaction. The projectile's energy loss ΔE is composed as follows:

$$\Delta E = E_D + E_{e2} + KER \qquad (1)$$

where E_D = 18 eV is the energy of the first dissociation limit of H_2^+ above the ground state of the neutral molecule. If we neglect the kinetic energy release because it is in most cases smaller than 1 eV, we see that E_{e2} is linearly linked with the energy loss which is continuous for direct ionization but takes discrete values for excitation. Hence, events from autoionization should employ energies for the emitted electron that can be associated with the energy transfers necessary to populate doubly-excited states of H_2. Those incidents can be identified in the left plot of fig. 2 where for E_{e2} between 5 and 12 eV increased count rate is registered, especially for KERs above 0.5 eV. Changing the direction of the molecular axis to aligned perpendicular to the momentum transfer (right plot in fig. 2) the count rate rapidly drops with larger kinetic energy releases at any value

of E_{e2}, showing that for this geometry GSD is the dominant process. From this we can already estimate that the autoionization rate depends stronger on the molecular alignment.

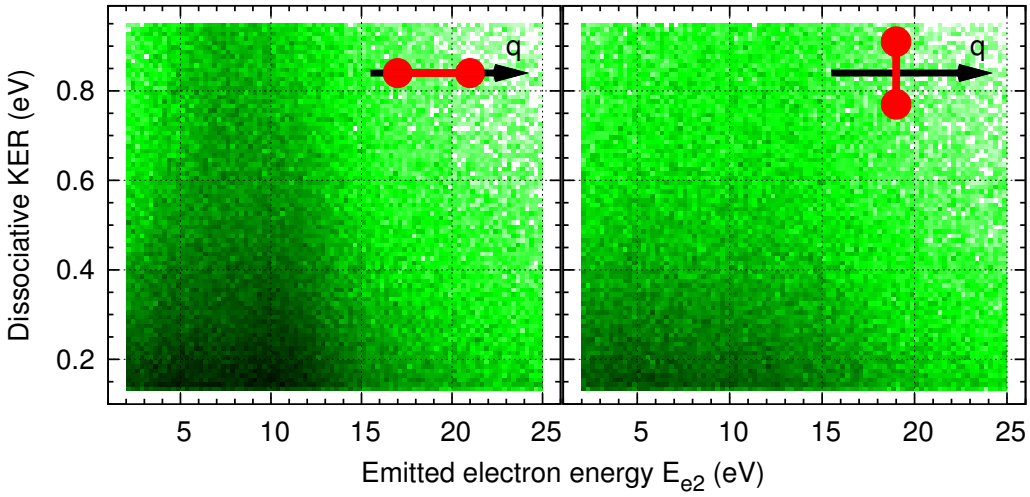

Figure 2: (color online) Measured kinetic energy released to the fragments of the dissociating H_2^+ ion versus the emitted electron's energy for molecules aligned parallel (left) and perpendicular (right) to the momentum transfer $\vec{q}$. The logarithmic color scales are identical in both images, with black representing the highest count rates.

In fig. 3 (b) to (d) the emission direction of the protonic fragment is plotted in the scattering plane system as defined in fig. 3 (a) for different electron energies E_{e2} and, consequently, energy losses ΔE. Fig. 3 (c) comprehends the region where autoionization is predicted due to the increased large KER count rate in fig 2(a). It clearly exhibits the strongest anisotropy of all distributions. We will postpone further discussion of autoionization to a future publication. However, for the energy ranges where GSD should be the sole contributing process, an increased rate for molecular alignment parallel to the momentum transfer has been measured as well (see fig. 3 (b) and (d)). To further investigate these findings, fig. 4 displays an exemplary 5DCS spectrum for ionization into the ground state of H_2^+. Hereby, the second electron's polar angle distribution is plotted for emission into the scattering plane at an energy of 3.5 eV while the scattering angle is fixed to 16°. Three distinct molecular alignments are selected. Other situations will be discussed in a subsequent publication.

Ground-state ionization has the advantage that its 5DCS can be calculated by stateof- the-art theoretical models. Here we present cross-sections obtained with the molecular 3-body distorted wave (M3DW) method [27]. They are displayed in the upper panel of fig. 4. The model has been used to normalize the experimental data. For all

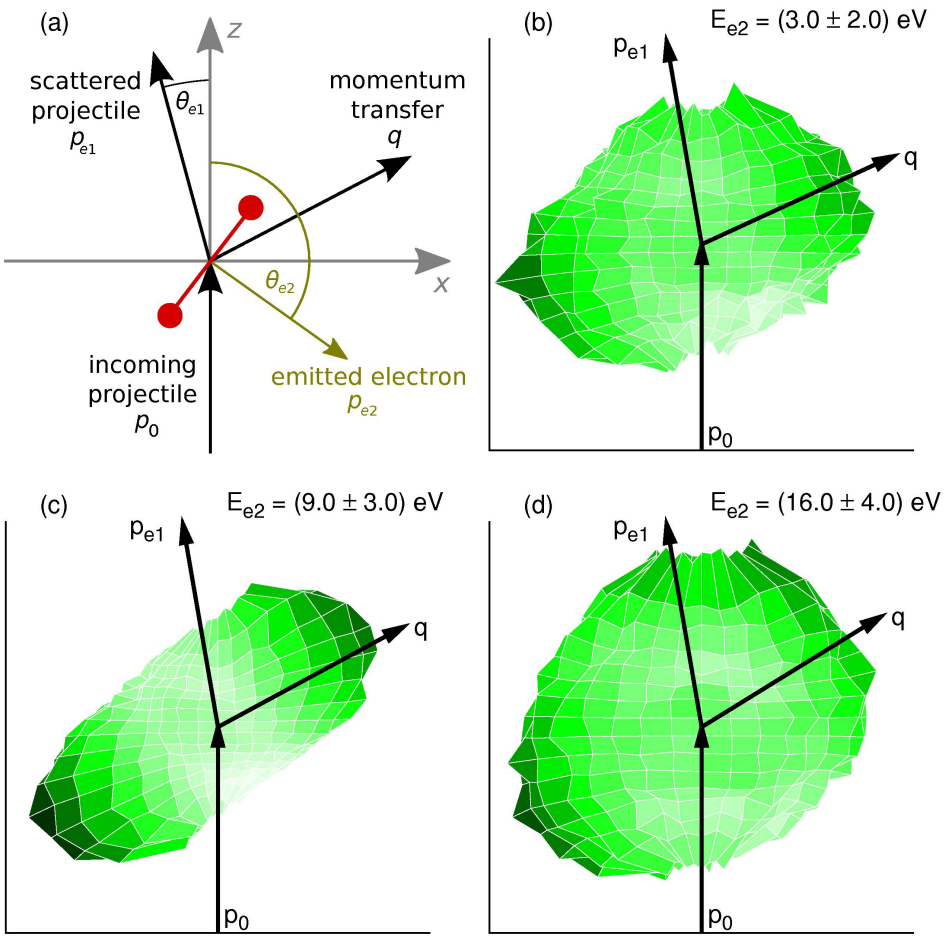

Figure 3: (color online) (a) Geometry of the ionizing collision in the scattering plane spanned by the incoming and scattered projectile momentum vectors. The sketched momentum of the emitted electron is exemplary. (b)–(d) Dependence of the ionization cross section on the emission direction of the protonic fragment. Summed over the whole detected solid angle for the two electrons while the emitted electron energy amounts (b) (3 ± 2) eV, (c) (9 ± 3) eV and (d) (16 ± 4) eV.

molecular alignments, the spectra resemble classical (e, 2e) spectra for the ionization of an atomic s-state (compare e.g. [28]). Generally, a reasonable agreement between M3DW calculation and experiment is found, especially in the binary region below 180◦ where the distinct experimental alignment dependence is well reproduced. At essentially all electron emission angles, parallel alignment of the molecule with respect to momentum transfer employs the highest cross-sections, while the perpendicular case features the lowest. An articulate disagreement between M3DW and experiment is found around 250°, where parallel alignment was found to show even higher rates. The origin of this is still not understood. At much lower energies, the time-dependent close-coupling (TDCC) method has recently predicted such strongly varying 5DCS for different molecular alignments. On the other hand, it has to be expected that in the dipole limit at very high electron energies, the ionization cross sections for GSD will become independent of the molecular alignment, as reported in photoionization experiments [29]. In the current case we seem to be in an intermediate regime where the location of the nuclei starts to play a role in the collision.

We have also investigated the experimental results in terms of the two-center picture developed by Stia et al [13] that predicts interference effects. Hereby, 5DCS are obtained by multiplying triply differential cross sections (3DCS) for an atomic target with an interference factor $I = 2\,[1+\cos((\vec{q}-\vec{p}_{e2})\bullet\vec{R})]$ depending on the molecular alignment $\vec{R}$. To demonstrate the effect of I we have currently employed 3DCS for the two-electron system helium calculated using 3C wavefunctions which were found to be in reasonable agreement to experimental data [28]. The resulting 5DCS are displayed in the lower panel of figure 4. Once again, the measured cross sections have been normalized to the calculations. Apparently, this model disagrees significantly with the experimental results. First, the cross sections of the distinct molecular alignments are reversed in order, i.e. the interference factor predicts highest probabilities when the molecular is perpendicular to momentum transfer. Additionally, the model exhibits much smaller overall alignment-dependence in the binary region than observed. From this we conclude that interference, at least in terms of Stia's model, is not able to explain the observed cross sections for ground-state ionization of H_2 at 200 eV impact energy. By having the additional information of alignment we can see that Stia's model is inadequate

while it was found to reproduce the binary-torecoil ratio in experimentswith randomly orientated molecules at comparable impact energy (Milne-Brownlie *et al* 2006). However, interference effects might certainly be present in a more subtle way and should be accounted for implicitly by the M3DW calculation.

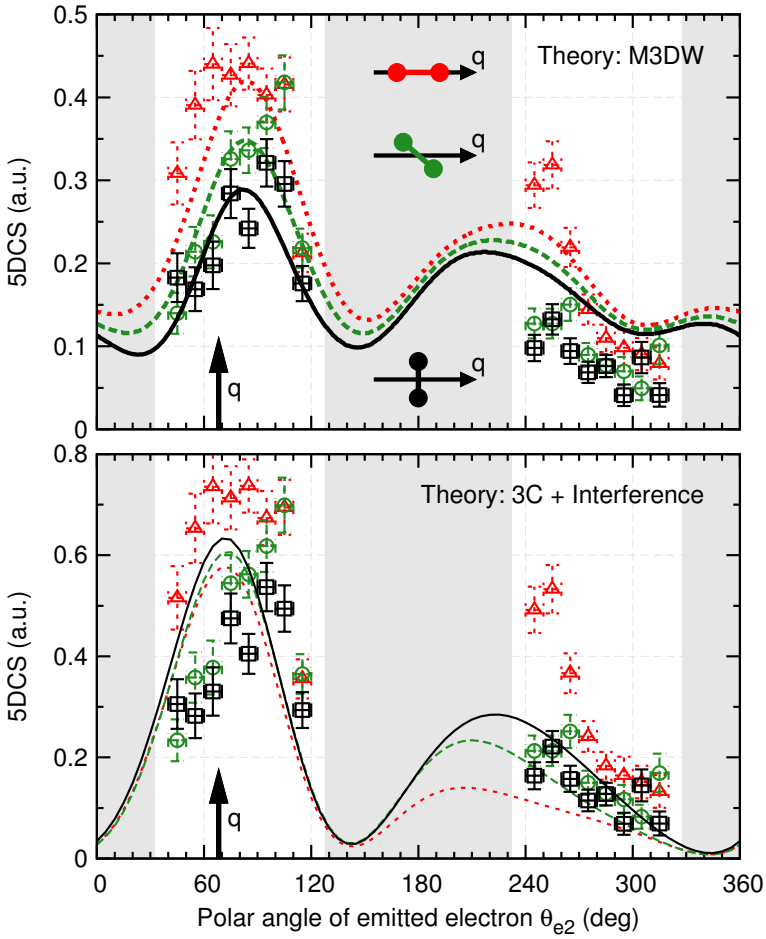

Figure 4: (color online) Five-fold differential cross sections (5DCS) as a function of the emitted electron's emission angle in the scattering plane. This electron's energy is (3.5 ± 2.0) eV and the projectile scattering angle is (16 ± 4) °. Points represent experimental results, lines model calculations, which is either M3DW (upper panel) or 3C for a helium target multiplied with the interference factor given by [13] (lower panel). For all data shown the molecule is aligned in the scattering plane, at angles of 0° (triangles/dotted line), 45° (circles/dashed line) or 90° (squares/solid line) relative to the momentum transfer $\vec{q}$. Shaded areas represent angular ranges outside the experimental acceptance.

To summarize, five-fold differential cross sections of electron impact ionization of molecular hydrogen have been successfully measured. Two dissociation channels leading to low energetic protons could be identified: Ground-state dissociation and autoionization. For GSD, experimental data was well matched by M3DW calculation, although unexplained discrepancies remain. On the other hand, atomic cross-sections multiplied with a alignment dependent interference factor failed to reproduce experimental 5DCS.

Acknowledgements

This work was partly supported by the USA National Science Foundation under Grant. No. PHY-0757749. The author OA-H would like to acknowledge the support of the Saudi Ministry of Higher Educationand the King Abdullah Bin Abdul-Aziz Scholarship. XR is grateful for support from DFG project No. RE 2966/1-1.

References

[1] G. H. Dunn and L. J. Kieffer, *Phys. Rev.* **132**, 2109 (1963).
[2] R. J. Van Brunt and L. J. Kieffer, *Phys. Rev*. A **2**, 1293 (1970).
[3] A. Crowe and J. W. McConkey, *J. Phys.* B: *At. Mol. Opt. Phys*. **6**, 2088 (1973).
[4] E. Weigold, S. T. Hood, I. E. McCarthy, and P. J. O. Teubner, *Phys. Lett.* A **44**, 531 (1973).
[5] M. Cherid, A. Lahmam-Bennani, A. Dugett, R. W. Zurales, R. R. Lucchese, M. C. Dal Cappello, and C. Dal Cappello, *J. Phys.* B: *At. Mol. Opt. Phys*. **22**, 3483 (1989).
[6] D. S. Milne-Brownlie, M. Foster, J. Gao, B. Lohmann, and D. H. Madison, *Phys. Rev. Lett.* **96**, 233201 (2006).
[7] A. J. Murray, *J. Phys.* B: *At. Mol. Opt. Phys*. **38**, 1999 (2005).
[8] E. M. Staicu Cassagrande, A. Naja, F. Mezdari, A. Lahmam-Bennani, P. Bolognesi, B. Joulakian, O. Chuluunbaatar, O. Al-Hagan, D. H. Madison, D. V. Fursa, et al., *J. Phys.* B: *At. Mol. Opt. Phys.* **41**, 052701 (2008).
[9] O. Al-Hagan, C. Kaiser, D. H. Madison, and A. J. Murray, *Nat. Phys*. **5**, 59 (2008).
[10] M. Takahashi, N. Watanabe, Y. Khajuria, K. Nakayama, Y. Udagawa, and J. H. D. Eland, J. *Electron Spectrosc. Relat. Phenom*. **141**, 83 (2004).
[11] M. Takahashi, N. Watanabe, Y. Khajuria, Y. Udagawa, and J. H. D. Eland, *Phys. Rev. Lett.* **94**, 213202 (2005).
[12] S. Bellm, J. Lower, E. Weigold, and D. W. Mueller, *Phys. Rev. Lett*. **104,** 023202 (2010).
[13] C. R. Stia, O. A. F´ojon, P. F. Weck, J. Hanssen, and R. D. Rivarola, *J. Phys.* B: *At. Mol. Opt. Phys.* **36**, L257 (2003).

[14] J. Colgan, M. S. Pindzola, F. Robicheaux, C. Kaiser, A. J. Murray, and D. H. Madison, *Phys. Rev. Lett*. **101**, 233201 (2008).
[15] J. Colgan, O. Al-Hagan, D. H. Madison, A. J. Murray, and M. S. Pindzola, *J. Phys*. B: *At. Mol. Opt. Phys*. **42**, 171001 (2009).
[16] T. E. Sharp, At. Data Nucl. *Data Tables* **2**, 119 (1970).
[17] S. L. Guberman, *J. Chem. Phys*. **78**, 1404 (1983).
[18] R. N. Zare, *J. Chem. Phys*. **47,** 204 (1967).
[19] R. M. Wood, Q. Zheng, A. K. Edwards, and M. A. Mangan, *Rev. Sci. Instrum*. **68**, 1382 8 (1997).
[20] M. D¨urr, A. Dorn, J. Ullrich, S. P. Cao, A. Czasch, A. S. Kheifets, J. R. G¨otz, and J. S. Briggs, *Physical Review Letters* **98,** 193201 (2007).
[21] A. Dorn, M. D¨urr, B. Najjari, N. Haag, C. Dimopoulou, D. Nandi, and J. Ullrich, J. *Electron Spectrosc. Relat. Phenom*. **161**, 2 (2007).
[22] O. Jagutzki, A. Cerezo, A. Czasch, R. D¨orner, M. Hattass, M. Huang, V.Mergel, U. Spillmann, K. Ullmann-Pfleger, T. Weber, et al., IEEE T. *Nucl. Sci*. **49**, 2477 (2002).
[23] H. B. Pedersen, S. Altevogt, B. Jordon-Thaden, O. Heber, L. Lammich, M. L. Rappaport, D. Schwalm, J. Ullrich, D. Zajfmann, R. Treusch, et al., *Phys. Rev*. A **80**, 012707 (2009).
[24] G. Laurent, J. Fern´andez, S. Legendre, M. Tarisien, L. Adoui, A. Cassimi, X. Fl´echard, F. Fr´emont, B. Gervais, E. Giglio, et al., *Phys. Rev. Lett.* **96**, 173201 (2006).
[25] A. K. Edwards, R. M. Wood, J. L. Davis, and R. L. Ezell, *Phys. Rev*. A **42**, 1367 (1990).
[26] B. Van Zyl and T. M. Stephene, Phys. Rev. A 50, 3164 (1994).
[27] J. Gao, D. H. Madison, J. L. Peacher, A. J. Murray, and M. J. H. Hussey, *J. Chem. Phys*. **124**, 194306 (2006).
[28] M. D¨urr, C. Dimopoulou, A. Dorn, B. Najjari, I. Bray, D. V. Fursa, Z. Chen, D. H. Madison, K. Bartschat, and J. Ullrich, *J. Phys*. B: *At. Mol. Opt. Phys*. **39,** 4097 (2006).
[29] Y. Hikosaka and J. H. D. Eland, *J. Electron Spectrosc. Relat. Phenom.* **133,** 77 (2003).

XI. Five-fold Differential Cross Sections for Ground-State Ionization of Aligned H_2 by Electron Impact

Arne Senftleben,[1] Ola Al-Hagan,[2] Thomas Pfl¨uger,[1] Xueguang Ren,[1] Don Madison,[2] Alexander Dorn,[1] and Joachim Ullrich[1]

[1]*Max-Planck-Institut fu¨r Kernphysik, Saupfercheckweg 1, 69117 Heidelberg, 5 Germany*

[2]*Department of Physics, Missouri University of Science & Technology, Rolla, 7 MO USA 65409*

Abstract

We discuss the ionization of aligned hydrogen molecules into their ionic ground state by 200 eV electrons. Using a reaction microscope, the complete electron scattering kinematics is imaged over a large solid angle. Simultaneously, the molecular alignment is derived from post-collision dissociation of the residual ion. It is found that the ionization cross section is maximized for small angles between the internuclear axis and the momentum transfer. Five-fold differential cross sections (5DCS) reveal subtle differences in the scattering process for the distinct alignments. We compare our observations with theoretical 5DCS obtained with an adapted molecular three-body distorted wave model that reproduces most of the results, although discrepancies remain.

1. Introduction

Ionization of molecules by charged particle impact is a fundamental reaction of great importance in many fields such as radiation tumor therapy, the physics and chemistry of planetary atmospheres, near-stellar clouds or reactive plasmas. The complete information of any specific process is contained in fully differential cross sections (FDCS) that can be obtained in kinematically complete experiments where all final state momenta are known. In electron impact single ionization, which we study here, there are usually three particles, two electrons and one ion. If the initial state momenta are well-defined, the detection of two fragments is sufficient to fully determine the kinematics, due to momentum conservation. In electron impact ionization traditionally the two final state electrons are detected, styling these studies as (e, 2e) experiments. Many atoms but also molecules have been investigated with this method [1], but for molecular targets they have so far neglected their alignment which defines the relative position of the constituent nuclei with respect to the incoming electron's direction. Madison and Al-Hagan have recently presented a review of the resent work in this area [2].

Due its role as a model system the ionization of H_2 has been extensively studied in the past for a broad range of impact energies. Much research was dedicated to total cross sections and their dependence on the alignment which is given by the relative angle between the internuclear axis and the incoming electron beam [3–5]. On the other hand, detailed studies on the final-state electron characteristics were performed for various kinematic settings [6–11]. In all of the latter studies, traditional (e, 2e) spectrometers were used to detect the two final state electrons with angle and energy selective analyzers. Recently, efforts have been made to combine this method with ion spectrometers to gain information on the molecular alignment [12–14], but no statistically significant FDCS were measured. The main reason for this was the small angular acceptance of the apparatus. We have overcome this problem using a reaction microscope, which allows to measure many different kinematic settings at the same time. The experiment has been introduced recently [15], while in this paper we will present the results obtained for ionization into the ionic ground state at different kinematic conditions.

On the other hand, studies on aligned hydrogen molecules have recently been performed in other settings. Molecular frame angular distributions of electrons emitted by one-photon single ionization have been the first fully differential cross sections obtained in any reaction of H_2 [16-19] Due to the absorption of the incoming photon, only two particles have to be detected in a kinematically complete experiment for photoionization. Ionic collisions with aligned H_2 were also investigated, but FDCS were not obtained, because up to now it has not been possible to fix the collision geometry simultaneously with the internuclear axis [20, 21].

On the theoretical side, FDCS for electron impact ionization of H_2 into the ground state of H_2^+ have been investigated recently [22–24], finding a distinct dependence of the electron scattering dynamics on the alignment. Some of the observed features, especially unexpected minima in the angular spectra were attributed to interference effects, either as a consequence of the two-center nature of H_2 [22] or by coherent superposition of partial waves [24]. Traces of two-center interference were predicted even in differential cross sections measured with randomly aligned molecules. Evidence for their experimental observation was reported at impact energies above 500 eV [10, 25] and at 250 eV [8], but excluded in investigations below 100 eV [9]. However, FDCS represent a much stricter test of the interference model which we have recently shown in an exemplary setting [15].

The general geometry of the ionizing collision is illustrated in fig. 1. In the present case the kinetic energy of the projectile (200 eV) is much higher than the ionization potential (15.4 eV without dissociation and at least 18 eV with dissociation). In this situation, asymmetric energy sharing between the two final state electrons is very likely, because the projectile is usually losing only a small part of its energy. Hence, in good approximation, we can label the fast electron scattered projectile with momentum $\vec{p}_{e1}$, whereas $\vec{p}_{e2}$ refers to an electron initially bound to the molecule and ejected during the collision. Without loss of generality, we can define the scattering plane spanned by $\vec{p}_0$ and $\vec{p}_{e1}$ as the (x, z)-plane of our collision-based coordinate system. The *x* component of the scattered projectile's momentum is by convention negative. As a consequence, the momentum transfer $\vec{q} = \vec{p}_0 + \vec{p}_{e1}$ is also located in the scattering plane

but has a positive x component. The emitted electron's momentums as well as the molecular axis are not restricted to the scattering plane. Hence, their orientation has to be characterized by the two angles φ and θ. FDCS for single ionization of a linear molecule are given as the five-fold differential cross sections (5DCS) $d^5\sigma / d\Omega_{e1} d\Omega_{e2} dE_{e2} d\phi_M d\theta_M$ where ϕ_M and θ_M fix the molecular alignment, E_{e2} is the energy of the emitted electron and Ω_{e1} (Ω_{e2}) is the solid angle of the scattered projectile and emitted electron, respectively.

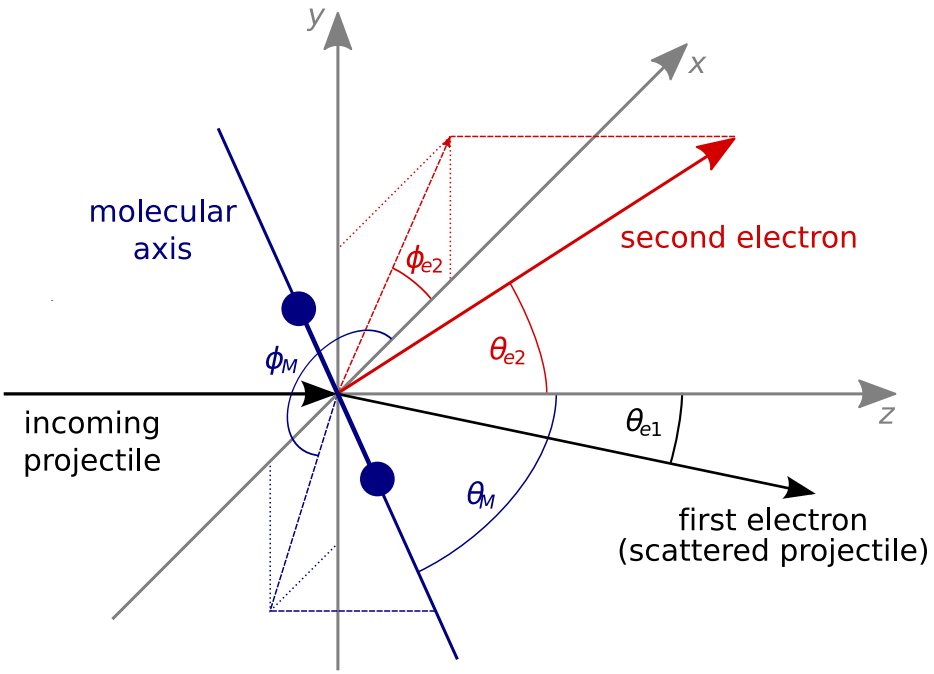

Figure 1: Geometry of the ionizing collision.

2. Theoretical framework

The details of the molecular three-body distorted wave (M3DW) approximation have been presented elsewhere [26-28] so only a brief overview will be presented here. The M3DW 5DCS is given by

$$\frac{d^5\sigma}{d\Omega_{e1} d\Omega_{e2} dE_2 d\phi_M d\theta_M} = \frac{1}{(2\pi)^5} \frac{k_{e1} k_{e2}}{k_0} \left(|T_{dir}|^2 + |T_{exc}|^2 + |T_{dir} - T_{exc}|^2 \right) \quad (1)$$

Where $\vec{k}_0$ is the initial state wave vector, and $\vec{k}_{e1}$ ($\vec{k}_{e2}$) is the wave vector for the scattered (ejected) electron. The direct and exchange amplitudes for oriented molecules are T_{dir} and T_{exc} respectively:

$$\begin{aligned} T_{dir} &= \left\langle \chi_{e1}^{-}(\vec{k}_{e1},\mathbf{r}_1)\chi_{e2}^{-}(\vec{k}_{e2},\mathbf{r}_2)C_{scat-eject}(r_{12})\,|\,V-U_i\,|\,\phi_{Dyson}(\mathbf{r}_2,\mathbf{R})\chi_0^{+}(\vec{k}_0,\mathbf{r}_1)\right\rangle \\ T_{exc} &= \left\langle \chi_{e1}^{-}(\vec{k}_{e1},\mathbf{r}_2)\chi_{e2}^{-}(\vec{k}_{e2},\mathbf{r}_1)C_{scat-eject}(r_{12})\,|\,V-U_i\,|\,\phi_{Dyson}(\mathbf{r}_2,\mathbf{R})\chi_0^{+}(\vec{k}_0,\mathbf{r}_1)\right\rangle \end{aligned} \quad (2)$$

In eqn. 2, $\mathbf{r}_1$ ($\mathbf{r}_2$) is the co-ordinate of the incident (bound) electron, χ_0, χ_{e1}, and χ_{e2} are the distorted waves for the incident, scattered, and ejected electrons respectively, $C_{scat-eject}$ is the Coulomb interaction between the scattered projectile and ejected electron, and the molecular wavefunction $\phi_{Dyson}(\mathbf{r}_{e1},\mathbf{R})$ is the so-called Dyson orbital which depends on the orientation of the molecule ($\mathbf{R}$). $\phi_{Dyson}(\mathbf{r}_{e1},\mathbf{R})$ is calculated using density functional theory (DFT) along with the standard hybrid B3LYP with the TZ2P (triple-zeta with two polarization functions) Slater type basis sets. The potential V is the initial state interaction between the projectile and the neutral molecule, and U_0 is the initial-state spherically symmetric distorting potential which is used to calculate the initial-state distorted wave χ_0.

The initial state molecular distorted waves are calculated using a spherically symmetric distorting potential U_0. The Schrödinger equation for the incoming electron wavefunction is given by

$$(\hat{T}_0 + U_0 - E_0)\chi_0^{+} = 0 \quad (3)$$

where $\hat{T}_0$ is the kinetic energy operator for the projectile, E_0 is the energy of the incoming projectile, and the '+' superscript on χ_0^{+} indicates outgoing wave boundary conditions. The initial state distorting potential contains three components $U_0 = U_S + U_E + U_{CP}$, where U_S is the initial state spherically symmetric static potential which is calculated from the molecular charge density obtained from the numerical orbitals averaged over all angular orientations, U_E is the exchange-distortion potential of Furness and McCarthy [29] (corrected for sign errors), and U_{CP} is the

correlation-polarization potential of Perdew and Zunger [30]. The two final channel distorted waves are obtained from a Schrödinger equation similar to eqn. 3.

3. Experimental procedure

3.1. Reaction microscope set-up

In our experiment, momentum vectors of the collisions products are measured using a reaction microscope as drawn in fig. 2. The set-up was designed to study atomic ionization by low and medium energetic electrons and has been described in previous works [31,32]. Briefly, a pulsed electron beam from a thermal source is crossed with a jet of cold gas created by supersonic expansion. Beam and target densities are kept low enough such that ionization will occur in less than every tenth shot. Charged collision products are accelerated and guided by well-defined electric and magnetic fields towards two position and time sensitive detectors. This information can be analyzed to retrieve the three-dimensional momentum vectors of the final state particles [33].

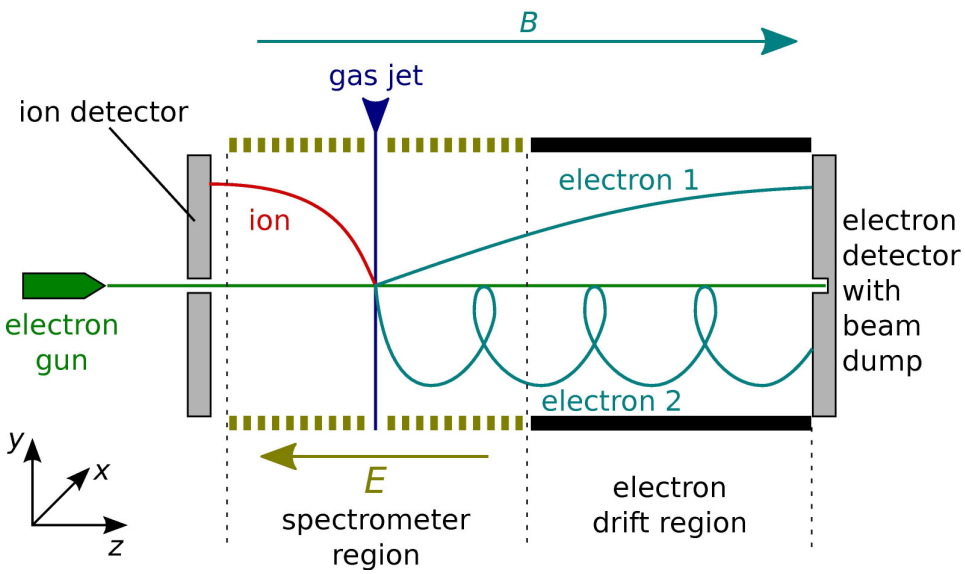

Figure 2: Schematic drawing of the employed reaction microscope.

The detectors employ pairs of 80mm micro channel plates for amplification of the single particle signal and hexagonal delay line anodes [34] to read out the position of the

incidence. While the electron detector has not been changed compared to previous works, the ion detector was significantly enlarged for the present study to achieve a better acceptance of fragments stemming from molecular dissociation. Furthermore, this structure needed to employ a central bore to allow the incoming beam to pass. Therefore the three individual delay lines of the detector were build with a gap to create hole in the center. This geometry requires the use of a sophisticated method to read out the position information similar to that described by Pedersen et al [35].

With the electric and magnetic field settings used we have been able to detect protons emerging from dissociation of H_2^+ over the complete solid angle for a kinetic energy release of up to 1 eV. The projectile was detected for a scattering angle between 3.3° and 25° while the emitted electron was measured over more than 90% of the full solid angle for energies between 1.5 and 25 eV. The neutral hydrogen atom also resulting from the fragmentation of H_2^+ was not detected, but its momentum can be calculated from momentum conservation, as the initial state momenta are well-defined.

3.2. Obtaining the molecular alignment

In our current experiment, the alignment of the internuclear axis is determined from fragmentation of the residual H_2^+ ion in the wake of the ionizing collision. Dissociation as investigated here can take two distinct reaction pathways which are illustrated in the potential curves diagram of fig. 3. On the one hand, it is possible to populate the vibrational continuum of the H_2^+ ground state. This channel is called ground-state dissociation (GSD) or direct ionization. It is known to yield a proton and a neutral hydrogen atom with a summed kinetic energy release (KER) of less than 1 eV [5]. Electronically, GSD is almost identical to non-dissociative single ionization of H_2, but it can only happen at sub-equilibrium internuclear distances. The second process is autoionization (AI) where a doubly-excited, repulsive level of the neutral molecule is populated. During the dissociation of this state, spontaneous emission of an electron is possible. The resulting molecular ion will fragment into a proton and a neutral atom when the energy A already gained by the nuclei exceeds the dissociation potential D. In

the following we will only consider GSD to study the alignment-dependence of ionization into the electronic ground state of H_2^+.

We have recently explained the separation of the two competing dissociation channels [15]: Although they employ different KER distributions a more articulate distinction can be found in the emitted electron's energy E_{e2}. Because of the low kinetic energy (< 1 eV) released in the ionic fragmentation, E_{e2} is directly connected with the energy ΔE transferred to the target. This takes continuous values in direct ionization but discrete values in excitation and, hence, autoionization. Therefore, we can select energy regions, where ground-state dissociation is the only contributing process.

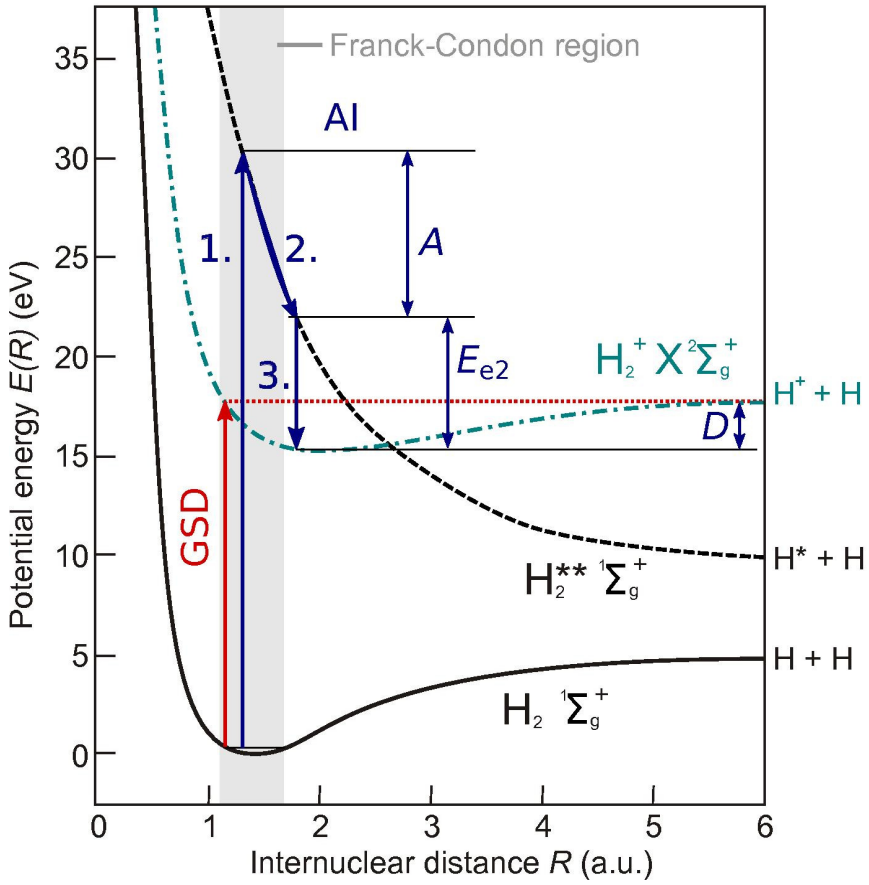

Figure 3: Selected potential curves of H_2 and H_2^+ (after [36,37]) with illustration of two dissociative ionization channels: Ground-state dissociation (GSD) and autoionization (AI).

Deriving the molecular alignment from the emission direction of dissociation fragments implies the validity of the axial recoil approximation [38], which is fulfilled if the H_2^+ ion fragments faster than it rotates. Using the method suggested by Wood et al [39] we have verified for ground-state dissociation that the alignment can be determined with an uncertainty of ±20° or less for kinetic energy releases above 0.13 eV.

Furthermore, we have to take into account that the measured protonic momentum $\vec{p}_{H^+}$ does not only contain the dissociation part $\vec{p}_{diss}$ but also the collisional recoil $\vec{p}_{rec}$. The latter can be derived from momentum conservation allowing to calculate $\vec{p}_{diss}$ which carries the information on the molecular alignment:

$$\vec{p}_{diss} = \vec{p}_{H^+} - \vec{p}_{rec} = \vec{p}_{H^+} - \frac{m_H}{m_{H_2}}(\vec{q} - \vec{p}_{e2}) \qquad (4)$$

where $(\vec{q} - \vec{p}_{e2})$ is the momentum transferred to the residual ion in the ionizing collision. Finally, the azimuthal and polar angles of the internuclear axis relative to the scattering plane as shown in fig. 1 can be obtained.

4. Results and discussion

4.1. General dependence of the ionization rate on the alignment

Both, the ground state of H_2 and its cation, employ Σ_g^+ symmetry. From this it can be expected that the total ionization cross section does not depend significantly on the molecular alignment [40]. This has been shown experimentally for electron (REF) and ion impact [41]. We have recently published [15] a slightly increased cross section for molecules aligned parallel to momentum transfer. Here we perform a more detailed analysis of these findings. In fig. 4 distributions of the angle γ spanned by the molecular axis and the direction of momentum transfer are displayed for various projectile scattering angles θ_{e1} and second electron energies. All data sets have been normalized to one at the maximum which corresponds to parallel alignment.

At high energies (right plot of fig. 4) of the emitted electron the anisotropy is essentially independent of the scattering angle, with the lowest cross section amounting to ≈ 80% of the maximum. The alignment-dependence is more articulate at low E_{e2} (left plot of fig. 4). Additionally, the anisotropy increases with larger scattering angles, with a

minimal relative cross-section around 60% for θ_{e1} = 16° and E_{e2} = 3 eV. For this kinematics, the emitted electron's momentum is significantly smaller than the magnitude of the momentum transfer q = 1.05 a.u., indicating that a significant interaction between projectile and the molecular core has taken place. It is assumed that such situations induce pronounced cross section differences for distinct alignments [23].

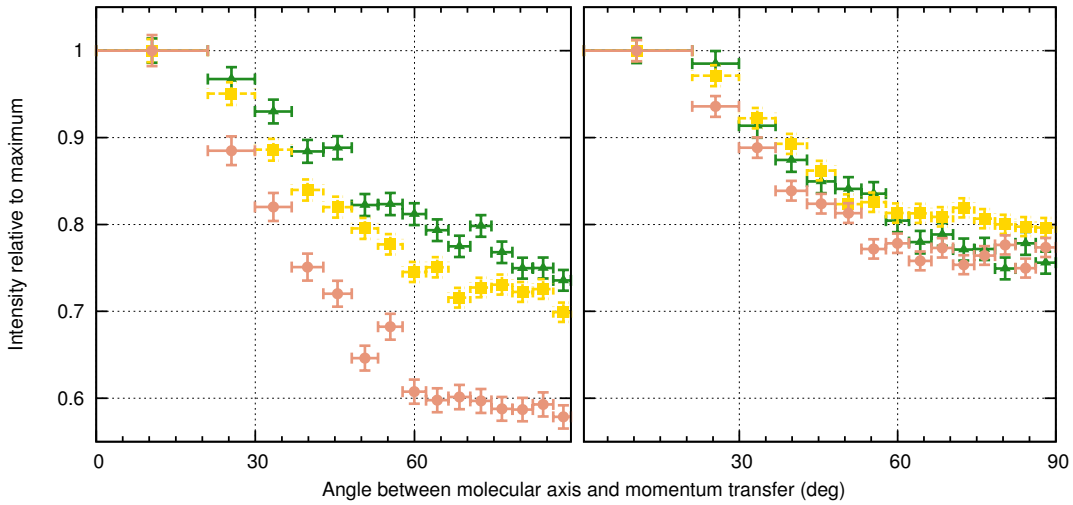

Figure 4: Dependence of the ionization cross-section for H_2 on the angle between the molecular axis and momentum transfer $\vec{q}$. The emitted electron's energy is (3 ± 2) eV (left) and (16 ± 4) eV (right) while the scattering angle varies from (5 ± 2)° (triangles) and (9.5 ± 2.5)° (squares) to (16 ± 4)° (circles). All data sets are normalized to one at their maximum.

4.2. Five-fold differential cross sections

We will present 5DCS for ground-state ionization of hydrogen molecules as emission spectra of the second electron for a fixed molecular alignment. A selection of spectra is shown in figures 6 and 8. A coplanar geometry is selected where the second electron was emitted within ±15◦ of the scattering plane. Three distinct alignments of the internuclear distance were chosen: 0◦ (red), 45◦ (green) and 90◦ (blue) with respect to $\vec{q}$ (see figure 5). In all cases the molecule was located in the scattering plane. Protons going in either direction were included, while the apex angle of the allowance cones was 50◦, corresponding in total to 9.4% of a spherical surface. The experimental values were

not available on an absolute scale. Therefore, the M3DW cross sections were used to normalize the data at the calculated maximum for the $\theta_M = 45^\circ$ geometry.

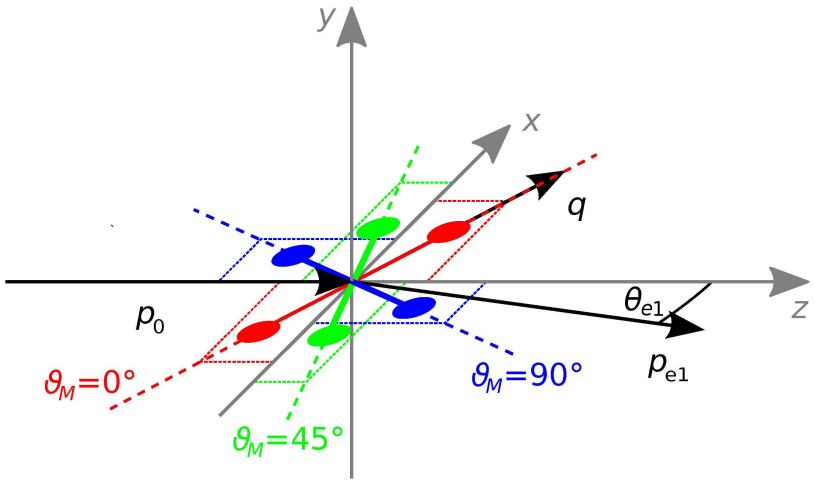

Figure 5: Illustration of the molecular alignments inside the scattering plane as considered in figs. 6, 8 and 7. $\varphi_M = 0°$ for all situations depicted.

Fig. 6 shows 3.5 eV electrons emitted into the scattering plane for three scattering angles. The characteristic (e, 2e) double-lobe structure is clearly shown by all curves: The binary peak corresponding to a clear knock-out collision is located roughly along $\vec{q}$, albeit shifted to larger angles due to repulsion of the two outgoing electrons while the recoil region represents electrons that have been backscattered by the ion after they have been hit by the projectile. Generally, the highest cross sections were determined for molecules aligned along the momentum transfer and the lowest for the perpendicular case. This trend is remarkably well reproduced by the M3DW calculation, especially in the binary lobe. The recoil peak is slightly overestimated by theory, which is well known feature of this model at low emitted electron energies [8].

Between the distinct molecular alignments hardly any pronounced structural differences can be seen in the cross sections. This is in agreement with photo-ionization

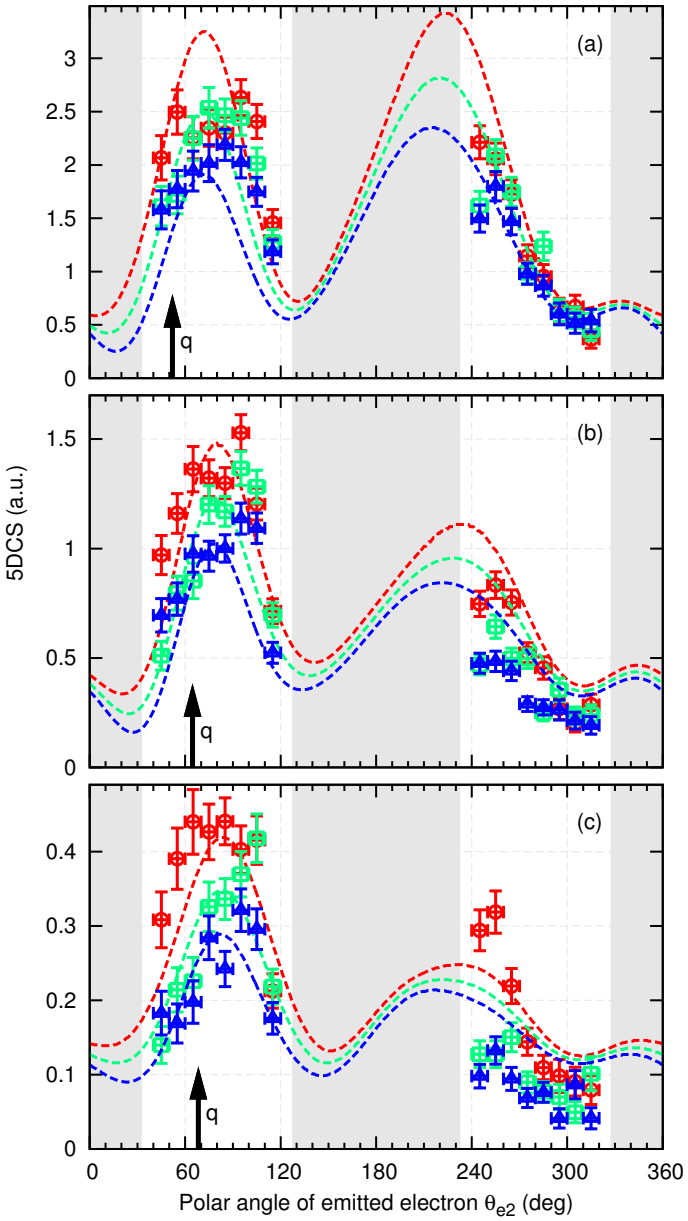

Figure 6: Coplanar 5DCS for molecules aligned in the scattering plane at an angle of 0° (red), 45° (green) and 90° (blue) relative to the momentum transfer $\vec{q}$ (compare fig. 5). The second electron energy is (3.5 ± 2.5) eV while the scattering angle is (a) (5 ± 2) °, (b) (9.5 ± 2.5) ° and (c) (16 ± 4) °. The lines are M3DW calculations. Shaded areas represent angular ranges without experimental acceptance.

studies into the H_2^+ ground state [16,17]. However, the experimental data exhibits an interesting feature at the scattering angle of 16° (Fig. 6 (c)) around 250° : The cross-sections for parallel alignment rises significantly above the typical level, which is not reproduced by theory. The origin of this discrepancy is unknown, but we assume that interaction with the molecular nuclei plays a role at this very specific geometry. If this is the case, articulate distinctions between the alignments are generally expected [23].

We want to highlight the structural differences in the 5DCS seen in fig. 6 (c) by displaying a different portion of the 3-dimensional electron emission picture that the reaction microscope is able to produce. Instead of the coplanar geometry, fig. 7 includes all electrons emitted into the (x, y) plane. This plane is oriented perpendicular to the projectile beam and is equivalent to imaging the azimuth φ_{e2} for a fixed polar angle θ_{e2} of 90°. The experimental values are scaled with the same factor as in fig. 6 (c). One can see that the cross sections are fairly similar for the three alignments, except the two intersections with the scattering plane at φ_{e2} = 0° and 180° (in the scattering plane this corresponds to θ_{e2} = 90° 12 and 270◦, respectively). From this, we can conclude that for the conditions investigated here, the largest dependence on the molecular alignment is found in coplanar geometry. A completely opposite behavior was predicted by the time-dependent close-coupling model [23].

Our M3DW cross sections also employ interesting features in this perpendicular plane. First of all, the 180° maximum for the θ_M = 0 alignment is excellently matching the experimental one. This is intriguing because measurement and model mismatch for this geometry in the coplanar recoil peak. The opposite situation unfolds for the 45° and 90◦ alignments: While the shape of the recoil lobe is in qualitative agreement in the scattering plane, a bump is predicted around φ_{e2} = 180° in the perpendicular geometry where the experimental cross sections are flat. Independent of the molecular alignment, the model always predicts higher 5DCS than the measurement in the azimuthal ranges between 30° and 100° as well as 260° and 330°. Additionally, the cross sections of the 45° and 90° alignments cross each other making the θ_M = 45° case the less probable in these areas. This effect is not resolved by the measurement and so far the origin of this disagreement is not known.

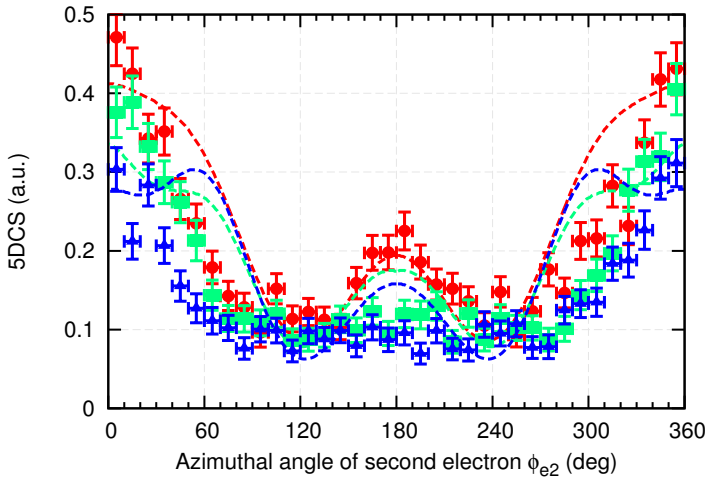

Figure 7: 5DCS in the plane perpendicular to the incoming beam at a scattering angle of (16 ± 4)° and second electron energy of (3.5 ± 2.0) eV, which are the kinematics of fig. 6 (c). Molecules are aligned in the scattering plane at an angle of 0° (red), 45° (green) and 90° (blue) relative to the momentum transfer $\vec{q}$ (compare fig. 5).

In fig. 8 coplanar electron emission spectra are shown for a second electron energy of 16 eV. Here, the plots are strongly dominated by the binary lobe, with little dependence of its magnitude and structure on the molecular alignment. But the trend of preferred ionization for small angles between the internuclear axis and $\vec{q}$ remains. In the recoil lobes it is difficult to mark out clear differences for the three alignments from the experimental data. But there are discrepancies to the M3DW results. Especially for scattering angles of 9.5° and 16° (Fig. 8 (b) and (c)) the recoil peak is significantly underestimated by the calculation. Only at 5◦ the general shape and height are reasonably reproduced whereas the complete structure is shifted about twenty degrees upwards in the experiment. Most notably, in fig. 8 (a) the theory predicts a central dip in the recoil structure that occurs only for a collinear alignment of the molecule with respect to the momentum transfer. Unfortunately, this feature cannot be tested in the present experiment because it is close to the spectrometer axis where there is no acceptance.

Up to now, we have only discussed results for internuclear axes located in the scattering plane. As the protons were essentially detected over the complete solid angle

we can also study other cases. However, as we have already observed in section IVA the ionization cross section is predominantly varying with the angle between molecular axis and momentum transfer but little with the azimuthal angle around $\vec{q}$. This effect can be verified with fully differential cross sections. In fig. 10 exemplary 5DCS are shown for different alignments where the molecule is always perpendicular to the momentum transfer. The geometries are illustrated in fig. 9. Opposite to the previous cross sections no general trend is visible: Especially in figure 10 (a) there seems to be no difference between the three alignments. With a few exceptions the binary peaks are well matched by the calculation, which also cannot find an articulate alignment-dependence. At the smaller emitted electron energy the theoretical cross sections intersect with each other twice to allow for a reversed order of the three molecular geometries in the binary and recoil regime. But the effect is too small to be identified with our experimental resolution.

5. Conclusion

Five-fold differential cross sections for ionization of hydrogen molecules into the ionic ground state by 200 eV electrons have been investigated for distinct molecular alignments, which was obtained from post-collision interaction. The highest rates were found when the internuclear axis is parallel to the momentum transfer direction, but the anisotropy varies with the electron kinematics. In general, good agreement between experimental data and M3DW calculations was found, especially in the binary peaks of the coplanar 5DCS spectra. Few structural differences in the cross sections for distinct alignments were found, but these were different in experiment and theory. Further investigation into this ionization process is suggested to reveal the underlying scattering mechanisms.

Acknowledgments

This work was partly supported by the USA National Science Foundation under Grant. No. PHY-0757749. The author OA-H would like to acknowledge the support of the Saudi Ministry of Higher Education's King Abdullah Bin Abdul-Aziz Scholarship.

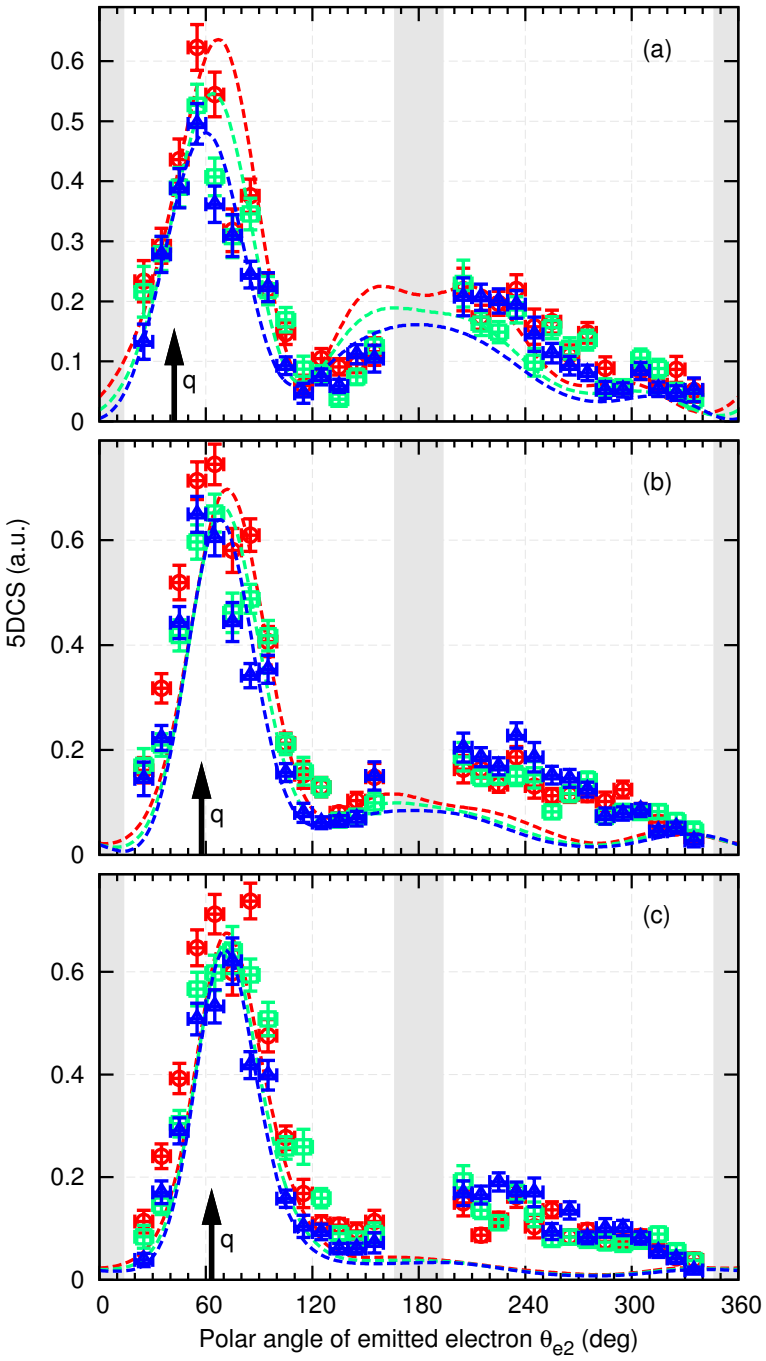

Figure 8: Same as figure 6, but at an energy of the second electron of (16 ± 4) eV.

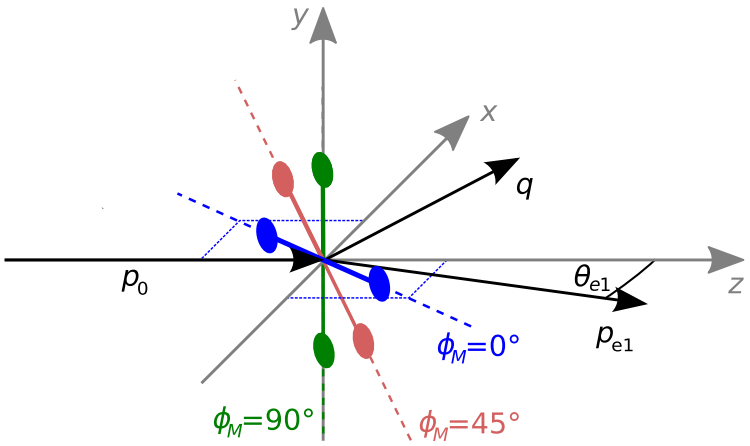

Figure 9: Illustration of the molecular alignments considered in figure 10. θ = 90° for all situations depicted, i.e. the internuclear axis is always located in the plane normal to $\vec{q}$.

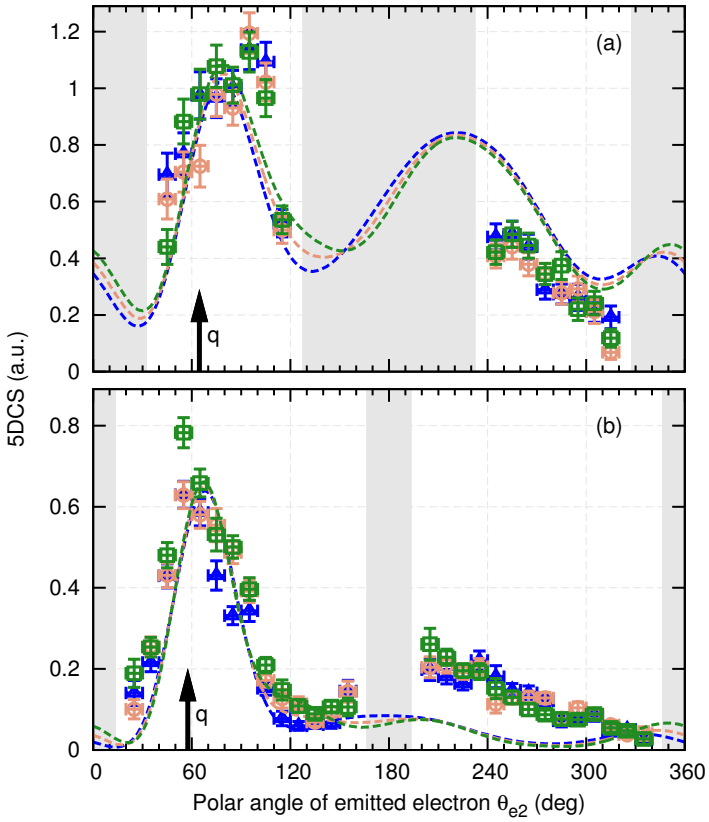

Figure 10: Coplanar 5DCS for molecules aligned perpendicular to $\vec{q}$ but with a relative angle towards the scattering plane of 0° (blue), 45° (salmon) and 90° (green) as illustrated in fig. 9. The scattering angle is fixed to (9.5 ± 2.5) ° while the plotted electron's energy is either (a) (3.5 ± 2.5) eV or (b) (16 ± 4) eV. Shaded areas represent angular ranges without experimental acceptance.

References

[1] E. McCarthy and E. Weigold, *Reports on Progress in Physics* **54**, 789 (1991).

[2] D. H. Madison and Ola Al-Hagan, *Journal of Atomic, Molecular, and Optical Physics,* **2010** 15 (2010).

[3] G. H. Dunn and L. J. Kieffer, *Phys. Rev.* **132**, 2109 (1963).

[4] R. J. Van Brunt and L. J. Kieffer, *Phys. Rev*. A **2**, 1293 (1970).

[5] K. Edwards, R. M. Wood, J. L. Davis, and R. L. Ezell, *Phys. Rev.* A **42**, 1367 (1990).

[6] E. Weigold, S. T. Hood, I. E. McCarthy, and P. J. O. Teubner, *Phys. Lett.* A **44,** 531 (1973).

[7] M. Cherid, A. Lahmam-Bennani, A. Dugett, R. W. Zurales, R. R. Lucchese, M. C. Dal Cappello, and C. Dal Cappello, *J. Phys.* B: *At. Mol. Opt. Phys*. **22**, 3483 (1989).

[8] D. S. Milne-Brownlie, M. Foster, J. Gao, B. Lohmann, and D. H. Madison, *Phys. Rev. Lett.* **96**, 233201 (2006).

[9] A. J. Murray, *J. Phys.* B: *At. Mol. Opt. Phys*. **38,** 1999 (2005).

[10] E. M. Staicu Cassagrande, A. Naja, F. Mezdari, A. Lahmam-296 Bennani, P. Bolognesi, B. Joulakian, O. Chuluunbaatar, O. Al-Hagan, D. H. Madison, D. V. Fursa, and I. Bray*, J. Phys.* B: *At. Mol. Opt. Phys*. **41**, 052701 (2008).

[11] O. Al-Hagan, C. Kaiser, D. H. Madison, and A. J. Murray, *Nat. Phys*. **5**, 59 (2008).

[12] M. Takahashi, N. Watanabe, Y. Khajuria, K. Nakayama, Y. Udagawa, and J. H. D. Eland, *J. Electron Spectrosc. Relat. Phenom*. **141**, 83 (2004).

[13] M. Takahashi, N. Watanabe, Y. Khajuria, Y. Udagawa, and J. H. D. Eland, *Phys. Rev. Lett.* **94**, 213202 (2005).

[14] S. Bellm, J. Lower, E. Weigold, and D. W. Mueller, *Phys. Rev. Lett.* **104**, 023202 (2010).

[15] A. Senftleben, T. Pflu¨ger, X. Ren, O. Al-Hagan, B. Najjari, D. Madison, A. Dorn, and J. Ullrich*, Phys. Rev. Lett*.(2010).

[16] A. Lafosse, M. Lebech, J. C. Brenot, P. M. Guyon, L. Spielberger, O. Jagutzki, J. C. Houver, and D. Dowek, *J. Phys.* B: *At. Mol. Opt. Phys.* **36**, 4683 (2003).

[17] Hikosaka and J. H. D. Eland, *J. Electron Spectrosc. Relat. Phenom*. **133**, 77 (2003).

[18] Y. Hikosaka and J. H. D. Eland, *Chem. Phys.* **277**, 53 (2002).

[19] K. Ito, J. ichi Adachi, R. Hall, S. Motoki, E. Shigemasa, K. Soejima, and A. Yagishita*, J. Phys.* B*: At. Mol. Opt. Phys*. **33**, 527 (2000).

[20] C. Dimopoulou, R. Moshammer, D. Fischer, P. D. Fainstein, C. H¨ohr, A. Dorn, J. R. Crespo L´opez Urrutia, C. D. Schr¨oter, H. Kollmus, R. Mann, S. Hagmann, and J. Ullrich, *J. Phys.* B: *At. Mol. Opt. Phys*. **38**, 593 (2005).

[21] G. Laurent, J. Fern´andez, S. Legendre, M. Tarisien, L. Adoui, A. Cassimi, X. Fl´echard, F. Fr´emont, B. Gervais, E. Giglio, J. P. Grandin, and F. Mart´ın, *Phys. Rev. Lett.* **96**, 173201 (2006).

[22] C. R. Stia, O. A. F´ojon, P. F. Weck, J. Hanssen, and R. D. Rivarola, J. Phys. B: *At. Mol. Opt. Phys.* **36**, L257 (2003).

[23] J. Colgan, M. S. Pindzola, F. Robicheaux, C. Kaiser, A. J. Murray, and D. H. Madison, *Phys. Rev. Lett.* **101**, 233201 (2008).

[24] J. Colgan, O. Al-Hagan, D. H. Madison, A. J. Murray, and M. S. Pindzola, *J. Phys.* B: *At. Mol. Opt. Phys*. **42**, 171001 (2009).

[25] S. Chatterjee, D. Misra, A. H. Kelkar, L. C. Tribedi, C. R. Stia, O. A. Foj´on, and R. D. Rivarola, *Phys. Rev.* A **78**, 052701 (2008).

[26] J. Gao, J. L. Peacher, and D. H. Madison, *J. Chem. Phys*. **123**, 204302 (2005).
[27] J. Gao, D. H. Madison, and J. L. Peacher, *J. Chem. Phys*. **123**, 204314 (2005).
[28] J. Gao, D. H. Madison, and J. L. Peacher, *J. Phys.* B: *At. Mol. Opt. Phys.* 39, 1275 (2006).
[29] J. B. Furness and I. E. McCarthy, *J. Phys.* B: *At. Mol. Opt. Phys*. **6**, 2280 (1973).
[30] J. P. Perdew and A. Zunger, *Phys. Rev*. B **23**, 5048 (May 1981).
[31] M. Du¨rr, A. Dorn, J. Ullrich, S. P. Cao, A. Czasch, A. S. Kheifets, J. R. G¨otz, and J. S. Briggs, *Physical Review Letters* **98**, 193201 (2007).
[32] A. Dorn, M. Du¨rr, B. Najjari, N. Haag, C. Dimopoulou, D. Nandi, and J. Ullrich, *J. Electron Spectrosc. Relat. Phenom.* **161**, 2 (2007).
[33] R. Moshammer, D. Fischer, and H. Kollmus, in Many-Particle Quantum Dynamics in Atomic and Molecular fragmentation, edited by J. Ullrich and V. P. Shevelko (*Springer, Berlin, 2003*) pp. 33–58.
[34] O. Jagutzki, A. Cerezo, A. Czasch, R. D¨orner, M. Hattass, M. Huang, V. Mergel, U. Spill mann, K. Ullmann-Pfleger, T. Weber, H. Schmidt-B¨ocking, and G. D. W. Smith, *IEEE T. Nucl. Sci*. **49**, 2477 (2002).
[35] H. B. Pedersen, S. Altevogt, B. Jordon-Thaden, O. Heber, L. Lammich, M. L. Rappaport, D. Schwalm, J. Ullrich, D. Zajfmann, R. Treusch, N. Guerassimova, M. Martins, and A. Wolf, *Phys. Rev.* A **80**, 012707 (2009).
[36] T. E. Sharp, At. *Data Nucl. Data Tables* **2**, 119 (1970).
[37] S. L. Guberman, *J. Chem. Phys*. **78**, 1404 (1983).
[38] R. N. Zare, *J. Chem. Phys*. **47,** 204 (1967).
[39] R. M. Wood, Q. Zheng, A. K. Edwards, and M. A. Mangan, *Rev. Sci. Instrum*. **68,** 1382 (1997).
[40] G. H. Dunn, *Phys. Rev. Lett*. **8,** 62 (1962). 350
[41] N. G. Johnson, R. N. Mello, M. E. Lundy, J. Kapplinger, E. Parke, K. D. Carnes, I. Ben Itzhak, and E. Wells, *Phys. Rev.* A **72,** 052711 (2005).

3. CONCLUSIONS

Although significant theoretical progress for calculating the FDCS for electron-impact ionization of molecules has been made in the last few years, there is still much to be done. While the experimental techniques are significantly ahead of the theoretical developments, this is an exciting time since experiments are able to produce excellent data with great detail, which provides very stringent tests for theoretical models. The work that has been done so far has provided some valuable insights into the mechanisms of molecular ionization as well as provided some unanswered questions. For example, is the simple model of Al-Hagan *et al*. in paper I correct? It states that molecules which have a nucleus at the center of mass will have strong back-to-back scattering in the perpendicular plane while molecules which do not have a nucleus at the center of mass will have weak back-to-back scattering? We have one data set supporting this model and one data set that does not support it.

For the simplest molecule H_2, the experimental data were compared with TDCC and M3DW calculations in the perpendicular plane for cases where the outgoing electrons had equal energies ranging from 1eV to 10eV and had unequal energies of 2 eV and 18 eV. The data for 10 eV exhibits peaks at 90° and 270° and a minimum at 180°. It was shown that the 90° and 270° peaks result from elastic scattering of the projectile from the target into the perpendicular plane followed by a classical binary collision between the projectile and target electrons. For the minimum at 180°, it was shown that PCI is unimportant at this energy, and that the electron-electron collision occurs between the nuclei where the net attractive force cancels on average, so that there is almost no 180° scattering. The data for 1 eV showed that the shape of the FDCS completely changed from two peaks centered at 90° and 270°, to a single peak at 180°. It was found that PCI changes from being unimportant at 10eV to being the dominant physical process for the case of 1 eV in which case the FDCS has a Gaussian shape centered on 180° as is predicted by the WPR threshold law.

For unequal and equal energy sharing (low incident energies) with different gun angles ψ, both the M3DW and TDCC give good agreement with measurements for large gun angle values, especially for the perpendicular geometry. At lower gun angles, and for

the coplanar geometry, the agreement between experiment and theory is not as satisfactory. The TDCC gives good shape agreement and relative normalization for out-of-plane angles greater than 45^0 and rather poor agreement for angles in and near the scattering plane. Surprisingly, the M3DW predicts the relative magnitudes of the cross section for different planes better than the TDCC.

At high incident energies, both the M3DW and FBA-TCC results are in qualitative agreement with the binary peak but in poor agreement with the recoil peak for ionization of H_2. This lack of agreement between experiment and theory for the simplest molecule is a major challenge that needs to be solved.

For the two-center double-slit interference effects in diatomic molecules, it has been predicted that the cross section for molecular hydrogen could be expressed as the cross section for atomic hydrogen times an interference factor. For higher energies and asymmetric kinematics for both H_2 and N_2, the molecular recoil peak is suppressed compared to atomic recoil peaks in accordance with the two-center predictions. Two experiments for H_2 and one experiment for N_2 have found evidence for interference using this method. For lower energy symmetric collisions, the N_2 results are in very good agreement with the experimental measurements and the M3DW results. The M3DW predicts a peak at 180^0 scattering which had previously been interpreted as a double scattering interference peak. Although this angular range is not accessible in the present measurements, the 180° peak is consistent with measurements which have been made. However, model calculations with different nuclear separations suggest that this peak does not result from electron scattering from two separate nuclei. Consequently, the present results suggest that two center effects can be seen in the ratio of the recoil peak to the binary peak. However, other peak structures predicted by the theory are probably due to some other type of interference which is yet to be determined.

In the case of low energy ionization of the $3a_1$ state of H_2O, results completely opposite to those for H_2 were found. For H_2, the best agreement between experiment and theory was in the perpendicular plane. For H_2O, the best agreement between experiment and theory is in the scattering plane and the worst agreement is in the perpendicular plane. For H_2, the largest cross section was found for $\psi = 45^0$; whereas, for H_2O the largest cross section is in the scattering plane. Since the M3DW has been moderately

successful for N_2, the big question is whether or not it will also work for even larger molecules. More theoretical and experimental work are required to answer this question.

For a larger molecule, such as formic acid, the fact that the M3DW produced reasonably good agreement with the high-energy EMS measurements is very encouraging and indicates the validity of the OAMO at least for the $10a'$ state. Unfortunately, the experimental data could not resolve the $10a'$ and $2a''$ states, and since the OAMO approximation is known to not be valid for the $2a''$ state, no definite conclusions can be made until either we have an improved experimental resolution or a M3DW calculation that does not make the OAMO approximation.

Overall, the M3DW results presented so far all rely on the OAMO approximation, which is potentially valid for a limited number of states and a limited range of scattering angles. Although the approximation has proved to be surprisingly successful for several cases, it is clearly highly desirable to develop a M3DW calculation that does not use this approximation.

Finally, the five-fold differential cross sections for ionization of hydrogen molecules into the ionic ground state by 200 eV electrons have been investigated for different molecular alignments. In general, good agreement between experimental data and M3DW calculations was found, especially in the binary peaks of the coplanar 5DCS spectra. Few structural differences in the cross sections for different alignments were found, but these were different in experiment and theory. Further investigation into this ionization process is suggested to reveal the underlying scattering mechanisms.

In future work, we hope that experimentalists will be able to do more measurements of the FDCS for a specific molecular orientation with respect to the electron beam for several molecules. These measurements will test recent predictions of the FDCS for ionization from oriented molecules and may also shed some light on the discrepancies which exist between theory and experiment for the FDCS as discussed here.

BIBLIOGRAPHY

[1] Rescigno T N, Baertschy M, Isaacs W A and McCurdy C W 1999 *Science* **286** 2474
[2] Bray I 2000 *J Phys. B* **33** 581
[3] Colgan J and Pindzola M S 2006 *Phys. Rev. A* **74** 012713
[4] Bartschat K and Bray I 1996 *J Phys. B* **29** L577
[5] Bray I 2002 *Phys. Rev. Lett.* **89** 273201
[6] Bray I, Fursa D V, Kheifets A and Stelbovics A T 2002 *J Phys. B* **35** R117
[7] Colgan J, Pindzola M S, Childers G and Khakoo M A 2006 *Phys. Rev. A* **73** 042710
[8] Weigold E and McCarthy I E 1999, '*Electron Momentum Spectroscopy'* (Kluwer Academic/Plenum Publishers, New York)
[9] Lahmam-Bennani A, Taouil I, Duguet A, Lecas M, Avaldi L and Berakdar J 1999 *Phys. Rev. A* **59** 3548
[10] Weck P, Joulakian B and Hervieux P A 1999 *Phys. Rev. A* **60** 3013
[11] Weck P, Fojón O A, Hanssen J, Joulakian B and Rivarola R D 2001 *Phys. Rev. A* **63** 042709
[12] Champion C, Hanssen J and Hervieux P A 2001 *Phys. Rev. A* **63** 052720
[13] Elboudali F and Joulakian B 2001 *J. Phys. B* **34** 4877
[14] Serov V V, Derbov V L, Joulakian B B and Vinitsky S I 2001 *Phys. Rev. A* **63** 062711
[15] Champion C, Hanssen J and Hervieux P A 2002 *Phys. Rev. A* **65** 022710
[16] Champion C, Hanssen J and Hervieux P A 2002 *J. Chem. Phys.* **117** 197
[17] Hussey M J and Murray A 2002 *J. Phys. B* **35** 3399
[18] Serov V V, Joulakian B B, Pavlov D V , Puzynin I V and Vinitsky S I 2002 *Phys. Rev. A* **65** 627081
[19] Stia C R, Fojón O A, Weck P F, Hanssen J, Joulakian B and Rivarola R D 2002 *Phys. Rev. A* **66** 052709
[20] Weck P, Fojón O A, Joulakian B, Stia C R, Hanssen J and Rivarola R 2002 *Phys. Rev. A* **66** 012711
[21] Fojón O A, Stia C R, Weck P F, Hanssen J, Joulakian B and Rivarola R D 2003 *Institute of Physics Conference Series* **172** 11
[22] Houamer S, Mansouri A, Dal Cappello C, Lahmam-Bennani A, Elazzouzi S, Moulay M and Charpentier I 2003 *J. Phys. B* **36** 3009
[23] Champion C, Hanssen J and Hervieux P 2004 *J. Chem. Phys.* **121** 9423
[24] Chuluunbaatar O, Joulakian B, Tsookhuu K and Vinitsky S I 2004 *J. Phys. B* **37** 2607
[25] Milne-Brownlie D S, Cavanagh S J, Lohmann B, Champion C, Hervieux P A and Hanssen P 2004 *Phys. Rev. A* **69** 032701
[26] Gao J, Madison D H and Peacher J L 2005 *Phys. Rev. A* Rapid Communications **72** 020701
[27] Gao J, Madison D H and Peacher J L 2005 *J. Chem. Phys.* **123** 204314
[28] Gao J, Madison D H and Peacher J L 2005 *Phys. Rev. A* **72** 032721
[29] Gao J, Peacher J L and Madison D H 2005 *J. Chem. Phys.* **123** 204302

[30] Hussey M J and Murray A J 2005 *J. Phys. B* **38** 2965
[31] Murray A J 2005 *J. Phys. B* **38**, 1999
[32] Serov V V, Joulakian B B, Derbov V L and Vinitsky S I 2005 *J. Phys. B* **38** 2765
[33] Dal Cappello C, Mansouri A , Houamer S and Joulakian B 2006 *J. Phys. B* **39** 2431
[34] Gao J, Madison D H, and Peacher J L 2006 *J. Phys B* **39** 1275
[35] Gao J, Madison D H, Peacher J L, Murray A J and Hussey M J 2006 *J. Chem. Phys.* **124** 194306
[36] Milne-Brownlie D S, Foster M, Gao J, Lohmann B and Madison D H 2006 *Phys. Rev. Lett.* **96** 233201
[37] Murray A J, Hussey M J, Gao J and Madison D H 2006 *J. Phys. B* **39** 3945
[38] Kaiser C, Spieker D, Gao J, Hussey M, Murray A J and Madison D H 2007 *J. Phys. B* **40** 2563
[39] Murray A J, Hussey M J, Kaiser C, Gao J, Peacher J L and Madison D H 2007 *Journal of Electron Spectroscopy and Related Phenomena* **161** 11
[40] Naja A, Staicu Casagrande E M, Lahmam-Bennani A, Nekkab M, Mezdari F, Joulakian B, Chuluunbaatar O and Madison D H 2007 *J. Phys. B* **40** 3775
[41] Serov V V, Derbov V L, Joulakian B B and Vinitsky S I 2007 *Phys. Rev. A* **75** 012715
[42] Staicu Casagrande E M, Naja A, Ren X G, Nekkab M, Catoire F, Mezdari F, Lahmam-Bennani A, Madison D, Chuluunbaatar O and Joulakian B 2007 *Journal of Physics: Conference Series* **88** 012010
[43] Champion C, Boudrioua O and Dal Cappello D 2008 *Journal of Physics: Conference Series* **101** 012010
[44] Chuluunbaatar O, Joulakian B B, Puzynin I V, Tsookhuu K and Vinitsky S I 2008 *J. Phys. B* **41** 015204
[45] Staicu Casagrande E M, Naja A, Mezdari F, Lahmam-Bennani A, Bolognesi P, Joulakian B, Chuluunbaatar O, Al-Hagan O, Madison D H, Fursa D V and Bray I 2008 *J. Phys. B:* **41** 025204
[46] Staicu Casagrande E M, Naja A, Lahmam-Bennani A, Kheifets A S, Madison D H and Joulakian B 2008 *J. Phys Conference Series* **141** 012016
[47] Colgan J, Pindzola M S, Robicheaux F J, Griffin D C and Baertschy M 2002 *Phys. Rev. A* **65** 042721
[48] Colgan J, Pindzola M S, Robicheaux F, Kaiser C, Murray A J and Madison D H 2008 *Phys. Rev. Lett.* **101** 233201
[49] Colgan J, Al-Hagan O, Madison D H, Murray A J and Pindzola M S 2009 *J. Phys. B* **42** 171001
[50] Kada I, Mansouri A, Dal Cappello C, Hervieux P A and Roy A C 2009 *J. Phys. B* **42** 025201
[51] Mansouri A, Dal Cappello C, Kada, I, Champion C and Roy A C 2009 *Phys. Lett. A* **373** 3151
[52] Duguet A M, Cherid A, Lahmam-Bennani, Franz A and Klar H 1987 *J. phys*. B **20** 6145
[53] Chérid M, Lahmam-Bennani A, Duguet A, Zurales R W, Lucchese R R, Dal Cappello M C and Dal Cappello C 1989 *J. Phys. B* **22** 3483
[54] McCarthy I E and Weigold E 1976 *Phys. Rep. C* **27** 275

[55] McCarthy I E and Weigold W 1988 *Rep. Prog. Phys.* **51** 299
[56] McCarthy I E and Rossi A M 1994 *Phys. Rev.* A **49** 4645
[57] Robicheaux F 1996 *J. Phys. B* **29** 779
[58] Deutch H and Becker K 1998 *J. Phys. Chem. A* **102** 8819
[59] Rioual G, Nguyen Vien and Pochat A1996 *Phys. Rev* A **54** 4968
[60] Madison D H, Calhoun R V and Shelton W N 1977 *Phys. Rev. A* **16** 552
[61] Monzani A L, Machado L E, Lee M T and Machado A M 1999 *Phys. Rev. A* **60** R21
[62] T´oth, R.I. Campeanu, V. Chi¸s1, and L. Nagy1, 2008 Eur. Phys. J. D **48**, 351–354
[63] Botero J and Macek J H 1992 *Phys. Rev. Lett.* **68** 576
[64] Whelan C T, Allan R J and Walters H R J 1993 *Journal De Physique IV : JP* **3** 39
[65] Whelan C T, Allan R J, Walters H R J and Zhang X 1993 *(e,2e) and Related Processes*, edited by Colm T.Whelan, H. R. J. Walters, A. Lahmam-Bennani and H. Ehrhardt (Kluwer Academic Publisher, Dordrecht)
[66] Kheifets A S, Naja A, Casagrande E M S and Lahmam-Bennani A 2008 *J. Phys* **41** 145201
[67] Kheifets A S, Naja A, Casagrande E M S and Lahmam-Bennani A 2008 *J. Phys* **41** 209801
[68] Ward S J and Macek J H 1994 *Phys. Rev. A* **49** 1049
[69] Al-Hagan O, Kaiser C, Madison D H and Murray A J 2009 *Nature Physics* **5** 59
[70] Nixon K L, Murray A J, Al-Hagan O, Madison D H and Ning C G 2010 *to be published (H_2O)*
[71] Brauner M, Briggs J S and Klar H 1989 *J. Phys. B* **22** 2265
[72] Jones S, Madison D H, Franz A and Altick P L 1993 *Phys. Rev. A* **48** R22-R25
[73] Jones S and Madison D H 1994 *J Phys. B* **27** 1423
[74] Rasch J, Whelan C T, Lucey S P, Dal Cappello C and Walters H R J 1998 *Computer Physics Communications* **114** 378
[75] Prideaux A and Madison D H 2003 *Phys. Rev. A* **67** 052710
[76] Perdew J P and Zunger A 1981 *Phys. Rev. B* **23** 5048
[77] Padial N T and Norcross D W 1984 *Phys. Rev. A* **29** 1742
[78] Joachain C J, 1983 ,Quantum collision theory, North-Holland physics Publishing: Amsterdam
[79] Takahashi M, Watanabe N, Khajuria Y, Udagawa Y, and J H D Eland 2005 *Phys. Rev. Lett.* **94**, 213202
[80] Dimopoulou C, Moshammer R, D Fischer, Fainstein P D, C Hohr, A Dorn, J R C L Urrutia, C D Schroter, H Kollmus, R Mann, S Hagmann, and J Ullrich, 2005 *J Phys. B* **38**, 593
[81] Senftleben Arne 2010
[82] Lee C, Yang W and Parr R G 1988 *Phys. Rev.* B **37** 785.
[83] Guerra *C* F *et al.* 1998 *Theor. Chem. Acc*. **99** 391.
[84] Furness J B and McCarthy I E 1973 *J. Phys B* **6** 2280
[85] Riley M E and Truhlar D G 1975 *J. of Chemical Physics* **63** 2182
[86] Martinez J M, Walters H R J and Whelan C T 2008 *J. Phys. B* **41** 065202

[87] Khare,P.S, 2002, Introduction to the theory of collisions of electrons with atoms and molecules , Kluwer Academic/Plenum Publisher, New York.

VITA

Ola Ali Al-Hagan was born and grew up in southwest Saudi Arabia. She graduated from the Girl's College of Education at Abha in Saudi Arabia with a Bachelor of Arts degree in Physics with highest honors. She enrolled in Northwest Missouri State University as graduate student, and in April 2005, she earned a master's degree in Business Administration (MBA). Then, she enrolled in the University of Missouri-Rolla (now Missouri University of Science and Technology) with support of the Saudi Ministry of Higher Education and the King Abdullah Bin Abdul-Aziz Scholarship Program and began work on her Ph.D. in Physics. She started working in the field of theoretical atomic physics in June 2006 and she earned her Ph.D. in May 2010.

Ola Ali Al-Hagan was the first place winner of the 14th Annual Laird D. Schearer Research Prize competition in November 2007 and the third place winner of the 16th Schearer Research Prize competition in December 2009. She was the winner of the GEC (Gaseous Electronics Conference) Student Award for Excellence, October 2008, held in Dallas, Texas. She served as the Physics Department representative for the Council of Graduate Students, and received the 2008 Council of Graduate Students Best Representative for the Valuable Services Award.

She has published 11 peer-reviewed articles, and presented research results at 8 national and international conferences. She was an invited speaker at the 2009 International Symposium on (e,2e), the Double Photoionization and Related Topics & 15th Int'l Symposium on Polarization and Correlation in Electronic and Atomic Collisions.